

**227**

## **Topics in Current Chemistry**

**Editorial Board:**

**A. de Meijere · K.N. Houk · H. Kessler**

**J.-M. Lehn · S.V. Ley · S.L. Schreiber · J. Thiem**

**B.M. Trost · F. Vögtle · H. Yamamoto**

**Springer**

*Berlin*

*Heidelberg*

*New York*

*Hong Kong*

*London*

*Milan*

*Paris*

*Tokyo*

# Colloid Chemistry II

**Volume Editor: Markus Antonietti**

With contributions by

J. Bibette, F. Caruso, F. Currie, A. Elaissari, K. Esumi,  
F. Ganachaud, C. Gruber, M. Häger, K. Holmberg,  
I. Kräuter, K. Landfester, F. Leal-Calderon,  
C. M. Paleos, C. Pichot, V. Schmitt, G. E. M. Tovar,  
D. Tsiourvas



**Springer**

The series *Topics in Current Chemistry* presents critical reviews of the present and future trends in modern chemical research. The scope of coverage includes all areas of chemical science including the interfaces with related disciplines such as biology, medicine and materials science. The goal of each thematic volume is to give the non-specialist reader, whether at the university or in industry, a comprehensive overview of an area where new insights are emerging that are of interest to a larger scientific audience.

As a rule, contributions are specially commissioned. The editors and publishers will, however, always be pleased to receive suggestions and supplementary information. Papers are accepted for *Topics in Current Chemistry* in English.

In references *Topics in Current Chemistry* is abbreviated *Top. Curr. Chem.* and is cited as a journal.

Springer WWW home page: <http://www.springer.de>  
Visit the TCC home page at <http://link.springer.de/series/tcc/>  
or <http://link.springer-ny.com/series/tcc/>

ISSN 0340-1022

ISBN 3-540-00418-1

DOI 10.1007/b10851

Springer-Verlag Berlin Heidelberg New York

Library of Congress Catalog Card Number 74-644622

This work is subject to copyright. All rights are reserved, whether the whole or part of the material is concerned, specifically the rights of translation, reprinting, reuse of illustrations, recitation, broadcasting, reproduction on microfilms or in any other ways, and storage in data banks. Duplication of this publication or parts thereof is only permitted under the provisions of the German Copyright Law of September 9, 1965, in its current version, and permission for use must always be obtained from Springer-Verlag. Violations are liable for prosecution under the German Copyright Law.

Springer-Verlag Berlin Heidelberg New York  
a member of BertelsmannSpringer Science+Business Media GmbH

<http://www.springer.de>

© Springer-Verlag Berlin Heidelberg 2003  
Printed in Germany

The use of general descriptive names, registered names, trademarks, etc. in this publication does not imply, even in the absence of a specific statement, that such names are exempt from the relevant protective laws and regulations and therefore free for general use.

Cover design: KunkelLopka, Heidelberg/design & production GmbH, Heidelberg  
Typesetting: Fotosatz-Service Köhler GmbH, 97084 Würzburg

02/3020 ra – 5 4 3 2 1 0 – Printed on acid-free paper

---

## Volume Editor

**Prof. Dr. Markus Antonietti**

Max Planck Institute of Colloids and Interfaces  
14424 Potsdam

Germany

*E-mail: pape@mpigk-golm.mpg.de*

## Editorial Board

**Prof. Dr. Armin de Meijere**

Institut für Organische Chemie  
der Georg-August-Universität  
Tammannstraße 2

37077 Göttingen, Germany

*E-mail: ameijer1@uni-goettingen.de*

**Prof. Dr. Horst Kessler**

Institut für Organische Chemie  
TU München

Lichtenbergstraße 4

85747 Garching, Germany

*E-mail: kessler@ch.tum.de*

**Prof. Steven V. Ley**

University Chemical Laboratory  
Lensfield Road

Cambridge CB2 1EW, Great Britain

*E-mail: svl1000@cus.cam.ac.uk*

**Prof. Dr. Joachim Thiem**

Institut für Organische Chemie  
Universität Hamburg

Martin-Luther-King-Platz 6

20146 Hamburg, Germany

*E-mail: thiem@chemie.uni-hamburg.de*

**Prof. Dr. Fritz Vögtle**

Kekulé-Institut für Organische Chemie  
und Biochemie der Universität Bonn

Gerhard-Domagk-Straße 1

53121 Bonn, Germany

*E-mail: voegt@uni-bonn.de*

**Prof. K.N. Houk**

Department of Chemistry and Biochemistry  
University of California

405 Hilgard Avenue

Los Angeles, CA 90024-1589, USA

*E-mail: houk@chem.ucla.edu*

**Prof. Jean-Marie Lehn**

Institut de Chimie

Université de Strasbourg

1 rue Blaise Pascal, B.P.Z 296/R8

67008 Strasbourg Cedex, France

*E-mail: lehn@chimie.u-strasbg.fr*

**Prof. Stuart L. Schreiber**

Chemical Laboratories

Harvard University

12 Oxford Street

Cambridge, MA 02138-2902, USA

*E-mail: sls@slsirir.harvard.edu*

**Prof. Barry M. Trost**

Department of Chemistry

Stanford University

Stanford, CA 94305-5080, USA

*E-mail: bmtrost@leland.stanford.edu*

**Prof. Hisashi Yamamoto**

School of Engineering

Nagoya University

Chikusa, Nagoya 464-01, Japan

*E-mail: j45988a@nucc.cc.nagoya-u.ac.jp*

## **Topics in Current Chemistry Also Available Electronically**

For all customers with a standing order for Topics in Current Chemistry we offer the electronic form via SpringerLink free of charge. Please contact your librarian who can receive a password for free access to the full articles by registration at:

<http://link.springer.de/orders/index.htm>

If you do not have a standing order you can nevertheless browse through the table of contents of the volumes and the abstracts of each article at:

<http://link.springer.de/series/tcc>

<http://link.springer-ny.com/series/tcc>

There you will also find information about the

- Editorial Board
- Aims and Scope
- Instructions for Authors

---

## Preface

Over the past forty years, good-old fashioned colloid chemistry has undergone something of a revolution, transforming itself from little more than a collection of qualitative observations of the macroscopic behavior of some complex systems into a discipline with a solid theoretical foundation and a whole toolbox of new chemical techniques. It can now boast a set of concepts which go a long way towards providing an understanding of the many strange and interesting behavior patterns exhibited by natural and artificial systems on the mesoscale.

This second volume of “Topics in Current Chemistry” on Colloid Chemistry, focuses on supramolecular approaches and new approaches towards polymer colloids, also with strong emphasis on biological and biomedical applications. Again topics were chosen which are expected to have broader relevance and to be interesting to a more general readership.

The volume opens with a contribution by C.M. Paleos in which new amphiphiles are presented which not only self-assemble to micelles or vesicles but also possess the ability to show specific recognition of complementary H-bridge patterns. Such structures might point a way to a rational addressing of surfaces and supramolecular structures by purely chemical means.

In the contribution by K. Esumi, the use of dendrimers or dendritic amphiphiles for the controlled generation of nanoparticles is reviewed. Depending on dendrimer generation, different well-defined particle sizes and hybrid morphologies can be made, whereas the outer shells are still given by the dendrimer and its functionality pattern on the outer rim. As in the previous contribution, such systems may be very relevant for controlled contrasting and recognition in biological systems.

Ascending the accessible length scales of colloid chemistry, K. Holmberg demonstrates how microemulsions can be favorably used to perform specific organic reactions in a highly efficient way. Microemulsions expose large, stable oil-water interfaces of up to  $1000 \text{ m}^2 \text{ g}^{-1}$  the control of which is the key factor whenever reactants/catalysts/products show very different polarity and live in different phases. This is especially worth considering when the reactions can be performed in the “green solvent” water.

The very high promise of reactions in heterophase systems is extended by K. Landfester who writes about the “boom-topic” miniemulsions. Miniemulsions are liquid/liquid dispersions with stable droplets with a size range between  $30 \text{ nm} < d < 300 \text{ nm}$ , and they are indeed the first convenient realization of

stable nanoreactors, with a number of perspectives especially for polymer, nanoparticle, and nanohybrid synthesis.

G. Tovar describes one of the novel chemical applications of modern colloidal systems by using such miniemulsions (in addition to classical suspension polymerization) for molecular imprinting. Here, the stable nanoreactor situation is used to “synthesize” particle surfaces with molecular sized cavities for biomedically relevant species or species to be separated from each other. Such “receptor” sites are nowadays preferentially made by the pathways of modern colloid chemistry.

It is again a special chemical surface design of polymer latex particles which is delineated in the contribution by A. Elaissari. Here, special routes have been developed to modify both the particle polarity, the surface charge and its chemical functionality to reveal specific binding with DNA and peptides. Obviously, such species are highly relevant for particle-based diagnostic and particle-based cell separation.

F. Caruso uses monodisperse polymer spheres and their colloidal crystals only as templates to create hollow capsules or extended opal arrays with the layer-by-layer technique. Again this is a typical colloid chemistry tool which is unparalleled in low molecular weight organic chemistry, and hollow mesostructures systems with astonishingly high complexity and chemical function can be generated.

The volume is closed with a contribution by J. Bibette who describes and illustrates a simplified process of making monodisperse emulsions and emulsion based particles with predictable size and size distribution by a simple shearing device. I regard this very flexible route as important for the conception of many future particle-based systems, devices and procedures, and it is rather the rule than the exception that colloid chemistry nicely integrates mechanical and engineering procedures to access the nanoscale in a rational way.

I think that the present two “Colloid Chemistry” issues of “Topics in Current Chemistry” nicely cover the width and the modern spirit of colloid science which (mostly just recently) has given chemists a whole new toolbox for treating and creating chemical nanostructures in a rational way. With this in mind, I hope that all the readers will find some inspiration and profit in the various contributions.

Markus Antonietti, Potsdam

March 2003



---

# Contents

<b>Molecular Recognition and Hydrogen-Bonded Amphiphiles</b>	
C. M. Paleos, D. Tsiourvas . . . . .	1
<b>Dendrimers for Nanoparticle Synthesis and Dispersion Stabilization</b>	
K. Esumi . . . . .	31
<b>Organic Reactions in Microemulsions</b>	
M. Häger, F. Currie, K. Holmberg . . . . .	53
<b>Miniemulsions for Nanoparticle Synthesis</b>	
K. Landfester . . . . .	75
<b>Molecularly Imprinted Polymer Nanospheres as Fully Affinity Receptors</b>	
G. E. M. Tovar, I. Kräuter, C. Gruber . . . . .	125
<b>Hollow Inorganic Capsules via Colloid-Templated Layer-by-Layer Electrostatic Assembly</b>	
F. Caruso . . . . .	145
<b>Biorelevant Latexes and Microgels for the Interaction with Nucleic Acids</b>	
A. Elaissari, F. Ganachaud, C. Pichot . . . . .	169
<b>Preparation of Monodisperse Particles and Emulsions by Controlled Shear</b>	
V. Schmitt, F. Leal-Calderon, J. Bibette . . . . .	195
<b>Author Index Volumes 201 – 227</b> . . . . .	217
<b>Subject Index</b> . . . . .	225

---

# **Contents of Volume 226**

## **Colloid Chemistry I**

**Volume Editor: Markus Antonietti**

ISBN 3-540-00415-7

**Amphiphilic Block Copolymers for Templating Applications**

S. Förster

**Nanocasting of Lyotropic Liquid Crystal Phases for Metals and Ceramics**

C. Göltner-Spickermann

**Nanoparticles Made in Mesoporous Solids**

L. M. Bronstein

**Nanocasting and Nanocoating**

R. A. Caruso

**Mineral Liquid Crystals from Self-Assembly of Anisotropic Nanosystems**

J.-C. P. Gabriel, P. Davidson

**Monodisperse Aligned Emulsions from Demixing in Bulk Liquid Crystals**

J. C. Loudet, P. Poulin

**Templating Vesicles, Microemulsions and Lyotropic Mesophases  
by Organic Polymerization Processes**

H.-P. Hentze, C. C. Co, C. A. McKelvey, E. W. Kaler

**Rational Material Design Using Au Core-Shell Nanocrystals**

P. Mulvaney, L. Liz-Marzán

# Molecular Recognition and Hydrogen-Bonded Amphiphiles

Constantinos M. Paleos, Dimitris Tsiourvas

Institute of Physical Chemistry, NCSR „Demokritos“, 15310 Aghia Paraskevi, Attiki, Greece

E-mail: [paleos@chem.demokritos.gr](mailto:paleos@chem.demokritos.gr)

Amphiphiles bearing polar heads capable of forming hydrogen bond(s) exhibit unique organizational and aggregational properties. Thus they are hierarchically organized in supramolecular assemblies, which in turn interact through hydrogen bonding with other complementary counterparts affording larger and more elaborated aggregates. For liposomes, which are primarily investigated in this review, a number of examples have demonstrated their interaction mode and the associated phenomena as related with the structural features of the supramolecular aggregates obtained. A limited number of molecular recognition experiments is discussed for micellar systems due to their dynamic character and non-clearly defined shape and interface. The recognition between cells, following incorporation of recognizable amphiphiles in their membranes, demonstrate the approximate resemblance of liposomes with cells as well as the similarities of liposomal interactions with those of the cells.

**Keywords.** Amphiphiles, Hydrogen bonding, Molecular recognition, Liposomes, Micelles

1	Introductory Remarks on the Hierarchical Aggregational Organization of Hydrogen-bonded Amphiphiles . . . . .	2
2	Interaction of Liposomal Dispersions with Molecules Dissolved in Water Through Hydrogen Bonding . . . . .	4
3	Inter-Liposomal Interactions via Hydrogen Bonding . . . . .	9
4	Molecular Recognition in Micellar Systems . . . . .	23
5	Cell-Cell Interactions Through Complementary Hydrogen Bonding Moieties Located at their External Surface . . . . .	26
6	Concluding Remarks and Future Prospects . . . . .	26
	References . . . . .	28

## List of Abbreviations

ADP	Adenosine-5'-diphosphate
AFM	Atomic force microscopy
AMP	Adenosine-5'-monophosphate

ATP	Adenosine-5'-triphosphate
CD	Circular dichroism
CHOL	Cholesterol
cmc	Critical micelle concentration
ITC	Isothermal titration microcalorimetry
NMR	Nuclear magnetic resonance
PC	Phosphatidylcholine
PEG	Poly(ethylene glycol)
SANS	Small angle neutron scattering
SDS	Sodium dodecyl sulfate
UV	Ultraviolet

## 1

### **Introductory Remarks on the Hierarchical Aggregational Organization of Hydrogen-bonded Amphiphiles**

The principle of molecular recognition [1] was introduced by Emil Fischer [2] in 1894 and proved very fruitful in non-covalent synthesis [3] which primarily involves hydrogen bonding interactions between complementary molecules. Molecular recognition of non-amphiphilic complementary molecules is effective in aprotic solvents [4] and also in the bulk melt phase affording a diversity of supramolecular systems. The research activity in this area has been included in numerous papers, but here suffice to mention some representative publications dealing with the preparation and properties of crystalline [5] and liquid crystalline materials [6]. For amphiphilic molecules, however, recognition occurs both in aprotic solvents and in water. In this case the preorganization-aggregation step of the amphiphiles leads to the formation of supramolecular organizates including liposomes, membranes, lyotropic liquid crystals, micelles or monolayers at the air-water interface.

The aggregation coupled with the organization of amphiphilic molecules is induced by the segregation of the polar moieties from their lipophilic segments. A consequence of the organization attained in supramolecular aggregates is the facilitation of interaction with their complementary counterparts [7]. In this second-level interaction, with the exception of the directional hydrogen bonding interactions, cooperative and multivalency effects [8] are also operating, providing the possibility for the complementary groups to interact more effectively with each other compared to isotropic media. Specifically, the binding efficiency is increased by a factor of  $10^2$ – $10^4$  each time one proceeds from isotropic to organized media, i.e. from the bulk water to microscopic interfaces of micelles or liposomes and finally to air-water macroscopic interfaces [9]. This is shown schematically in Fig. 1 depicting the association of guanidinium and phosphate moieties in different media. Even under the disrupting action of water on hydrogen bonds, amphiphilic molecules bearing hydrogen-bonding moieties can form supramolecular organizates with elaborated structures in certain cases, which are distantly comparable to biological systems. This process is illustrated by the initial formation of complementary liposomes which further interact at a

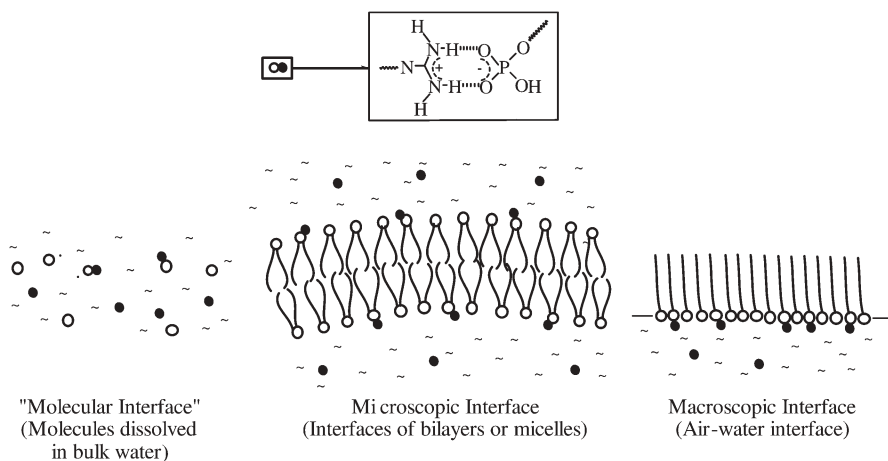


**Fig. 1.** Binding patterns of guanidinium and phosphate moieties in media of varying degree of organization

second-stage, simulating in a way cell-cell or cell-liposome recognition. In fact, in biological cells, the receptor is located at their surface at fixed spatial arrangements, facilitating interaction and adhesion with other cells [10]. Furthermore, the aggregation of amphiphilic molecules is simultaneously associated with compartmentalization of the so-formed supramolecular organizes, giving rise to selective solubilization of various compounds. This latter property is shared by liposomes and is finding application in drug delivery. Thus, the main characteristics of biological cells such as organization, compartmentalization and recognition are in a way also shared by liposomes. It therefore justifies the characterization of liposomes, especially of the giant ones [11], as the closest artificial analogs of cells.

Interaction of hydrogen-bonded amphiphiles has also been investigated at air-water interfaces and was reviewed some years ago [12]. As mentioned above, air-water interface strongly favours the organization of amphiphiles and, since a higher organization is obtained compared to liposomes hydrogen bonding, interaction of complementary molecules is more effective [9]. Air-water interfaces however lack colloidal properties and therefore they will not be discussed any further in this review.

Taking into consideration the above introductory remarks, molecular recognition between liposomes will be primarily discussed within the framework of hydrogen bonding interactions of complementary moieties located at their surfaces. The functionalization of the external surface of liposomes for rendering these particles recognizable is achieved at their preparation stage by employing established methods [13]. The mode of molecular recognition in liposomes and the associated phenomena will be discussed in conjunction with the supramolecular structures obtained. Examples of recognition occurring in colloidal micellar systems are rarely reported in the literature. This is due to the dynamic equilibrium between micelles and their non-aggregated amphiphiles, resulting

in a non-clearly defined shape and interface. Finally, in order to illustrate the approximate resemblance of liposomes to cells, the recognition of the latter will be discussed following incorporation of a synthetic recognizable amphiphile in cell membranes.

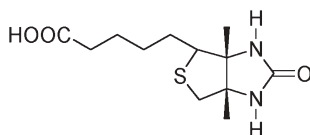
## 2

### Interaction of Liposomal Dispersions with Molecules Dissolved in Water Through Hydrogen Bonding

The interactions of liposomes with simple molecules dissolved in water will precede the discussion of inter-liposomal processes. Liposomes are rendered recognizable by the introduction of hydrogen bonding groups at their external surface, through incorporation of appropriate lipids during their preparation. Liposomes are therefore susceptible to interaction with complementary molecules dissolved in water through hydrogen bonding. Molecules with more than one recognizable moieties can act as “sticky material”, binding liposomes together. The following examples will illustrate the processes occurring in liposomal dispersions in the presence of complementary molecules.

The association of biotin, **1**, (vitamin H) with streptavidin or avidin, two homologous water soluble proteins with molecular weights of 60 KDa and 68 KDa respectively, has been extensively investigated [14], being one of the first systems employed for assembling liposomes. The hydrogen bonding system of biotin is recognized by each of the four identical subunits of streptavidin as shown in Fig. 2A. Recent crystallographic data [15] support this view. This recognition reaction has an exceptionally high binding constant,  $10^{15} \text{ M}^{-1}$  corresponding to a binding energy of the order of a covalent bond. Therefore binding of biotin to avidin/streptavidin is virtually irreversible.

In this context Chiruvolu et al. [16] prepared mixed unilamellar liposomes based on dilauroylphosphatidylcholine and incorporating dipalmitoylphosphatidylethanolamine-conjugated biotin as a recognizable amphiphile. When streptavidin was added to the biotinylated liposomal dispersion, aggregation occurred followed by precipitation. The resulting liposomal aggregates were studied by cryoelectron microscopy and it was shown that only minimal changes in their shape and size occurred. Tethered liposomes were formed through biotin-streptavidin bridges shown schematically in Fig. 2B. Most of the liposomes formed large aggregates while only few free liposomes were observed. The aggregates were bound strongly, withstanding breakage even during the relatively large shears exerted in preparing samples for cryoelectron microscopy.



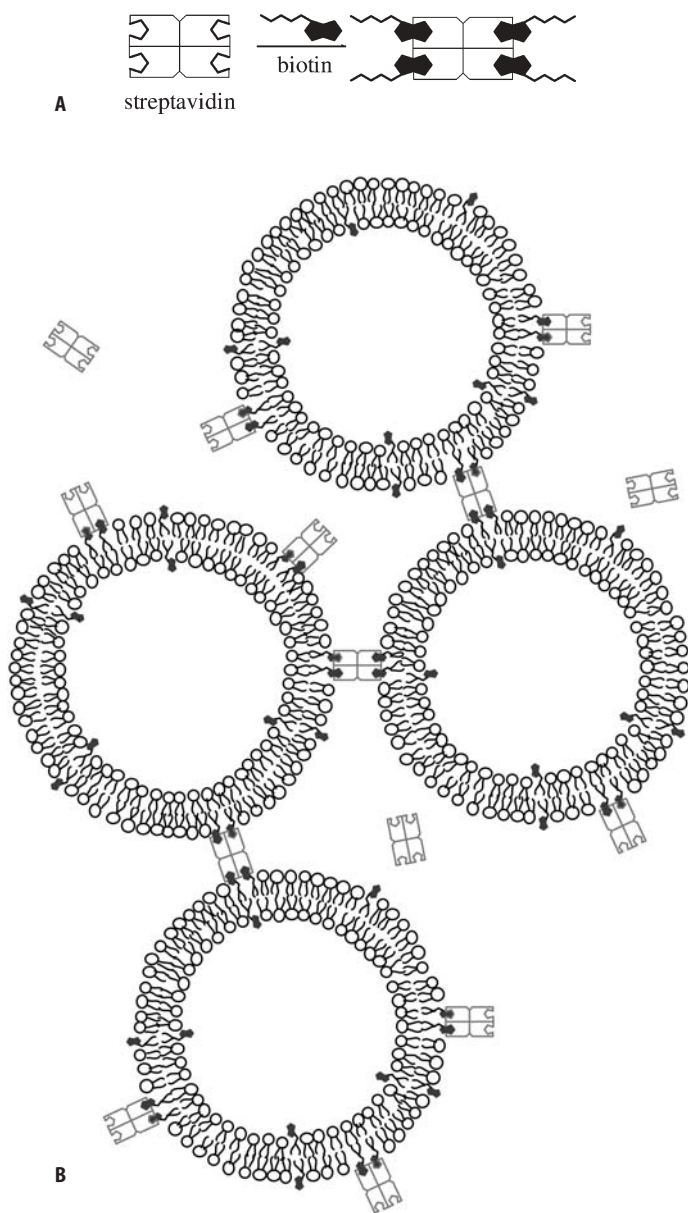


**Fig. 2.** **A** Interaction of biotin with the tetrameric protein streptavidin. **B** Schematic representation of the aggregation of biotinylated liposomes induced by the tetrameric streptavidin protein (taken from [16])

Following the previous early report on the biotin-streptavidin system the surface of liposomes were structurally elaborated in order their external surface to approximately mimic the functional behaviour of cell surfaces. Thus, mixed recognizable liposomes were obtained [17] by introducing biotin at their external surface through the incorporation of biotin-(CH<sub>2</sub>)<sub>n</sub>-hexadecylphosphatidylethanolamine amphiphile. In addition, for providing a repulsive steric barrier, poly(ethylene glycol) of molecular weight 750 (PEG<sup>750</sup>) was also linked at the head group of another component of these liposomes, i.e. of distearoylphosphatidylethanolamine. The comparatively short-chain PEG<sup>750</sup> moiety was chosen as a steric barrier since it was found not to inhibit completely adsorption of avidin at low biotin concentrations. It should also be noted that PEG<sup>750</sup> prevented non-specific van der Waals adhesion between the two liposomes in the absence of biotin-avidin-biotin cross-bridges. The placement of these recognizable groups on a liposomal bilayer and PEG<sup>750</sup> are shown schematically in Fig. 3.

The interaction effectiveness of biotin with avidin was enhanced by the introduction of a poly(methylene) spacer between the polar head of the lipid and

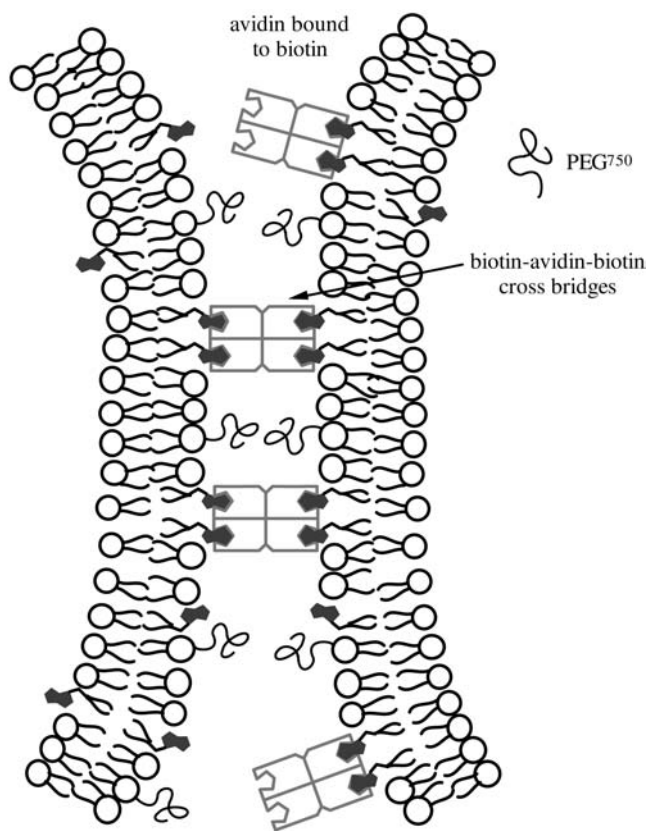


**Fig. 3.** Schematic representation of interacting PEG-coated liposome bilayers bearing the recognizable biotin group with avidin molecules dissolved in water



biotin moiety. Separately prepared avidin-coated liposomes when interacted with biotinylated liposomes lead to liposome-liposome adhesion. In both cases the detection of avidin on the biotinylated vesicle surface and in adherent contact zones is made possible by fluorescently labelled avidin. With these molecularly engineered liposomal surfaces the main results of the detailed study were summarized in the following:

1. The rate of avidin absorption was found to be four times less with 2 mol% PEG<sup>750</sup> than the unmodified surface while 10 mol% PEG<sup>750</sup> completely suppressed binding of avidin to biotin.
2. The rate of cross-bridges accumulation was consistent with the diffusion of the lipid-linked “receptors” into the contact zone. PEG<sup>750</sup> did not influence the mechanical equilibrium established between the bilayers because it was not compressed in the contact zone but on the contrary PEG performed an important function by eliminating non-specific adhesion.

In a recent work [18] liposomes bearing recognizable groups were allowed to interact with dendrimers to which complementary groups had been introduced at their external surface. Thus, phosphatidylcholine based liposomes incorporating dihexadecylphosphate as a recognizable lipid interacted with partially guanidinylated poly(propylene imine) complementary dendrimers of the fourth and fifth generation. The interaction is schematically shown in Fig. 4 and the main conclusions are summarized in the following:

1. The higher generation dendrimeric derivative proved more effective in its interaction with liposomes. This behaviour was attributed to multivalent effects, exhibited at a greater extent by this dendrimeric derivative. Under an equal concentration of functional moieties the reactivity is favoured when the groups are located in a smaller number of particles. Thus the dendrimeric materials act as molecular “glue” causing adhesion of liposomal particles.
2. Redispersion of the resulting aggregates was achieved by the addition of a phosphate buffer. Therefore the process is reversible.
3. The stability of the liposomal membranes during the collapse and redispersion processes was assessed by the calcein fluorescence method, TEM and AFM. It was established that liposomes are not disrupted during these processes and their TEM images after redispersion of the liposomal aggregates are shown in Fig. 5.

Molecular recognition of the biotin-streptavidin system was also used for preparing, among others, multicompartmental aggregates of tethered liposomes encapsulated within large liposomes. These aggregates were called vesosomes [19] and were prepared by an elegant but rather tedious procedure. Large aggregates of unilamellar liposomes were prepared as described above [16] by the addition of streptavidin to unilamellar liposomes based on dilauroylphosphatidylcholine and incorporating dipalmitoylphosphatidylethanolamine-conjugated biotin as a recognizable amphiphile, the size of which was reduced through extrusion. With this method a dispersion of liposomes with diameters ranging from 0.3 to 1.0  $\mu\text{m}$  was prepared. These aggregates were encapsulated within an outer bilayer through interaction with cochleate cylinders, which are

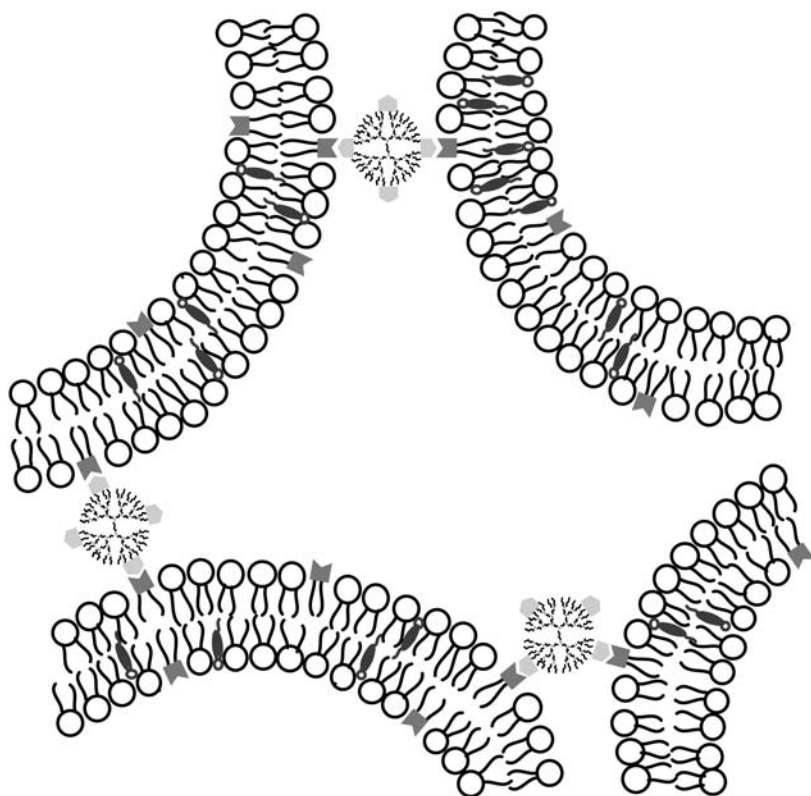


**Fig. 4.** Schematic representation of the aggregation of liposome bilayers induced by complementary dendrimers

biotin functionalized multilamellar lipid tubules formed spontaneously by certain negative phospholipids such as phosphatidylserine in the presence of  $\text{Ca}^{II}$ . This scheme of formation is shown pictorially in Fig. 6. The formation of vesosomes not only establishes the ability of molecular recognition to construct elaborate biomimetic structures but it also provides an elegant method for the preparation of vehicles for multifunctional or multicomponent drug delivery systems.

The interaction of liposomes leading to the formation of tethered liposomes and/or large aggregates, as mentioned above, cannot however be generalized. Depending on the interacting species transformation to other type of aggregates of the original liposomes may occur. For instance, in the interaction of dihexadecylphosphate liposomes with increasing quantities of guanidinium cations ( $\text{C}(\text{NH}_2)_3^+$ ) or its derivatives, the size of liposomes decreases and the aggregates are finally transformed into micelles at 1:1 molar concentration of the interacting moieties [20]. In this case the guanidinium counterions are bound to the phosphate groups by combined electrostatic and hydrogen bonding forces,

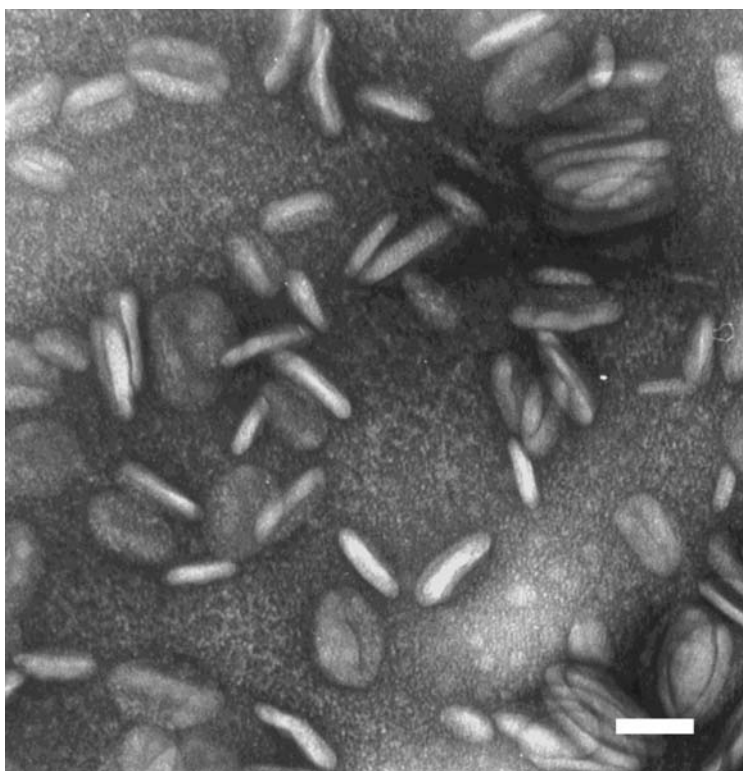


**Fig. 5.** TEM images of mixed phosphatidylcholine-dihexadecylphosphate liposomes originating after the redispersion of liposome-dendrimer aggregates with phosphate buffer. The bar represents 100 nm

and in analogy with simple ionic counterions, the surfactant parameter requirement [21],  $v/\alpha\ell < 1/3$  was fulfilled and therefore micelles were formed. In this formula  $v$  is the volume per hydrocarbon chain, or of the hydrophobic region of the surfactant,  $\ell$  is an optimal hydrocarbon chain length related to the maximum extended length and  $\alpha$  is the head group area.

### 3

#### Inter-Liposomal Interactions via Hydrogen Bonding

Molecular engineering of liposomal surfaces, by the introduction of functional groups having the ability to form hydrogen bonds with complementary moieties introduced in other liposomes, is leading to the formation of large aggregates. During this interaction the following two processes may be encountered [22]: a) adhesion or aggregation in which the liposomes are simply conjoined but retain separate inner compartments and b) fusion in which the liposomes merge sharing a common inner compartment. In this second process a sequence of events

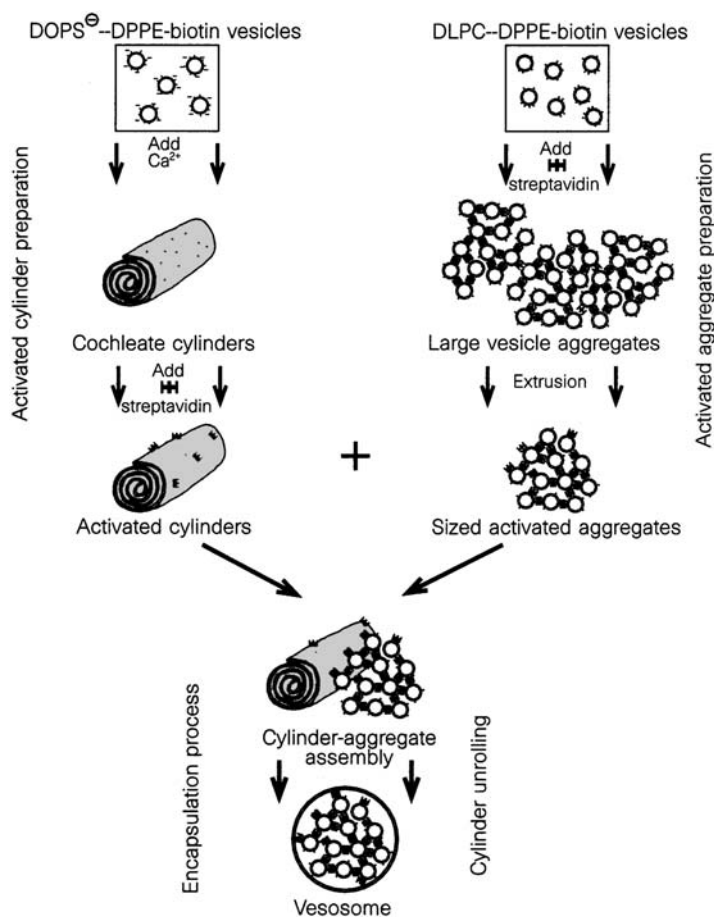


**Fig. 6.** Schematic representation of the process for the preparation of vesosomes. DLPC=di-lauroylphosphatidylcholine, DOPS=1,2-dioleoylphosphatidylserine, DPPE=dipalmitoylphosphatidylethanolamine (taken from [19])

occurs giving rise to the mixing of the aqueous content of liposomes with or without leakage or rupturing of the fused vesicles. Concerning the mechanism of membrane fusion two processes have been investigated and which are shown schematically in Fig. 7, i.e. the conventional one involving the non-lamellar fusion (Fig. 7, upper half) and the method proceeding through restructuring and ultimately merging of the membrane on a less ordered basis (Fig. 7, lower part). It is supported that both mechanisms are energetically favourable at least for small-scale fusion. However it has to be noted that small liposomes, e.g. with diameters of about 45 nm comprising of less than 10000 molecules, do not have sufficient number of amphiphiles to form a non-lamellar phase without disintegrating; these liposomes are however known to fuse extensively, apparently through membrane restructuring [22]. Taking into account the above-men-

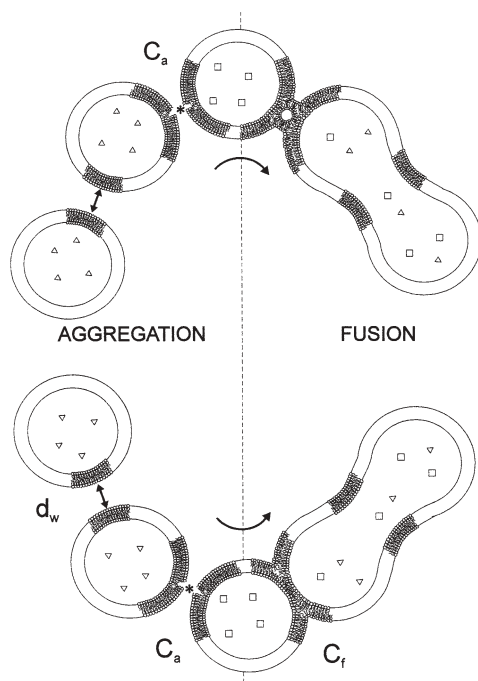
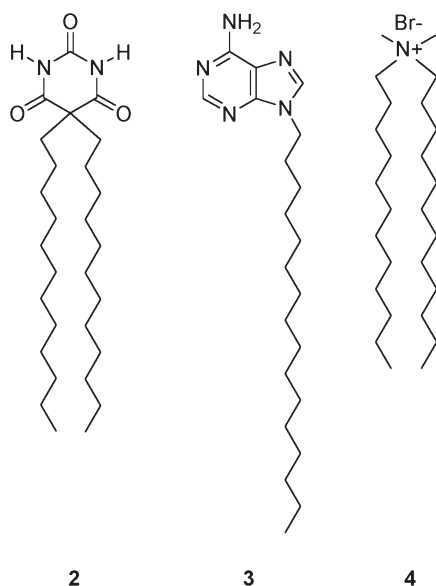


**Fig. 7.** Schematic representation of the mechanisms of membrane fusion. Conventional process involving the non-lamellar fusion (*upper*) and method proceeding through restructuring and ultimately merging of the membrane on a less order basis (*lower*) (taken from [22])

tioned associative mechanisms, processes such as the exchange of amphiphiles or the effect of liposomal size on the efficiency of interaction should also have a bearing on the binding of liposomes. With these considerations in mind and with the understanding that the fusion of phospholipid liposomes has been used as a model for simulating biological membrane fusion, the cited examples on liposome interactions will be discussed. Fusion has been studied extensively in recent years [22] and experimentally the process has been monitored by a diversity of techniques [23] including differential scanning calorimetry, optical, electron and scanning probe microscopies, light scattering and gel filtration. For giant liposomes [24], by employing video-enhanced optical microscopy techniques these transformations were observed in real-time.

As previously mentioned, the functionalization of the external surface of liposomes was achieved through the preparation of mixed liposomes. In this manner, the functional moieties at the external surface originate from the amphiphilic components, which were incorporated in these mixed liposomes. It was thus possible to monitor the reactivity of liposomes by changing the type and concentration of the incorporated recognizable lipid.

In an early experiment [25] the amphiphiles 5,5-didodecylbarbituric acid, 2, and 9-hexadecyladenine, 3, were incorporated separately at an approximately



1/7 molar ratio to didodecyldimethylammonium bromide, **4**, based liposomes. The interaction effectiveness was evaluated indirectly by phase contrast optical and atomic force microscopies, which have shown that larger aggregates were formed. In Fig. 8 are shown the AFM images (tapping mode) of liposomes before and after recognition. These liposomes were mainly built from the positively charged and strongly hydrated didodecyldimethylammonium bromide lipid and therefore they would normally repel each other. It is interesting to note that the mixed liposomes of **4** with **2** or **3** exhibit excellent stability and one has to add more than about 40% alcohol in order to destroy them. This is shown in Fig. 9 in which the turbidity of the liposomal dispersions is plotted relative to the added volume of ethanol; the constancy of turbidity value is an indication of the stability of liposome dispersions. It is evident that the incorporation of amphiphilic barbituric and adenine derivatives results in the stabilization of these liposomes.

The recognition of a complementary pair of liposomes based on lecithin containing amphiphilic derivatives of barbituric acid, **5**, and triaminopyrimidine, **6**, respectively up to 10% molar ratio was the subject of detailed and thorough recent investigations from Lehn's group [26]. The recognition of the complementary moieties was facilitated by the insertion of a suitable spacer in between the recognizable and polar groups. In the first preliminary experiments [26a], it was established that the complementary particles aggregate and fuse generating larger aggregates as shown in Fig. 10 at various time intervals by employing freeze-fracture electron microscopy.

In a recent study from the same laboratory [26b] the same complementary pair was employed and the consequence of the recognition features on aggregation, adhesion and fusion were investigated, identifying the physicochemical pa-

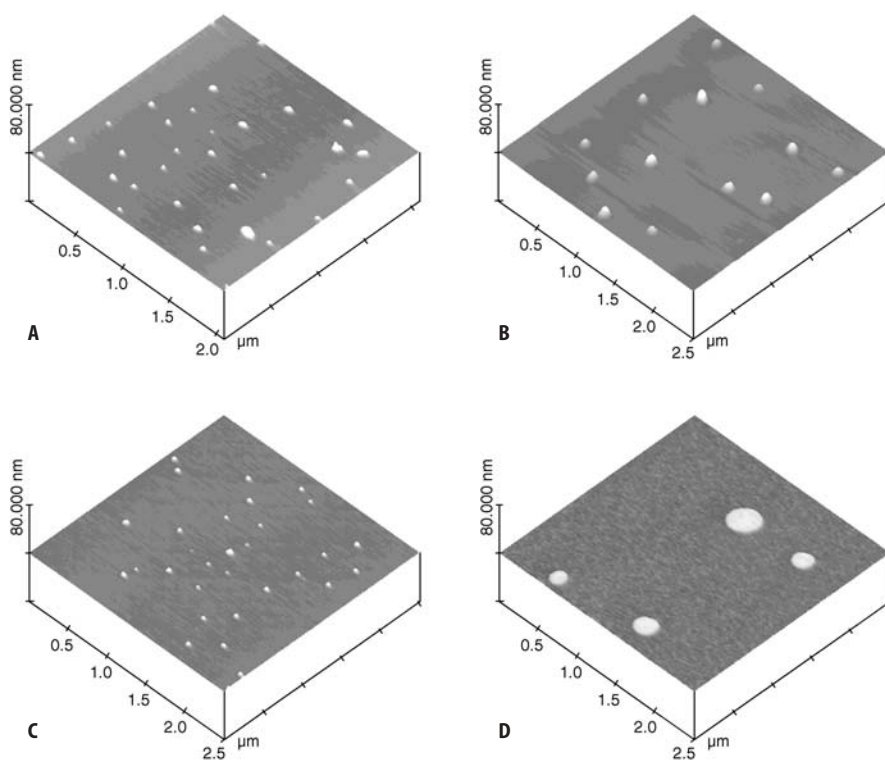


**Fig. 8A–D.** Images obtained with AFM microscopy of simple vesicles derived: **A** from **4**; **B** from mixed vesicle originating from **2**; **C** from mixed vesicle originating from **3**; **D** vesicles obtained after the interaction of **B** and **C** liposomes



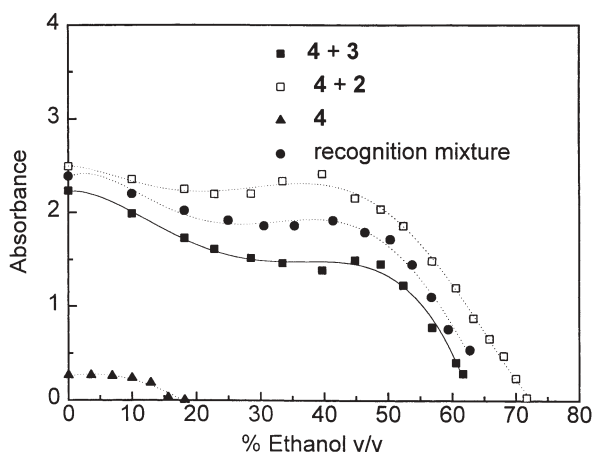


**Fig. 9.** Stability of vesicles as judged by turbidity studies by the addition of increasing quantities of alcohol in their dispersion

rameters that participate in these processes. The main conclusions of this study are summarized in the following:

1. Rapid and selective aggregation (in less than 30 s) occurs between the complementary liposomes, which is followed by lipid exchange (within 30 min after mixing). The lipid exchange, which takes place when the membranes are in contact, results either in fusion or, if fusion does not occur, to a redispersion of the liposomes within 17 h.
2. The aggregation process of the system under investigation can be weakened by decreasing the ionic strength, through the addition of a soluble barbituric competitor or by decreasing the concentration of the recognizable amphiphiles. The effect of ionic strength underlines the basic role of electrostatic interaction in the initial aggregation step. On the other hand the effect of the concentration of the recognizable amphiphiles supports the view according to which the recognizable system stabilizes the adhesion state.
3. The fusion process was observed by electron microscopy and remained at a low level, not resulting in an intermixing of the aqueous pools of the liposomes in significant proportion. It seems that fusion resulted from the collapse of mixed triaminopyridine/barbituric acid liposomes with neighbouring liposomes.
4. The size of the liposomes affects crucially the recognition phenomena. Thus aggregation was not observed when giant liposomes were encountered. The recognizable groups do not interact strongly enough to stabilize a contact between giant liposomes. A rapid adhesion however occurs between complementary large and giant unilamellar liposomes.

Cholesterol is a basic constituent of cell membranes and is known to affect their properties [10]. Thus experiments with liposomes incorporating varying amounts of cholesterol may simulate the function of cholesterol in cell mem-



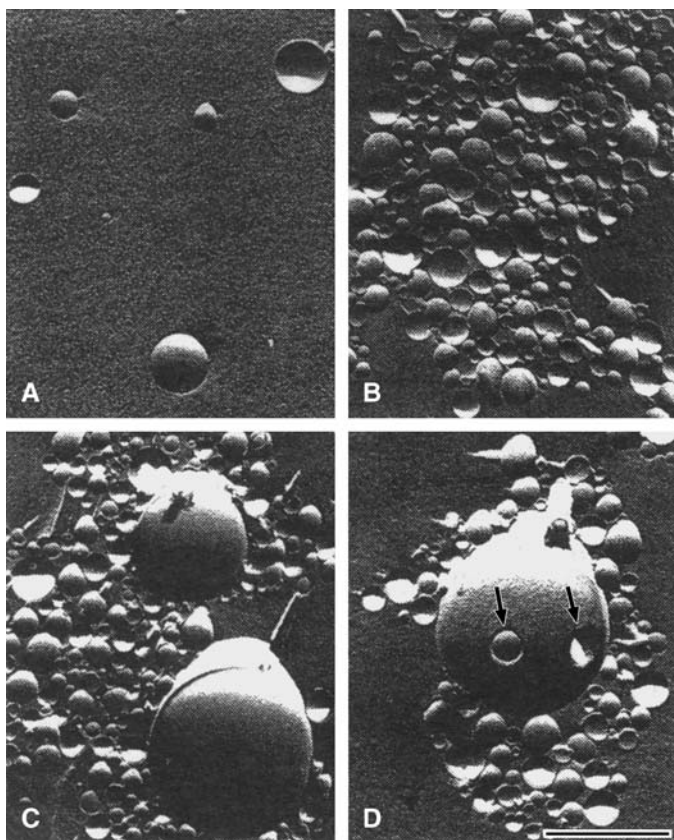


**Fig. 10A–D.** Freeze-fracture electron micrographs of mixed liposomes composed of lecithin and lipids 5 or 6 before and after mixing: **A** image of lecithin liposomes containing lipid 5 or 6 before mixing; **B** aggregation immediately following mixing of the complementary liposomes; **C,D** images obtained after incubation for at least 15 minutes (taken from [26a])

branes and recognition. For this purpose a pair of liposomes was used [27] prepared from hydrogenated phosphatidylcholine (PC) and various amounts of cholesterol also incorporating di-*n*-hexadecylphosphate, 7, and 1-(4-(dihexadecylcarbamoyl)butyl)guanidinium *p*-toluenesulfonate, 8, as recognizable molecules respectively. The complementary pair of guanidinium and phosphate groups interact strongly (Fig. 11) due to combined action of electrostatic forces and hydrogen-bonding [9]. The initially prepared small complementary liposomes cannot be observed by optical microscopy; however they interacted spontaneously following their mixing and the resulting liposomal aggregates were observed by phase contrast optical microscopy. This observation was made possible since the initially formed aggregates, due to unreacted recognizable moieties, interact further resulting in even larger aggregates, which in certain cases encapsulate smaller liposomes as shown in Fig. 12. This behaviour is reminiscent of previous

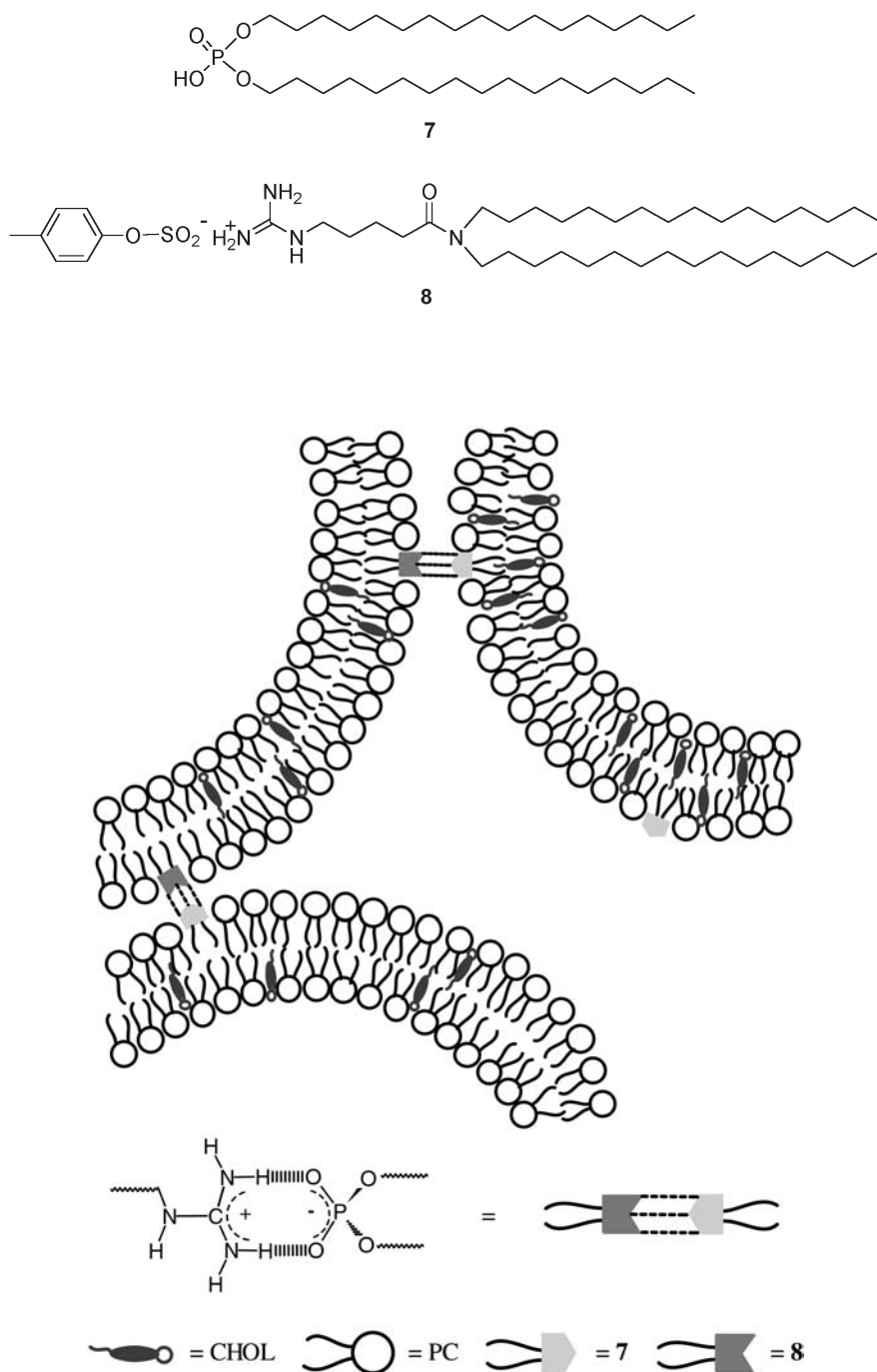


**Fig. 11.** Schematic representation of molecular recognition of phosphatidylcholine-cholesterol based liposomes bearing the complementary guanidinium and phosphate moieties

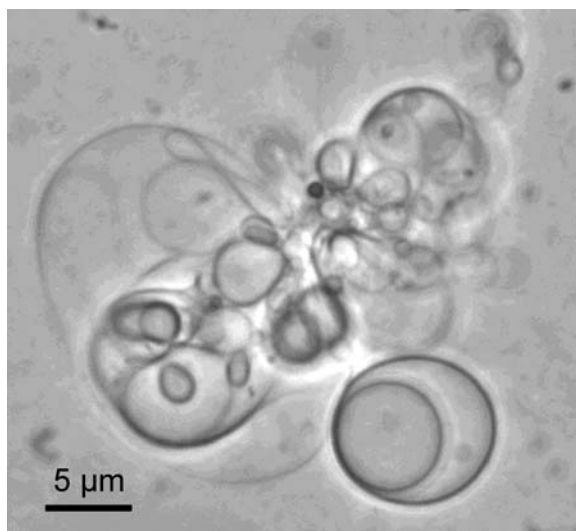


**Fig. 12.** Phase-contrast optical microscopy images after mixing phosphatidyl-cholesterol based liposomes bearing the complementary guanidinium and phosphate moieties

experiments [19] obtained during the recognition of liposomal aggregates with cochleate cylinders, which led to encapsulation of liposomal aggregates.

Furthermore, as derived from turbidimetric measurements and isothermal titration calorimetry, cholesterol incorporated in liposomes significantly enhances their molecular recognition effectiveness. The enhancement in molecular recognition ability, observed when cholesterol is incorporated into mixed liposomes at concentration levels of 10–50%, can be attributed to the structural features of lipid-cholesterol bilayers. In this case the membrane structure is such that contributes to a favourable exposure of the complementary groups of the lipids and the interaction is thus more efficient. As discussed [27] this is in agreement with the effect of cholesterol upon the molecular order of the lipid bilayer membrane summarized in a widely accepted phase diagram [28]. According to this phase diagram at the temperatures employed in these experiments and with cholesterol in amounts higher than 25 mol% the so-called liquid-ordered phase is obtained. The bilayer is in a fluid form from the point of view of lateral disorder and diffusion and therefore it affects the mobility of membrane-incorporated compounds. Since in these experiments the incorporated recognizable lipids are at low concentrations (1:19 molar ratio), their presence will not appreciably perturb, as mentioned before, the molecular order of the PC-cholesterol bilayer and therefore the interacting moieties would most likely encounter the previously described organized environment. It is thus possible to tune the association ability of liposomes by changing the incorporated amounts of cholesterol in the liposomal bilayer. Based on these findings, model liposomal systems may be produced in order to explore the role of cholesterol in molecular recognition in cell membranes and drug delivery targeting.

In a recent work [29] the recognizable amphiphiles 5,5-didodecylbarbituric acid, **2**, and 9-hexadecyladenine, **3**, previously incorporated in didodecyltrimethylammonium bromide liposomes, were employed in another lipid environment for inducing again recognition between liposomes. They were incorporated in liposomes based on neutral lipids, i.e. hydrogenated PC and cholesterol (CHOL) in a PC:CHOL 2:1 molar content. In this case a relatively high molar content of the recognizable molecules **2** or **3** (1:4 with respect to PC) was needed for quantitatively assessing liposomes recognition properties and obtaining measurable thermodynamic parameters. At these high concentrations of recognizable molecules incorporated in the PC and the PC-cholesterol based liposomes, the bilayer order may be severely affected and merits investigation. In fact the effects of additives on bilayer order and other properties of liposomes was a matter of meticulous investigations since the mid-1980s [30] and it is still the focus of intense research [30b]. Thus, for the PC:CHOL unilamellar liposomes the high molar concentration of **2** and **3** relative to PC enforces a considerable degree of lateral heterogeneity in the bilayer and the lipids are not in the liquid-ordered phase but instead in a solid-ordered/liquid-ordered phase coexistence region [29].

Molecular recognition of liposomes becomes most effective at 1:1 molar ratio of the recognizable molecules as deduced from turbidity studies. In addition the incorporation of cholesterol in the bilayer of liposomes enhanced the molecular recognition effectiveness a result in agreement with the previous studies [27]. Also AFM microscopy (tapping mode) proved the interaction since liposomes with diameters 50–140 nm were transformed to aggregates with sizes between 300 and 450 nm. Furthermore the initially collapsing and aggregating particles are relatively stable since no detectable disruption of the liposomes was observed as judged by calcein experiments.

Quantitative investigation of recognition of this pair of liposomes was performed with isothermal titration microcalorimetry (ITC). It has been found that one-to-one binding between adenine and barbituric acid in the lipid/water/lipid interface occurs. However at  $T=58^{\circ}\text{C}$ , above the main lipid phase transition, the situation is different and no liposomal binding is detected. This is mainly due to the molecular disorder within the bilayer (liquid-disordered/liquid ordered phase coexistence) that limits the capacity of complementary moieties to bind, due to the weakening of the hydrogen bonds at these high temperatures.

The inhibitory role of protective poly(ethylene glycol) (PEG) coating on molecular recognition was assessed by employing complementary liposomes based on hydrogenated PC and cholesterol [31]. The liposomes contained as recognizable lipids either octadecylguanidine hydrochloride, **9**, or *N*-[3-(*N,N* dioctadecylamino)propyl] guanidine hydrochloride, **10**, and di-*n*-hexadecylphosphate, **7**, respectively. PEG (molecular weight 5000) coating at the interface of liposomes was introduced by incorporating varying amounts of PEGylated cholesterol, **11**, which was anchored inside the membrane by the cholesteryl moiety. Segments of the interacting complementary particles are shown in Fig. 13.

The interaction effectiveness between liposomes with the above-mentioned recognizable pair of lipids was assessed by turbidimetry. A number of PEGylated cholesterol concentrations were tested in order to determine the optimum concentration at which both the interaction ability and the protection of liposomes

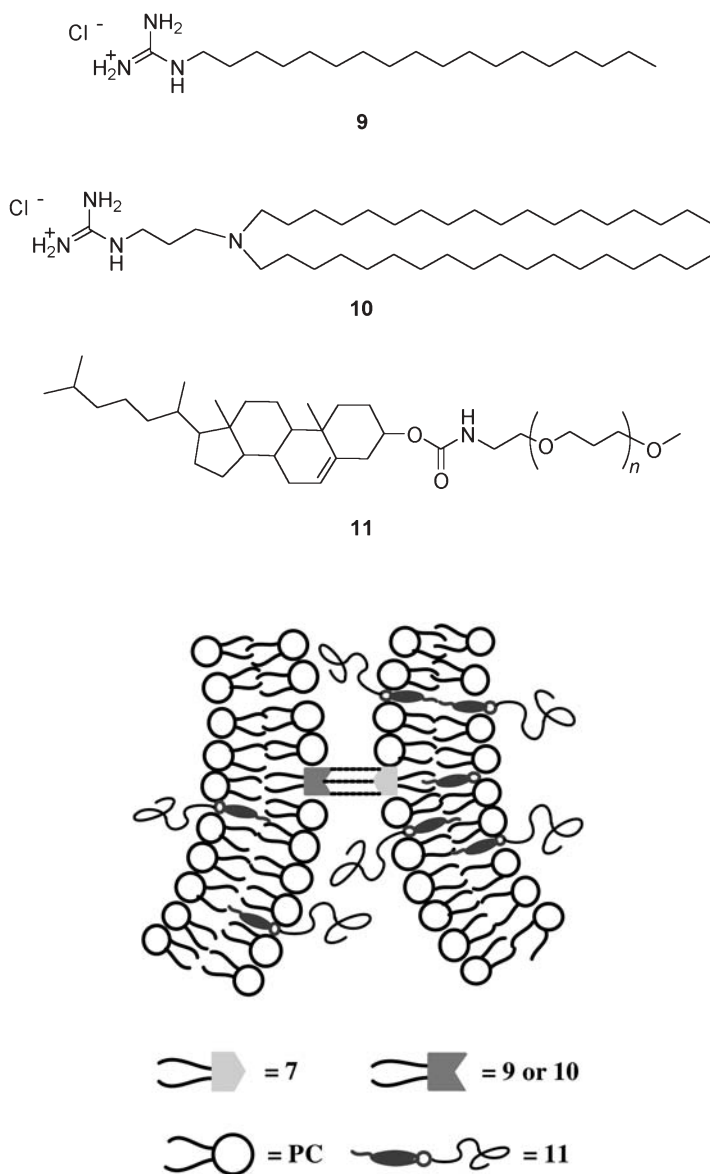


**Fig. 13.** Schematic representation of molecular recognition between phosphatidyl-cholesterol based liposomes protected with PEG and bearing the complementary guanidinium and phosphate moieties respectively

is secured. As shown in Fig. 14A, interaction between liposomes is significant at a 5% molar incorporation of PEGylated cholesterol, i.e. at a concentration in which effective protection is achieved in biological systems. Furthermore analogous results were obtained when **9** was replaced by **10**, i.e. a double chain amphiphile with the recognizable group attached through a spacer at the end of the lipophilic moiety. The interaction between liposomes incorporating **10** is rather more effective compared to liposomes incorporating **9**. Larger aggregates were obtained, resulting in more turbid dispersions. This may be due to a better arrangement of the double-chain amphiphile within the bilayer coupled with the presence of the spacer, which makes the recognizable group to protrude outside of the external surface of the bilayer. The same enhanced recognition was also observed for liposomes incorporating PEGylated cholesterol and **10** (Fig. 14B). It should be noted that in this case even with a 15% molar content in PEGylated cholesterol, interaction was effective while for liposomes containing **9** (Fig. 14A), 15% PEGylated derivative almost completely suppressed liposomes ability for interaction.

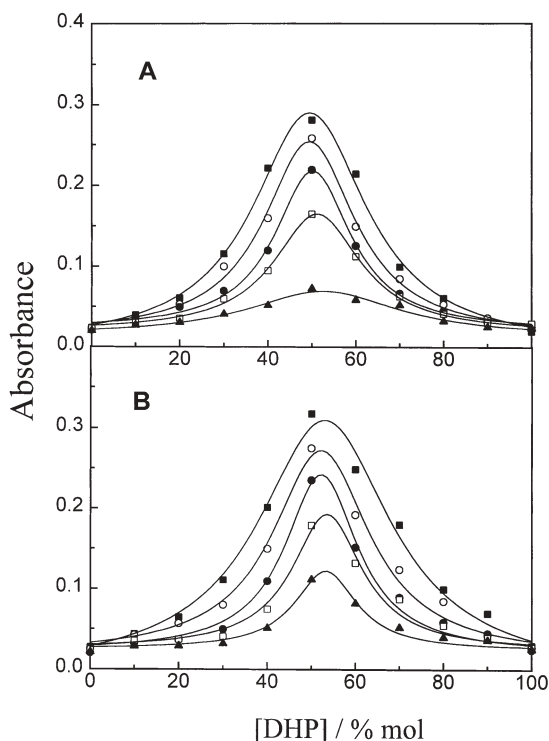


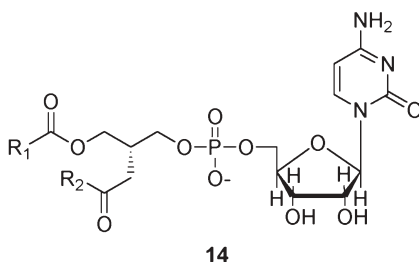
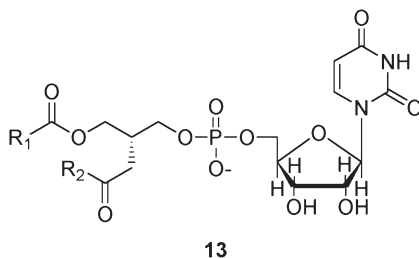
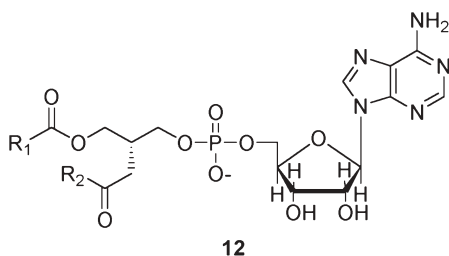
**Fig. 14A,B.** Turbidity change during interaction experiments between PC-CHOL-DHP and: A PC-CHOL-ODG; B PC-CHOL-DODG liposomes. Both liposome dispersions incorporate PEGylated cholesterol at various concentrations. The X axis represents the percent concentration of liposomes based on DHP in the aqueous dispersion: (filled squares) 0%, (open circles) 1%, (filled circles) 5%, (filled triangles) 15% PEG-cholesterol

Analogous results were also obtained microscopically. Interactions occurred spontaneously and large aggregates were formed, which were visible with phase contrast optical microscopy. These particles interact further giving rise to even larger aggregates, which in certain cases encapsulate smaller aggregates.

Association of the liposomes by this guaninium-phosphate pair did not lead to disruption. As deduced from fluorescence experiments, calcein fluorescences only slightly because of self-quenching since it remains entrapped at high concentrations in the interior of the liposomes [32]. However if liposomes were disrupted, calcein would be diluted in the bulk aqueous phase resulting in enhanced fluorescence since quenching was reduced.

Anchoring amphiphilic recognizable molecules and PEGylated cholesterol in the membrane of PC-cholesterol based liposomes may lead to a promising model system for drug delivery. At these concentrations of the recognizable and protective functional moieties a liposomal system was prepared that exhibited significant stability together with targeting ability.

Molecular recognition has also been achieved though hydrogen bonding interactions between complementary liposomes originating from phosphatidyl-nucleoside-based amphiphiles [33] 12–14. In this case the phosphate groups, among other things, reproduce the charge of the repeating units in nucleic acids.





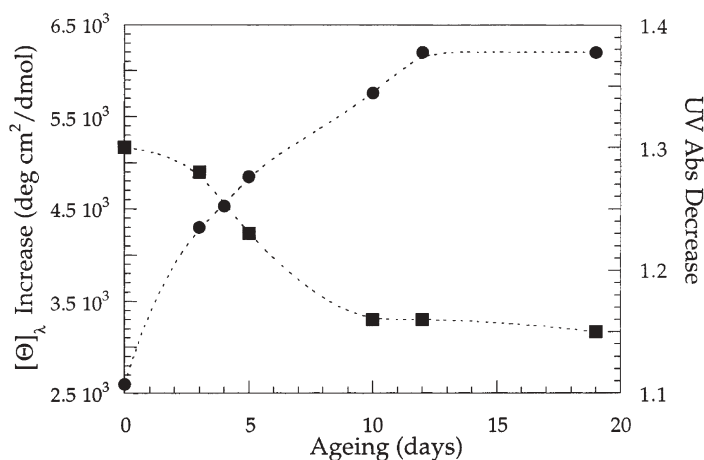


**Fig. 15.** Time dependence of UV hypochromicity (*squares*) compared to circular dichroism (CD) increase in ellipticity (*circles*) occurring when mixing diolelphosphatidyl (DOP)-adenosine and DOP-uridine (taken from [33])

The UV-vis spectroscopic behaviour of samples obtained from pure phospholiponucleosides remains constant for over 2–3 weeks. A quite different behaviour was however displayed upon mixing of complementary liposomes. Thus, when liposomes derived from 12 were mixed with liposomes prepared from 13, the absorption at 260 nm decreases slowly with time as shown in Fig. 15. Since the size distribution of the dispersion remains constant, indicating that aggregation does not occur, the onset of a hypochromic effect can be ascribed to adenosine-uridine interaction. Non-complementary liposomes, originating from 12 and 14 do not show the hypochromic effect observed for the complementary phospholiponucleosides. It should be noted that these UV changes that were obtained during mixing are the same as those obtained from the “mechanical” equimolar mixture of two complementary nucleobase lipids, i.e. when the two complementary lipids were first mixed and subsequently used for the preparation of liposomes. This UV hypochromicity of the nucleobases, was coupled to a large increase in circular dichroism (CD), Fig. 15, whereas the CD spectra of simple component liposomes were comparable to those of adenosine monophosphate and uridine monophosphate. The increase of CD intensity has been observed in nucleobase pairing interactions of polynucleotides in solution. The time-scale of the CD changes occurring upon mixing of complementary nucleobase liposomes was the same as the UV changes shown in Fig. 15. The slow progress of the spectral changes is most likely determined by the mechanism of lipid exchange between liposomes. In fact it was established that lipid exchange in phosphatidylcholine liposomes is very slow and in this case the re-adjusting for base pairing may require an additional slower step.



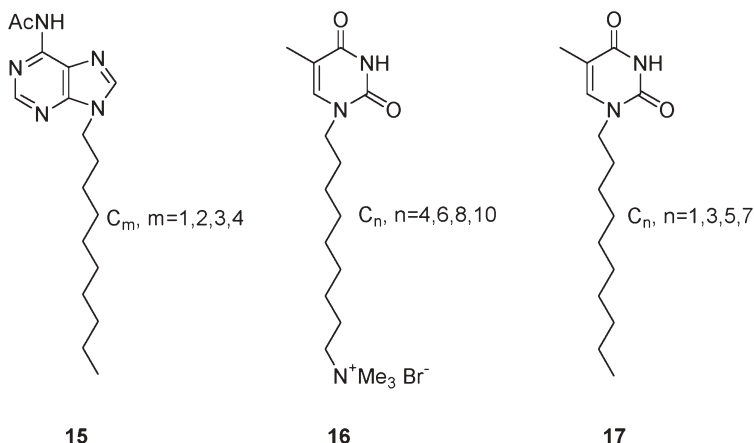
## 4

## Molecular Recognition in Micellar Systems

Micelles are in dynamic equilibrium with their non-aggregated amphiphiles in solution; a consequence of this is that micellar interfaces are not clearly defined and micelles are rather flexible supramolecular systems. Thus micelles, although easily prepared through simple dissolution of amphiphiles in water, are not sufficiently organized to favour interaction of the moieties located at their interface. For this reason only a limited number of examples of micellar interactions, occurring through molecular recognition between complementary moieties at micellar interfaces, has been reported. The micellar interior however, due to its non-polar character, provides the appropriate microenvironment for molecular recognition to occur between complementary moieties of the solubilized molecules.

Molecular recognition of complementary amphiphiles was achieved in the micellar core of sodium dodecyl sulphate (SDS) employing adenine derivatives, **15**, and positively charged (thyminyllalkyl)ammonium salts, **16** [34]. Binding occurs at 1:1 molar ratio as established by NMR studies and the Job's plot method and is shown schematically in Fig. 16. The binding of complementary molecules was affected by the lipophilicity of adenine substrate, the position of the thymine group within the micelles and the role of SDS. For investigating these factors the length of the alkyl group attached on adenine, the length of the aliphatic chain of the thymine derivative and the concentration of SDS were varied. It was found that the lipophilicity of adenine derivatives affect more efficiently the association constant  $K_{\text{obs}}$ . According to the proposed model the adenine derivative partitions between the external water phase and the interior of the micelle where it pairs with the thymine derivative.

Employing the above-mentioned complementary pair the same authors [35] replaced the charged (thyminyllalkyl)ammonium salts, by 1-alkylthymine derivatives **17**, which again interact with the complementary adenine derivatives in the interior of SDS micelles while stacking occurs in its absence. NMR titration



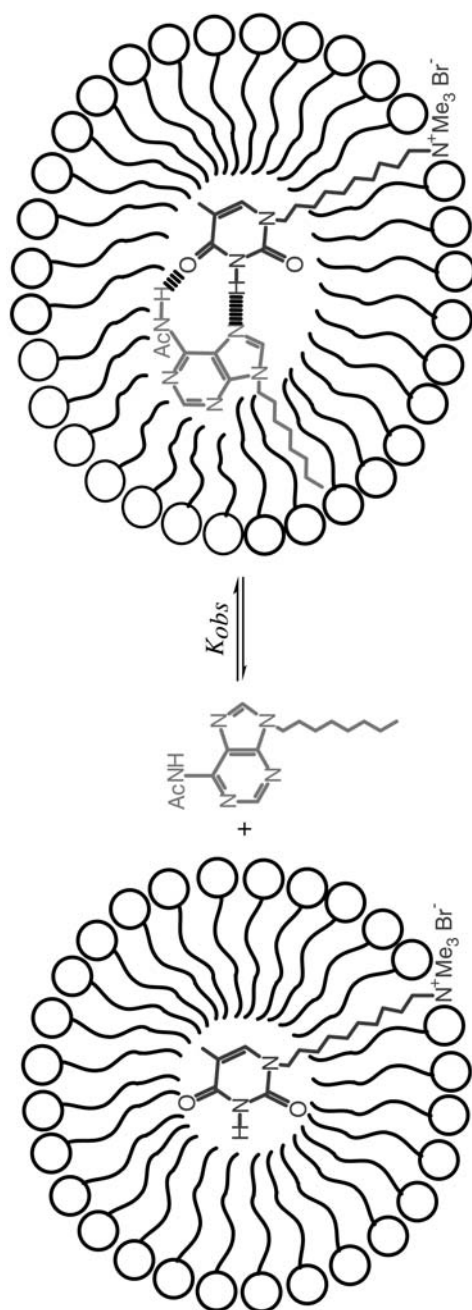
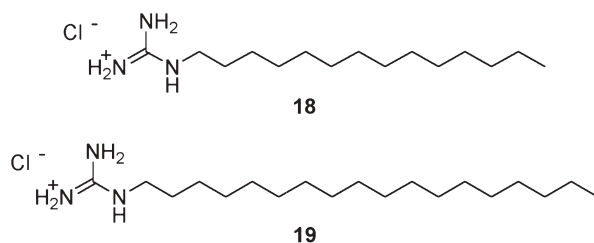


**Fig. 16.** Molecular recognition in SDS micelles of adenine derivatives 16 with (thyminylalkyl) quaternary ammonium salts 17



showed that adenine and thymine moieties play different roles in the binding process, i.e. the thymine derivative acts as the receptor, with the adenine derivative as the ligand. For efficient base pairing to occur the alkylthymine must be very hydrophobic in order to be solubilized within the micelles. In contrast the adenine derivative may be considerably less hydrophobic and it is not required to be largely incorporated in the micelles. However, higher binding constants ( $K_{\text{obs}}$ ) are determined with adenine derivatives of higher lipophilicity. According to the proposed model the alkylated adenine derivative partitions between the exterior and the interior of the micelles and thymine is bound to adenine derivative, which is solubilized in the core of the micelle.

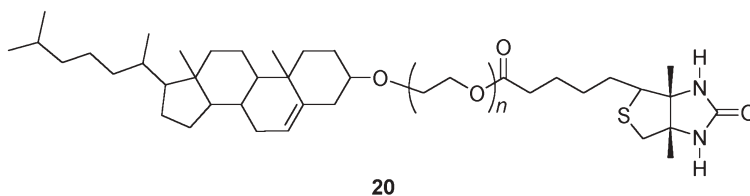
Following the recognition experiments occurring in the micellar core, Kunitake et al. [9] reported that recognition can also take place at the interface of the micelles. For this purpose monoalkyl guanidinium amphiphiles **18** and **19** were prepared which form micelles in water. The guanidinium moiety located at the interface of the micelles interacted with the phosphate group of AMP, ADP and ATP nucleotides. The binding constants were in the range of  $10^2$ – $10^4$   $\text{M}^{-1}$ . These values are significantly larger than that of  $1.4$   $\text{M}^{-1}$  found for guanidinium chloride and a simple phosphate in bulk water. Thus, water molecules at the interface of the aggregates provide much less interference for binding of the guanidinium with the phosphate group.

Replacing the long aliphatic chains of the previously discussed phosphatidyl-nucleoside-based amphiphiles, **12**–**14**, i.e. of oleoyl by octanoyl, micelles were formed [33] through self-assembly. A first indication of recognition between these complementary amphiphiles results from their cmc values, determined by light scattering. A negative deviation of the cmc for the 1:1 complementary pair is observed with respect to the pure components. In principle, preferential interactions exercised between amphiphiles with complementary nucleobases should be reflected in the structural properties of micellar aggregates. In this connection neutron scattering has proved a powerful method, allowing the determination of micellar structures and the intermicellar correlations resulting from their interactions. A meaningful decrease of the polar head group size in the 1:1 complementary pair was therefore observed, which was ascribed to a favourable interaction between polar head groups undergoing molecular recognition. The area contraction, determined by SANS data analysis, shows a good correlation with UV-vis, CD and NMR spectroscopy investigations; this proves that molecular recognition occurs between the complementary lipids not being observed for non-complementary nucleobases.

## 5

**Cell-Cell Interactions Through Complementary Hydrogen Bonding Moieties Located at their External Surface**

For establishing the usefulness of the notions described above in the real biological world a cell-cell system was investigated by employing synthetically prepared recognizable amphiphiles, which were incorporated in their bilayers. In this case the aggregation of the cells was achieved by properly functionalized poly(ethyleneoxides), **20** [35]. Specifically, unsymmetrically substituted PEGs bearing at one end a hydrophobic cholesteryl group and at the other end a hydrophilic biotin group were anchored in the membrane of SubT1 cells (a human CD4 expressing T-lymphoblastoid cell line) via their cholesteryl group following an incubation for 4 h at 37°C. The length of the PEG spacer must be such as to protrude the glycocalyx of the cell in order to be accessible for interaction with the added streptavidin. Therefore the molecular weight of PEG spacer chain was varied between 2000 and 35,000 g mol<sup>-1</sup>, i.e. its root-mean-square end-to-end distance being approximately 6–20 nm. The scheme of the interaction between biotinylated cell membranes and streptavidin is shown pictorially in Fig. 17 together with optical microscopy images of the cells. It is interesting to note that aggregation is reversed by addition in the cell dispersion of a large excess of free biotin. It is therefore reasonable to assume that the biotinylated polymer has a significantly lower binding affinity for streptavidin compared to free biotin. As claimed by the authors, streptavidin aggregation is not only shared by lymphoblastoid cells but it can also occur with hepatocytes or bacteria.



## 6

**Concluding Remarks and Future Prospects**

The incorporation into liposomes of amphiphiles bearing moieties capable of forming hydrogen bond(s) with each other induces their molecular recognition. These liposomes form large supramolecular aggregates of usually more elaborate structure compared to their interacting counterparts. The functional groups that render liposomes recognizable were introduced at the stage of their preparation with the strategy of non-covalent synthesis. Specifically mixed liposomes were prepared by the established methods, where one lipid bears at its polar head a recognizable moiety. Complementarity of the functional groups and a favourable interplay [37] of entropic and enthalpic effects are the driving forces for the formation of these aggregational-based biomaterials, which in cer-

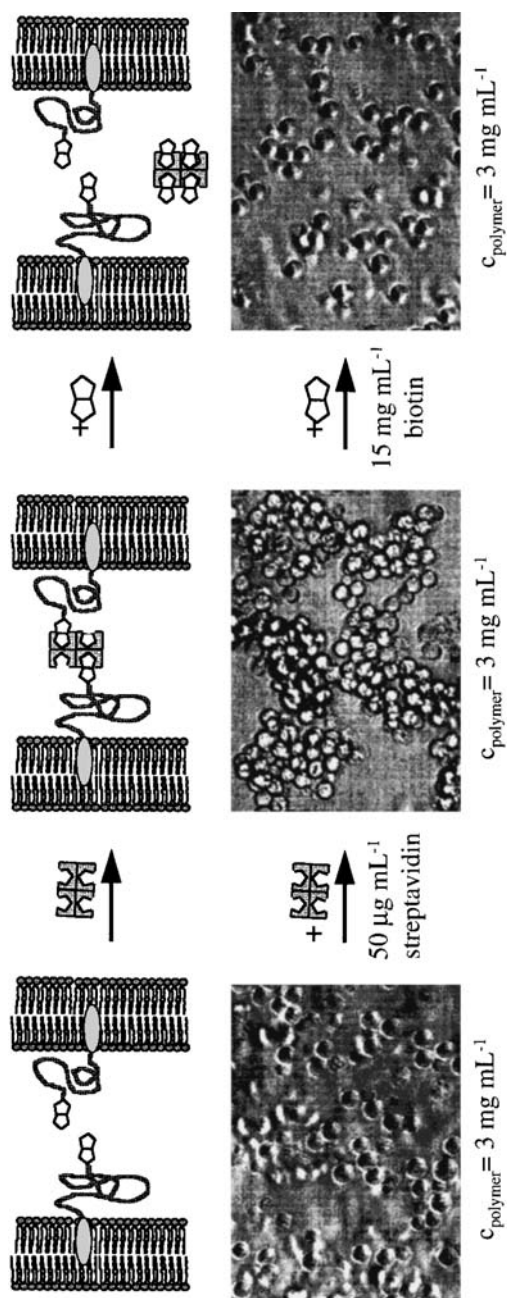


**Fig. 17.** Schematic representation of the reversible binding between biotinylated cell membranes via streptavidin and photomicrographs of the same process using Sub T1 cells (taken from [36])

tain cases exhibit multicompartmental properties. Although research activity in this area is still far from its ultimate goal, i.e. that of building tissue-like materials, the first steps have already been made and intensification of the effort together with elaborated experiments are required for accomplishing this goal. More nearby, analogous studies could form a firm basis for tackling current research problems associated with liposomal drug delivery.

## References

1. a) Lichtenthaler FW (1994) *Angew Chem Int Ed Engl* 33:2364; b) Koshland DE Jr (1994) *Angew Chem Int Ed Engl* 33:2375; c) Rebek J Jr (1996) *Acta Chem Scand* 50:707
2. Fischer E (1894) *Ber Dtsch Chem Ges* 27:2985
3. a) Whitesides GM, Simanek EE, Mathias JP, Seto CT, Chin DN, Mammen D, Gordon DM (1995) *Acc Chem Res* 28:37; b) MacDonald C, Whitesides GM (1994) *Chem Rev* 94:2383; c) Fyfe MC, Stoddart JF (1997) *Acc Chem Res* 30:401; d) Prins LJ, Reinhoudt D, Timmerman P (2001) *Angew Chem Int Ed Engl* 40:2382
4. a) Hamilton AA (1990) *J Chem Educ* 67:821; b) Schneider H-J (1991) *Angew Chem Int Ed Engl* 30:1417; c) Smithrud DB, Sanford EM, Chao I, Ferguson SB, Carcanague DR, Evanseck JD, Houk KN, Diederich F (1990) *Pure Appl Chem* 62:2227; d) Rebek J Jr (1996) *Chem Soc Rev* 255; e) Mecozzi S, Rebek J Jr (1998) *Chem Eur J* 4:1016
5. a) Fan E, Vicent C, Geib SJ, Hamilton AD (1994) *Chem Mater* 6:1113; b) Etter MC, Reutzel SM (1991) *J Am Chem Soc* 113:2586; c) Desiraju GR (1995) *Angew Chem Int Ed Engl* 34:2311; d) Lehn J-M (1996) *Supramolecular chemistry*. VCH Weinheim New York; e) Etter MC (1990) *Acc Chem Res* 23:120; f) Lawrence DS, Jiang T, Levett AM (1995) *Chem Rev* 95:2229; g) Philp D, Stoddart JF (1995) *Angew Chem Int Ed Engl* 35:2311; h) Hosseini MW, De Cian A (1998) *Chem Commun* 727; i) Niemeyer CM (2001) *Angew Chem Int Ed Engl* 40:4128
6. a) Paleos CM, Tsiourvas D (1995) *Angew Chem Int Ed Engl* 34:1696; b) Kato T (1998) Hydrogen-bonded systems. In: Demus D, Goodby J, Gray GW, Spiess HW, Vill V (eds) *Handbook of liquid crystals*. Wiley-VCH, Weinheim, p 969; c) Blunk D, Praefcke K, Vill V (1998) Amphotropic liquid crystals. In: Demus D, Goodby J, Gray GW, Spiess HW, Vill V (eds) *Handbook of liquid crystals*. Wiley-VCH, Weinheim, p 305; d) Paleos CM, Tsiourvas D (2001) *Liq Cryst* 28:1127
7. Kawasaki T, Tokuhiko M, Kimizuka N, Kunitake T (2001) *J Am Chem Soc* 123:6792
8. Mammen M, Choi S-K, Whitesides GM (1998) *Angew Chem Int Ed Engl* 37:2754
9. Onda M, Yoshihara K, Koyano H, Ariga K, Kunitake T (1996) *J Am Chem Soc* 118:8524
10. a) Cooper GM (1997) *The cell. A molecular approach*. ASM Press, Washington DC, p 467; b) Paleos CM, Sideratou Z, Tsiourvas D (2001) *ChemBioChem* 2:305–310
11. a) Käs J, Sackmann E (1991) *Biophys J* 60:825; b) Decher G, Ringsdorf H, Venzmer J, Bittersuermann D, Weisberger C (1990) *Biochim Biophys Acta* 1023:357; c) Menger FM, Lee SJ (1995) *Langmuir* 11:3685; d) Bradley J-C, Guedeau-Boudeville M-A, Jandeau G, Lehn J-M (1997) *Langmuir* 13:2457
12. a) Paleos CM, Tsiourvas D (1997) *Adv Mater* 9:695 and references cited therein; b) Ariga K, Kunitake T (1998) *Acc Chem Res* 31:371 and references cited therein
13. New RRC (1990) *Liposomes, a practical approach*. IRL Press, Oxford
14. Ahlers M, Mueller W, Reichert A, Ringdorf H, Venzmer J (1990) *Angew Chem Int Ed Engl* 29:1269
15. a) Rosano C, Arosio P, Bolognesi M (1999) *Biomol Eng* 16:5; b) Freitag S, Le Trong I, Klumb LA, Chu V, Chilkoti A, Stayton PS, Stenkamp RE (1999) *Biomol Eng* 16:13; c) Scief WR, Edwards T, Frey W, Koppenol S, Stayton PS, Vogel V (1999) *Biomol Eng* 16:29
16. Chiruvolu S, Walker S, Israelachvili J, Schmitt FJ, Leckband D, Zasadzinski JA, (1994) *Science* 264:1753

17. Noppi-Simpson DA, Needham D (1996) *Biophys J* 70:1391–1401
18. Sideratou Z, Foundis J, Tsiourvas D, Nezis IP, Papadimas G, Paleos CM (2002) *Langmuir* 18:5036
19. Walker SA, Kennedy MT, Zasadzinski JA (1997) *Nature* 387:61
20. Paleos CM, Tsiourvas D, Kardassi D (1999) *Langmuir* 15:282
21. Evans DF, Ninham BW (1986) *J Phys Chem* 90:226
22. Cevc G, Richardsen H (1999) *Adv Drug Delivery Rev* 38:207
23. a) Duezguenes N, Wilschut J (1993) *Methods Enzymol* 230:3; b) Hoekstra D, Duezguenes N (1993) *Methods Enzymol* 230:15
24. Menger FM, Keiper JS, Lee SJ (1997) *Langmuir* 13:4614
25. Paleos CM, Sideratou Z, Tsiourvas D (1996) *J Phys Chem* 100:13,898
26. a) Marchi-Artzner V, Jullien L, Gulik-Krzywicki T, Lehn J-M (1997) *Chem Commun* 117; b) Marchi-Artzner V, Gulik-Krzywicki T, Guedeau-Boudeville M-A, Gosse C, Sanderson JM, Dedieuand L-C, Lehn J-M (2001) *ChemPhysChem* 2:367–376
27. Sideratou Z, Tsiourvas D, Paleos CM, Tsortos A, Nounesis G (2000) *Langmuir* 16:9186
28. a) Ipsen JH, Karlström G, Mouritsen OG, Wennerström H, Zuckermann MJ (1987) *Biochim Biophys Acta* 905:162; b) Thewalt LJ, Bloom M (1992) *Biophys J* 63:1176; c) Vist MR, Davis JH (1990) *Biochemistry* 29:451; d) Trandum C, Westh P, Jørgensen K, Mouritsen OG (2000) *Biophys J* 78:2486
29. Sideratou Z, Tsiourvas D, Paleos CM, Tsortos A, Pyrpassopoulos S, Nounesis G (2002) *Langmuir* 18:829
30. a) A thorough discussion of the subject in: *Faraday Discuss Chem Soc* (1986) 77, 209, 340, 341 (81 pages); b) Söderlund T, Jutila A, Kinnunen PKJ (1999) *Biophys J* 76:896
31. Pantos A, Sideratou Z, Paleos CM (2002) *J Colloid Interface Sci* 253:435
32. Komatsu H, Okada S (1997) *Chem Phys Lipids* 85:67
33. a) Berti D, Franci L, Baglioni P, Luisi PL (1997) *Langmuir* 13:3438; b) Berti D, Luisi PL, Baglioni P (2000) *Colloids Surf A Physicochem Eng Aspects* 167:95
34. a) Nowick JS, Chen JS (1992) *J Am Chem Soc* 114:1107; b) Nowick JS, Chen JS, Noronha G (1993) *J Am Chem Soc* 115:7636
35. Nowick JS, Cao T, Noronha G (1994) *J Am Chem Soc* 116:3285
36. Meier W (2000) *Langmuir* 16:1457
37. Lemieux RU (1996) *Acc Chem Res* 29:373



# Dendrimers for Nanoparticle Synthesis and Dispersion Stabilization

Kunio Esumi

Department of Applied Chemistry and Institute of Colloid and Interface Science,  
Tokyo University of Science, Kagurazaka, Shinjuku-ku, Tokyo 162-8601, Japan  
E-mail: [kuesumi@rs.kagu.tus.ac.jp](mailto:kuesumi@rs.kagu.tus.ac.jp)

Since dendrimers consisting of regularly branched structure are controlled by chemical structure, molecular weight, and its distribution as well as molecular size and molecular shape, they are unique macromolecules with many functional properties.

By using dendrimers as templates, dendrimer-metal nanoparticles are synthesized in aqueous and non-aqueous media. Particle sizes of metals are significantly affected by many factors including concentration of dendrimers and generation of dendrimers. In particular, structure of dendrimer-metal nanoparticles is characterized by TEM, SANS, and SAXS.

Synthesis of dendrimer-semiconductor nanoparticles such as CdS and CuS is also described.

**Keywords.** Dendrimer, Metal nanoparticles, Semiconductor nanoparticles, Nanocomposites

<b>1</b>	<b>Introduction</b>	<b>31</b>
<b>2</b>	<b>Synthesis and Structure of Dendrimers</b>	<b>32</b>
2.1	Synthesis of Dendrimers	32
2.2	Structure of Dendrimers	34
<b>3</b>	<b>Synthesis of Dendrimer-Metal Nanoparticles</b>	<b>36</b>
3.1	Synthesis of Dendrimer-Metal Nanoparticles in Aqueous Solutions	38
3.2	Synthesis of Dendrimer-Metal Nanoparticles in Non-Aqueous Solutions	45
<b>4</b>	<b>Synthesis of Dendrimer-Semiconductor Nanoparticles</b>	<b>49</b>
	<b>References</b>	<b>51</b>

## 1 Introduction

Dendrimers are macromolecules with a regular and highly branched three-dimensional architecture. The first example of an iterative synthetic procedure toward well-defined branched structures has been reported by Vögtle et al. [1], who named this procedure a “cascade synthesis”. The paper concerning den-



drimers, which has received widespread attention, was presented by Tomalia et al. [2] at the first international polymer conference at Kyoto in 1984 and was published in *Polymer Journal* in 1985. Tomalia's poly(amidoamine)dendrimer (PAMAM) and Newkome's arborol [3] have been obtained by the divergent method, while Hawker and Fréchet [4] introduced the convergent approach for precise synthesis of dendrimers.

Since dendrimers consisting of regularly branched structure are controlled by chemical structure, molecular weight, and its distribution as well as molecular size and molecular shape, they are unique macromolecules with many functional properties. In addition, it is possible to make a molecular design of dendrimers with respect to core, branched chain, and surface functional groups and the pore space of dendrimers can also be utilized. Dendrimers can provide a dimensional functionality which is different from conventional linear polymers; although conventional linear polymers can be modified by grafting branched chains, dendrimers have superior properties to build up three-dimensional molecular architectures [5–8]. Dendrimers have many applicable potentials such as nanocapsules, gene vectors, catalysis, magnetic resonance imaging agents, electron conduction, and photon transduction. The science of dendrimers has grown by a strong connection with disciplines that include physical and materials chemistry, biotechnology, and applied physics. At present, PAMAM and poly(propyleneimine)dendrimers are available commercially which are made by the divergent method.

In this chapter we introduce structures and physicochemical properties of dendrimers. Then synthesis and characterization of dendrimer-nanoparticles are discussed.

## 2 Synthesis and Structure of Dendrimers

### 2.1 Synthesis of Dendrimers

Two different methods for the construction of high-generation dendrimers have been proposed: the divergent and convergent approaches.

In the divergent method, the dendrimer is grown in a stepwise manner from a central core, implying that numerous reactions are performed on a single molecule. This method provides a high yield. PAMAM dendrimers and poly(propyleneimine)dendrimers have been synthesized commercially by this method. Figure 1 shows the reaction steps of divergent method for PAMAM dendrimers.

In the convergent method, the synthesis of dendrimers starts from the periphery and ends at the core. In this method, a constant and low number of reaction sites is warranted in every reaction step throughout the synthesis. As a consequence, only a small number of side products can be formed in each reaction. It is necessary to employ a purification process in order to remove unreacted dendrons or defected dendrons after reaction. Accordingly it seems difficult to produce dendrimers on a large scale by this method. However, dendrimers synthesized convergently can provide defect-free ones.



In the divergent method, the presence of a small number of statistical defects cannot be avoided unless the substitution by branched reaction is perfect at every step. In particular, the defects are apparently seen when the generation of dendrimers increases. Considering the dendrimers as useful and potential functional molecules and materials, the influence of a small number of defects will be negligible from the standpoints of basic research and industrial application. It should be mentioned that highly purified dendrimers can be synthesized by the divergent method through a process of size exclusion chromatography.

## 2.2

### Structure of Dendrimers

Dendrimers consisting of core with symmetrical branched structures can be recognized as a spherical molecule when the generation increases. According to numerical calculations [9–12] using the kinetic growth model it can be predicted that the ends of the branches are not positioned at the surface but are severely backfolded. These results suggest that we can provide proper freedom and fluidity to the surface end groups as well as flexible movement of inner molecules of the dendrimers.

Since dendrimers have regular branched structures, their shape and size can be controlled systematically. Dendrimers are of a nanometer-size scale and their size increases with generation. Table 1 shows the relationship between molecular weight, number of end groups, and diameter for PAMAM dendrimers [13]. Although the diameter is relatively wider from the stretching of the branched chains, the diameter is well controlled compared to that of conventional linear polymers. The size of dendrimers is larger than a fullerene with diameter of 0.7 nm, but smaller than fine particles with diameters of 0.1–10  $\mu\text{m}$ . It is apparent that molecular construction of nanoscale dimension becomes significantly feasible by using dendrimers. In nature, there are many biopolymers, e.g., proteins, whose sizes are nanoscale with constant molecular shapes. Accordingly it is easily understood that a significant advance in the precision of molecular con-

**Table 1.** Effect of generation on selected properties of poly(amidoamine) PAMAM dendrimers (ammonia core)

Generation	Calculated diameter (nm)	No. of surface groups	Molecular weight <sup>a</sup>
0	0.96	3	359
1	1.28	6	1043
2	1.76	12	2411
3	2.41	24	5147
4	3.06	48	10619
5	3.85	96	21563
6	4.75	192	43451
7	6.18	384	87227

<sup>a</sup> Corey-Pauling-Koltun (CPK) model.

struction can be achieved with dendrimers from the standpoint of the molecular shape as well as the molecular size.

The size and shape of dendrimers have been estimated using transmission electron microscopy [14]. Producing better images of dendrimers may supply answers to fundamental questions such as whether dendrimers have truly uniform sizes, spherical shapes, and dense cores. The visualization of dendrimer assemblies would also be helpful to confirm the structure and morphology for many applications of dendrimers. The positively stained PAMAM dendrimers are shown in Fig. 2 for G10 to G5, respectively. The dendrimer molecules appear as dark objects on a light background of the amorphous carbon substrate and they are well separated from each other. The shapes of the stained molecules are spherical to a first approximation for G10 to G7, with some molecules showing

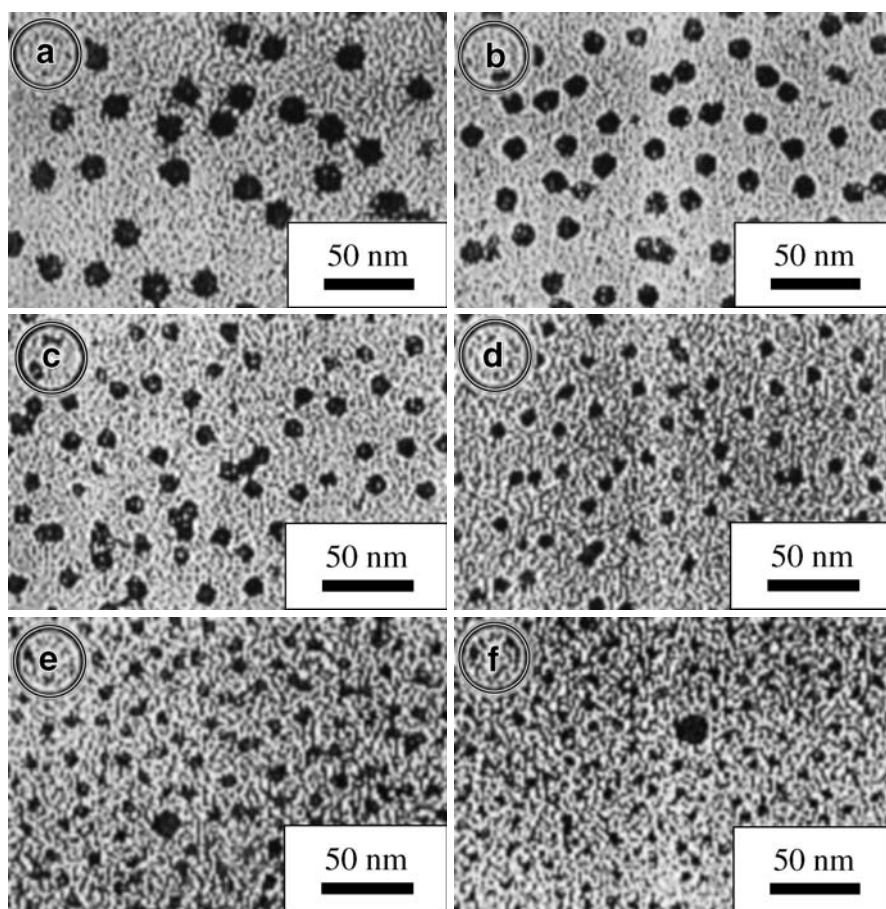


**Fig. 2a–f.** TEM images of PAMAM dendrimers positively stained with 2% aqueous sodium phosphotungstate: a G10; b G9; c G8; d G7; e G6; f G5. Reprinted with permission from [14]. Copyright 2002 American Chemical Society

**Table 2.** Size measurements on poly(amidoamine)PAMAM dendrimers (ethylenediamine core) from computer analysis of TEM images

Generation	Mean diameter (nm)	Median diameter (nm)	No. of dendrimers	Standard deviation
5	4.3	4.3	285	0.7
6	6.9	6.9	239	0.5
7	8.0	8.0	576	0.7
8	10.2	10.3	459	0.8
9	12.4	12.5	1331	0.8
10	14.7	14.8	413	1.1

“edges” or slightly polyhedral shapes. For G6 and G5 the shapes become more indistinct because the carbon substrate is closer in size to the molecule and the edges become more difficult to delineate. The mean and median diameters of each generation are listed in Table 2, along with the standard deviation of the measurement. In general, the agreement between the mean and median diameters is good, indicating that the distribution is approximately Gaussian in shape. The mean diameters range from 14.7 nm for G10 to 4.3 nm for G5. The mean diameters of PAMAM dendrimers measured by TEM on the stained specimens compare well with SAXS measurements in methanol. The close agreement between the techniques suggests that the staining done on wet dendrimer molecules locks in the size of the dendrimer in solution.

PAMAM dendrimers in the G5–G10 range have been imaged by tapping mode atomic force microscopy (AFM) [15]. Individual dendrimer molecules can be clearly observed in the AFM images, which show that these dendritic particles appear to be monodispersed, dome-shaped, and randomly distributed on the mica surface (Fig. 3). Molecular diameter and height can also be measured from each particle’s profile section from the AFM line scans. The diameter and height data are used to calculate the molecular volume of each single molecule. Absolute molecular weight and polydispersity are then estimated for each dendrimer generation. The calculated molecular weights for G5–G8 are in very good agreement with the theoretical ones. Although individual molecules of lower generations such as G4 cannot be imaged due to their lower rigidity, the smaller number of surface functional groups, and as well as the ability of the branches of lower generations to interpenetrate easily one another, the surface morphology of G4 dendrimer films on mica at different surface densities is observed by AFM.

### 3

#### Synthesis of Dendrimer-Metal Nanoparticles

Synthesis of metal particles has been intensively investigated because metal nanoparticles have been applied to electrooptical devices, electronic devices, imaging materials, catalysis, and so on [16]. Fabrication of nanoparticles becomes one of important topics in nanotechnology. For that purpose, it is neces-

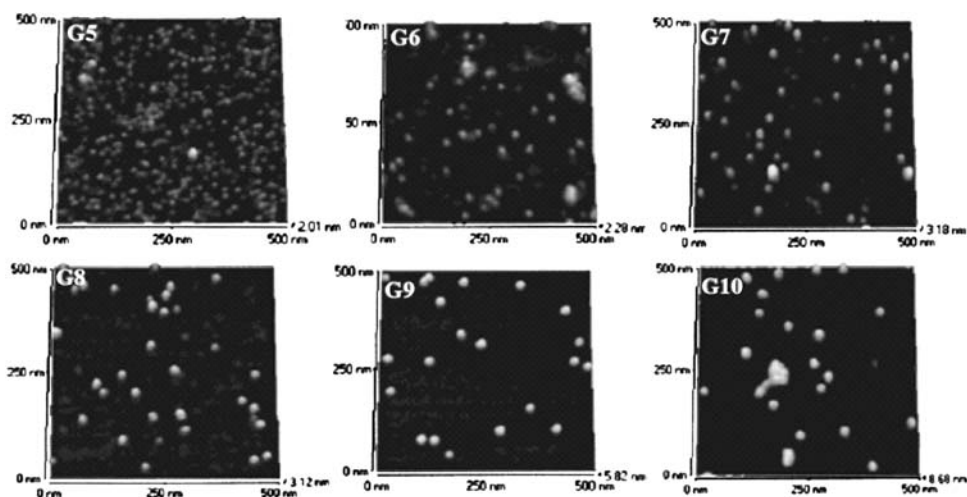


**Fig. 3.** Tapping mode AFM 3D images of PAMAM dendrimers from G5 to G10. Dendrimer molecules (0.001 wt%) are deposited on the mica surface by spin coating. Reprinted with permission from [15]. Copyright 2002 American Chemical Society

sary for reliable nanoscale devices to control particle size, shape, and size distribution of metal nanoparticles.

Since dendrimers contain a large number of regularly spaced internal and external functional groups, it is expected that they operate as templates to grow inorganic crystal in the internal or external region of dendrimers which provide organic-inorganic hybrid nanostructures.

When metal ions mix with PAMAM dendrimers in solutions, complex formation by ligand-metal ion interaction, acid-base interaction, etc. might occur at the surface or inside the dendrimers. After the reduction the location of metal nanoparticles strongly depends on the place of complex formation. Accordingly, dendrimer-metal nanoparticle structures can be schematically illustrated in Fig. 4. In Fig. 4a, metal ions interact with surface functional groups of the dendrimers and the resulting nanoparticles are present on the surface of the dendrimers. Also, for lower generation dendrimers whose diameters are smaller than those of metal nanoparticles, a nanocomposites structure like in Fig. 4a might be suggested. When metal ions are diffused into the dendrimers complexed with the binding sites, metal particles after the reduction might be encapsulated into the dendrimers as shown in Fig. 4b. Such encapsulation might occur at higher generation dendrimers. In addition, there is a possibility of a mixed structures of Fig. 4a,b. Results obtained from dendrimer-metal nanoparticles prepared so far are discussed below.

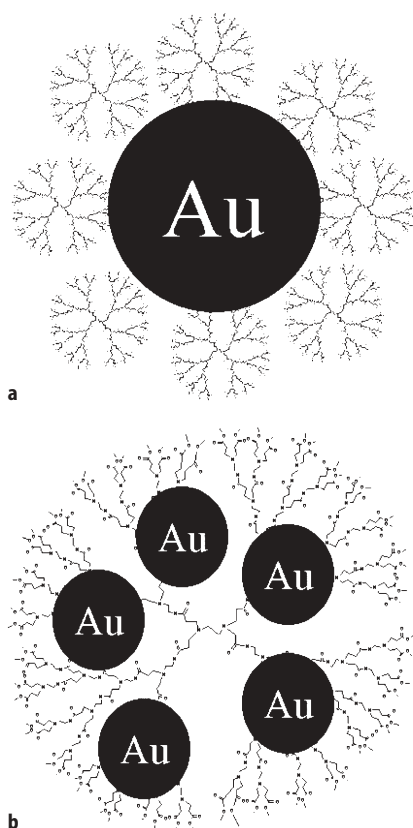


**Fig. 4a,b.** Possible structures of dendrimer-metal nanoparticles: **a** lower generation dendrimers; **b** higher generation dendrimers

### 3.1

#### Synthesis of Dendrimer-Metal Nanoparticles in Aqueous Solutions

The dendrimer-copper nanoparticles were first synthesized using PAMAM dendrimers with various surface functional groups [17, 18]. In the case of copper sulfate and dendrimer with surface hydroxyl group, chemical reduction of  $\text{Cu}^{2+}$ -loaded generation fourth dendrimer (G4-OH) with a fivefold molar excess of sodium borohydride results in intradendrimer Cu clusters. The solution color immediately changes from blue to golden brown: the absorbance bands originally present at 605 and 300 nm disappear and are replaced with a monotonically increasing spectrum of nearly exponential slope toward shorter wavelengths. This behavior results from the appearance of a new interband transition arising from the formation of intradendrimer Cu clusters. TEM results indicate the presence of intradendrimer Cu clusters after reduction. Micrographs of Cu clusters within G4-OH reveal particles having a diameter less than 1.8 nm, much



smaller than the 4.5 nm diameter of G4-OH. Clusters formed in the presence of G4-OH are stable for at least one week in an oxygen-free solution. However, in air-saturated solutions the clusters revert to intradendrimer  $\text{Cu}^{2+}$  ions overnight. When G4 dendrimers with surface amino group are used as template, they adsorb  $\text{Cu}^{2+}$  ions which bind primarily to the surface amino groups. Reduction of a solution shows a formation of Cu clusters >5 nm in diameter. This larger size is a consequence of agglomeration of Cu particles adsorbed to the unprotected dendrimer exterior. Another study of the synthesis of dendrimer-copper nanoparticles using copper acetate and hydrazine as a reductant suggests that copper particles are present at both the interior and exterior of the dendrimer with surface amino groups. Thus, depending on the polarity of the dendrimer surface substitutes, the metallic particles may be directed primarily near the dendrimer surface or deeper into the interior. Using poly(propylene imine) dendrimers Cu nanoparticles have also been synthesized. The geometry of the dipropylenetriamine- $\text{Cu}^{2+}$  end-group complexes is reported and the Cu size decreases with increasing dendrimer generation [19].

The dendrimer-gold nanoparticles are synthesized by reduction of  $\text{AuCl}_4^-$  with irradiation of UV in aqueous solution [20]. The absorption band of gold particles appears at around 520 nm, and its intensity increases with an increase of the irradiation time. In the case of lower generations at low concentrations, the plasmon band is shifted to longer wavelength with increasing UV irradiation due to coagulation of gold particles. Typical TEM images of gold particles obtained in the presence of G5-NH<sub>2</sub> and their particle size distributions are shown in Fig. 5. At a ratio of [surface amino group]/[ $\text{HAuCl}_4$ ]=1, the particle size of gold particles is 2–18 nm, having a broad distribution. When the ratio is increased to 4, monodispersed gold particles with a diameter less than 1 nm are obtained. The changes in the average particle size with the surface amino group concentration of G(0–5) dendrimers are shown in Fig. 6. The average particle size decreases with an increase of the concentration of surface amino group for each dendrimer. At a ratio of [surface amino group]/[ $\text{HAuCl}_4$ ]=1, the average particle size is not dependent on the generation of the dendrimers, but at [surface amino]/[ $\text{HAuCl}_4$ ] $\geq 4$  it becomes smaller with an increase of the dendrimer generation. These results suggest that the dendrimers of lower generation G0 do not operate an effective protective colloid, but the dendrimers of higher generations provide sites for complex formation as well as an effective protective action.

By addition of reductants such as sodium borohydride into noble metal ions-dendrimers aqueous solutions, dendrimer-noble metal nanoparticles (gold, silver, platinum, palladium) are also synthesized [21, 22]. The average sizes of gold decreases with an increase of the concentration of surface amino groups for G(3–5) dendrimers, while the average sizes of platinum are insensitive against the generation of the dendrimers above a certain ratio of [amino group]/[ $\text{Pt}^{4+}$ ] (Figs. 7 and 8). A fact that higher dendrimer concentrations are required for obtaining stable platinum particles compared to that for gold particles suggest that the interaction between platinum particles and the dendrimers is weaker than that between gold particles and the dendrimers. In fact, FT-IR spectra of the dendrimer-platinum nanoparticles show that the absorption band due to the in-



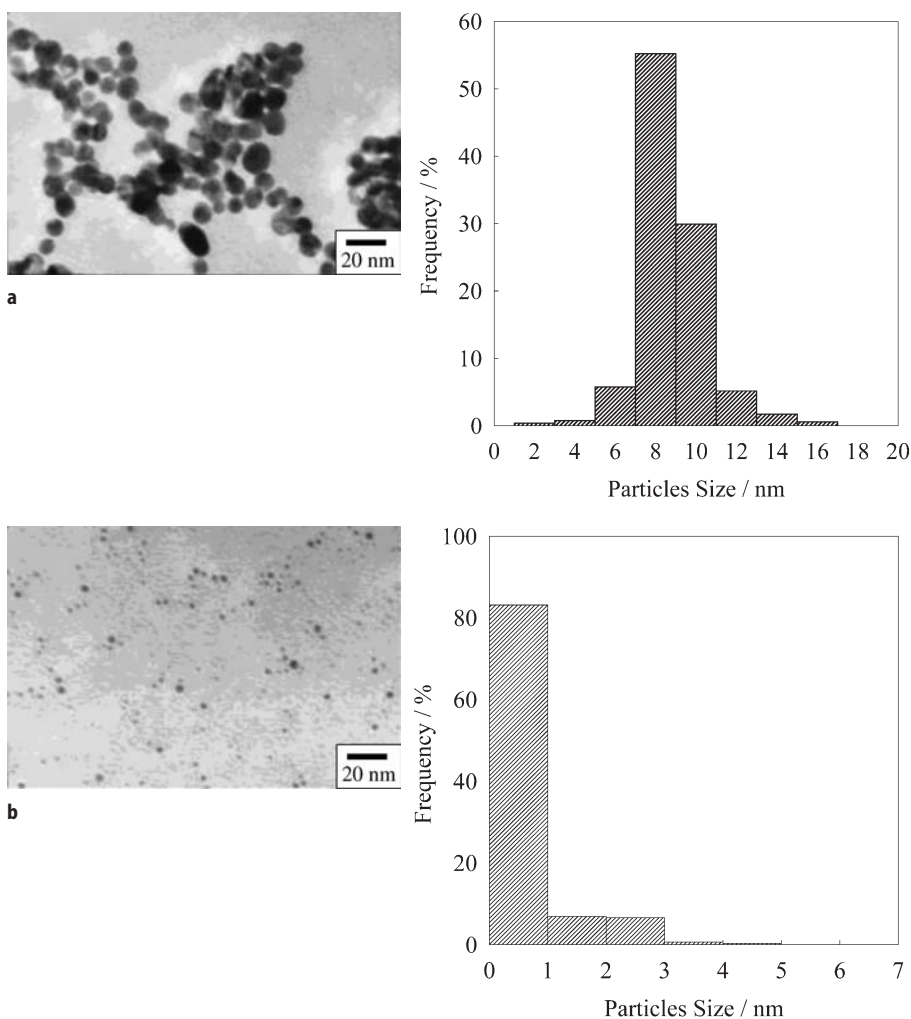


**Fig. 5a,b.** TEM images and size distribution of gold nanoparticles, molar ratio of surface amino group of G5 and  $\text{HAuCl}_4$ : **a** 1:1; **b** 4:1. Reprinted with permission from [20]. Copyright 2002 American Chemical Society

teraction between platinum particles and amino groups of the dendrimers is very weak.

Since it is anticipated that  $\text{Ag}^+$  ions strongly adsorb on the dendrimers with surface carboxyl groups through electrostatic attractive forces, synthesis of dendrimer-silver nanoparticles is carried out by the reduction of  $\text{AgNO}_3$  with sodium borohydride in the presence of dendrimers with surface carboxyl groups (G(3.5–5.5)). When  $\text{Ag}^+$  ions are reduced with sodium borohydride in the presence of dendrimers, the color of silver particles changes with an increase of G5.5 concentration; yellow at the ratio of  $[\text{carboxyl group}]/[\text{Ag}^+]=1$  turns to or-

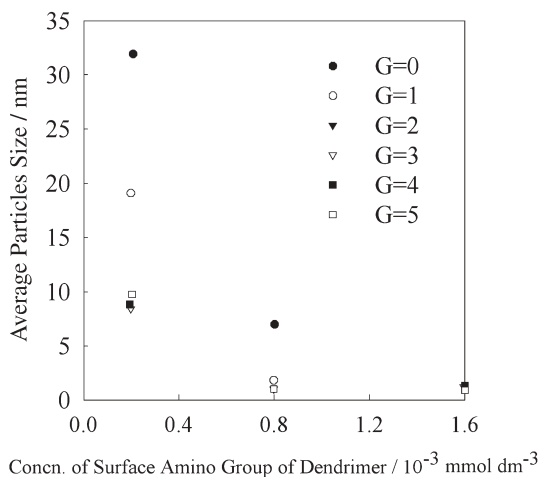


**Fig. 6.** Change of the average particle size of gold with the dendrimer concentration (surface amino group). The feed concentration of  $\text{HAuCl}_4$  is  $0.2 \text{ mmol dm}^{-3}$ . Reprinted with permission from [20]. Copyright 2002 American Chemical Society

ange at the higher ratios. In the cases of G3.5 and G4.5 dendrimers, a similar color change is observed as that of G5.5 dendrimer. It is interesting to note that the time required for the color change to yellow or orange after addition of sodium borohydride increases with an increase of the dendrimer concentration because of the repulsive action of  $\text{BH}_4^-$  with negatively charged dendrimers that carry reacting  $\text{Ag}^+$  ions [23]. Unfortunately, at above the ratio of  $[\text{carboxyl group}]/[\text{Ag}^+]=5$  we could not observe any silver nanoparticles by TEM because the particle size is too small to detect in this experimental condition. The absorption spectra of silver particles show that a typical plasmon band of silver particles is observed at 380 nm at the ratio of  $[\text{carboxyl group}]/[\text{Ag}^+]=1$  and another band at around 450 nm appears with an increase of the ratio (Fig. 9). A similar absorption band at 440 nm for silver clusters has been observed when the reduction of  $\text{Ag}^+$  ions on polyacrylate in aqueous solution has been carried out by  $\gamma$ -irradiation.

On the other hand, by using fourth-generation PAMAM dendrimer with surface hydroxyl group it is suggested that platinum or palladium nanoparticles can be encapsulated inside the dendrimer [22]. This is probably due to different interactions of platinum or palladium nanoparticles with the functional groups of the dendrimers. Note that the hydrogenation reaction rates can be controlled by using dendrimer-metal nanoparticles, i.e., the rates decrease with an increase of the dendrimer generation. In addition, it has also been pointed out [24] that the structure of dendrimer-gold or silver nanoparticles is the function of the dendrimer structure and surface functional groups as well as the formation mechanism and chemistry involved.

To verify the structure of dendrimer-gold nanoparticles, gold nanoparticles synthesized by reduction of  $\text{HAuCl}_4$  with sodium borohydride in the presence of

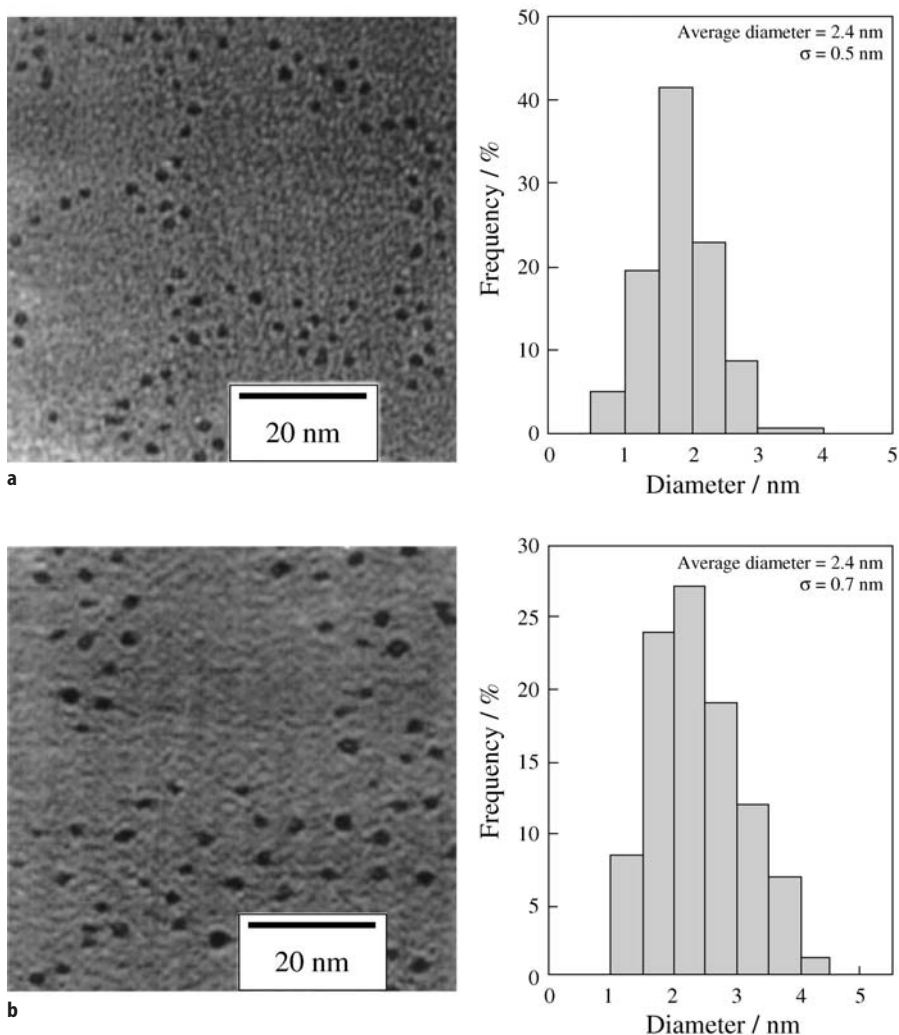


**Fig. 7a,b.** TEM images and size distribution of platinum nanoparticles obtained in the presence of dendrimer: **a**  $[\text{H}_2\text{PtCl}_6]=0.1 \text{ mmol dm}^{-3}$ ,  $[\text{G4}]=8.0 \text{ mmol dm}^{-3}$ ; **b**  $[\text{H}_2\text{PtCl}_6]=0.1 \text{ mmol dm}^{-3}$ ,  $[\text{G5}]=8.0 \text{ mmol dm}^{-3}$ . Reprinted with permission from [21]. Copyright 2002 American Chemical Society

PAMAM dendrimers with surface amino groups (G2–G10) are characterized by TEM, SANS, and SAXS [25]. Figure 10 shows TEM image of gold particles containing G9 dendrimer. The image indicates that gold particles are formed inside the dendrimer. Under slow reaction condition, one gold particle per dendrimer is predominantly formed. The sizes estimated for the dendrimer and gold are 13 and 4 nm, respectively. The results obtained by SANS and SAXS are in good agreement with that by TEM. Further, it is suggested for the dendrimers with

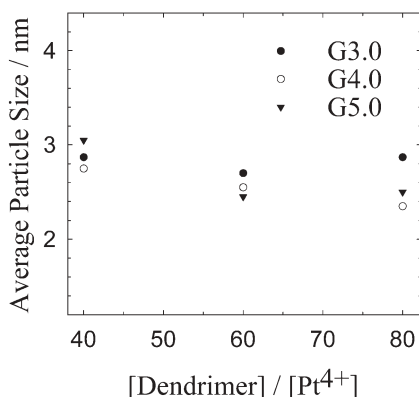


**Fig. 8.** Change in the average particle size of platinum with dendrimer concentration

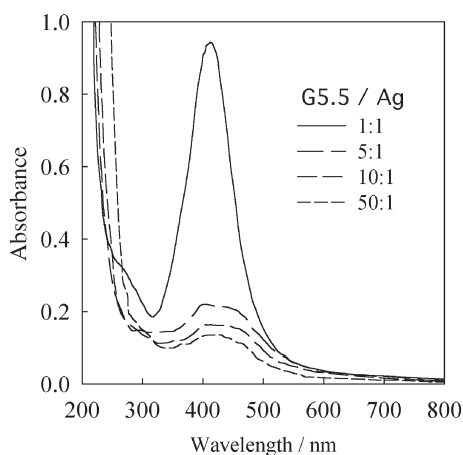


**Fig. 9.** Absorption spectra of silver nanoparticles synthesized in the presence of dendrimer. Reprinted with permission from [21]. Copyright 2002 American Chemical Society

various generations that several dendrimers surround the surface of gold particle formed for G2–G4 dendrimers, while gold particles are completely formed inside individual dendrimers for G6–G10 dendrimers. For G10, multiple gold particles within one dendrimer are formed due to the more crowded volume inside the dendrimer. Thus such a transition has been shown from colloid stabilization by low molecular mass molecules to polymer nanotemplating with increase of molecular mass but unchanged chemistry of the stabilizing species.

For metal ions that do not form either covalent bonds or strong complexes with the interior amine groups of PAMAM dendrimers, a new method for the synthesis of dendrimer-encapsulated metal nanoparticles has been reported [26]. For example, when G6 dendrimer (with surface hydroxyl group) -encapsulated copper is exposed to a solution containing ions more noble than copper,

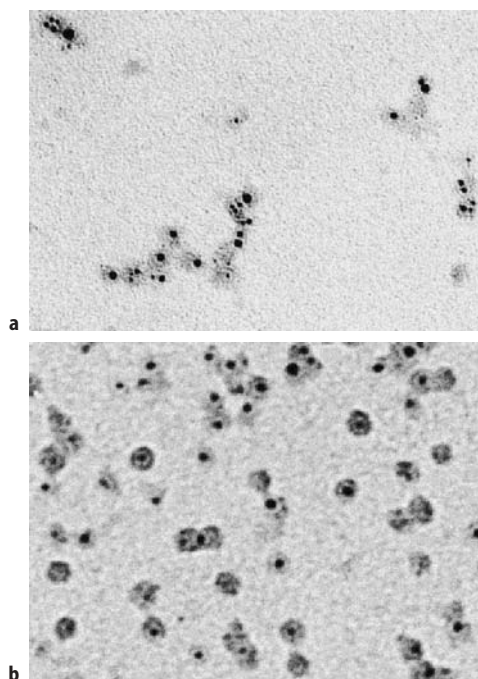


**Fig. 10a,b.** TEM images of gold nanoparticles containing PAMAM G9 dendrimer obtained at 1:1 loading. The dendrimers have been stained with phosphotungstic acid and appear gray; the gold colloids appear black: **a** fast reduction; **b** slow reduction. Reprinted with permission from [25]. Copyright 2002 American Chemical Society

the copper is displaced and the more noble ions are reduced. By using this method, silver, gold, palladium, and platinum dendrimer-encapsulated metal particles have been obtained.

Gold and silver nanoparticles can also be synthesized in the presence of sugar-persubstituted PAMAM dendrimers (sugar ball) without reductants [27]. Actually, the hydroxyl groups of glucose residue of sugar ball can operate as reductant. In the case of silver nanoparticles, the addition of NaOH is required to reduce  $\text{Ag}^+$  ions. It is suggested that several sugar balls adsorb on the surface of gold or silver particles, resulting in a stable dispersion in aqueous solution. Their diameters are ranged between 2 and 6 nm. In addition, the kinetics of the formation of gold and silver nanoparticles is affected by the generation of sugar ball as well as the additive concentration of sugar ball. The observed rate constants increase with the concentration of sugar ball, where the rate constants for early generation sugar ball are greater than those for late generation. Such sugar ball-gold nanoparticles are of considerable interest in biochemical and medical applications.

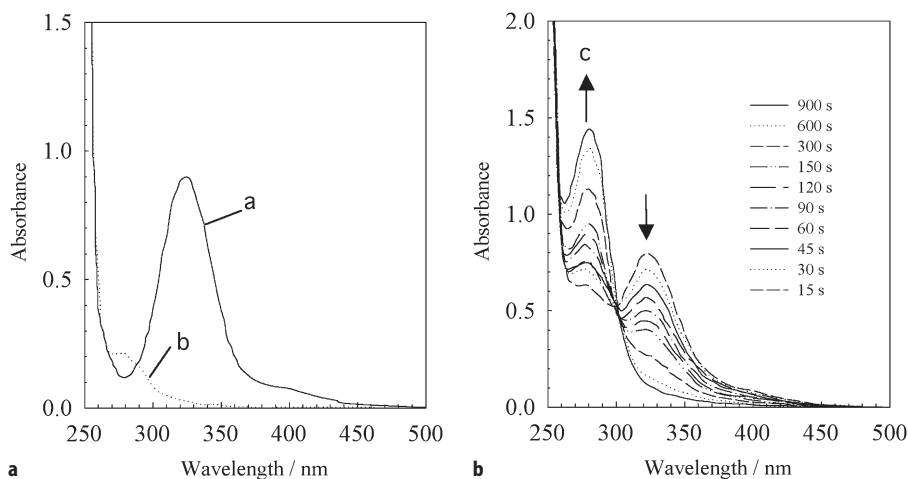


**Fig. 11.** **a** UV-visible absorption spectra of  $\text{HAuCl}_4$  (0.2  $\text{mmol dm}^{-3}$ ) in ethyl acetate; **b** PAMAM G5.5 (13  $\text{mmol dm}^{-3}$  in tertiary amine concentration) in ethyl acetate; **c** Evolution of UV-visible absorption spectra after mixing  $\text{HAuCl}_4$  with PAMAM G5.5. Reprinted with permission from [28]. Copyright 2002 Academic Press

### 3.2

#### Synthesis of Dendrimer-Metal Nanoparticles in Non-Aqueous Solutions

Gold and platinum nanoparticles are synthesized in ethyl acetate by reduction of respective metal salts with dimethylamineborane in the presence of PAMAM dendrimers with surface methyl ester groups [28–30]. When  $\text{HAuCl}_4$  in ethyl acetate is added to dendrimers in ethyl acetate, a formation of dendrimer- $\text{Au}^{3+}$  is observed (Fig. 11) [28]. As shown in Fig. 11a,  $\text{HAuCl}_4$  in ethyl acetate shows an intense absorption at 324 nm which can be assigned to LMCT band of  $\text{AuCl}_4^-$ . On the other hand, G5.5 dendrimer shows a small absorption maximum at 278 nm, as shown in Fig. 11a. A new band develops at 280 nm at the expense of 324 nm band and the latter band completely disappears in 15 min of stirring. In addition, an isobestic point is found at 304 nm, indicating that a ligand substitution from  $\text{AuCl}_4^-$  to another  $\text{Au}^{3+}$  complex occurs through a participation of the dendrimer. It is also found from FT-IR measurements that the bands for surface methyl ester groups at 1044, 1200, 1438, and 1736  $\text{cm}^{-1}$  scarcely change by introducing  $\text{Au}^{3+}$ , while amide I band at 1647  $\text{cm}^{-1}$  for interior amide groups undergoes a high-frequency shift to 1649  $\text{cm}^{-1}$  and a single peak for amide II band splits into two peaks by addition of  $\text{Au}^{3+}$ .  $\text{Au}^{3+}$  ions in the presence of the dendrimers in ethyl acetate are readily reduced by adding an excess amount of dimethylamineborane. Interestingly it is found that above the ratio of  $[\text{G}]/[\text{Au}^{3+}] \geq 10$  the maximum particle size of gold is less than the hydrodynamic diameter of the dendrimer (G3.5 and G5.5), whereas in the case of G1.5 dendrimer the maximum size of gold is larger than that of G1.5 dendrimer (Fig. 12). These results may suggest that the encapsulation of gold nanoparticles by G3.5

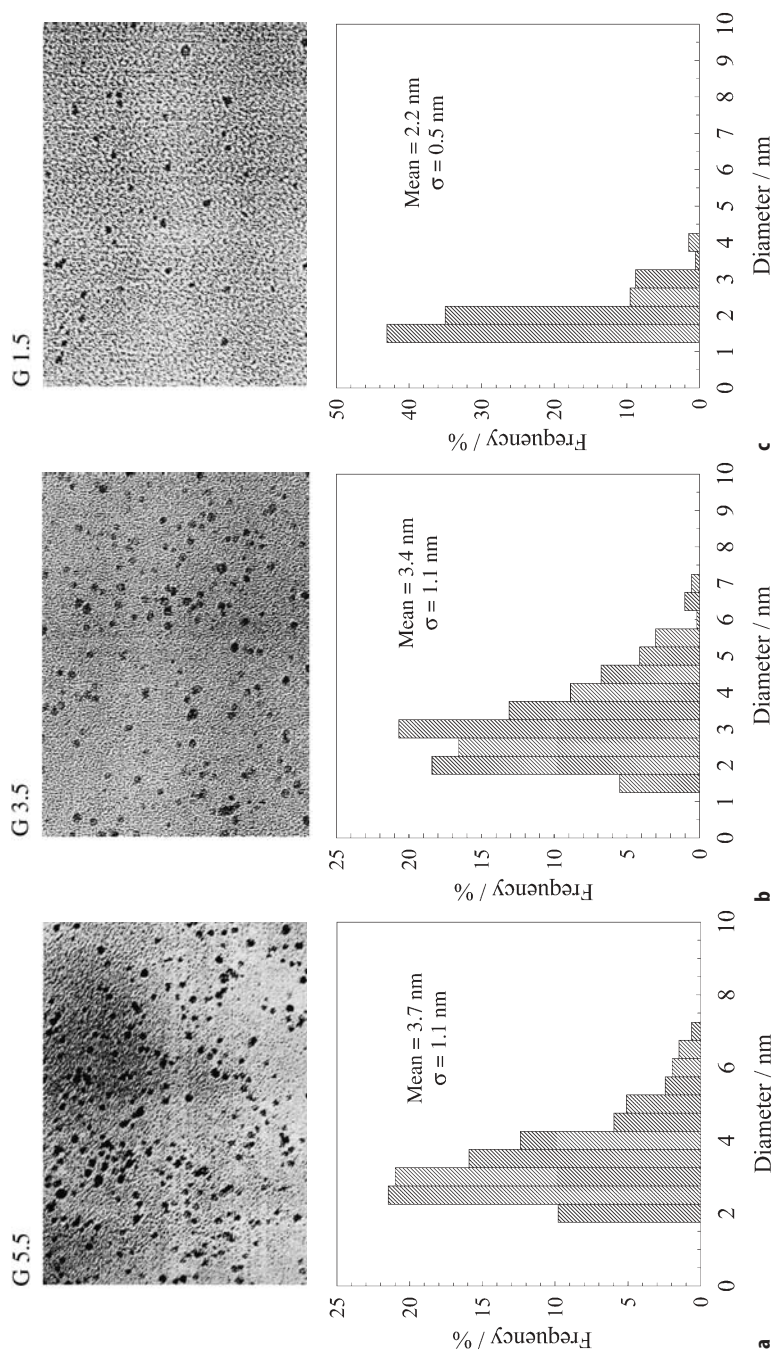


**Fig. 12a–c.** TEM images and size distribution of gold nanoparticles synthesized using: **a** PAMAM G5.5; **b** PAMAM G3.5; **c** PAMAM G1.5.  $[\text{HAuCl}_4] = 0.2 \text{ mmol dm}^{-3}$ ,  $[\text{PAMAM}] = 10 \text{ mmol dm}^{-3}$ ,  $[\text{dimethylamine borane}] = 2 \text{ mmol dm}^{-3}$ . Reprinted with permission from [28]. Copyright 2002 Academic Press



or G5.5 dendrimer predominantly occurs, while G1.5 dendrimers adsorb on the surface of gold nanoparticle.

When  $\text{HAuCl}_4$  in formamide solutions in the presence of PAMAM dendrimers with surface methyl ester groups is reduced by addition of sodium borohydride, gold nanoparticles are also obtained whose size decreases with an increase of the dendrimer concentration as well as the generation [29]. Further, the particle size of gold is affected by the elapsed time for the solution before reduction since  $\text{HAuCl}_4$  in formamide is reduced to some extent. In *N,N*-dimethylformamide in the presence of dendrimer, relatively monodispersed gold nanoparticles are obtained. It may be suggested that stable gold nanoparticles are prepared by adsorbing a low generation dendrimers on the nanoparticles, while dendrimer-encapsulated gold nanoparticles are obtained in the case of a higher generation dendrimers.

Platinum nanoparticles have also been synthesized in ethyl acetate in the presence of PAMAM dendrimers with surface methyl ester groups [30]. Different from the preparation of gold nanoparticles, the elapsed time after mixing of  $\text{H}_2\text{PtCl}_6$  and the dendrimer in ethyl acetate is very important to control the particle size. Figure 13 shows TEM images of platinum nanoparticles obtained in the presence of G5.5 dendrimer at 5 min of elapsed time after mixing. One can see that even at different concentrations of dimethylamineborane, large (about 18 nm in diameter) and small (about 3 nm in diameter) platinum particles are formed. In particular, when the concentration of dimethylamineborane is 90 times that of  $\text{H}_2\text{PtCl}_6$ , it is visualized that the large particles are coated by G5.5 dendrimer, where the thickness of coating is about 4–5 nm and is smaller than the hydrodynamic diameter (7.6 nm) of G5.5 dendrimer determined by dynamic light scattering measurements in ethyl acetate. It is suggested that G5.5 dendrimers are flattened on the surface of the platinum particle. Actually, the structural distortion of the dendrimers on gold surfaces has been reported [31]: the height of generation 8 of PAMAM dendrimer on a naked gold surface ranges from 3.5 to 4.0 nm, which is less than the ideal-sphere diameter of 9.7 nm. On the other hand, it is seen that the small platinum particles are encapsulated by G5.5 dendrimer in which the diameter of G5.5 dendrimer-encapsulated platinum is about 10 nm. It seems that the G5.5 dendrimer-encapsulated platinum particle is flattened on the grid surface. Microstructural studies of dendrimer adsorption at solid surfaces also indicate that the dendritic macromolecules are flattened on the surfaces [32]. When the concentration of dimethylamineborane is reduced to ten times that of  $\text{H}_2\text{PtCl}_6$ , the image of visualized dendrimers is not observed, although similar large and small platinum particles are obtained. It should be noted that the visualization of G5.5 dendrimer from mixtures of dimethylamineborane and G5.5 dendrimer is not observed, suggesting that platinum particles play an important role for the visualization of G5.5 dendrimer. Such a formation of large and small platinum particles at short elapsed time may occur due to nonuniform distribution of  $\text{Pt}^{4+}$  ions in the solution and in the G5.5 dendrimer. When the elapsed time after mixing is increased, the average particle diameter decreases: the average diameters are about 1.7 nm (standard deviation, 0.3 nm) at one day of the elapsed time and 0.8 nm (standard deviation, 0.1 nm) at three days of the elapsed time. Since the particle size is consid-



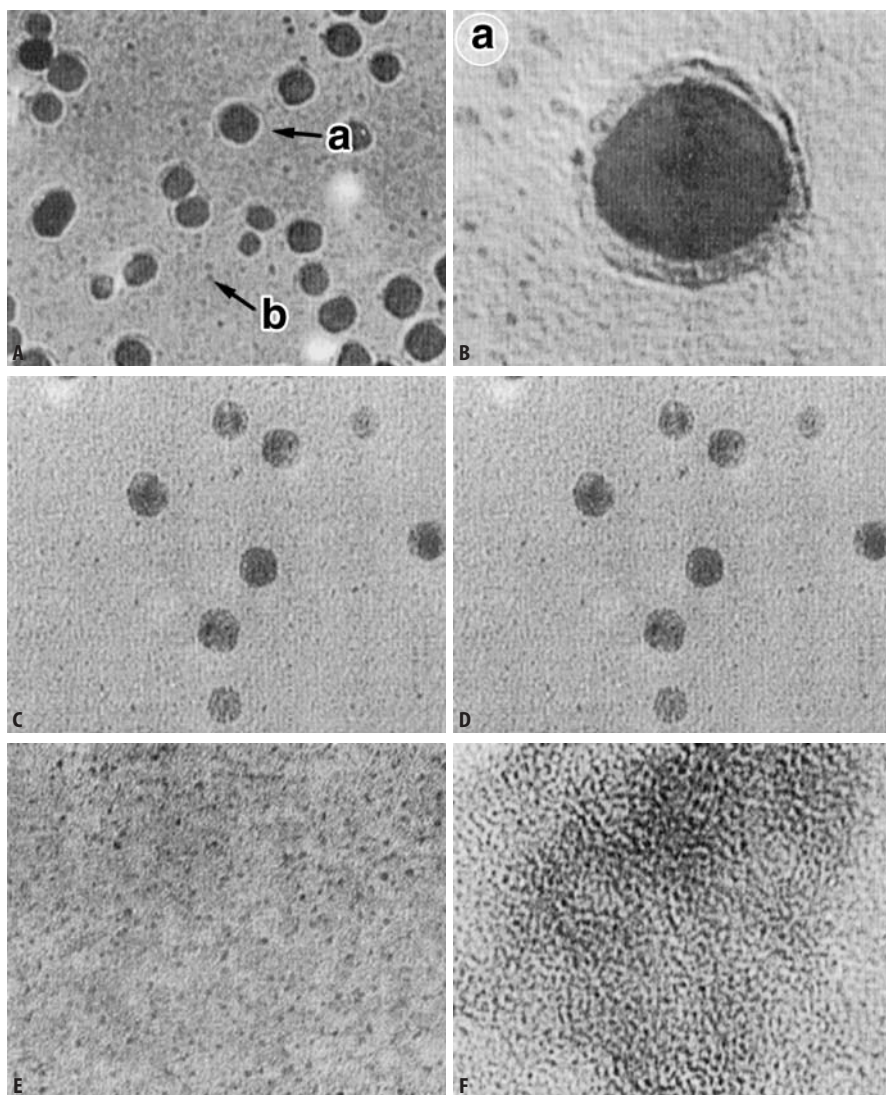


**Fig. 13A–F.** TEM images of platinum nanoparticles obtained by reduction of  $\text{Pt}^{4+}$  ions in the presence of PAMAM G5.5 in ethyl acetate at a mixing ratio of dendrimer:  $\text{H}_2\text{PtCl}_6=150:1$ ; **A** 5 min of elapsed time and concentration of dimethylamine borane  $18 \text{ mmol dm}^{-3}$ ; **B** enlargement of particle a; **C** enlargement of particle b; **D** 5 min of elapsed time and concentration of dimethylamine borane  $2 \text{ mmol dm}^{-3}$ ; **E** one day of elapsed time and concentration of dimethylamine borane  $18 \text{ mmol dm}^{-3}$ ; **F** three days of elapsed time and concentration of dimethylamine borane  $18 \text{ mmol dm}^{-3}$ . The concentration of  $\text{H}_2\text{PtCl}_6$  is  $0.2 \text{ mmol dm}^{-3}$ . Reprinted with permission from [30]. Copyright 2002 American Chemical Society

erably smaller than the diameter of G5.5 dendrimer at longer elapsed times, it is conceivable that many clusters of platinum are entrapped in the interior of G5.5 dendrimer. When the mixing ratio of  $[G5.5]/[H_2PtCl_6]$  is varied from 150 to 50, the average diameter of platinum is not appreciably changed. In addition, it is suggested that G3.5 dendrimer-encapsulated platinum particles are formed, while G1.5 dendrimers adsorb on the surface of platinum particles because the particle size of platinum obtained is larger than the diameter of G1.5 dendrimer.

In toluene, which is less polar organic solvent than ethyl acetate, dendrimer-gold nanoparticles have been synthesized using a hydrophobically modified PAMAM dendrimer [33]. The modified dendrimer is synthesized by reaction of PAMAM dendrimer with surface amino group with 1,2-epoxydodecane [34]. Solution of the hydrophobically modified dendrimer in toluene is carefully layered on top of  $HAuCl_4$  aqueous solution. After the solution stands for several hours at room temperature, a bright yellow color emerges in toluene. The extraction experiment is continued for one day. Since  $HAuCl_4$  is not soluble in toluene alone, it is reasonable to consider that  $AuCl_4^-$  ions should be incorporated in the interior of the hydrophobically modified dendrimer in toluene. Then, by addition of dimethylamineborane-toluene solution,  $AuCl_4^-$  ions are reduced. The average diameters of gold nanoparticles obtained range between 2.5 and 3.4 nm which is smaller than the diameter (4.5 nm) of G4 PAMAM dendrimer. A similar result has also been obtained using chloroform.

Another approach for the preparation of dendrimer-noble metal nanoparticles in toluene is a process driven by acid-base chemistry and ion pairing [35]. At first, palladium nanoparticles are prepared by reducing aqueous  $K_2PdCl_4$  with sodium borohydride in the presence of G4 dendrimer where the pH of dendrimer solution is adjusted to about 2. The low pH protonates the exterior amines to a greater extent than the less basic interior tertiary amines. Accordingly,  $Pd^{2+}$  binds preferentially to the interior tertiary amines and upon reduction palladium particles form within the dendrimer interior. After the complete reduction, the pH of solutions is adjusted back to about 8.5. Then, these nanocomposites can be quantitatively transported from the aqueous phase into toluene containing 10–20% of dodecanoic acid. The transition is visualized by the color change: brown aqueous solution of dendrimer-palladium nanoparticles becomes clear after addition of the acid, while the toluene layer turns brown.

## 4

### Synthesis of Dendrimer-Semiconductor Nanoparticles

Semiconductor nanoclusters (quantum dots) possess chemical and physical properties that differ substantially from those of the analogous bulk solids [36–38]. Quantum dots have been synthesized using hosts such as zeolites [39], porous glass [40], micelles [41], membranes [42], and anionic polymers [43]. The synthesis and characterization of CdS quantum dots in dendrimer hosts have been studied [44–48]. Here, two PAMAM dendrimers are used; one is G3.5 with surface carboxyl group and the other is G4 with surface amino group. Mixing solutions of  $Cd^{2+}$  and  $S^{2-}$  in pure methanol result in a yellow precipitate of

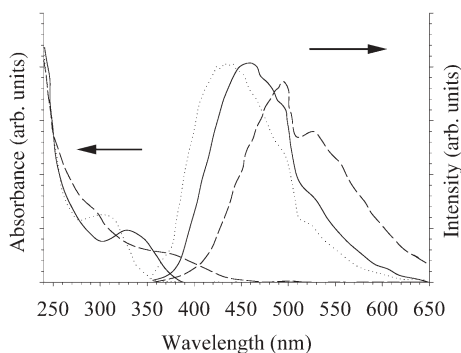


**Fig. 14.** Absorption (*left*) and photoluminescence (*right*) of CdS/COOH-D nanocomposites prepared in MeOH (*dotted curves*) and CdS/NH<sub>2</sub>-D nanocomposites prepared in MeOH (*solid curves*) and in water (*dashed curves*). Reprinted with permission from [45]. Copyright 2002 Wiley-VCH

bulk CdS after 10 min. However, mixing Cd<sup>2+</sup> and S<sup>2-</sup> in a methanol solution of dendrimer (either type) produces no precipitate. Photon correlation spectroscopy data show that these dendrimer-stabilized CdS clusters slowly associate to produce aggregates. At higher temperatures and reactant concentrations, aggregate diameter increases as a power of time, suggesting diffusion-limited colloidal aggregation. The dendrimer-stabilized CdS nanocluster aggregates remain colorless and free of precipitate for at least two months storage at -10°C. X-ray energy dispersive analysis confirms the presence of CdS in these solutions. It is postulated for the aggregation behavior that rapid nucleation and growth of CdS nanoclusters are followed by slow aggregation where nucleation occurs within the dendrimers. The most remarkable feature of the dendrimer-CdS nanocomposites is their optical properties. Absorbance measurements indicate that methanol solutions of dendrimer do not absorb light at wavelengths greater than about 250 nm. On the other hand, methanol solutions of dendrimer-CdS nanocomposites show significant absorption of UV light (Fig. 14) but almost none in the visible part of the spectrum (400–750 nm). These results indicate the presence of very small semiconducting CdS clusters. The size of these CdS clusters can be estimated from the absorption edge using Brus' effective mass model. From absorption edge values of 382 nm (CdS/NH<sub>2</sub>-D) and 349 nm (CdS/COOH-D), the Brus model predicts CdS cluster diameters of 2.8 and 2.4 nm, respectively.

Upon excitation with light at a wavelength of 340 nm, the same solutions manifest strong photoluminescence with emission maximizing at about 450 nm. Although the peak height varies in magnitude for samples prepared under identical conditions, the emission spectra have the same general features. In all cases, bright blue-green emission is observed. The emission quantum yield has been determined by comparing the integrated emission of CdS/NH<sub>2</sub>-D to that of a standard solution of Coumarin 47. The quantum yield of 0.22 has been obtained which is extremely larger than the quantum yield of less than 0.001 for CdS colloids. These results suggest that nanoparticles can provide a new class of lu-

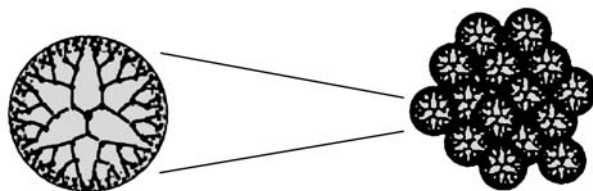


**Fig. 15.** Schematic representation of the model nanomolecular composite structure from SANS and SAXS measurements. *Left*, individual dendrimer molecule with CuS trapped at its periphery. *Right*, multimolecular cluster of individual dendrimer/CuS particles. Reprinted with permission from [49]. Copyright 2002 Elsevier Science

minophores for use in chemical sensing, DNA sequencing, high throughput screening, and other biotechnology applications. Linear polymer such as poly(ethylene imine) analogue of the dendrimer molecules can be used to make CdS nanocomposites with similar optical properties in solution, albeit with reduced quantum yield of emission.

Dendrimer-CuS nanocomposites have also been synthesized using G4 PA-MAM with surface hydroxyl group [49]. Complexation is accomplished by adding copper(II) acetate to a dilute solution of PAMAM dendrimer in deuterated water. Then, the solution is reacted with a slow stream of hydrogen sulfide gas. The structure of dendrimer-CuS nanocomposites has been studied by a combination of SAXS and SANS techniques. The physical size of the dendritic molecule is not perturbed by internal complexation of  $\text{Cu}^{2+}$  ions, or by the subsequent conversion of these ions into the neutral CuS species. Comparisons between SANS and SAXS measurements of dendrimer-copper complexes and dendrimer-CuS nanocomposites in solution indicate that the ions in the complexes are primarily distributed throughout the dendrimer molecules, but that conversion of the  $\text{Cu}^{2+}$  ions to neutral CuS molecules results in a redistribution of the inorganic species. The results imply that the CuS molecules in the nanocomposites are localized at the periphery of individual dendrimer molecules. In addition, a strong evidence of aggregation in the nanocomposite system suggests that the stable form of the dendrimer-CuS hybrid species in solution is in supermolecular clusters containing more than 50 individual dendrimer-copper sulfide molecules. A schematic representation of the dendrimer-CuS nanocomposites is shown in Fig. 15.

## References

1. Buhleier E, Wehner W, Vögtle F (1978) *Synthesis* 155
2. Tomalia DA, Baker H, Dewald JR, Hall M, Kallos G, Martin S, Roeck J, Ryder J, Smith PA (1985) *Polym J* 17:117
3. Newkome GR, Yao Z, Baker GR, Gupta VK (1985) *J Org Chem* 50:2003
4. Hawker CJ, Fréchet JMJ (1990) *J Am Chem Soc* 112:7638
5. Zeng F, Zimmerman SC (1997) *Chem Rev* 97:1681
6. Newkome GR, He E, Moorefield CN (1999) *Chem Rev* 99:1689

7. Bosman AW, Janssen HM, Meijer EW (1999) *Chem Rev* 99:1665
8. Astruc D, Chardac F (2001) *Chem Rev* 101:2991
9. de Gennes PG, Hervert HJ (1983) *J Phys Lett* 44:351
10. Lescanec RL, Muthukumar M (1990) *Macromolecules* 23:2280
11. Mansfield ML, Klushin LI (1993) *Macromolecules* 26:4262
12. Naidoo KJ, Hughes SJ, Moss JR (1999) *Macromolecules* 32:331
13. Tomalia DA, Naylor AM, Goddard WA III (1990) *Angew Chem Int Ed Engl* 29:138
14. Jackson CJ, Chanzy HD, Booy FP, Drake BJ, Tomalia DA, Bauer BJ, Amis EJ (1998) *Macromolecules* 31:6259
15. Li J, Piehler LT, Qin D, Baker JR Jr, Tomalia DA (2000) *Langmuir* 16:5613
16. Feldheim DL, Foss CA Jr (2002) (eds) *Metal nanoparticles*. Marcel Dekker, New York
17. Zhao M, Sun Li, Crooks RM (1998) *J Am Chem Soc* 120:4877
18. Balogh L, Tomalia DA (1998) *J Am Chem Soc* 120:7355
19. Floriano PN, Noble CO IV, Schoonmaker JM, Poliakoff ED, McCarley RL (2001) *J Am Chem Soc* 123:10,545
20. Esumi K, Suzuki A, Aihara N, Usui K, Torigoe K (1998) *Langmuir* 14:3157
21. Esumi K, Suzuki A, Yamahira A, Torigoe K (2000) *Langmuir* 16:2604
22. Zhao M, Crooks RM (1999) *Angew Chem Int Ed* 38:364
23. Ershov BG, Henglein A (1998) *J Phys Chem* 102:10,667
24. Balogh L, Valluzzi R, Laverdure KS, Gido SP, Hagnauer GL, Tomalia DA (1999) *J Nanoparticle Res* 1:353
25. Gröhn F, Bauer BJ, Akpalu YA, Jackson CL, Amis EJ (2000) *Macromolecules* 33:6042
26. Zhao M, Crooks RM (1999) *Chem Mater* 11:3379
27. Esumi K, Hosoya T, Suzuki A, Torigoe K (2000) *J Colloid Interface Sci* 226:346
28. Torigoe K, Suzuki A, Esumi K (2001) *J Colloid Interface Sci* 241:346
29. Esumi K, Kameo A, Suzuki A, Torigoe K (2001) *Colloids Surf A* 189:155
30. Esumi K, Nakamura R, Suzuki A, Torigoe K (2000) *Langmuir* 16:7842
31. Hierlemann A, Cambell JK, Baker LA, Crooks RM, Ricco AJ (1998) *J Am Chem Soc* 120:5323
32. Tsukruk VV, Rinderspacher F, Bliznyuk VN (1997) *Langmuir* 16:2171
33. Esumi K, Hosoya T, Suzuki A, Torigoe K (2000) *J Colloid Interface Sci* 229:303
34. Sayed-Sweet Y, Hedstrand DM, Spinder R, Tomalia DA (1997) *J Mater Chem* 7:1199
35. Chechik V, Zhao M, Crooks RM (1999) *J Am Chem Soc* 121:4910
36. Kamat PV (1997) *Prog Inorg Chem* 44:273
37. Vossmeier T, Katsikas L, Giersig M, Popovic IG, Diesner K, Chemseddine A, Eychmüller A, Weller H (1994) *J Phys Chem* 98:7665
38. Alivisatos AP (1996) *Science* 271:933
39. Herron N, Wang Y, Eddy MM, Stucky GD, Cox D, Moller K, Bein T (1989) *J Am Chem Soc* 111:350
40. Mathieu H, Richard T, Allegre J, Lefebvre P, Arnaud G, Granier W, Boudes L, Marc JL, Pradel A, Ribes M (1995) *J Appl Phys* 77:287
41. Pileni MP (1993) *Adv Colloid Interface Sci* 46:139
42. Zhao XK, Barai S, Orlando R, Fendler JH (1988) *J Am Chem Soc* 110:1012
43. Smotkin ES, Brown RM, Rahenberg LK, Salomon K, Bard AJ, Campion A, Fox MA, Mallouk TE, Webber ES, White JM (1990) *J Phys Chem* 94:7543
44. Lemon BI, Crooks RM (2000) *J Am Chem Soc* 122:12,886
45. Sookal K, Hanus LH, Ploehn HJ, Murphy CJ (1998) *Adv Mater* 10:1083
46. Luckowicz JR, Gryczynski I, Gryczynski Z, Murphy CJ (1999) *J Phys Chem B* 103:7613
47. Huang J, Sooklal K, Murphy CJ, Ploehn HJ (1999) *Chem Mater* 11:3595
48. Hanus LH, Sooklal K, Murphy CJ, Ploehn HJ (2000) *Langmuir* 16:2621
49. Beck Tan NC, Balogh L, Trevino SF, Tomalia DA, Lin JS (1999) *Polymer* 40:2537

# Organic Reactions in Microemulsions

Maria Häger<sup>1</sup>, Fredrik Currie<sup>2</sup>, Krister Holmberg<sup>2</sup>

<sup>1</sup> Institute for Surface Chemistry, P.O. Box 5607, 114 86 Stockholm, Sweden  
*E-mail: Maria.Hager@surfchem.kth.se*

<sup>2</sup> Chalmers University of Technology, Department of Applied Surface Chemistry,  
41296 Göteborg, Sweden,  
*E-mail: fcurrie@surfchem.chalmers.se, E-mail: kh@surfchem.chalmers.se*

The use of microemulsions as media for organic reactions is a way to overcome the reagent incompatibility problems that are frequently encountered in organic synthesis. In this sense, microemulsions can be regarded as an alternative to phase transfer catalysis. The microemulsion approach and the phase transfer approaches can also be combined, i.e. the reaction can be carried out in a microemulsion in the presence of a small amount of phase transfer agent. A very high reaction rate may then be obtained. The reaction rate in a microemulsion is often influenced by the charge at the interface and this charge depends on the type of surfactant used. For instance, reactions involving anionic reactants may be accelerated by cationic surfactants. The surfactant counterion also plays a major role for the reaction rate. The highest reactivity is obtained with small counterions, such as acetate, that are only weakly polarizable. Large polarizable anions, such as iodide, bind strongly to the interface and may prevent other anionic species to reach the reaction zone.

**Keywords.** Microemulsion, Surfactant, Organic synthesis, Catalysis, Nucleophilic substitution

1	Introduction . . . . .	54
2	Overcoming Reagent Incompatibility . . . . .	54
2.1	General . . . . .	54
2.2	Reaction in Winsor Systems . . . . .	55
2.3	Substitution Reactions . . . . .	57
2.4	Hydrolysis Reactions . . . . .	59
2.5	Miscellaneous Reactions . . . . .	61
3	Microemulsions vs Phase Transfer Catalysis . . . . .	62
4	Effect of the Surfactant and Surfactant Counterion on Reactivity . .	66
5	Inducing Regiospecificity . . . . .	70
6	Concluding Remarks . . . . .	72
	References . . . . .	72



## 1

### Introduction

Microemulsions are used as reaction media for a variety of chemical reactions. The aqueous droplets of water-in-oil microemulsions can be regarded as minireactors for the preparation of nanoparticles of metals and metal salts and particles of the same size as the starting microemulsion droplets can be obtained [1–3]. Polymerisation in microemulsions is an efficient way to prepare nanolatexes and also to make polymers of very high molecular weight. Both discontinuous and bicontinuous microemulsions have been used for the purpose [4]. Microemulsions are also of interest as media for enzymatic reactions. Much work has been done with lipase-catalysed reactions and water-in-oil microemulsions have been found suitable for ester synthesis and hydrolysis, as well as for transesterification [5, 6].

Microemulsions, being microheterogeneous mixtures of oil, water and surfactant, are excellent solvents for both polar and non-polar compounds. The capability of microemulsions to solubilize a broad spectrum of substances in a one-phase formulation has been found useful in preparative organic synthesis. Microemulsions are one way, out of several, to overcome the reagent incompatibility problems that one frequently encounters in preparative organic chemistry. The capability of microemulsions to compartmentalise and concentrate reagents can lead to unusual reactivity in organic synthesis. Attempts have also been made to use the oil-water interface of microemulsions as a template to induce regiospecificity of organic reactions.

This chapter deals with the use of microemulsions as media for organic synthesis. The distinguishing characteristics of microemulsion-based reactions, as well as typical examples of syntheses carried out in such media, will be discussed. Emphasis will be put on recent development in the area.

## 2

### Overcoming Reagent Incompatibility

#### 2.1

##### General

A common practical problem in synthetic organic chemistry is to attain proper phase contact between non-polar organic compounds and inorganic salts. There are many examples of important reactions where this is a potential problem: hydrolysis of esters with alkali, oxidative cleavage of olefins with permanganate-periodate, addition of hydrogen sulfite to aldehydes and to terminal olefins, preparation of alkyl sulfonates by treatment of alkyl chloride with sulfite or by addition of hydrogen sulfite to  $\alpha$ -olefin oxides. The list can be extended further. In all examples given there is a compatibility problem to be solved if the organic component is a large non-polar molecule.

There are various ways to solve the problem of poor phase contact in organic synthesis. One way is to use a solvent or a solvent combination capable of dissolving both the organic compound and the inorganic salt. Polar, aprotic sol-

vents, such as dimethylsulfoxide (DMSO) and tetrahydrofuran (THF), are sometimes useful for this purpose but many of these are unsuitable for large-scale work due to toxicity and/or difficulties in removing them by low vacuum evaporation.

Alternatively, the reaction may be carried out in a mixture of two immiscible solvents. The contact area between the phases may be increased by agitation. Phase transfer reagents, in particular quaternary ammonium compounds, are useful aids in many two-phase reactions. Also, crown ethers are very effective in overcoming phase contact problems; however, their usefulness is limited by high price. (Open-chain polyoxyethylene compounds often give a 'crown ether effect' and may constitute practically interesting alternative phase transfer reagents.)

Microemulsions are excellent solvents both for hydrophobic organic compounds and for inorganic salts. Being macroscopically homogeneous yet microscopically dispersed, they can be regarded as something between a solvent-based one-phase system and a true two-phase system. In this context microemulsions should be seen as an alternative to two-phase systems with phase transfer reagents. As will be shown below, the microemulsion and the phase transfer catalysis approaches can be combined. Addition of a phase transfer agent to a microemulsion can give very high reactivity.

Micellar solutions have also been used as media for organic reactions. Reactions in micellar solutions have much in common with reactions in microemulsions but the capability to solubilize hydrophobic components is much smaller in micellar solutions than in microemulsions. Micellar solutions are therefore of limited value for preparative purposes. For both systems separation of the surfactant from the product may constitute a work-up problem.

## 2.2

### Reaction in Winsor Systems

Organic reactions in microemulsions need not be performed in one-phase systems. It has been found that most reactions work well also in two-phase Winsor I or Winsor II systems, i.e. an oil-in-water microemulsion coexisting with excess oil or a water-in-oil microemulsion coexisting with excess water, respectively [7, 8]. A Winsor III system, i.e. a three-phase system in which a middle phase microemulsion coexists with both oil and water, has also been successfully used as reaction medium [9]. The transport of reactants from the excess oil or water phase to the microemulsion phase, where the reaction takes place, is evidently fast compared to the rate of the reaction. This is a practically important aspect on the use of microemulsions as media for chemical reactions because it simplifies the formulation work. Formulating a Winsor I or Winsor II system is usually much easier than formulating a one-phase microemulsion of the whole reaction mixture. Winsor systems can also be of value to simplify the work-up process, in particular to separate the product from the surfactant, as will be discussed below in Sect. 2.4 (see also [6]).

Figure 1 illustrates the use of Winsor I and Winsor II systems as reaction media for the synthesis of 1-phenoxyoctane from sodium phenoxide and 1-bromooctane. The reaction was performed in microemulsions based on various



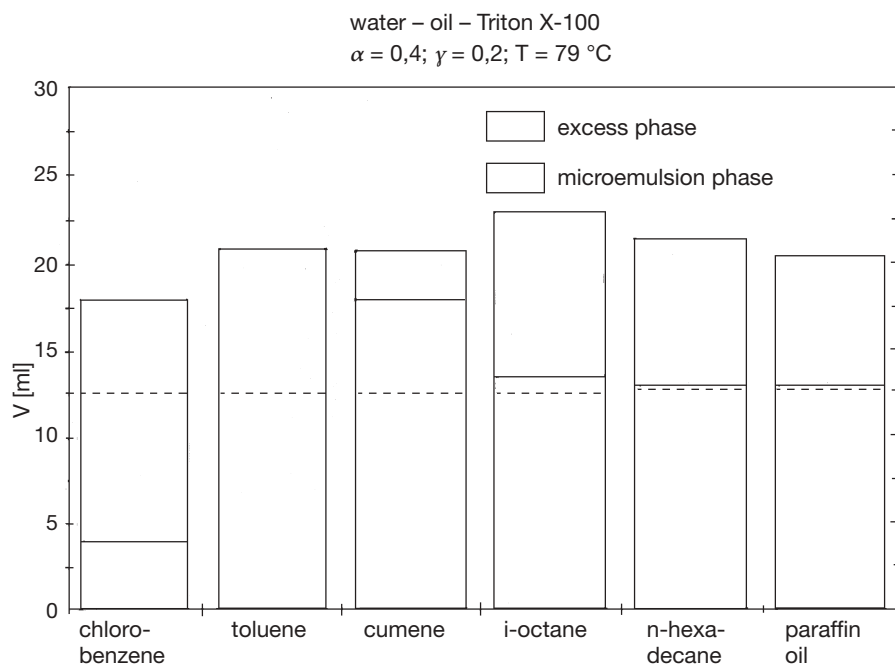


**Fig. 1.** Change of the phase volumes caused by variations of the oil component in the system oil-water-nonionic surfactant (redrawn from [8]). The microemulsions were used as reaction media for the reaction between sodium phenoxide and 1-bromooctane to give 1-phenoxyoctane

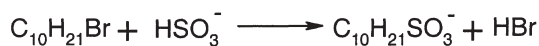
aliphatic and aromatic hydrocarbons as oil and with an octylphenol ethoxylate as surfactant [8]. The figure shows the relative phase volumes obtained with the different hydrocarbons. A one-phase microemulsion is only obtained with toluene as oil component. The more hydrophobic oils, i.e. cumene, isooctane, hexadecane and paraffin oil, all give a microemulsion in equilibrium with an excess oil phase, i.e. a Winsor I system. With the more hydrophilic chlorobenzene as oil a microemulsion coexisting with an excess water phase, i.e. a Winsor II system, is obtained. As is also shown in Fig. 1, the reactivity is highest in the chlorobenzene- and paraffin oil-based microemulsions, i.e. in the systems that are at the extremes in terms of phase separation. The relative reactivity is believed to be governed by the solubility of the surfactant in the oil. The higher the solubility, the less surfactant is available to form the interface. Since the reaction occurs exclusively at the interface (sodium phenoxide has no solubility in the oil and 1-bromooctane is insoluble in water), it is important to have as large an interface as possible.

The use of Winsor systems as reaction media is not unique to organic synthesis. Winsor I and Winsor II systems, as well as three-phase systems of Winsor III type, have been successfully employed as media for a variety of enzymatic reactions [7, 10–12].

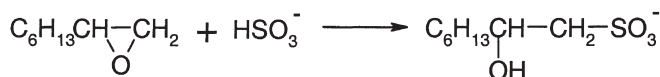
## 2.3

## Substitution Reactions

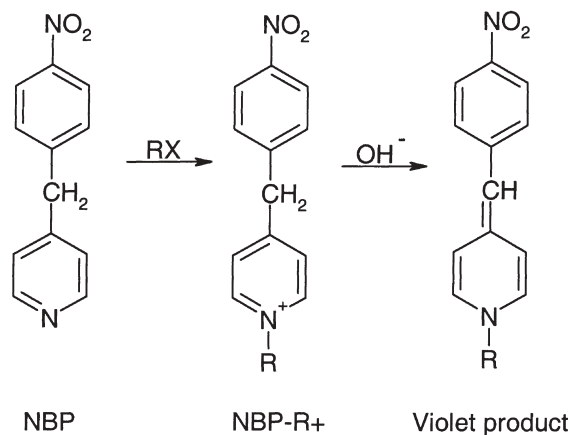
The majority of organic reactions that have been performed in microemulsions are substitution reactions, most commonly bimolecular nucleophilic substitutions, i.e.  $S_N2$  reactions. Figure 2 shows representative examples of such reactions that have been investigated in microemulsion media. Some of the reactions will be discussed below. Previous reviews can be consulted for other examples [13–15].



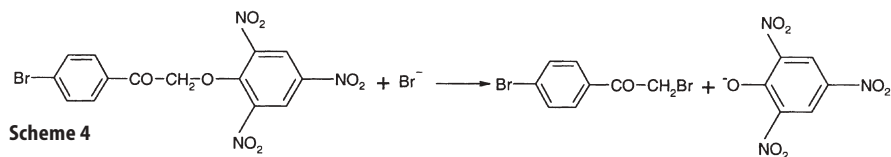
Scheme 1



Scheme 2



Scheme 3



Scheme 4

**Fig. 2.** Examples of nucleophilic substitution reactions performed in microemulsions. Scheme 1: synthesis of decyl sulfonate from decyl bromide and hydrogen sulfite. Scheme 2: synthesis of 2-hydroxyoctyl sulfonate from 1,2-epoxyoctane and hydrogen sulfite. Scheme 3: reaction of 4-nitrobenzylpyridine (NBP) with an alkyl halide (RX) followed by alkaline hydrolysis of the N-alkyl derivative (NBP-R<sup>+</sup>) formed. Scheme 4: a reaction involving displacement of the trinitrophenoxide ion by bromide

Oh et al. [16] have demonstrated that a microemulsion based on a nonionic surfactant is an efficient reaction system for the synthesis of decyl sulfonate from decyl bromide and sodium sulfite (Scheme 1 of Fig. 2). Whereas at room temperature almost no reaction occurred in a two-phase system without surfactant added, the reaction proceeded smoothly in a microemulsion. A range of microemulsions was tested with the oil-to-water ratio varying between 9:1 and 1:1 and with approximately constant surfactant concentration. NMR self-diffusion measurements showed that the 9:1 ratio gave a water-in-oil microemulsion and the 1:1 ratio a bicontinuous structure. No substantial difference in reaction rate could be seen between the different types of microemulsions, indicating that the curvature of the oil-water interface was not decisive for the reaction kinetics. More recent studies on the kinetics of hydrolysis reactions in different types of microemulsions showed a considerable dependence of the reaction rate on the oil-water curvature of the microemulsion, however [17]. This was interpreted as being due to differences in hydrolysis mechanisms for different types of microemulsions.

In a related reaction Anderson et al. used a microemulsion for ring opening of a long-chain epoxide with sodium hydrogen sulfite (Scheme 2 of Fig. 2) [9]. In two-phase systems with no surfactant added the reaction was very sluggish. Microemulsions based on alcohol ethoxylates proved to be efficient reaction media, giving almost complete conversion of epoxide to hydroxysulfonate in 2 h at 75°C. A microemulsion based on the anionic surfactant sodium dodecylsulfate gave a slower rate of epoxide consumption. In addition, the dodecylsulfate anion took an active part in the reaction, competing with the hydrogen sulfite ion as ring opening reagent. This may be a side reaction to consider in many cases where a microemulsion based on an anionic surfactant is used as medium for a nucleophilic substitution reaction.

Scheme 3 of Fig. 2 shows alkylation of 4-nitrobenzylpyridine (NBP) with alkyl halide (RX) followed by reaction with hydroxide ion to form a violet product. The reaction, which is used for the detection of alkylating agents, is a good example of the advantage of using a microemulsion as reaction medium [18, 19]. In the conventional procedure a non-aqueous solvent is employed to dissolve the oil soluble NBP and the RX. This solution is then treated with an aqueous base in a two-step process since NBP and base, when combined, slowly react to form an interfering blue colour. However, the use of an anionic microemulsion permits a combination of the two reagents in the same solution. The addition of  $\text{Ag}^+$  is required to effect alkylation by methyl iodide. The suggested mechanistic explanation is as follows: NBP is solubilized in the oil phase and is exposed to only a very low hydroxide ion concentration since  $\text{OH}^-$  is electrostatically repelled by the anionic interface. Added methyl iodide, aided by  $\text{Ag}^+$ , which is concentrated at the negatively charged interface, reacts with the NBP to form 4-nitrobenzyl-1-methylpyridinium ion ( $\text{NBP-Me}^+$ ). This more water-soluble ion is accessible to attack by  $\text{OH}^-$  to form the final violet product. Due to accumulation of  $\text{Ag}^+$  (from  $\text{AgNO}_3$ ) and  $\text{OH}^-$  (from  $\text{NaOH}$ ) in different domains of the microemulsion, the solubility product of  $\text{AgOH}$  is never exceeded.

Bunton and de Buzzaccarini have studied the kinetics of substitution reactions in microemulsions and compared the result with the reaction kinetics in

micellar solutions and also in true solutions. Scheme 4 of Fig. 2 shows an example of an  $S_N2$  reaction that has been investigated in some detail [20]. The reaction was performed in microemulsions based on the cationic surfactant cetyltrimethylammonium bromide (CTAB). It was found that the second-order rate constants in the microemulsion droplets were similar to those in CTAB micelles in water and in alcohol-water mixtures. The rates were slightly higher than those estimated for the reaction in water but smaller than rate constants in alcohol-water mixtures of low water content.

Microemulsions can be formulated with carbon dioxide in supercritical state instead of a hydrocarbon as nonaqueous solvent. Fluorinated surfactants are commonly used to prepare such microemulsions. Water-in-carbon dioxide microemulsions can be made and the droplet size has been found to be similar to the size of the droplets of water-in-hydrocarbon microemulsions with similar composition [21]. Such a microemulsion was used for conversion of benzyl chloride to benzyl bromide using KBr as hydrophilic nucleophile. The yield was an order of magnitude higher in the carbon dioxide microemulsion than in a conventional microemulsion at similar conditions, a fact that has been ascribed to low interfacial viscosity [22]. The big advantage with these microemulsions is the environmental friendliness and the ease of work-up associated with carbon dioxide as solvent.

## 2.4

### Hydrolysis Reactions

Many types of hydrolysis reactions have been performed in microemulsions and some examples are given in Fig. 3.

Mackay and coworkers have studied in detail alkaline hydrolysis of 4-nitrophenyl diphenyl phosphate, Scheme 1 of Fig. 3. This work has been driven by an interest to use microemulsions as a medium for decontamination of toxic substances such as chemical warfare agents [23–26]. Because the reacting species is the hydroxyl ion, the reaction is promoted by cationic surfactants and retarded by anionic surfactants. In the cationic microemulsion the intrinsic rate constant is approximately the same as in micelles. The observed rate constant, however, is higher in micelles due to their greater surface potentials. It is also observed that there is no effect of ionic strength on the rate of reaction up to an added electrolyte concentration of 0.5 mol/l, a clear indication of the reaction taking place in the microemulsion interfacial region where the effective ion strength is of the order of 3 mol/l. The effect of cosurfactant was investigated in some detail. It was found that some quaternary ammonium compounds, notably tri(octyl-decyl)methyl ammonium chloride, gave much faster reactions than the common alcohol cosurfactants. This could be a useful observation.

Scheme 2 of Fig. 3 shows an elegant way of catalysing the hydrolysis of a phosphate ester [26–28]. Iodosobenzoates, such as the one shown in the figure, are strong nucleophiles and are efficient agents for splitting of phosphate ester bonds. The iodosobenzoate of Fig. 3, Scheme 2 is fully ionised at pH 8 in a microemulsion based on a cationic surfactant. The same hydrolysis rate was obtained at pH 8 in the presence of the iodosobenzoate as at pH 11 in the absence of the

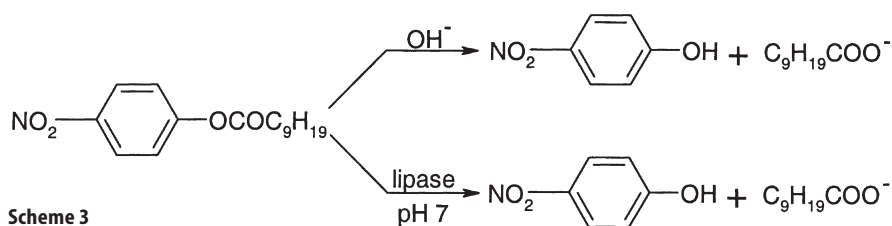
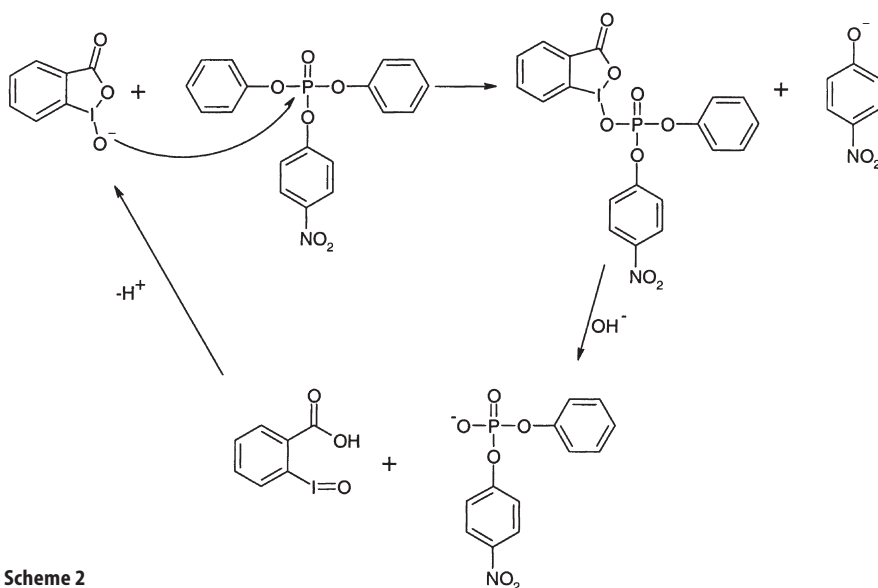
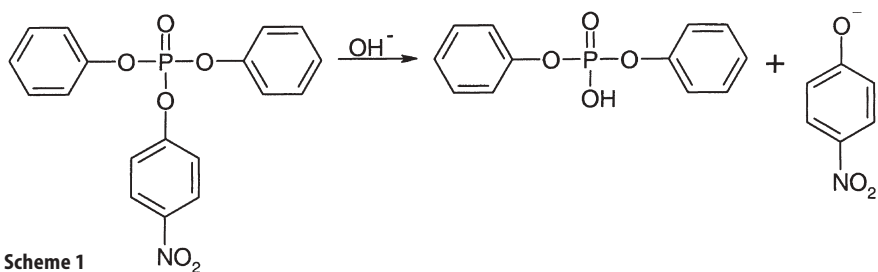


**Fig. 3.** Examples of hydrolysis reactions performed in microemulsions. Scheme 1: alkaline hydrolysis of 4-nitrophenyldiphenyl phosphate. Scheme 2: catalysis of phosphate ester hydrolysis by an iodosobenzoate. Scheme 3: alkali- and lipase-catalysed hydrolysis of 4-nitrophenyldecanoate

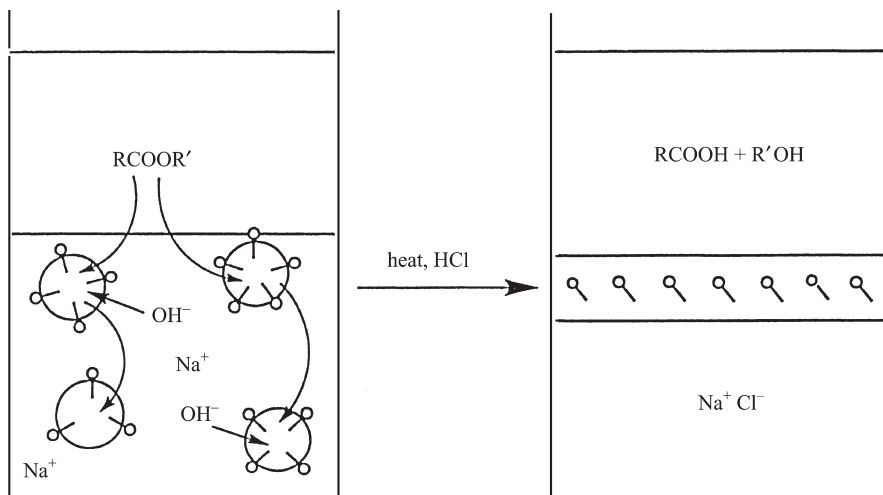


**Fig. 4.** Ester hydrolysis in a Winsor I system followed by heat-induced transition into a Winsor III system

iodosobenzoate. Thus, addition of the iodosobenzoate is a way to perform the detoxification reaction in a microemulsion under much milder conditions. As is seen from the figure, the reaction is a true catalytic reaction with no net consumption of the iodosobenzoate.

Lif and Holmberg have demonstrated the efficiency of microemulsions as a medium for both organic and bioorganic hydrolysis of a 4-nitrophenyl ester; see Scheme 3 of Fig. 3 [7]. The reactions were performed in a Winsor I type microemulsion and took place in the lower phase oil-in-water microemulsion. After the reaction was complete a Winsor I→III transition was induced by a rise in temperature. The products formed, 4-nitrophenol and decanoic acid, partitioned into the upper oil phase and could easily be isolated by separation of this phase and evaporation of the solvent. The principle is outlined in Fig. 4. The surfactant and the enzyme (in the case of the lipase-catalysed reaction) resided in the middle-phase microemulsion and could be reused.

## 2.5

### Miscellaneous Reactions

A wide variety of reactions other than substitutions and hydrolyses have been performed in microemulsions. Examples include alkylations [29], Knoevenagel condensations [13], oxidations [30, 31], reductions [32], formation and decomposition of Meisenheimer complexes [33], aromatic substitution reactions such as nitration and bromination [34–36], nitrosation [37] and lactone formation, i.e. esterification [38–40]. Microemulsions have also been used for photochemical and electrochemical reactions [41–45].

Figure 5 shows bromination of a small series of aromatic compounds performed in a microemulsion based on cationic surfactants. The bromide ion is at

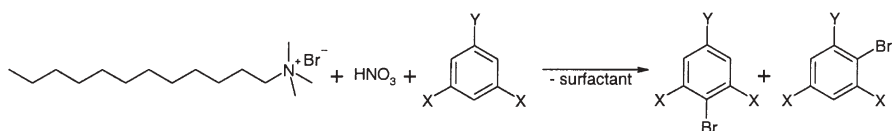


**Fig. 5.** Bromination of phenols and anisols using a quaternary ammonium bromide in combination with nitric acid as bromination reagent. Y is OH and OCH<sub>3</sub> for phenols and anisols, respectively. X is H or CH<sub>3</sub>

the same time surfactant counterion and source of the brominating agent. The reaction gives a quantitative yield of monobrominated species and an advantage compared to conventional bromination is that the procedure avoids the use of elemental bromine or other unpleasant bromination reagents.

### 3 Microemulsions vs Phase Transfer Catalysis

Use of a microemulsion to overcome reagent incompatibility can be seen as an alternative to the more conventional approach of carrying out the reaction in a two-phase system with the use of a phase transfer catalyst. The latter is usually either a quaternary ammonium salt or a crown ether. There are several examples in the literature of comparisons between the microemulsion concept and phase transfer catalysis. The topic has also recently been reviewed [46].

An early example of a comparison between the microemulsion approach and the process of phase transfer catalysis was a study by Menger et al. on the hydrolysis of trichlorotoluene to form sodium benzoate; see Fig. 6 [47]. As can be seen from Table 1, hydrolysis in the presence of the cationic surfactant

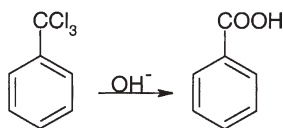


**Fig. 6.** Alkaline hydrolysis of trichlorotoluene

**Table 1.** Hydrolysis of trichlorotoluene to sodium benzoate using 20% NaOH at 80°C [47]. CTAB, C<sub>12</sub>E<sub>23</sub> and TBAB stand for cetyltrimethylammonium bromide, tricoso(ethylene glycol)monododecyl ether and tetrabutylammonium bromide, respectively

Additive	Reaction time (h)	Yield (%)
CTAB (0.01 mol/l)	1.5 <sup>a</sup>	98
None	1.5	0
Dioxane (20%)	1.5	0
C <sub>12</sub> E <sub>23</sub> (0.006 mol/l)	11 <sup>a</sup>	97
TBAB (0.02 mol/l)	15 <sup>a</sup>	98
None	60 <sup>a</sup>	97

<sup>a</sup> This is roughly the minimum time required for completion of the reaction.

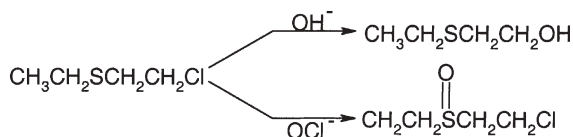


**Fig. 7.** Transformation of 2-chloroethylethyl sulfide (half-mustard) into 2-hydroxyethylethyl sulfide by alkali or into 2-chloroethylethyl sulfoxide by hypochlorite

cetyltrimethylammonium bromide (CTAB) required 1.5 h. The reaction without the surfactant took 60 h. The nonionic surfactant tricos(ethylene glycol)monododecyl ether ( $\text{C}_{12}\text{E}_{23}$ ) also accelerated the reaction but to a lesser extent than did CTAB. The commonly used phase transfer agent tetrabutylammonium bromide (TBAB) gave a rate enhancement comparable to that of the nonionic surfactant. Evidently the solubilizing power of a properly formulated microemulsion was at least as effective as phase transfer catalysis for overcoming the compatibility problems common to hydrolyses of lipophilic organic compounds.

In another comparison between the microemulsion approach and the use of phase transfer agents, Menger and Elrington investigated the decontamination of chemical agents, in particular bis(2-chloroethyl)sulfide, commonly known as mustard [30]. Mustard is a well-known chemical warfare agent. Although it is susceptible to rapid hydrolytic deactivation in laboratory experiments where rates are measured at low substrate concentrations, its deactivation in practice is not easy. Due to its extremely low solubility in water, it remains for months on a water surface. The addition of strong alkali does not increase the rate of reaction. Microemulsions were explored as media for both hydrolysis and oxidation of 'half-mustard',  $\text{CH}_3\text{CH}_2\text{SCH}_2\text{CH}_2\text{Cl}$ , a less toxic mustard model (Fig. 7). Oxidation with hypochlorite turned out to be extremely rapid in both oil-in-water and water-in-oil microemulsions. In formulations based on either an anionic, a nonionic or a cationic surfactant oxidation of the half-mustard sulfide to sulfoxide was complete in less than 15 s. The same reaction took 20 min when a two-phase system, together with a phase transfer agent, was employed [48]. Menger and Rourk have more recently made further progress in optimising microemulsion formulations for decontamination of chemical warfare agents [49].

Different types of microemulsions were evaluated as reaction media for synthesis of the surface active compound sodium decyl sulfonate from decyl bromide and sodium sulfite (Scheme 1 of Fig. 2). The reaction rates of the nucleophilic substitution reaction performed in microemulsions were compared with the rates obtained by phase transfer catalysis using either a quaternary ammonium salt (tetrabutylammonium hydrogen sulfate) or a crown ether (18-crown-6) as catalyst [50]. The microemulsions were based on the nonionic surfactant penta(ethylene glycol)monododecyl ether ( $\text{C}_{12}\text{E}_5$ ) and two compositions were used, one in the water-in-oil region (the L2 phase) and the other in the bicontinuous region. The reaction profiles are shown in Fig. 8. As can be seen, the reaction was much faster in the microemulsions than in the two-phase systems with added phase transfer agent. In the reference system, hydrocarbon-water with neither a surfactant, nor a phase transfer agent, there was virtually no reaction at all.



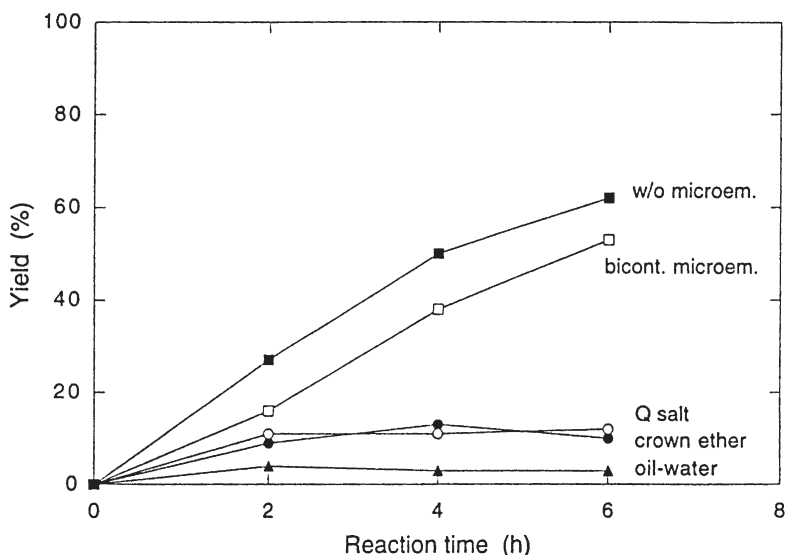


**Fig. 8.** Reaction profiles for synthesis of sodium decyl sulfonate from decyl bromide and sodium sulfite in either a microemulsion or a two-phase system with or without added phase transfer agent (from [50])

As can be seen from Fig. 8, the addition of a phase transfer agent to the two-phase system did not much affect the reaction rate. It has been suggested that the reason why phase transfer agents are not effective as catalysts in this reaction is that the product formed, decyl sulfonate, is a much more lipophilic anion than the inorganic ions. Hence,  $Q^+$  will prefer to form an ion pair with  $R-SO_3^-$  rather than with  $HSO_3^-$ , which means that transfer of the latter ion across the oil-water interface will decline as more and more decyl sulfonate is being produced during the course of the reaction. Figure 9 illustrates the competing processes.

Schomäcker compared the use of nonionic microemulsions with phase transfer catalysis for several different types of organic reactions and concluded that the former was more laborious since the pseudo-ternary phase diagram of the system had to be determined and the reaction temperature needed to be carefully monitored [13, 29]. The main advantage of the microemulsion route for industrial use is related to the ecotoxicity of the effluent. Whereas nonionic surfactants are considered relatively harmless, quaternary ammonium compounds exhibit considerable fish toxicity.

The use of a two-phase system with added phase transfer catalyst and the use of a microemulsion are two alternative approaches to overcome reagent incompatibility problems in organic synthesis. Both routes have proved useful but on entirely different accounts. In phase transfer catalysis the nucleophilic reagent is carried into the organic phase where it becomes highly reactive. In the microemulsion approach there is no transfer of reagent from one environment to another; the success of the method relies on the very large oil-water interface at which the reaction occurs.

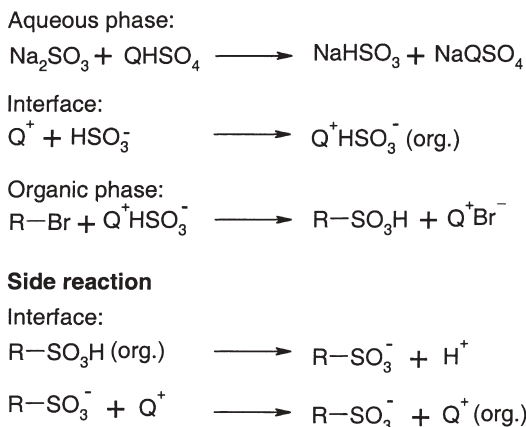


**Fig. 9.** Reaction steps involved in the synthesis of decyl sulfonate from decyl bromide and sodium sulfite using phase transfer catalysis. Q stands for tetrabutylammonium

In an attempt to combine the two approaches of accelerating organic reactions, a nucleophilic substitution reaction has been carried out in a microemulsion in the presence of a phase transfer agent [51]. The aim of the work was to investigate if a combination of the two approaches would give a reaction rate higher than that obtained in either the microemulsion approach or in a two-phase system using phase transfer catalysis.

The reaction chosen was ring-opening of 1,2-epoxyoctane by sodium hydrogen sulfite, Scheme 2 of Fig. 2. The synthesis was performed in an oil-in-water microemulsion based on a chlorinated hydrocarbon, water and surfactant with tetrabutylammonium hydrogen sulfate added to the formulation. Attempts to formulate a microemulsion with standard nonionic surfactants containing polyoxyethylene chains as polar head group failed, probably due to too high solubility of these surfactants in the oil domain. Polyol surfactants are less soluble in chlorinated hydrocarbons and a microemulsion with a relatively broad range of existence could be obtained by using a combination of two alkylglucoside surfactants. Figure 10 shows the reaction profiles for the synthesis carried out in a two-phase system with and without the phase transfer catalyst and in a microemulsion containing the catalyst. As can be seen, the combined approach leads to a very fast reaction. Obviously a substitution reaction in a microemulsion can be greatly accelerated by addition of a phase transfer catalyst.

An attempt was also made to accelerate the same reaction performed in a microemulsion based on water, nonionic surfactant and hydrocarbon oil [9]. The reaction was performed in a Winsor III system and the same Q salt, tetrabutyl ammonium hydrogen sulfate, was added to the formulation. In this case the addition of the phase transfer catalyst gave only a marginal increase in reaction rate. Similar results have been reported for an alkylation reaction performed in different types of micellar media [52]. The addition of a Q salt gave no effect for a system based on cationic surfactant, a marginal increase in rate for a system based on nonionic surfactant and a substantial effect when an anionic

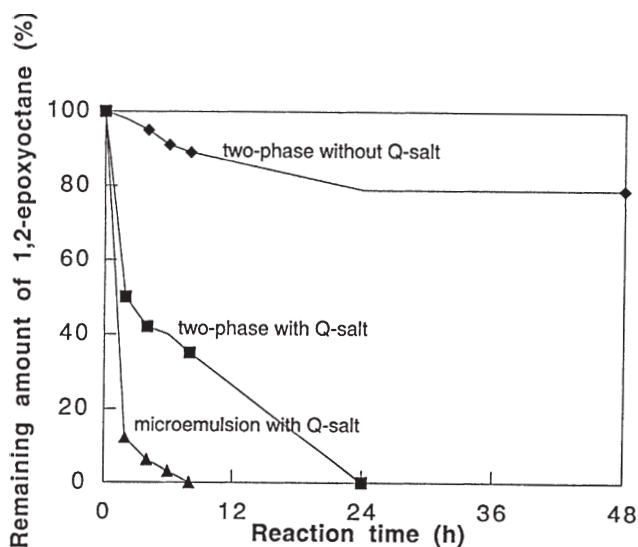


**Fig. 10.** Reaction profiles for synthesis of 2-hydroxyoctyl sulfonate from 1,2-epoxyoctane and hydrogen sulfite using either a two-phase system with or without added Q salt or a microemulsion with added Q salt as reaction medium. Q stands for tetrabutylammonium (from [51])

surfactant was used. The last system, also with Q salt added, gave lower yield than the first two, however, most likely due to electrostatic repulsion of the negatively charged nucleophile by the anionic micelles, as discussed above for microemulsion-based reaction media.

#### 4

#### Effect of Surfactant and Surfactant Counterion on Reactivity

Microemulsion droplets and micellar aggregates can catalyse or inhibit chemical reactions by compartmentalization and by concentration of reactants and products. The catalytic effect in micelles has been widely studied, a typical reaction being base catalysed hydrolysis of lipophilic esters. This rate enhancement is normally referred to as micellar catalysis. The analogous effect occurring in microemulsions may be called microemulsion catalysis.

The groups of Menger and Bunton have made early significant contributions to the understanding of the effect organized media has on catalysis of organic reactions [53, 54]. A number of kinetic studies, on hydrolysis and other reactions, have been made in micellar systems, i.e. aqueous solutions of surfactants at concentrations above the critical micelle concentration. The rate enhancement in such systems is often very substantial. The effect of micelle formation on reaction rates is primarily a consequence of reactant compartmentalization. Inclusion or exclusion of reactants from the Stern layer has either an accelerating or an inhibitory effect on the reaction rate, depending on reaction type and the nature of the micelle. The most widely used model to

describe these phenomena is the pseudophase kinetic model. This approach assumes that micelles act as a phase (pseudophase) apart from water. Further, it is assumed that effects on reaction rates are due primarily to the distribution of reactants between the micellar and aqueous pseudophases [55, 56]. The rate of a chemical reaction is then the sum of adjusted rates in the aqueous and micellar pseudophases. Although it has been clearly demonstrated that hydrolysis reactions of hydrophobic substrates can be strongly accelerated when carried out in micelles, true micellar catalysis is of limited preparative value (except when the surfactant itself is the reacting species) since the reactant concentration is normally too low. A micellar solution has a limited solubilization capacity. By introducing a nonpolar solvent into the system, i.e. by creating a microemulsion, a much higher solubilization capacity will be achieved. The pseudophase model has been successfully applied to microemulsion systems [56–58].

An excellent example of the importance of the surfactant charge for the reaction rate is given in Fig. 11. The reaction studied, iodosobenzoate-catalysed hydrolysis of a phosphate ester, was previously shown in Scheme 2 of Fig. 3 [26]. As can be seen from the figure, the reaction is slow and independent of water content when a nonionic amphiphile is used as microemulsion surfactant. In microemulsions based on a cationic surfactant the reaction is much faster and the rate is highly dependent on the relative amount of water. The reason for the higher reactivity in cationics-based microemulsions is obviously related to the charge of the interface; the negatively charged nucleophile is attracted by the positively charged surfactant palisade layer. The increase in reaction rate with an increase in water content is interpreted as an effect of increasing counterion, i.e. bromide, dissociation. An increase in counterion dissociation leads to a higher surface potential and, consequently, to a higher concentration of the anionic nucleophile in the interfacial zone, where the reaction occurs.

It has been shown that the addition of a small amount of the anionic surfactant sodium dodecyl sulfate (SDS) to a microemulsion based on nonionic surfactant increased the rate of decyl sulfonate formation from decyl bromide and sodium sulfite (Scheme 1 of Fig. 2) [59, 60]. Addition of minor amounts of the cationic surfactant tetradecyltrimethylammonium gave either a rate increase or a rate decrease depending on the surfactant counterion. A poorly polarizable counterion, such as acetate, accelerated the reaction. A large, polarizable counterion, such as bromide, on the other hand, gave a slight decrease in reaction rate. The reaction profiles for the different systems are shown in Fig. 12. More recent studies indicate that when chloride is used as surfactant counterion the reaction may at least partly proceed in two steps, first chloride substitutes bromide to give decyl chloride, which reacts with the sulfite ion to give the final product [61].

The effect of surfactant charge on the reaction rate was investigated for a related reaction, ring opening of 1,2-epoxyoctane with sodium hydrogen sulfite (Scheme 2 of Fig. 2). The reaction, which was performed in a Winsor III microemulsion, was fast when a nonionic surfactant was used as the sole surfactant and considerably more sluggish when a small amount of SDS was added to the formulation [9].

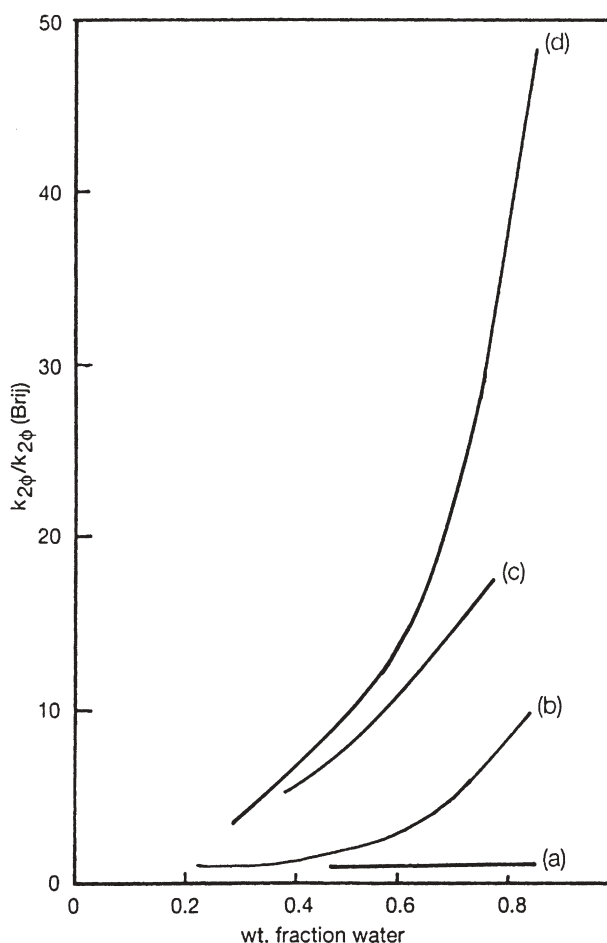


**Fig. 11.** Relative phase volume-corrected rate constants vs weight fraction water for the iodosobenzoate-catalysed hydrolysis of a phosphate ester in water/hexadecane microemulsions stabilized by various surfactant/cosurfactant mixtures. Curve (a) Brij 96/1-butanol; curve (b) CTAB/I-butanol; curve (c) CTAC/dibutylformamide; curve (d) CTAB/2-methylpyrrolidone and Adogen 464 (from [26])

An interesting example of a specific ion effect in microemulsions is a strong increase in reactivity found for large, polarizable anions such as iodide. The tendency for such ions to interact with, and accumulate at, the interface can be taken advantage of for preparative purposes. The increased concentration of such ions in the interfacial zone, where the reaction takes place, will lead to an increase in reaction rate. Expressed differently, the reactivity of iodide and other highly polarizable ions [62, 63] will be very high in such systems. The microemulsions need not be based on cationic surfactants that would drive the anions to the interface by electrostatic attraction. Also microemulsions based on non-ionic surfactants display the effect because large, polarizable anions interact

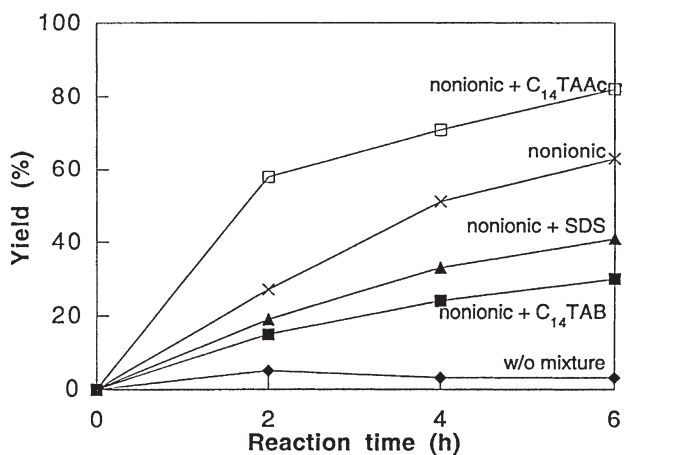


**Fig. 12.** Effect of addition of ionic surfactant to a microemulsion based on a nonionic surfactant on the rate of synthesis of decyl sulfonate from decyl bromide and sodium sulfite (from [60])

with the hydrophobic surface by dispersion forces [64]. The mechanism of attraction (and the background for the increased concentration of reacting species) is, thus, different from that of micellar catalysis, which is basically an ion exchange process [65].

In a recent work 4-*tert*-butylbenzylbromide was reacted with potassium iodide to give 4-*tert*-butylbenzyl iodide (Fig. 13). The reaction was performed in a microemulsion based on the nonionic surfactant penta(ethylene glycol)monododecyl ether (C<sub>12</sub>E<sub>5</sub>) and the temperature was varied from 23 to 29°C, which is the total temperature range of the isotropic L1 region of this system [66]. It was found that the reaction rate decreased considerably when the temperature was increased from 23 to 29°C. <sup>125</sup>I-NMR showed a marked temperature effect on line broadening; the lower the temperature the broader the signals (within the temperature range 23 to 29°C). This indicates that the iodide ion interacts more strongly with the interface at lower temperature, which is likely to be the reason for the inverse temperature-reactivity relationship. Thus, ion binding to the microemulsion interface can have a pronounced effect on reactivity also in microemulsions based on uncharged surfactants.



**Fig. 13.** Synthesis of 4-*tert*-butylbenzyl iodide from 4-*tert*-butylbenzyl bromide and sodium iodide

## 5 Inducing Regiospecificity

Organic molecules with one more polar and one less polar end will accumulate at the oil-water interface of microemulsions. They will orient at the interface so that the polar part of the molecule extends into the water domain and the non-polar part extends into the hydrocarbon domain. This tendency for orientation at the interface can be taken advantage of to induce regiospecificity in an organic reaction. A water-soluble reagent will react from the 'water side', i.e. attack the polar part of the amphiphilic molecule and a reagent soluble in hydrocarbon will react with the other end of the amphiphilic molecule. Figure 14 shows an example of the principle although the reaction in this case is performed in a micellar solution, not in a proper microemulsion [67]. The micelle-water interface is used as a template to control the regioselectivity of a Diels-Alder reaction in which both reactants are surface active. The diene (*a*), as well as the dienophile (*b*), is a lipophilic molecule with a trimethylammonium head group. This Diels-Alder system should display no regiochemical preference in the absence of orientational effects because the substituents at carbons 2 and 3 within *a* and those at carbons 1 and 2 within *b* are close to being both electronically and sterically equivalent with respect to the diene and dienophile reaction centres.

The two possible regioisomers of the reaction are shown in Fig. 15. When the reactions were run in an organic solvent, i.e. in absence of micellar orientational effects, the two regioisomers were obtained in equal amounts. When, on the other hand, the reactions were carried out in an aqueous buffer, in which the reagents form mixed micelles, a regioisomer ratio *c* to *d* of 3 was obtained. Product *c* is the expected regioisomer if *a* and *b* react in their preferred orientations within a mixed micelle, with the quaternary ammonium head groups at the outside of the aggregate and the remainder of the reactant molecules extended into the micelle interior. The fact that regioselectivity is not complete seems to indicate that a fraction of the reaction occurs outside of the micelles.

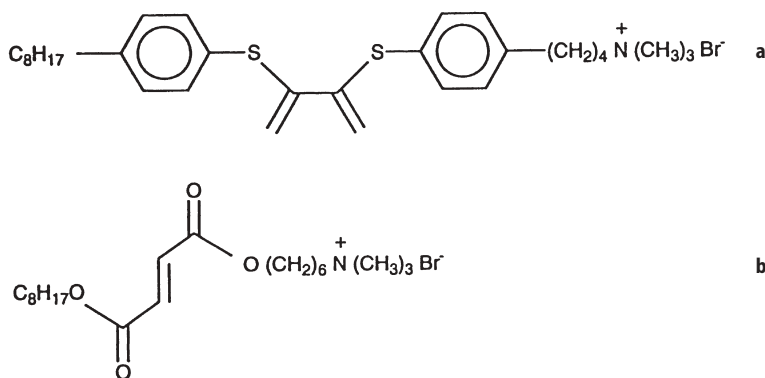


**Fig. 14.** A surface-active: **a** diene; **b** dienophile used as reagents in a Diels-Alder reaction

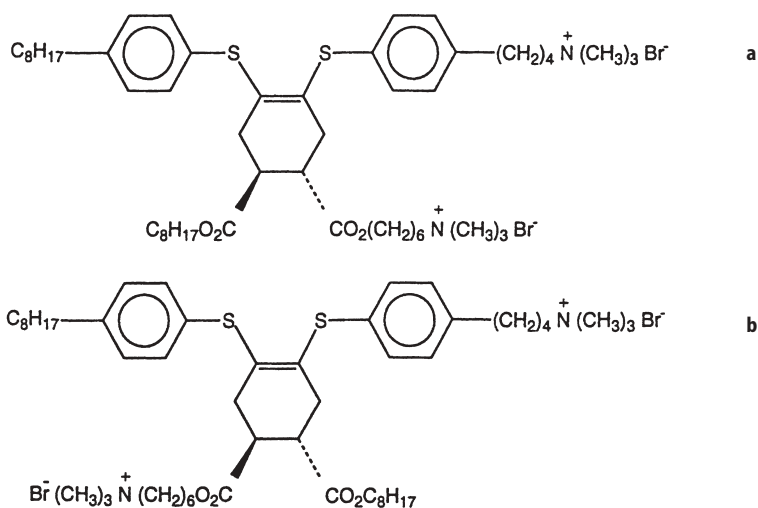


**Fig. 15a,b.** The two possible regioisomers formed by Diels-Alder reaction of the diene and the dienophile of Fig. 14

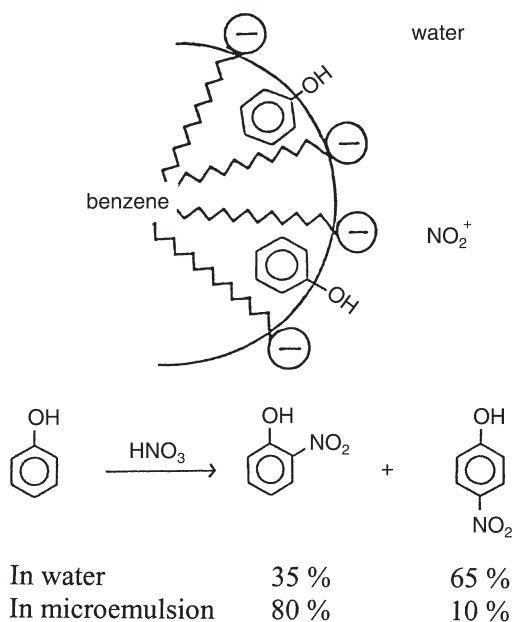


**Fig. 16.** Nitration of phenol in water and microemulsion (redrawn from [34])



Another example, this time in a proper microemulsion, is the stereoselective nitration of phenol, shown in Fig. 16. It has been claimed that the reaction in an oil-in-water microemulsion gives a preference for ortho nitration whereas conventional nitration in a homogeneous reaction system gives predominantly para nitration [34]. The results have been questioned, however, and nitration in microemulsion seems not to give very different ortho to para ratio than nitration in a homogeneous medium [36]. A related reaction, bromination of phenols and anisols (Fig. 5), gives a higher para to ortho ratio than conventional bromination [36]. The strong preference for para substitution can be of preparative value.

## 6

### Concluding Remarks

This review shows that microemulsions are of interest as media for organic reactions on several accounts. First of all they can be used as a means to overcome reagent incompatibility, which frequently occurs between a lipophilic organic compound and an inorganic salt. Used for this purpose they can be regarded as an alternative to the use of a two-phase system with added phase transfer catalyst. The concept of a microemulsion medium and phase transfer catalysis can also be combined to give a system of very high reactivity.

The reaction rate in microemulsions can be high not only because of the large internal interface but also because there can be a catalytic effect related to the interface. First, a charged interface, i.e. an oil-water interface stabilized by an ionic surfactant, will attract species, such as reacting nucleophiles, of opposite charge. Second, large polarizable ions, such as iodide or thiocyanate, will accumulate in the interfacial region due to strong interaction with the interface. This can substantially increase the rate of reactions involving such species.

The oil-water interface of microemulsions can also be used as a template for organic molecules with one more polar and one less polar end, thus inducing regioselectivity of reactions. Water-soluble reagents will attack the amphiphilic compound from the water side and oil-soluble species will react from the oil side.

### References

1. Pileni MP (1993) *J Phys Chem* 97:6961
2. Nagy JB (1999) In: Kumar P, Mittal KL (eds) *Handbook of microemulsion science and technology*. Marcel Dekker, New York, p 499
3. Pileni MP (2002) In: Rosoff M (ed) *Nano-surface chemistry*. Marcel Dekker, New York, p 315
4. Candau F (1999) In: Kumar P, Mittal KL (eds) *Handbook of microemulsion science and technology*. Marcel Dekker, New York, p 679
5. Holmberg K (1997) In: Solans C, Kunieda H (eds) *Industrial applications of microemulsions*. Surfactant science series 66. Marcel Dekker, New York, p 69
6. Holmberg K (1999) In: Kumar P, Mittal KL (eds) *Handbook of microemulsion science and technology*. Marcel Dekker, New York, p 713

7. Lif A, Holmberg K (1997) *Colloids Surf A* 129/130:273
8. Bode G, Lade M, Schomäcker R (2000) *Chem Eng Technol* 23:5
9. Andersson K, Kizling J, Holmberg K, Byström S (1998) *Colloids Surf A* 144:259
10. Sonesson C, Holmberg K (1991) *J Colloid Interface Sci* 141:239
11. Backlund S, Rantala M, Molander O (1994) *Colloid Polym Sci* 272:1098
12. Towey TF, Rees GD, Steytler DC, Price AL, Robinson BH (1994) *Bioseparation* 4:139
13. Schomäcker R (1992) *Nachr Chem Tech Lab* 40:1344
14. Holmberg, K (1994) *Adv Colloid Interface Sci* 51:137
15. Sjöblom J, Lindberg R, Friberg SE (1996) *Adv Colloid Interface Sci* 95:125
16. Oh S-G, Kizling J, Holmberg K (1995) *Colloids Surf A* 97:169
17. Hao J (2000) *J Dispersion Sci Technol* 21:19
18. Mackay RA, Seiders RP (1985) *J Dispersion Sci Technol* 6:193
19. Mackay RA (1991) *Actual Chim May/Jun*:161
20. Bunton CA, de Buzzaccarini F (1982) *J Phys Chem* 86:5010
21. Johnson KP, Lee CT, Li G, Psathas P, Holmes JD, Jacobson GB, Yates MZ (2001) In: Texter J (ed) *Reactions and synthesis in surfactant systems. Surfactant science series 100*. Marcel Dekker, New York, p 349
22. Jacobson GB, Lee CT, Johnston KP (1999) *J Org Chem* 64:1201
23. Mackay RA, Hermansky C (1981) *J Phys Chem* 85:739
24. Knier BL, Durst HD, Burnside BA, Mackay RA, Longo FR (1988) *J Solution Chem* 17:77
25. Mackay RA, Burnside BA, Garlick SM, Knier BL, Durst HD, Nolan PM, Longo FR (1988/1989) *J Dispersion Sci Technol* 9:493
26. Mackay RA (2001) In: Texter J (ed) *Reactions and synthesis in surfactant systems. Surfactant science series 100*. Marcel Dekker, New York, p 373
27. Garlick SM, Durst HD, Mackay RA, Haddaway KG, Longo FR (1990) *J Colloid Interface Sci* 135:508
28. Mackay RA, Longo FR, Knier BL, Durst HD (1987) *J Phys Chem* 91:861
29. Schomäcker R, Stickdorn K, Knoche W (1991) *J Chem Soc Faraday Trans* 87:847
30. Menger FM, Elrington AR (1991) *J Am Chem Soc* 113:9621
31. Häger M, Holmberg K, d'A Rocha Gonsalves AM, Serra AC (2001) *Colloids Surf A* 183/185:247
32. Jaeger DA, Ward MD, Martin CA (1984) *Tetrahedron* 40:2691
33. Bunton CA, de Buzzaccarini F, Hamed FH (1983) *J Org Chem* 48:2461
34. Chhatre AS, Joshi RA, Kulkarni BD (1993) *J Colloid Interface Sci* 158:183
35. Currie F, Holmberg K, Westman G (2001) *Colloids Surf A* 182:321
36. Currie F, Holmberg K, Westman G (2003) *Colloids Surfaces* (in press)
37. Garcia-Rio L, Leis JR, Pena ME (1993) *J Phys Chem* 97:3437
38. Gonzales A, Holt SL (1981) *J Org Chem* 46:2594
39. Galli C, Mandolini L (1982) *J Chem Soc Chem Commun* 251
40. Kumar A, Morén A-K, Holmberg K (2002) *J Dispersion Sci Technol* (in press)
41. Jones CE, Mackay RA (1978) *J Phys Chem* 82:63
42. Mackay RA (1994) *Colloids Surf A* 82:1
43. Willner I, Ford WE, Ottvos JW, Calvin M (1979) 280:823
44. Rusling JF (2001) In: Texter J (ed) *Reactions and synthesis in surfactant systems. Surfactant science series 100*. Marcel Dekker, New York, p 323
45. Thomalla M (2001) In: Texter J (ed) *Reactions and synthesis in surfactant systems. Surfactant science series 100*. Marcel Dekker, New York, p 295
46. Holmberg K, Häger M (2002) In: Mittal KL, Moudgil B, Shah DO (eds) *Proceedings of the 13th International Symposium on Surfactants in Solution*. Marcel Dekker, New York (in press)
47. Menger FM, Rhee JU, Rhee HK (1975) *J Org Chem* 40:3803
48. Ramsden JH, Drago RS, Riley R (1989) *J Am Chem Soc* 111:3958
49. Menger FM, Rourke MJ (1999) *Langmuir* 15:309
50. Gutfelt S, Kizling J, Holmberg K (1997) *Colloids Surf A* 128:265
51. Häger M, Holmberg K (2000) *Tetrahedron Lett* 41:1245

52. Siswanto C, Battal T, Schuss OE, Rathman JF (1997) *Langmuir* 13:6047
53. Menger FM, Portnoy CE (1967) *J Am Chem Soc* 89:4698
54. Bunton CA, Robinson L (1968) *J Am Chem Soc* 90:5972
55. Bunton CA (1991) In: Mittal KL, Shah DO (eds) *Surfactants in solution*, vol 11. Plenum, New York, p 17
56. Romsted LS, Bunton CA, Yao J (1997) *Curr Opinion Colloid Interface Sci* 2:622
57. Mackay RA (1982) *J Phys Chem* 86:4756
58. Bunton CA, de Buzzaccarini F (1982) *J Phys Chem* 86:5010
59. Oh S-G, Kizling J, Holmberg K (1995) *Colloids Surf A* 104:217
60. Holmberg K, Oh S-G, Kizling J (1996) *Progr Colloid Polym Sci* 100:281
61. Husein MM, Weber ME, Vera JH (2000) *Langmuir* 16:9159
62. Hofmeister F (1888) *Arch Exp Pathol Pharmacol* 24:247
63. Collins KD, Washabaugh MWQ ((1985) *Rev Biophys* 4:323
64. Ninham BW, Yaminsky VV (1997) *Langmuir* 13:2097
65. Romsted LS (1977) In Mittal KL (ed) *Micellization, solubilization and microemulsions*, vol 2. Plenum, New York, p 509
66. Häger M, Currie F, Holmberg K, Olsson U (2002) (to be submitted)
67. Jaeger DA, Wang J (1992) *Tetrahedron Lett* 33:137

# Miniemulsions for Nanoparticle Synthesis

K. Landfester

Max Planck Institute of Colloids and Interfaces, Research Campus Golm, 14424 Potsdam, Germany. E-mail: [katharina.landfester@mpikg-golm.mpg.de](mailto:katharina.landfester@mpikg-golm.mpg.de)

Miniemulsions are specially formulated heterophase systems consisting of stable nanodroplets in a continuous phase. The narrowly size distributed nanodroplets of 50 to 500 nm can be prepared by shearing a system containing oil, water, a surfactant, and an osmotic pressure agent which is insoluble in the continuous phase. Since each of the nanodroplets can be regarded as a batch reactor, a whole variety of reactions can be carried out starting from miniemulsions clearly extending the profile of classical emulsion polymerization. This article gives an overview about the mechanism of formation of and polymerizations in miniemulsions and reviews the current standing of the field for both the synthesis of new polymers and of dispersed hybrid systems.

**Keywords.** Polymer latex, Miniemulsion, Heterophase polymerization, Polymer nanoparticles, Composite particles

<b>1</b>	<b>Introduction</b>	<b>76</b>
<b>2</b>	<b>Miniemulsions and Miniemulsion Polymerization</b>	<b>78</b>
2.1	Emulsion Stability Against Ostwald Ripening, Collisions, and Coalescence	78
2.2	Techniques of Miniemulsion Preparation and Homogenization	79
2.3	Influence of the Surfactant	81
2.4	Influence of the (Ultra)hydrophobe	84
2.5	Inverse Miniemulsions	86
2.6	Preservation of Particle Identity Throughout Miniemulsion Polymerization	88
2.7	Surfactant Variation	88
2.8	Checklist for the Presence of a Miniemulsion	90
<b>3</b>	<b>Radical Polymerizations of Miniemulsions</b>	<b>91</b>
3.1	Mechanisms and Kinetics in Miniemulsion Polymerization	91
3.2	Droplet Size	92
3.3	Initiators	93
<b>4</b>	<b>Different Polymerization Reactions in Miniemulsions</b>	<b>95</b>
4.1	Radical Homopolymerization in Regular Miniemulsions	95
4.2	Formation of Particles in Non-Aqueous Solvents	96

4.3	Formation of Particles in Inverse Miniemulsion . . . . .	97
4.4	Nanocrystalline Polymers . . . . .	99
4.5	Radical Copolymerization . . . . .	100
4.5.1	Hydrophobic/Hydrophobic Copolymers . . . . .	100
4.5.2	Amphiphilic Copolymers . . . . .	101
4.6	Catalytic Chain Transfer in Miniemulsion . . . . .	103
4.7	Controlled Free-Radical Miniemulsion Polymerization . . . . .	103
<b>5</b>	<b>Hybrid Nanoparticles by Miniemulsion Technologies . . . . .</b>	<b>104</b>
5.1	Polymer-Polymer Hybrids . . . . .	104
5.2	Encapsulation of Pigments by Direct Miniemulsification . . . . .	105
5.3	Encapsulation of Carbon Black by Co-Miniemulsion . . . . .	107
5.4	Encapsulation of a Liquid – Formation of Nanocapsules . . . . .	107
5.5	Surface Coating of Miniemulsions with Inorganic Nanoparticles and Crystalline Building Blocks . . . . .	111
5.5.1	Miniemulsions with Silica Nanoparticles . . . . .	112
<b>6</b>	<b>Non-Radical Polymerizations in Miniemulsion . . . . .</b>	<b>114</b>
6.1	Polyaddition . . . . .	114
6.2	Anionic Polymerization . . . . .	116
6.3	Metal Catalyzed Polymerization Reactions . . . . .	116
<b>7</b>	<b>Inorganic Miniemulsions . . . . .</b>	<b>117</b>
<b>8</b>	<b>Conclusion . . . . .</b>	<b>119</b>
	<b>References . . . . .</b>	<b>120</b>

## 1

### Introduction

The synthesis and application of polymeric nanoparticles dispersed in a continuous media enjoy great popularity in academy and industry. This is due to a number of reasons. On the one hand the formulation of polymers without the use of organic solvents is of high importance because of security, health, and environmental reasons. Consequently, the formulation in an environmentally friendly solvent, in general water, is highly desired. This is why polymer science is confronted with the problems of dispersing or synthesizing more and more polymers in water, although dispersion in water might interfere with the polymerization process.

On the other hand, there is a technological trend towards a high solid content of polymer formulations, e.g., to minimize shrinkage effects or to shorten processing times. A high polymer content at reasonable processing viscosities can only be obtained by polymer dispersions, either in water or hydrocarbon solvents.

As a third advantage, polymer particles in dispersions allow one to control or imprint an additional length scale into a polymer bulk material, given by the diameter of the particle, which is offered by the process of film formation. That way, polymer materials can be generated employing rational structure design not only on the molecular scale, but also on the mesoscale.

Usually or most widely applied, polymer latexes are made by emulsion polymerization [1]. Without any doubt, emulsion polymerization has created a wide field of applications, but in the present context one has to be aware that an inconceivable restricted set of polymer reactions can be performed in this way. Emulsion polymerization is good for the radical homopolymerization of a set of barely water-soluble monomers. Already heavily restricted in radical copolymerization, other polymer reactions cannot be performed. The reason for this is the polymerization mechanism where the polymer particles are the product of kinetically controlled growth and are built from the center to the surface, where all the monomer has to be transported by diffusion through the water phase. Because of the dictates of kinetics, even for radical copolymerization, serious disadvantages such as lack of homogeneity and restrictions in the accessible composition range have to be accepted.

There are a variety of other techniques to generate polymer dispersions, such as polymerization of microemulsions, suspension polymerization, or the generation of secondary dispersions by precipitation, which will be discussed in more detail below. All of them found their applications which, however, cannot really be extended to more general procedures in polymer science since they are handicapped by serious disadvantages such as excessive use of surfactant, insufficient colloidal stability, or costly procedures. It is therefore an idealized concept in heterophase polymerization to generate small, homogeneous, and stable droplets of monomer or polymer precursors, which are then transferred by (as many as possible) polymer reactions to the final polymer latexes, keeping their particular identity without serious exchange kinetics being involved. This means that the droplets have to become the primary locus of the initiation of the polymer reaction. Then, polymerization or polyaddition should proceed as in a hypothetical bulk state, where the continuous phase is still good to transport initiators, side products, and heat. This is a state we call 'nanoreactors', since every droplet behaves as an independent reaction vessel without being seriously disturbed by all the other events.

With the concept of 'nanoreactors' one can take advantage of an additional mode control for the design of nanoparticles where both thermodynamic aspects as well as shear history enter the particle size and the inner structure of the latexes or hybrid particles. The polymerization in such nanoreactors takes place in a highly parallel fashion, i.e., the synthesis is performed in  $10^{18}$ – $10^{20}$  nanocompartments per liter that are separated from each other by a continuous phase. In miniemulsion polymerization, the principle of small nanoreactors is realized as demonstrated in Fig. 1.

In a first step of the miniemulsion process, small stable droplets in a size range between 30 and 500 nm are formed by shearing a system containing the dispersed phase, the continuous phase, a surfactant, and an osmotic pressure agent. In a second step, these droplets are polymerized without changing their identity.

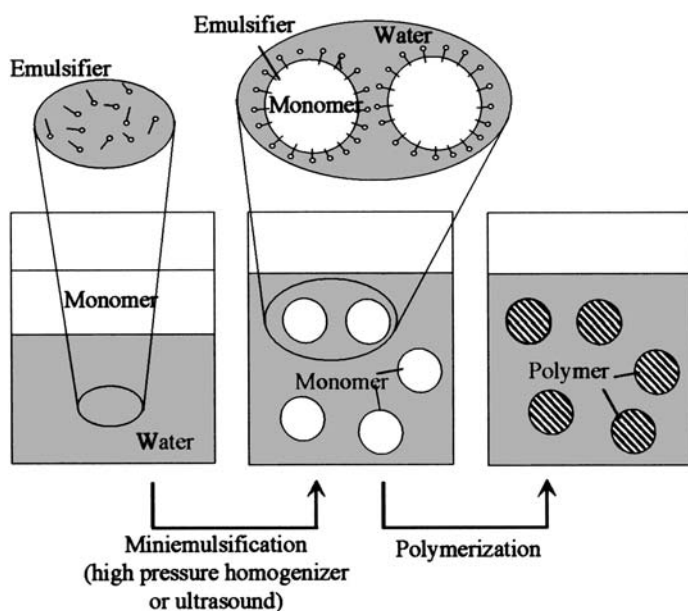


Fig. 1. The principle of miniemulsion polymerization

The main focus of this article is a detailed description of the working principles of miniemulsions, the examination of kinetics during the polymerization process, and the generation of different particle structures by appropriate handling of interface effects. It will be shown that miniemulsions are indeed not restricted to radical polymerization in water, but open the way to new polymers via a liquid/liquid technology both in direct (aqueous solvent) and inverse (organic or hydrocarbon solvent) situations. It will be shown that this principle is also highly favorable for the generation of nanoparticulate metals and ceramics, and for the encapsulation of nanoparticles into polymer shells to generate nanocomposites with high stability and processibility.

## 2

### Miniemulsions and Miniemulsion Polymerization

#### 2.1

##### Emulsion Stability Against Ostwald Ripening, Collisions, and Coalescence

Emulsions are understood as dispersed systems with liquid droplets (dispersed phase) in another, non-miscible liquid (continuous phase). Either molecular diffusion degradation (Ostwald ripening) or coalescence may lead to destabilization and breaking of emulsions. In order to create a stable emulsion of very small droplets, which is, for historical reasons, called a miniemulsion (as proposed by Chou et al. [2]), the droplets must be stabilized against molecular diffusion degradation (Ostwald ripening, a unimolecular process or  $\tau_1$  mechanism) and

against coalescence by collisions (a bimolecular process or  $\tau_2$  mechanism). Stabilization of emulsions against coalescence can be obtained by the addition of appropriate surfactants, which provide either electrostatic or steric stabilization to the droplets.

Mechanical agitation of a heterogeneous fluid containing surfactants always leads to a distribution of droplet sizes results. Even when the surfactant provides sufficient colloidal stability of droplets, the fate of this size distribution is determined by their different droplet or Laplace pressures, which increase with decreasing droplet sizes resulting in a net mass flux by diffusion between the droplets. If the droplets are not stabilized against diffusional degradation, Ostwald ripening occurs which is a process where small droplet will disappear leading to an increase of the average droplet size [3].

In 1962, Higuchi and Misra examined the quantitative aspects of the rate of growth of the large droplets and the rate of dissolution of the small droplets in emulsion for the case in which the process is diffusion controlled in the continuous phase [4]. It was proposed that unstable emulsions may be stabilized with respect to the Ostwald ripening process by the addition of small amounts of a third component, which must distribute preferentially in the dispersed phase [4]. The obtained stability in miniemulsions is said in the literature to be *metastable* or *fully stable*. The stabilization effect by adding a third component was recently theoretically described by Webster and Cates [5]. The authors considered an emulsion whose droplets contain a trapped species, which is insoluble in the continuous phase, and studied the emulsion's stability via the Lifshitz-Slyozov dynamics (Ostwald ripening).

The rate of Ostwald ripening depends on the size, the polydispersity, and the solubility of the dispersed phase in the continuous phase. This means that a hydrophobic oil dispersed as small droplets with a low polydispersity already shows slow net mass exchange, but by adding an 'ultrahydrophobe', the stability can still be increased by additionally building up a counteracting osmotic pressure. This was shown for fluorocarbon emulsions, which were based on perfluorodecaline droplets stabilized by lecithin. By adding a still less soluble species, e.g., perfluorodimorphinopropane, the droplets' stability was increased and could be introduced as stable blood substitutes [6, 7].

## 2.2

### Techniques of Miniemulsion Preparation and Homogenization

In order to obtain emulsification, a premix of the fluid phases containing surface-active agents and further additives is subjected to high energy for homogenization. Independent of the technique used, the emulsification includes first deformation and disruption of droplets, which increase the specific surface area of the emulsion, and second, the stabilization of this newly formed interface by surfactants.

In early papers, miniemulsions were prepared by using mechanical homogenization, e.g., by simple stirring or by the use of an omni-mixer and an ultra-turax. However, the energy transferred by these techniques is not sufficient to obtain small and homogeneously distributed droplets [8]. A much higher energy



for the comminuting of large droplets into smaller ones is required, significantly higher than the difference in surface energy  $\gamma\Delta A$  (with  $\gamma$  the surface/interfacial tension and  $\Delta A$  the difference between former and the newly formed interface), since the viscous resistance during agitation absorbs most of the energy.

In high force dispersion devices, ultrasonication is used today especially for the homogenization of small quantities, whereas rotor-stator dispersers with special rotor geometries, microfluidizers, or high-pressure homogenizers are best for the emulsification of larger quantities.

Power ultrasound emulsification was first reported in 1927 [9]. There are several possible mechanisms of droplet formation and disruption under the influence of longitudinal density waves [10–12]. Cavitation is the mechanism generally regarded as crucial under practical conditions [13, 14]. Parameters positively influencing cavitation in liquids improve emulsification in terms of smaller droplet size of the dispersed phase right after disruption. Imploding cavitation bubbles cause intensive shock waves in the surrounding liquid and the formation of liquid jets of high velocity with enormous elongational fields [15]. This may cause droplet disruption in the vicinity of the collapsing bubble. However, the exact process of droplet disruption, due to ultrasound as a result of cavitation, is not yet fully understood.

Using a high-pressure homogenizer with an orifice valve [16], it was shown that the time droplets spend in the laminar flow is long enough for a large number of disruption steps to take place subsequently, because the deformation time is much lower than the mean residence time in the elongation flow. During the deformation and break-up of a single droplet, almost no surfactant molecule adsorbs at the newly forming interface because the adsorption time is longer than one disruption step. This is why a special mechanical design to ensure either highly turbulent flow after disruption or sufficient residual times in the elongational flow is necessary to enable surfactant adsorption at the newly formed droplets. Then the disruption process can be facilitated by the presence of surfactants.

In direct miniemulsions, the droplet size is in turn determined by the amount of oil and water, the oil density, the oil solubility, and the amount of surfactant. It is found for direct miniemulsions that the droplet size is initially a function of the amount of mechanical agitation [17, 18]. The droplets also change rapidly in size throughout sonication in order to approach a pseudo-steady state, assuming a required minimum amount of energy for reaching this state is used. Once this state is reached, it was found that the size of the droplet does not change any more. At the beginning of homogenization, the polydispersity of the droplets is still quite high, but by constant fusion and fission processes the polydispersity decreases, and the miniemulsion then reaches a steady state (see Fig. 2) [19].

The process of homogenization can be followed by different methods, e.g., by turbidity, by conductivity, and by surface tension measurements. With increasing time of ultrasound, the droplet size decreases and therefore the entire oil/water interface increases. Since a constant amount of surfactant has now to be distributed onto a larger interface, the interfacial tension as well as the surface tension at the air/emulsion interface increases since the droplets are not fully covered by surfactant molecules. The surface tension can reach a value

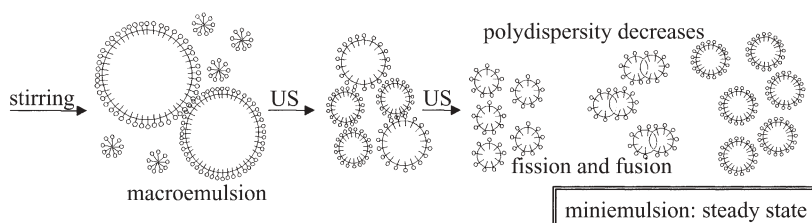


**Fig. 2.** Scheme for the formation of a miniemulsion by ultrasound (US)

close to  $60 \text{ mN m}^{-1}$ , indicating that the coverage of the droplets is indeed very low (calculated as 10% of a dense layer). The conductivity of the system is characterized by the surfactant and its distribution between the different bound states only. The conductivity due to free surfactant molecules, to surfactant micelles as well as the conductivity of charged dispersion droplets will also differ significantly. Increasing the droplet number during ultrasonication will decrease the free surfactant molecules and micelles; this is always accompanied with a strong decrease of the conductivity till an equilibrium is reached as seen in Fig. 3. The surface tension and the conductivity measurements are sensitive to the total oil/water interface, but both techniques can hardly distinguished between polydisperse and monodisperse systems as long as the overall interfacial area in the system is the same. Supplementing turbidity measurements (included in Fig. 3), which are sensitive to the size and size distribution of the droplets, equilibrate later than the surface tension or conductivity measurements, indicating the complexity of the underlying equilibration process.

The droplet size and size distribution seems to be controlled by a Fokker-Planck type dynamic rate equilibrium of droplet fusion and fission processes, i.e., the primary droplets are much smaller directly after sonication, but colloidally unstable, whereas larger droplets are broken up with higher probability. This also means that miniemulsions reach the minimal droplet sizes under the applied conditions (surfactant load, volume fraction, temperature, salinity, etc.), and therefore the resulting nanodroplets are at the critical borderline between stability and instability. This is why miniemulsions directly after homogenization are called 'critically stabilized' [19, 20]. Practically speaking, miniemulsions potentially make use of the surfactant in the most efficient way possible.

## 2.3

### Influence of the Surfactant

Colloidal stability is usually controlled by the type and amount of the employed surfactant. In miniemulsions, the fusion-fission rate equilibrium during sonication and therefore the size of the droplets directly after primary equilibration depends on the amount of surfactant. For sodium dodecylsulfate (SDS) and styrene at 20% dispersed phase, it spans a range from 180 nm (0.3% SDS relative to styrene) down to 32 nm (50 rel.% SDS) (Fig. 4a). Again, it is anticipated that rapidly polymerized latexes also characterize the parental miniemulsion. As

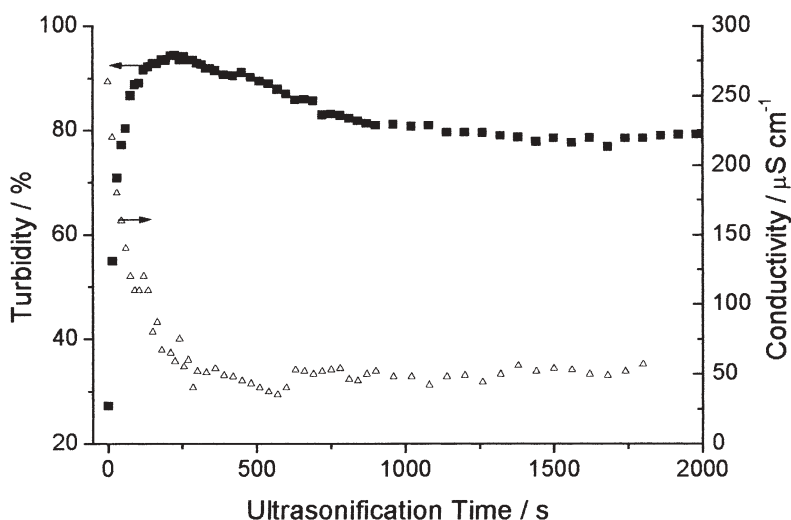


**Fig. 3.** Homogenization process followed by surface tension and conductivity measurements until a steady state is reached

compared to emulsion- and microemulsion polymerization, those particles are – with respect to the amount of used surfactant – very small, comparable to the best emulsion polymerization recipes. A latex with a particle size of 32 nm is already translucent and very close to the size, which was obtained in a microemulsion polymerization process with no hydrophobe, but the fourfold amount of a SDS/alcohol mixture [21].

The area per surfactant molecule on the particle surface,  $A_{\text{surf}}$ , also show a strong dependence on the particle size. It is seen that the entire range from a dense surfactant monolayer ( $A_{\text{surf}}$  about  $0.4 \text{ nm}^2$ ) for small particles to very incompletely covered latex particles ( $A_{\text{surf}}$  about  $7 \text{ nm}^2$ ) is obtained (see Fig. 4b). This reflects the fact that smaller particles have at comparable volume fractions a higher particle number density, a shorter averaged surface-to-surface distance, a higher relative mobility, and lower potential barriers, and therefore rely on denser surfactant layers to become colloidally stable. Since surfactant layer densities also influence the chemistry of such objects, e.g., permeation rates through the interface or enrichment of polar components within the droplet, this effect is important to remember: certain effects and reactivities might depend on the droplet size and work better for larger particles, which is somewhat counterintuitive.

It is a matter of course that the different surfactant coverages are also reflected in the corresponding surface tensions  $\gamma$  of the latexes (see Fig. 4b). An increase of the surface tension with increasing diameter is observed. The miniemulsions based on polystyrene particles exceeding 100 nm have a surface tension of close to the one of pure water ( $72 \text{ mN m}^{-1}$ ). This is due to the fact that the bare particle surface is so large that adsorption equilibrium ensures a very low surfactant solution concentration. Smaller particles with their higher sur-

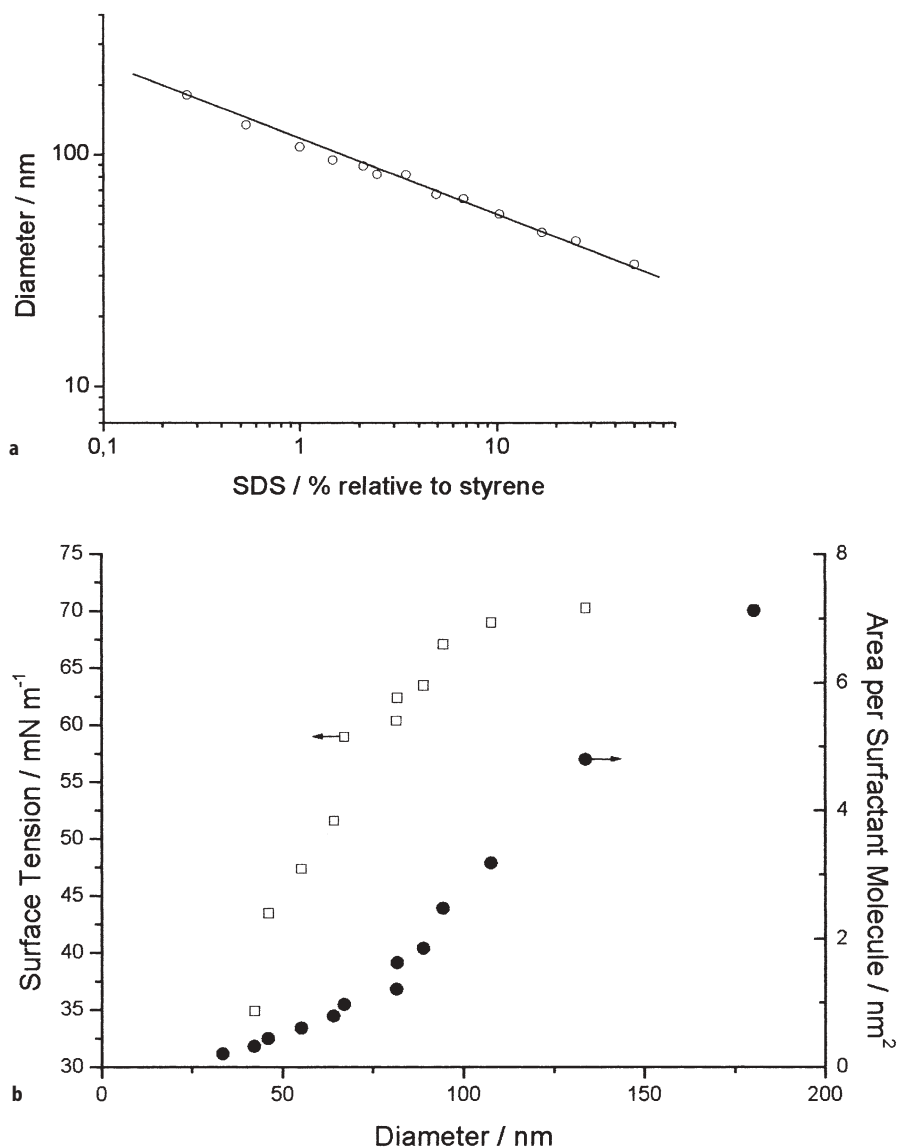


**Fig. 4.** a Polystyrene particle size vs amount of SDS (KPS as initiator); b Surface tension of the latexes and coverage of the particles in dependence of particle size

face coverage also have a higher equilibrium concentration of free surfactant, but the concentration usually still stays well below the critical micelle concentration value (cmc). This means that in miniemulsions there are no free micelles present. This is very important for the chemical reactivity and the polymerization kinetics in such systems. Just in the case of the highest surfactant load (50% SDS), a dense surface layer and a  $\gamma$  value typical for a micellar phase are observed. Here we leave the composition region for well-defined miniemulsions.

## 2.4

### Influence of the (Ultra)hydrophobe

As stated above, the destabilization of nanodroplets by Ostwald ripening after the homogenization process can be efficiently slowed down by an addition of a hydrophobic agent to the dispersed phase, which now counteracts the droplet or Laplace pressure of the droplet. The agent has to be chosen so that it is trapped in each droplet and cannot diffuse from one droplet to the other. The effectiveness of the hydrophobe increases with decreasing water solubility in the continuous phase and there is a low but finite hydrophobe content in order to become operative to efficiently suppress Ostwald ripening. Many ultrahydrophobes can be used for the formulation of miniemulsions: beside hexadecane as a model [22, 23], other alkanes with different chain lengths [24], hydrophobic dyes [25], hydrophobic comonomers [26, 27], chain transfer agents [28, 29], hydrophobic initiators [30, 31], plasticizers, silanes, siloxanes, isocyanates, polyester, fluorinated alkanes [20], or other additives are effective agents to prevent Ostwald ripening. Long chain alcohols which acts as a hydrophobe and a cosurfactant at the same time [32, 33] are less effective.

A steady-state of miniemulsification is reached if an efficient homogenization process is performed and an adequate amount of hydrophobe is used. After stopping sonication, a rather rapid and minor equilibration process has to occur where the effective chemical potential in each droplet (which can be expressed as an effective net pressure) is equilibrating. Since the droplet number after sonication is fixed, the averaged size is also not influenced by this process, but the droplet size distribution usually undergoes very fast change. It can be calculated that the Laplace pressure within the resulting nanodroplets and the osmotic pressure created by the hydrophobe are still far away from being equal: the Laplace pressure is still larger than the osmotic pressure. It was found that steady-state miniemulsification results in a system 'with critical stability', i.e., the droplet size is the product of a rate equation of fission by ultrasound and fusion by collisions, and the minidroplets are as small as possible for the time scales involved [19].

The Laplace pressure  $p_{\text{Laplace}}$  and the osmotic pressure can be calculated as shown in [20]. For a typical hexadecane concentration of 2 mol% relative to styrene, this results in an osmotic pressure of 4.5 bar, which is usually well below the Laplace pressure of 12 bar in a typical miniemulsion system (1.7% SDS relative to styrene, ca. 100 nm diameter). This means that right after steady-state miniemulsification the droplet size is not given by an effective zero droplet pressure, i.e.,  $p_{\text{Laplace}} - \Pi_{\text{osm}} = 0$ , which would represent a real thermodynamic

equilibrium state, but it is rather characterized by a state of equal pressure in all droplets. Minor statistical differences of the pressure directly after sonication are presumably rapidly equilibrated, since changing the particle size leads to an adaptation of the Laplace pressure with  $R^{-1}$ , whereas the osmotic pressure goes with  $R^{-3}$ . This means that minor changes in size change the pressure balance significantly.

The equality of droplet pressures makes such systems insensitive against net mass exchange by diffusion processes (after the very fast equilibrium process at the beginning), but the net positive character of the pressure makes them sensitive to all changes of the droplet size. Experimental observations were made [19] that steady-state homogenized miniemulsions, which are critically stabilized, undergo droplet growth on the timescale of hundreds of hours, presumably by collisions or by hydrophobe exchange. The droplets seem to grow until a zero effective pressure is reached. Accordingly to Webster and Cates these miniemulsions are then fully stable [5]. It is, however, possible to obtain immediate long-term colloidal stability of miniemulsions by addition of an appropriate second dose of surfactant after the dispersion step. This dose is not used to increase the particle number, but goes to the bare interface of the preformed miniemulsion droplets in order to decrease the interfacial tension between the oil and the water phase and to decrease the coupled Laplace pressure. Such post-stabilized miniemulsions do not change their droplet size on the timescale of days and even several months. This leads to the conclusion that most miniemulsions described in the literature are indeed thermodynamically only metastable, i.e., with respect to conservation of particle number they are in a local minimum of the chemical potential, which, however, is deep enough to allow chemical reactions without significant change of the particle size and structure.

The particle size of rapidly polymerized minidroplets does not or does just weakly depend on the amount of the hydrophobe [34–36]. It was found that doubling the amount of hydrophobe does not decrease the radius by a factor of 2 (as expected from a zero effective pressure), it is just that the effective pressure (pressure difference) has to be the same in every droplet, a mechanism which in principle does not depend on the amount of hydrophobe [19]. However, a minimum molar ratio of the hydrophobe to the monomer of about 1:250 is required in order to build up a sufficient osmotic pressure in the droplets exceeding the influence of the first formed polymer chains. This also explains the fact that a small amount of high molecular weight polymer, e.g., polystyrene, can barely act as an osmotic stabilizing agent; here stabilization can only be achieved for the time of polymerization [37, 38].

The investigation of the droplet size is also an important issue in the literature. The size of the *polymer particles* is easily determined by light scattering or microscopic methods since the dispersions can be diluted without changing the particles. Few attempts have been made at measuring *droplet sizes* in emulsions directly. Ugelstad et al. [24] and Azad et al. [39] stained miniemulsions with  $\text{OsO}_4$  and used transmission electron microscopy. However, the treatment can alter the sizes. Goetz and El-Aasser [40] made some attempts to determine droplet sizes using light scattering and transmission electron microscopy. Miller et al. [41] used capillary hydrodynamic fractionation (CHDF). Nevertheless, for those

measurements the emulsions had to be diluted, which seriously changes the system. Even if the emulsion is diluted with monomer-saturated water [42], the size of the droplets will change slightly due to different solubility effects.

Measurement of characteristics of the emulsion droplets in concentrated media is indeed a difficult task. Some indirect methods have been used. The interfacial area and therefore the droplet size were determined by measuring the critical micelle concentration of miniemulsions [43]. Erdem et al. determined droplet sizes of concentrated miniemulsions via soap titration, which could be confirmed by CHDF measurements [44]. Droplet sizes without diluting the system can much better be estimated by small angle neutron scattering (SANS) measurements [23].

## 2.5

### Inverse Miniemulsions

The concept of emulsion stabilization is not restricted to direct miniemulsions, but it could also be extended to inverse miniemulsions where the osmotic pressure is built up by an agent insoluble in the continuous oily phase, a so-called 'lipophobe'. Ionic compounds, simple salts or sugars, show a low solubility in organic solvents and can be used as lipophobes in water-in-oil miniemulsions [45]. Another adaptation of the process is that for the dispersion of polar monomers in non-polar dispersion media; surfactants with low HLB (hydrophilic-lipophilic balance) values are required. A number of surfactants were screened, including standard systems such as  $C_{18}EO_{10}$ , sodium bis(2-ethylhexyl)-sulfosuccinate (AOT), sorbitan monooleate (Span80), and the nonionic block copolymer stabilizer poly(ethylene-co-butylene)-*b*-poly(ethylene oxide) (PE/B-EO) consisting of hydrophilic and hydrophobic block lengths of about  $3700 \text{ g mol}^{-1}$ , respectively. PE/B-EO turned out to be most efficient due to its polymeric and steric demanding nature, providing maximal steric stabilization which is the predominant mechanism in inverse emulsions. A comparison of the direct and inverse miniemulsion is given in Fig. 5.

The extraordinarily high droplet stability against exchange processes can be demonstrated in a very illustrative way by the formation of a nickel murexid complex inside the droplets: One miniemulsion with droplets containing a Murexid solution, and one miniemulsion containing a  $Ni(NO_3)_2$  solution are mixed. As seen in Fig. 6a, the mixed miniemulsion stays orange-red for weeks, which indicates that the droplets with the different species stay separated as colloidal entities on the time scale of most chemical reactions. Repetition of the same experiment with two microemulsion or micellar solutions would lead to an immediate reaction because of unblocked droplet exchange. In miniemulsions, the exchange can be stimulated by mechanical energy, such as ultrasonication used to prepare the original miniemulsions. In this case, fusion and fission processes are induced, and with increasing ultrasonication the miniemulsion indeed turns yellow (see Fig. 6b).

Also in the inverse case, the droplet size throughout the miniemulsification process runs into an equilibrium state (steady-state miniemulsion) which is characterized by a dynamic rate equilibrium between fusion and fission of the



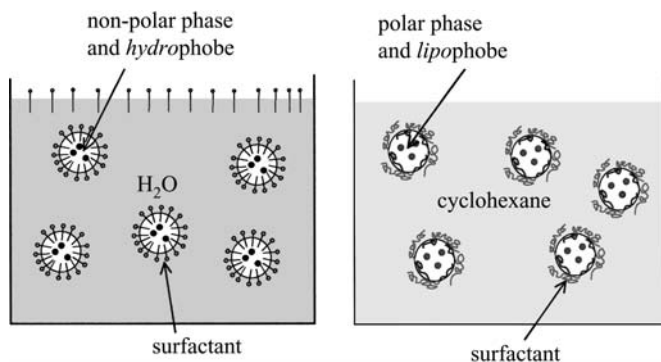


Fig. 5. Comparison between direct and inverse miniemulsion

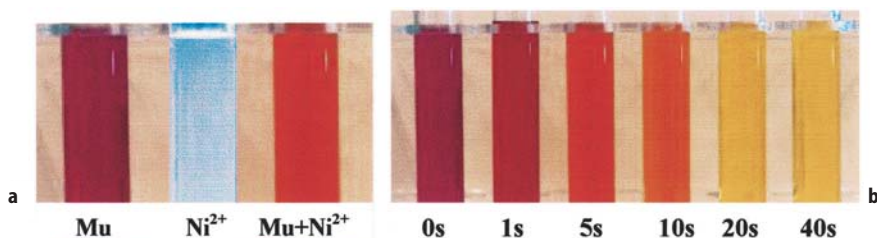


Fig. 6. a Mixing of two inverse miniemulsions, one containing Murexid solution, the other one  $\text{Ni}(\text{NO}_3)_2$ ; b Mixed miniemulsion of b during the process of ultrasonication

droplets, as it can be determined by turbidity measurements. High stability of the droplets *after* the high shear treatment, however, is obtained with the osmotic agent. The type of lipophile has no influence on the stability of the inverse miniemulsion. The droplet size depends, unlike in regular miniemulsions, on the amount of osmotic agent [46]. It seems that in inverse miniemulsions the droplets experience shortly after miniemulsification a real zero-effective pressure situation (the osmotic pressure counterbalances the Laplace pressure) which makes them very stable. This is speculatively attributed to the different stabilization mechanism and mutual particle potentials, which make a pressure equilibration near the ultrasonication process possible. This is why it is believed that inverse miniemulsions are not critically stabilized, but are fully stable systems.

Nevertheless, for inverse miniemulsions the surfactant is used in a very efficient way, at least as compared to inverse microemulsions [47, 48] or inverse suspensions [49] which are used for subsequent polymerization processes. Again, the surface coverage of the inverse miniemulsion droplets with surfactant is incomplete and empty inverse micelles are absent. Again this is important for the interpretation of the reaction mechanism.

The fusion/fission mechanism of minidroplet formation also results in the typical triangular relation between the amount of surfactant, the resulting par-



ticle size, and the surface coverage. With increasing amount of the surfactant, the particle size decreases. The smaller the particles, the higher the coverage of the particles by surfactant. For inverse miniemulsions these relations also depend on the amount of hydrophobe.

## 2.6

### **Preservation of Particle Identity Throughout Miniemulsion Polymerization**

The idea of miniemulsion polymerization is to initiate the polymerization in each of the small stabilized droplets, without major secondary nucleation or mass transport processes involved. Preservation of particle number and particle identity is therefore a key issue. Therefore, the growth of minidroplets is ideally slower than the polymerization time, and a situation very close to a 1:1 copying of the monomer droplets to polymer particles is obtained. From today's point of view, it is either possible to polymerize a freshly prepared, steady-state miniemulsion with minimal particle size, freezing the critically-stabilized state by rapid polymerization, or by adding an adequate second dose of surfactant (controlled by surface tension measurements to saturate the particle surface avoiding the presence of free micelles). The growth of the minidroplets is then effectively suppressed, and polymerization avoids any 'racing' situation.

The preservation of particle character and size throughout polymerization itself is very hard to determine. The size of the final polymer particles is easily determined by light scattering or microscopic methods since the dispersions can be diluted without changing the particle size. Measurements of the emulsion droplets in concentrated media on the other hand are a very difficult task and have already been discussed above.

Indirect techniques, such as conductivity measurements and the determination of the surface tension were carried out to get more information about the surfactant distribution during the polymerization and were applied to characterize the droplet or particle sizes before and after the polymerization without diluting the system [23]. As a powerful method small angle neutron scattering experiments were applied to characterize the droplet or particle sizes before and after the polymerization without diluting the system [23].

## 2.7

### **Surfactant Variation**

The majority of the recipes described in the literature are based on the anionic sodium dodecylsulfate (SDS) as a model system. The possibility of using cationic surfactants such as octadecyl pyridinium bromide for the preparation of miniemulsions was first exploited in 1976. However, the emulsions were prepared by stirring and the resulting emulsions showed broadly distributed droplet sizes [2, 39, 50]. Recent work on steady-state miniemulsions showed that cationic and nonionic surfactants form well-defined miniemulsions for further miniemulsion polymerization processes, resulting in narrow size distributed stable cationic and nonionic latex particles [51]. Similar molecular amounts of the simple cationic surfactant, cetyltrimethylammonium bromide or chloride

(CTAM-Br or -Cl), compared to the anionic surfactant, SDS, result in similar particle sizes showing that the particle size is essentially controlled by a limit of the surfactant coverage of the latex particles. From surface tension measurement results, this surface coverage was determined to be of the order of 30%, which proves the very efficient use of surfactants in the miniemulsification process. A new class of cationic surfactants with sulfonium headgroups was also effectively employed for the synthesis of miniemulsions. The ring-opening reaction of epoxides with thioethers, followed by addition of organic acids, is a versatile approach towards a broad variety of different sulfonium surfactant structures. By use of a wide variety of accessible reactants, the sulfonium surfactant architecture was varied in terms of (a) the hydrophobic chain length, (b) the counterion of the sulfonium headgroup, (c) the structure of the sulfonium headgroup, and (d) the surfactant architecture, i.e., single-chain or bola- or star-shaped surfactants [52].

Nonionic miniemulsions can be made by using 3–5% of a poly(ethylene oxide) derivative as surfactant, resulting in larger, but also very well defined latexes [51]. Chern and Liou used a nonionic surfactant nonylphenol polyethoxylate with an average of 40 ethylene oxide units per molecule [53]. Particle sizes between 135 and 280 nm were realized. The particle size mainly depends on the type and amount of the hydrophobe and therefore on the degree of the suppression of Ostwald ripening [53].

Capek described the use of a macromonomer in miniemulsion polymerization [54]. Lim and Chen used poly(methyl methacrylate-*b*-(diethylamino)ethyl methacrylate) diblock copolymer as surfactant and hexadecane as hydrophobe for the stabilization of miniemulsions [55]. Particles with sizes between about 150 and 400 nm were produced. It is possible to create stable vinyl acetate miniemulsions employing nonionic polyvinyl alcohol (PVA) as surfactant and hexadecane as hydrophobe [56].

The favorable use of an amphiphilic graft copolymer comprised of octadecyl acrylate and acrylic or methacrylic acid groups for the formation of polystyrene miniemulsion latexes has been demonstrated in our laboratory by Baskar et al. [57]. The comb-like polymers had molecular weights of about  $4 \times 10^4 \text{ g mol}^{-1}$ . In this case, the polymer acts as a surfactant and a hydrophobe at the same time which is of large industrial significance. Since those polymers neither dissolve homogeneously in monomer or water, the polymers are anticipated to be located only at the oil-water interface [57]. Compared to the surface-active cetyl alcohol, the water solubility is shown to be very low, which ensures the stability of the miniemulsion droplets.

By variation of the relative amount of the surfactant, it was possible to vary the particle size over a wide range [58]. Figure 7 shows that, depending on the type of the surfactant, different size ranges can be achieved. Latexes synthesized with ionic surfactants, e.g., sodium dodecyl sulfate (SDS), CTAB, or the  $C_{12}$  sulfonium surfactant show about the same size-concentration curve, i.e., the efficiency of the surfactants and the size dependent surface coverage is very similar, independent of the sign of charge. The efficiency of the nonionic surfactants is lower in contrast to the ionic ones and the whole size-concentration curve is shifted to larger sizes. This is attributed to the lower efficiency of the steric sta-

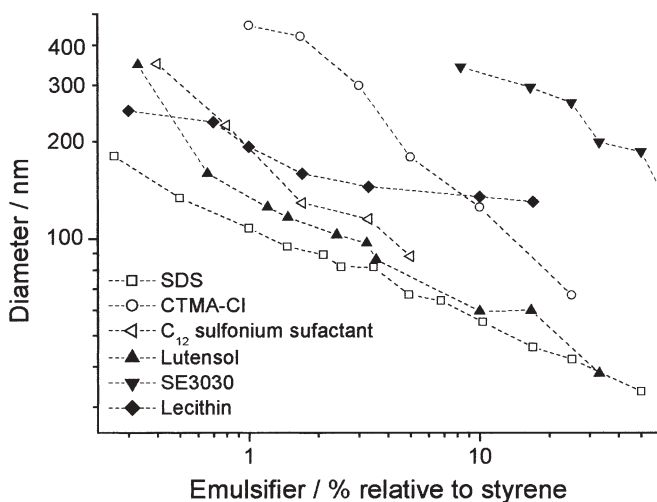


**Fig. 7.** Variation of the particle size by changing the amount and type of surfactant in a styrene miniemulsion

bilization as compared to electrostatic stabilization and the fact that steric stabilization relies on a more dense surfactant packing to become efficient. As can be derived from the surface tension of the latexes and surfactant titrations, the nonionic particle surfaces are, nevertheless, incompletely covered by surfactant molecules and the latexes show surface tensions well above the values of the saturated surfactant solution where saturated surfactant layers occur. Also, the bio-surfactant lecithin can be used for the preparation of stable miniemulsions.

## 2.8

### Checklist for the Presence of a Miniemulsion

In some crucial cases it might be not obvious whether the system represents a miniemulsion or not. Therefore a short checklist summarizing the characteristics of miniemulsions is provided:

1. Steady-state dispersed miniemulsions are stable against diffusional degradation, but critically stabilized with respect to colloidal stability.
2. The interfacial energy between the oil and water phase in a miniemulsion is significantly larger than zero. The surface coverage of the miniemulsion droplets by surfactant molecules is incomplete.
3. The formation of a miniemulsion requires high mechanical agitation to reach a steady state given by a rate equilibrium of droplet fission and fusion.
4. The stability of miniemulsion droplets against diffusional degradation results from an osmotic pressure in the droplets, which controls the solvent or monomer evaporation. The osmotic pressure is created by the addition of a substance, which has extremely low water solubility, the so-called hydrophobe. This crucial prerequisite is usually not present in microemulsions, but

can be added to increase the stability. Such miniemulsions can still undergo structural changes by changing their average droplet number to end up in a situation of zero effective pressure, however, on very long time scales. This secondary growth can be suppressed by an appropriate second dose of surfactant added after homogenization.

5. Polymerization of miniemulsions occurs by droplet nucleation only.
6. During the polymerization, the growth of droplets in miniemulsions can be suppressed. In miniemulsions the monomer diffusion is balanced by a high osmotic background of the hydrophobe, which makes the influence of the firstly formed polymer chains less important.
7. The amount of surfactant or inherent surface stabilizing groups required to form a polymerizable miniemulsion is comparably small, e.g., with SDS between 0.25 and 25% relative to the monomer phase, which is well below the surfactant amounts required for microemulsions.

### 3

## Radical Polymerizations of Miniemulsions

### 3.1

#### Mechanisms and Kinetics in Miniemulsion Polymerization

In miniemulsion polymerization the nucleation of the particles mainly starts in the monomer droplets themselves. Therefore, the stability of droplets is a crucial factor in order to obtain droplet nucleation. The better the droplets are stabilized against Ostwald ripening, the higher is the droplet nucleation.

In Fig. 8 the calorimetric curve of a typical miniemulsion polymerization for 100-nm droplets consisting of styrene as monomer and hexadecane as hydrophobe with initiation from the water phase is shown. Three distinguished intervals can be identified throughout the course of miniemulsion polymerization. According to Harkins' definition for emulsion polymerization [59–61], only intervals I and III are found in the miniemulsion process. Additionally, interval IV describes a pronounced gel effect, the occurrence of which depends on the particle size. Similarly to microemulsions and some emulsion polymerization recipes [62], there is no interval II of constant reaction rate. This points to the fact that diffusion of monomer is in no phase of the reaction the rate-determining step.

The first interval is the interval of particle nucleation (interval I) and describes the process to reach an equilibrium radical concentration within every droplet formed during emulsification. The initiation process becomes more transparent when the rate of polymerization is transferred into the number of active radicals per particle  $\bar{n}$ , which slowly increases to  $\bar{n} \approx 0.5$ . Therefore the start of the polymerization in each miniemulsion droplet is not simultaneous, so that the evolution of conversion in each droplet is different. Every miniemulsion droplet can be perceived as a separate nanoreactor, which does not interact with others. After having reached this averaged radical number, the polymerization kinetics is slowing down again and follows nicely an exponential kinetics as known for interval III in emulsion polymerization or for suspension polymer-

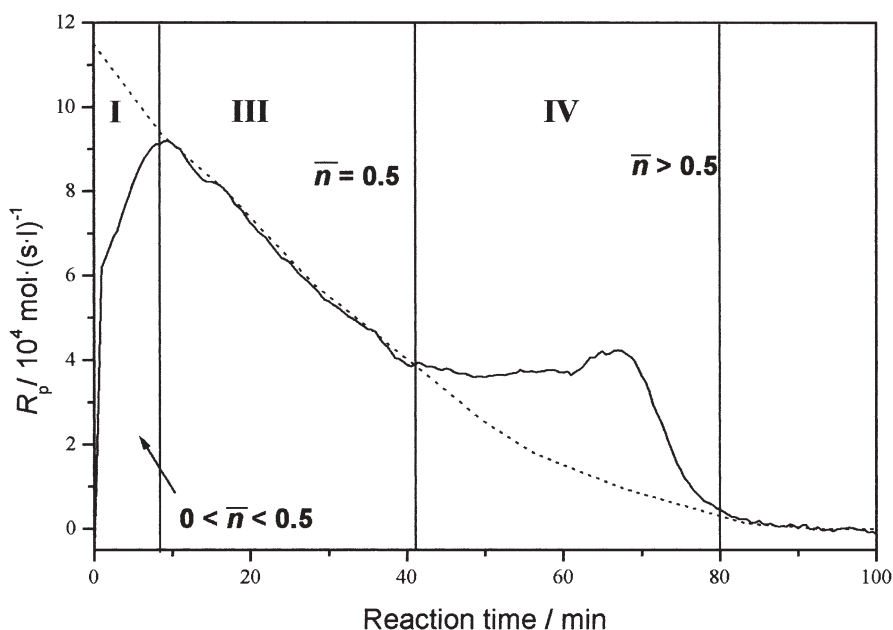


**Fig. 8.** Calorimetric curve of a typical miniemulsion polymerization consisting of 20% styrene in water, 1.2% SDS (relative to styrene), and KPS as initiator

ization. As reasoned by the droplet nucleation mechanism, only the monomer in the droplet is available for polymerization, which is exponentially depleted from the reaction site. The average number of radicals per particle,  $\bar{n}$  during interval III is quite accurately kept at 0.5, implying that the on/off mechanism known from emulsion polymerization [63] upon entry of additional radicals into such small latex particles is strictly valid.

The boost found in interval IV is the typical gel-peak well known also from suspension polymerization, which is due to the viscosity increase inside the particles and the coupled kinetic hindrance of the radical recombination. This is also reflected in a steep rise of  $\bar{n}$ .

### 3.2

#### Droplet Size

The polymerization kinetics is governed by the droplet size. Tang et al. found that the polymerization of styrene miniemulsions created by the microfluidizer was faster than that of miniemulsions created by the omnimixer [64]. This behavior can mainly be attributed to the different droplet size prior to polymerization. In the first case, the droplets are smaller than in the second case [65]. Fontenot and Schork observed similar behavior for MMA miniemulsions. With increasing shear and increasing concentration of surfactant, the polymerization rate increases [22]. This again can be explained by different sizes of the initial droplets.

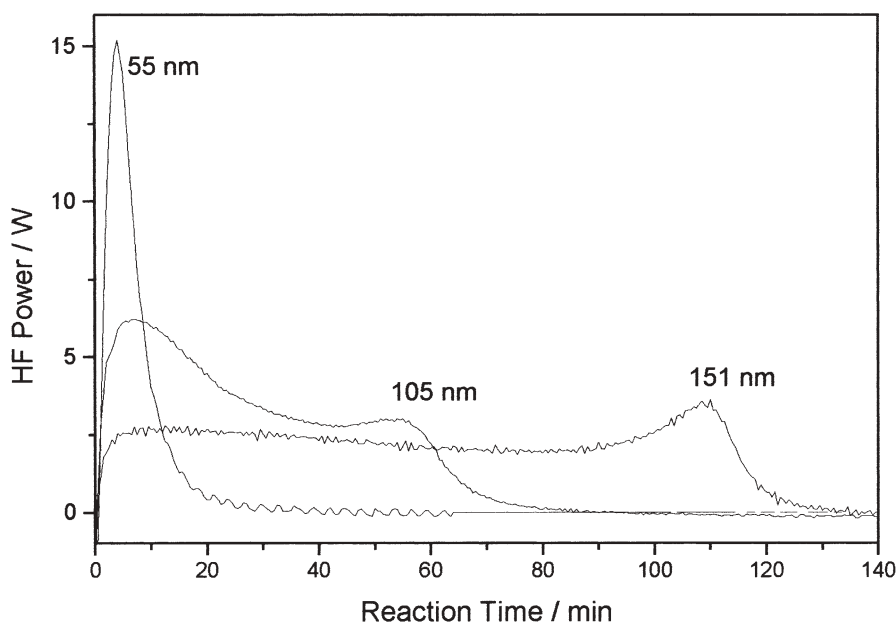


**Fig. 9.** Calorimetric curves for styrene miniemulsion polymerizations with different SDS contents, e.g., different particle sizes (0.3 rel.% SDS leads to 151-nm, 1.0 rel.% SDS to 105-nm, and 10 rel.% SDS to 55-nm particles)

In steady-state or mechanically equilibrated miniemulsions, the droplet size can be easily varied by variation of the amount of surfactant. Depending on the droplet size of the miniemulsions, we obtained calorimetric curves with various kinetic features which are shown in Fig. 9 [66]. Disregarding the complexity of the kinetics and the existence of the three intervals, the reaction time to reach 95% conversion depends as a rule of thumb about linearly on the particle size and thus varies between 20 and 120 min.

Independent of the size of the droplets, interval I (see also Fig. 8) has a similar duration and takes about 5 min, which again supports the concept that this interval is only influenced by processes in the continuous aqueous phase which do not depend on the droplet size. The maximum reaction speed, however, shows a strong particle size dependence and is proportional to the particle number, i.e., the smaller the particles are, the faster is the reaction.

### 3.3

#### Initiators

For miniemulsion polymerization, the initiator can be either oil- or water-soluble. In the case of an oil-soluble initiator, the initiator is dissolved in the monomeric phase prior to miniemulsification. Then the reaction starts within the droplets. This is comparable to suspension polymerization where the initia-

tion is carried out in the large droplets. Because of the finite size of the miniemulsions droplets, radical recombination is here the problem to face. Also a water-soluble initiator can be used to start the polymerization from the water phase. The start from the continuous phase is similar to the conventional emulsion polymerization where usually water-soluble initiators are used.

It was found that the chain length of the resulting polymer is inversely proportional to the square root of the initiator concentration [66], underlining that the reaction in miniemulsion is rather direct and close to an ideal radical polymerization. It could be shown that the amount of initiator used for polymerizing the latex does not have an effect on the number of nucleated droplets which shows that droplet nucleation is by far the dominant mechanism over the whole range of initiator concentrations.

For the styrene/hexadecane system, the amount of initiator does not have an effect on the particle number, but in the case of more water-soluble monomers, for example MMA and vinyl chloride [67], secondary particle formation was observed. Here, the amount of new particles increases with the concentration of the water-soluble initiator. Homogeneous nucleation in the water phase can be restrained by using a water-soluble redox initiator, e.g.,  $(\text{NH}_4)_2\text{S}_2\text{O}_8/\text{NaHSO}_3$  at lower temperature (45°C) [68] or even more efficiently by using an interfacial acting redox initiator (cumene hydroperoxide/ $\text{Fe}^{2+}$ /ethylenediamine tetraacetate (EDTA)/sodium formaldehyde sulfoxylate (SFS)) [69, 70] to initiate the miniemulsion polymerization. The hydrophobic radicals decrease the homogeneous nucleation in the aqueous phase.

The miniemulsion polymerization also allows the use of oil-soluble initiators which is the preferential choice for monomers with either high water solubility (e.g., MMA in order to prevent secondary nucleation in the water phase) or for monomers with an extremely low water solubility (e.g., LMA) where the monomer concentration in the water phase is not high enough to create oligoradicals which can enter the droplets.

The ability of initiators with different water solubilities, namely lauroyl peroxide (LPO), benzoyl peroxide (BPO) and 2,2'-azoisobutyronitrile (AIBN) in stabilizing monomer droplets against degradation by molecular diffusion and their efficiency for polymerization was investigated [30]. Upon heating, the initiator decomposes, and a sufficiently long polymer chain will be formed only when a single radical appears. 'Single radicals' refer to radicals that appear in the monomer droplets one at a time as opposed to pair generation in which, due to initiator decomposition, two radicals appear in the monomer droplet at the same time. Single radicals can be formed by desorption of one of the radicals formed by initiator decomposition and by entry of a radical from the aqueous phase. This makes oil-soluble initiators effective only when one or both of the formed radicals are sufficiently hydrophilic to undergo desorption. Comparing different oil-soluble initiators, the probability of nucleation is much larger for AIBN than in the cases of LPO and BPO.

## 4

### Different Polymerization Reactions in Miniemulsions

The process of miniemulsion allows in principle the use of all kinds of monomers for the formation of particles, which are not miscible with the continuous phase. In case of prevailing droplet nucleation or start of the polymer reaction in the droplet phase, each miniemulsion droplet can indeed be treated as a small nanoreactor. This enables a whole variety of polymerization reactions that lead to nanoparticles (much broader than in emulsion polymerization) as well as to the synthesis of nanoparticle hybrids, which were not accessible before.

#### 4.1

##### Radical Homopolymerization in Regular Miniemulsions

As a model monomer for radical homopolymerization of hydrophobic monomers, styrene is described in many papers. The polymerization of acrylates and methacrylates is also well known. It could also be shown that the miniemulsion process also easily allows the polymerization of the ultrahydrophobic monomer lauryl methacrylate without any carrier materials as necessary in emulsion polymerization [71].

Not only hydrophobic but also fluorinated monomers were applied for the synthesis of latexes in the size range of 100–250 nm by employing rather low doses of protonated surfactants [72]. As a model system, the fluorine-containing monomer tridecafluorooctyl methacrylate ( $\text{CH}_2=\text{C}(\text{CH}_3)\text{CO}_2(\text{CH}_2)_2(\text{CF}_2)_6\text{F}$ ) was used for the miniemulsion procedure. Indeed, this monomer could be miniemulsified using perfluoromethyldecane or the polymerizable heptadecafluorodecyl methacrylate ( $\text{CH}_2=\text{C}(\text{CH}_3)\text{CO}_2(\text{CH}_2)_2(\text{CF}_2)_8\text{F}$ ) as hydrophobes and the standard hydrocarbon surfactant sodium dodecyl sulfate (SDS). The use of this simple standard surfactant is worth mentioning, since most other recipes relied on fluorinated surfactants or long chain alkyl surfactants (dense packing). Already at surfactant loads as low as 0.66 rel.% (weight percent SDS relative to the dispersed phase), a stable miniemulsion could be obtained. Due to the low water solubility of the monomer, it was not possible to perform initiation from the water phase, and the polymerization was started inside the droplets by using AMBN (2,2'-azobis(2,4-dimethylbutyronitrile)) as a hydrophobic initiator. With 0.66 rel.% SDS, coagulate-free latexes with particle diameters of about 200 nm were obtained. The size of the final particles could be easily decreased by increasing the amount of surfactant from about 200 nm (0.66% SDS) to 100 nm (5.33% SDS). As compared to polystyrene latexes made under similar conditions, all fluoromethacrylate latexes are slightly larger, thus expressing the more hydrophobic surface and the connected higher packing density of surfactant required for stabilization. On the other hand, the latexes are smaller than those made from lauryl methacrylate (see Fig. 10a), which we interpret with a higher average surface energy for the fluoromethacrylate due to the fact that methacryloyl units are also pointing to the water phase.

The hydrophobic monomer vinylanthracene also forms at temperatures above its melting temperature miniemulsions and the miniemulsion droplets



can be polymerized, resulting in polymer particles with a refractive index of the polymer particles of 1.6818 which is one of the highest known for polymers (see Fig. 10b). Since the scattering intensity for particles with the same diameter is proportional to  $\Delta(n_1 - n_2)^2$  (where  $n_1$  and  $n_2$  are the refractive indexes of the particles and the continuous medium respectively), the scattering intensity of polynaphthalene latex particles is twice as high ( $\Delta(n_1 - n_2)^2 = 0.1213$ ) as for styrene latex particles with the same size ( $\Delta(n_1 - n_2)^2 = 0.0660$ ).

The polymerization of more hydrophilic monomers is also possible, as shown for MMA and vinyl acetate [36, 56, 73]. In the case of monomers with a pronounced water solubility, the nucleation in water should be efficiently suppressed in order to avoid secondary nucleation in the water phase. This can be achieved, e.g., by using an oil-soluble initiator and the polymerization of acrylonitrile or by adding a termination agent to the continuous phase. A typical calorimetric curve of MMA polymerization using a hydrophobic initiator shows a fast conversion.

PVC latex particles consisting of two size populations can be generated in a miniemulsion polymerization. The mechanism for the formation of two discrete particle families relies upon polymerization of two distinct kinds of droplets [74].

## 4.2

### Formation of Particles in Non-Aqueous Solvents

It was shown that the principle of aqueous miniemulsions could be transferred to non-aqueous media [45]. Here, polar solvents, such as formamide or glycol, replace water as the continuous phase, and hydrophobic monomers are miniemulsified with a hydrophobic agent, which stabilizes the droplets against molecular diffusion processes. It turned out that steric nonionic surfactants based on poly(ethylene oxide) tails are far more efficient than ionic stabilizers,

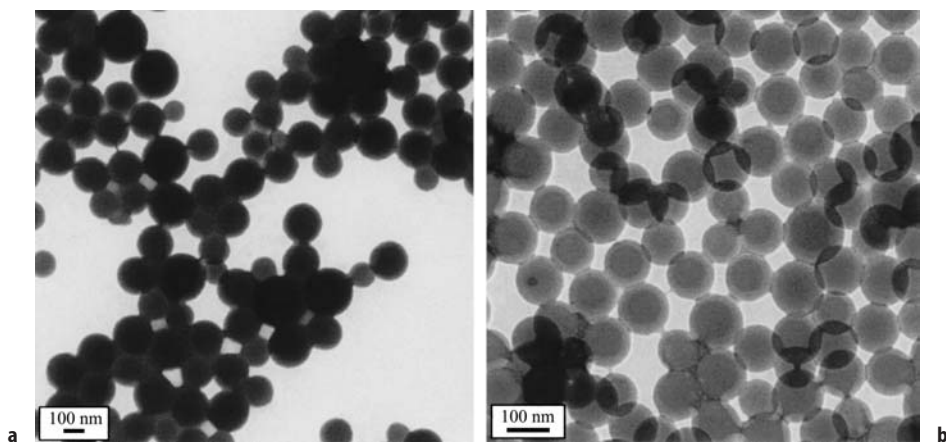


**Fig. 10a,b.** TEM photographs: **a** polylaurylmethacrylate latex particles; **b** polynaphthalene latex particles

which is speculatively attributed to a low degree of ion solvation and degree of dissociation in formamide. It is possible to make particles as small as 70 nm, which is unusually small for non-aqueous heterophase polymerization techniques. An increase of the particle size with decreasing amounts of surfactant is detected. For the polymerization of the monomer droplets, both AIBN and KPS were employed as initiators. AIBN dissolves in both organic phases leading to an aggregation of the particles since the polymerization can be started simultaneously and uncontrolled in the droplets and in the continuous phase. The hydrophilic initiator KPS, however, turned out to be suitable, since it starts the polymerization controlled from the continuous phase.

### 4.3

#### Formation of Particles in Inverse Miniemulsion

In the case of inverse systems, hydrophilic monomers such as hydroxyethyl acrylate, acrylamide, and acrylic acid were miniemulsified in non-polar media, e.g., cyclohexane or hexadecane [45, 46]. Rather small and narrow distributed latexes in a size range between  $50 \text{ nm} < d < 200 \text{ nm}$  were synthesized with nonionic amphiphilic block copolymers. Depending on the system, the surfactant loads can be as low as 1.5 wt% per monomer, which is very low for an inverse heterophase polymerization reaction and clearly underlines the advantages of the miniemulsion technique.

For the moderately hydrophilic hydroxyethyl methacrylate, cyclohexane and hexadecane were chosen as the continuous phase. As initiators, PEGA200 which is soluble in the monomer phase, but not in cyclohexane, turned out to be applicable. AIBN which is mainly soluble in the cyclohexane phase could also be successfully used. KPS cannot be employed as initiator due to solubility problems. Small amounts of water act as lipophobe, and it could be shown by turbidity measurements that the addition of water increases the emulsion stability.

Rather small latex particles in the size range between 80 nm and 160 nm and narrow size distributions are obtained. The systems are stable down to 1.6 wt% surfactant relative to the monomer; at lower amounts the systems tend to coagulate. With increasing amount of surfactant, the particle size decreases as expected. The area per surfactant molecule,  $A_{\text{surf}}$ , decreases with decreasing particle size and follows the same trend as in the case of direct miniemulsions shown earlier. This means that again the surface coverage is a function of the particle size: for smaller particles more surfactant is required in order to obtain stable latexes. It is remarkable that the final dispersions are stable for longer time even at low surface coverage.

For the synthesis of acrylamide in a miniemulsion polymerization process, the solid crystalline monomer has to be dissolved in water, and therefore a higher amount of water was applied for the synthesis. As the continuous phase, cyclohexane or IsoparM were chosen. The miniemulsions after sonication show only a low stability (less than 1 h) without the addition of a strong lipophobe (1 mol/l NaCl); its presence increases the stability of the miniemulsions to the timescale of several days. A polymerization started with AIBN from the continuous phase resulted in stable polymer dispersions, as shown in Fig. 11.

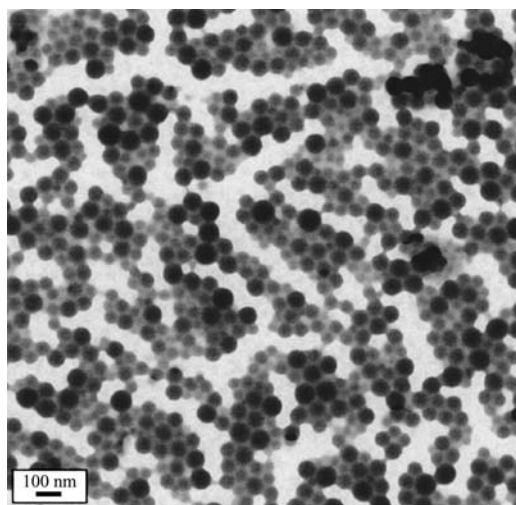


**Fig. 11.** Hydrophilic polyacrylamide particles obtained in inverse miniemulsion polymerization in IsoparM

The high homogeneity and rather well-defined character of those latexes is clearly observed. Again, already surfactant loads as low as 1.8% relative to the dispersed phase result in stable latexes. The particle size is getting smaller with increasing amounts of the surfactant, and the surface area per surfactant molecule  $A_{\text{surf}}$  is between 18 nm<sup>2</sup> at low surfactant amounts (1.8 rel.%) and 7 nm<sup>2</sup> for higher surfactant amounts (7.1 rel.%), depending on the particle size.

Acrylic acid was polymerized in inverse miniemulsions together with 4 wt% of the crosslinking agent diethylene glycol diacrylate in order to obtain homogeneous polyelectrolyte microgels, which can be redispersed and characterized in water. However, the solubility of acrylic acid in cyclohexane is not negligible. The addition of water to acrylic acid already decreases the solubility of acrylic acid in cyclohexane significantly. Therefore, a 5 mol/l NaOH solution at a 1:1 ratio NaOH solution/acrylic acid was used in order to shift the partitioning of acrylic acid more into the water phase. NaOH not only acts as a lipophobe, but also neutralizes the acid, which leads to a higher hydrophilicity of the component. Starting from a critical surfactant amount of 2.5 rel.% to prevent the formed polymer particles from aggregation, stable latex particles of about 100 nm diameter were produced. Increasing the surfactant amount leads to smaller particles. The surfactant efficiency or the stabilized area per surfactant molecule,  $A_{\text{surf}}$  is very high. In the case of low surfactant concentration,  $A_{\text{surf}}$  is as big as 25 nm<sup>2</sup> per stabilizing molecule and decreases to 13.2 nm<sup>2</sup> in the case of higher amounts of surfactant.

As compared to classical inverse heterophase polymerization techniques such as polymerization in inverse microemulsions [47] or dispersion polymerization [75, 76], polymerization of inverse miniemulsions is favored by the very efficient use of surfactant and the copying process from the droplets to the par-

ticles. This leads to a homogeneous structure and composition of the resulting particles (no kinetic effects are involved). The latter feature is especially important for homogeneous crosslinking or copolymerization in inverse heterophase polymerization.

#### 4.4

##### Nanocrystalline Polymers

Polyacrylonitrile, which is a semicrystalline polymer, can be used for many engineering applications, such as fiber spinning or for housing and package applications. A peculiarity of polyacrylonitrile is that it is insoluble in its monomer. This makes it very difficult to homopolymerize acrylonitrile in an emulsion polymerization process since nucleated polymer particles cannot grow by monomer swelling.

Polymerization in miniemulsion is a very suitable technique to avoid this problem since each droplet acts as a nanoreactor. As a result, pure polyacrylonitrile (PAN) nanoparticles were obtained in the size range  $100\text{ nm} < d < 180\text{ nm}$  depending on the amount of surfactant as usually observed in miniemulsion systems (2.0 rel.% SDS leads to 180-nm particles, 6 rel.% to 98-nm particles) [77]. As compared to a standard styrene miniemulsion system, it has to be considered that the solubility of acrylonitrile in water is rather high (7.35%). For a miniemulsion with 20 wt% acrylonitrile, just about 70% of the monomer is located inside the droplets, whereas 30% is dissolved in the water phase. This is no restriction for a miniemulsion polymerization process, and the use of a hydrophobic initiator 2,2'-azobis(2-methylbutyronitrile) allows the preservation of the droplets as the reaction sites by droplet nucleation (see Fig. 12). Initiation of the

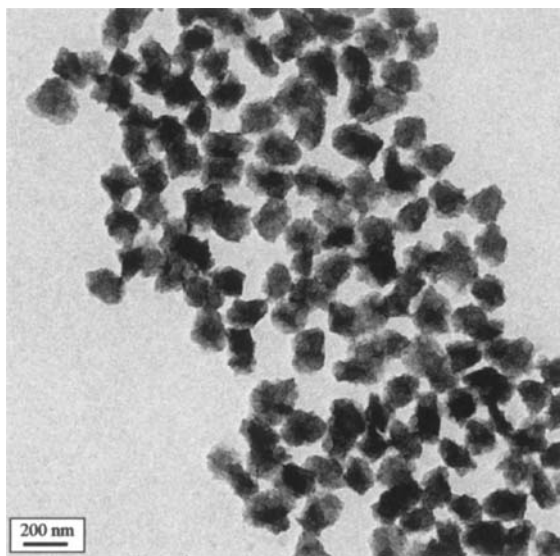


**Fig. 12.** Transmission electron micrograph of PAN latex particles

mini-emulsion in the water phase would lead to polymerization in the water phase and secondary nucleation of new polymer particles. However, it has to be noted that the more SDS is used and therefore the smaller the droplets are, the more difficult it is to control the fast polymerization within the droplets.

Due to the insolubility of the polymer in the monomer, the formed polymer precipitates and crystallizes during the polymerization within the droplets; ca. 10-nm large polymer nanocrystals are formed. Pure PAN latexes have a crumpled appearance where the single polymer nanocrystals remain in the final structure and are easily identified by their sharp edges and flat surfaces.

## 4.5

### Radical Copolymerization

#### 4.5.1

##### *Hydrophobic/Hydrophobic Copolymers*

Mini-emulsion copolymerization of a 50:50 styrene/methyl methacrylate monomer mixture, using hexadecane as hydrophobe, was carried out by Rodriguez et al. [78]. The mechanism of mass transfer between mini-emulsion droplets and polymer particles in the mini-emulsion copolymerization of styrene-methyl methacrylate (AIBN as initiator, hexadecane as hydrophobe) was studied, analyzing the mass transfer of highly water-insoluble compounds from mini-emulsion droplets to polymer particles by both molecular diffusion and collisions between droplets and particles [79, 80].

Copolymerization of styrene and butyl acrylate was successfully carried out by Huang et al. using the redox initiator system  $(\text{NH}_4)_2\text{S}_2\text{O}_8/\text{NaHSO}_3$  at lower temperature [68]. The rate of the mini-emulsion polymerization increases with increasing butyl acrylate concentration and decreases with increasing styrene concentration. This was attributed to differences in the water solubility. The lower water solubility of styrene either increases the desorption rate of the radicals or reduces the radical absorption of the monomer droplet [81].

Inaba et al. prepared a series of model styrene/butyl acrylate copolymer latexes with glass transition temperatures at room temperature. The functional monomer 2-(3-isopropenylphenyl)-2-methylethylisocyanate (TMI) was used as monomer/crosslinking agent for further film formation. A small amount of methacrylic acid was introduced in some formulations in order to enhance the crosslinking reaction. A redox initiation system was used to reduce premature crosslinking during the polymerization [82].

The copolymerization of monomers where one of the monomers acts as the hydrophobe was reported by Reimers and Schork [26]. MMA was copolymerized with *p*-methylstyrene, vinyl hexanoate, or vinyl 2-ethylhexanoate. The resulting copolymer composition tended to follow the predictions of the reactivity ratios, i.e., the reaction progresses as a bulk reaction. In contrast, copolymer compositions obtained from the (macro)emulsion copolymerizations tended to be more influenced by the relative water solubility of the comonomer and mass transfer. Wu and Schork used monomer combinations with large differences in reactivity ratios and water solubility: vinyl acetate/butyl acrylate,

vinyl acetate/dioctyl maleate, and vinyl acetate/*N*-methylol acrylamide. The miniemulsion system follows more closely the integrated Mayo-Lewis equations than the comparable emulsion system [73].

The copolymer composition in miniemulsion copolymerization of vinyl acetate and butyl acrylate during the initial 70% conversion was found to be less rich in vinyl acetate monomer units [34]. Miniemulsion polymerization also allowed the synthesis of particles in which butyl acrylate and a PMMA macromonomer [83, 84] or styrene and a PMMA macromonomer [85] were copolymerized. The macromonomer acts as compatibilizing agent for the preparation of core/shell PBA/PMMA particles. The degree of phase separation between the two polymers in the composite particles is affected by the amount of macromonomer used in the seed latex preparation.

In a previous chapter the polymerization of fluorinated monomers in miniemulsion polymerization was shown. The fluorinated monomers can also be copolymerized with protonated monomers. It was shown in our laboratory that miniemulsification of such mixed monomer species allows one to perform efficient copolymerization reactions with standard hydrophobic and hydrophilic monomers in a common heterophase situation, resulting either in core-shell latexes or in statistical copolymers. In contrast to the pure fluorinated polymers, these copolymers dissolve in organic solvents but still show the profitable interface properties of the fluorinated species. In order to obtain a negatively charged surface, the surfactant SDS and small amounts of acrylic acid were used, whereas positively charged particles are expected to be obtained by cetyl trimethylammonium chloride as surfactant and MADQUAT as polymerizable comonomer. In all cases, coagulum-free and stable polymer latexes were obtained. It could be shown that the use of AA or MADQUAT did not significantly affect the particle size. However, the size distribution is broader than for the pure fluorinated polymer particles. An increase in the surfactant amount leads often to bimodal distributions; 1.3% surfactant seems to be well suited.

#### 4.5.2

##### ***Amphiphilic Copolymers***

Small amounts of carboxylic monomers (acrylic acid (AA) or methacrylic acid (MAA)) [86] or 2-hydroxyalkyl methacrylates [87] could be easily used in a styrene miniemulsion polymerization, using DMA or SMA as hydrophobe and SDS as emulsifier.

The polymerization process of two monomers with different polarities in similar ratios is a difficult task due to the solubility problems. Using the miniemulsion process, it was possible to start from very different spatial monomer distributions, resulting in very different amphiphilic copolymers in dispersion [88]. The monomer, which is insoluble in the continuous phase, is miniemulsified in order to form stable and small droplets with a low amount of surfactant. The monomer with the opposite hydrophilicity dissolves in the continuous phase (and not in the droplets). As examples, the formation of acrylamide/methyl methacrylate (AAM/MMA) and acrylamide/styrene (AAM/Sty) copolymers was chosen using the miniemulsion process. In all cases the synthe-



ses were performed in water as well as in cyclohexane as the continuous phase. If performing the synthesis in water, the hydrophobic monomer with a low water solubility (styrene or methyl methacrylate) mainly forms monomer droplets, whereas the hydrophilic monomer acrylamide with a high water solubility will be mainly dissolved in the water phase. In the case of inverse miniemulsion, the hydrophilic monomer is expected to form the droplets, whereas the hydrophobic monomer is dissolved in the continuous phase.

Starting from those two dispersion situations, the locus of initiation is expected to have a great influence on the reaction products and the quality of the obtained copolymers. Therefore three different initiators were used, an oil-soluble initiator (e.g., 2,2'-azobis(2,4-dimethylvaleronitrile (ADVN)), an interfacial active initiator (e.g., PEGA200), and a water-soluble initiator (e.g., potassium peroxydisulfate (KPS)) in order to initiate the polymerization selectively in one of the phases or at the interface.

In the system AAm/MMA, the best copolymer with respect to low content of homopolymers, low blockiness, and good redispersibility in polar and non-polar solvents was obtained in inverse miniemulsion with initiation in the continuous phase cyclohexane. In this case, the MMA chains grow in the continuous phase till they become insoluble and precipitate onto the AAm-droplets which enables the radicals to cross the interface; then AAm units can be added to the polymer chain. In the system AAm/Sty, the best copolymer was also obtained in the inverse miniemulsion process, but using interfacial initiation. This leads to almost homopolymer free copolymer samples with low blockiness indicating a fast change of the growing radical between the phases in order to add Sty and AAm units. A copolymerization in the direct miniemulsion with water as continuous phase using the interfacial initiator PEGA200 (see Fig. 13) results in a higher homo-AAm content. This can be attributed to the fact that the initiator

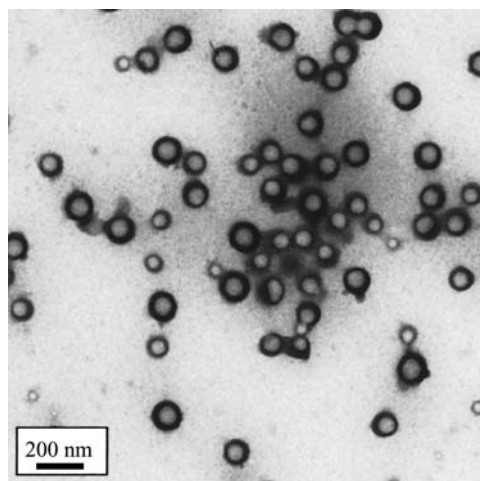


**Fig. 13.** TEM micrograph of the PMMA/AAm copolymer obtained in a direct miniemulsion polymerization with interfacial initiation stained with  $\text{RuO}_4$

due to its hydrophilicity has a slightly higher tendency to be in the water phase where AAm units can be captured. In order to obtain also in this direct case a statistical copolymer, the hydrophilicity of the interfacial initiator will be changed by in further experiments.

#### 4.6

##### Catalytic Chain Transfer in Miniemulsion

The employment of a cobalt catalytic chain transfer agent in miniemulsion polymerization allows the direct control of the molecular weight [89]. The solubility of the cobalt catalyst was found to have a large influence on the mechanism of the reaction. Cobaltoxime boron fluoride partitions approximately equally between the water and oil phases. In this case, the reaction was found to be extremely sensitive to the selection of the initiator, displaying poor catalytic activity in the presence of oxygen-centered radicals (derived from potassium sulfate), which can be explained by a poisoning and/or deactivation of the catalyst. By contrast, tetraphenylcobaltoxime boron fluoride resides exclusively in the oil phase. The catalytic activity proved to be independent of the initiator type, as the catalyst does not come in direct contact with the initiator-derived radicals. Therefore, miniemulsions allow effective isolation from the initiator radicals, thereby allowing a batch reaction to proceed without significant loss of catalytic activity.

#### 4.7

##### Controlled Free-Radical Miniemulsion Polymerization

Living free-radical polymerization represents a promising technique to produce polymers with highly controlled structures. Different possible systems known from bulk polymerizations have been used in miniemulsions. The living free radical polymerization of, e.g., styrene via the miniemulsion approach allows one to eliminate the drawback of the bulk system where an increase in polydispersity was found at high conversions due to the very high viscosity of the reaction medium [90].

Four different approaches for controlled radical polymerization have been adapted to the miniemulsion polymerization process:

1. The controlled free-radical miniemulsion polymerization of styrene was performed by Lansalot et al. and Butte et al. in aqueous dispersions using a *degenerative transfer process* with iodine exchange [91, 92]. An efficiency of 100% was reached. It has also been demonstrated that the synthesis of block copolymers consisting of polystyrene and poly(butyl acrylate) can be easily performed [93]. This allows the synthesis of well-defined polymers with predictable molar mass, narrow molar mass distribution, and complex architecture.
2. In a *stable free-radical polymerization* (SFRP), the initiated polymer chains are reversibly capped by a stable radical, for example, the 2,2,6,6-tetramethylpyridin-1-oxyl radical (TEMPO). Stable PS dispersions via miniemulsion polymerization were prepared by MacLeod et al. with an optimized ratio



and amount of surfactant, hydrophobe, nitroxide and KPS as initiator at 135°C [94]. TEMPO in combination with BPO was used by Prodpran et al. [95]. Utilizing TEMPO-terminated oligomers of polystyrene also results in stable latexes, but the particle size distribution is unexpectedly broad [96]. In order to decrease the reaction temperature below 100°C, an acrylic  $\beta$ -phosphonylated nitroxide in combination with the KPS/ $\text{Na}_2\text{S}_2\text{O}_5$  redox initiator system was used [97].

3. *Living radical polymerizations* in miniemulsions have also been conducted by de Brouwer et al. using reversible addition-fragmentation chain transfer (RAFT) and nonionic surfactants [98]. The polydispersity index was usually below 1.2. The living character is further exemplified by its transformation into block copolymers.
4. *Reverse atom transfer radical polymerization* (ATRP) of butyl methacrylate was successfully conducted in miniemulsions by Matyaszewski et al. using the water-soluble initiator V50 and the hydrophobic ligand 4,4'-di(5-nonyl)-4,4'-bipyridine (dNbpy) to complex the copper ions. Although the forming radical mediator Cu(II) complex had a large water-partitioning coefficient, the rapid transfer of Cu(II) between the organic and aqueous phases assured an adequate concentration of the deactivator in the organic phase. As a result, controlled polymerization was achieved [99, 100].

## 5

### Hybrid Nanoparticles by Miniemulsion Technologies

#### 5.1

##### Polymer-Polymer Hybrids

Water-insoluble materials such as resins by dissolution or dispersion can be incorporated easily in the organic phase by using the miniemulsion process. Miniemulsion copolymerizations were carried out with acrylic monomers (methyl methacrylate, butyl acrylate, and acrylic acid) in the presence of alkyd resin in order to produce stable polymer-polymer hybrid latex particles incorporating an alkyd resin into acrylic coating polymers [42]. Throughout the reaction, the resin simultaneously acts as a hydrophobe and allows the stabilization of the miniemulsion. The double bonds served as grafting sites of the alkyd onto the polyacrylate and predominantly poly(acrylate-g-alkyd) was formed [101]. Despite a high degree of crosslinking (>70%), residual double bonds were still present in the polymer-polymer hybrid latex for curing reactions during film formation [102].

Polymerizing acrylic monomers in the presence of oil-modified polyurethane leads also to a grafting onto the polyacrylics, resulting in dispersions suitable for stable water-borne latexes with good adhesion properties and fair hardness properties [103].

Oil-acrylate hybrid-emulsions were formed using the fatty-acid hydroperoxides as initiator system for the miniemulsion polymerization of acrylate. The initiation took place at the droplet interface and resulted in the formation of triglycide modified polyacrylate molecules which act as compatibili-

zers between the oil and the PMMA phase, resulting in more homogeneous particles [104].

## 5.2

### Encapsulation of Pigments by Direct Miniemulsification

For the encapsulation of pigments by miniemulsification, two different approaches can be used. In both cases, the pigment/polymer interface as well as the polymer/water interface have to be carefully chemically adjusted in order to obtain encapsulation as a thermodynamically favored system. The design of the interfaces is mainly dictated by the use of two surfactant systems, which govern the interfacial tensions, as well as by employment of appropriate functional comonomers, initiators, or termination agents. The sum of all the interface energies has to be minimized.

For a successful incorporation of a pigment into the latex particles, both type and amount of surfactant systems have to be adjusted to yield monomer particles, which have the appropriate size and chemistry to incorporate the pigment by its lateral dimension and surface chemistry. For the preparation of the miniemulsions, two steps have to be controlled (see Fig. 14). First, the already hydrophobic or hydrophobized particulate pigment with a size up to 100 nm has to be dispersed in the monomer phase. Hydrophilic pigments require a hydrophobic surface to be dispersed into the hydrophobic monomer phase, which is usually promoted by a surfactant system 1 with low HLB value. Then, this common mixture is miniemulsified in the water phase employing a surfactant system 2 with high HLB, which has a higher tendency to stabilize the monomer (polymer)/water interface.

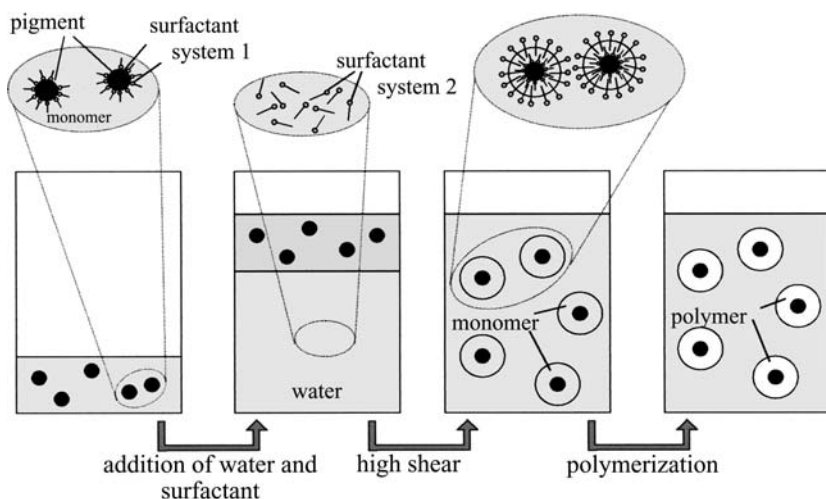
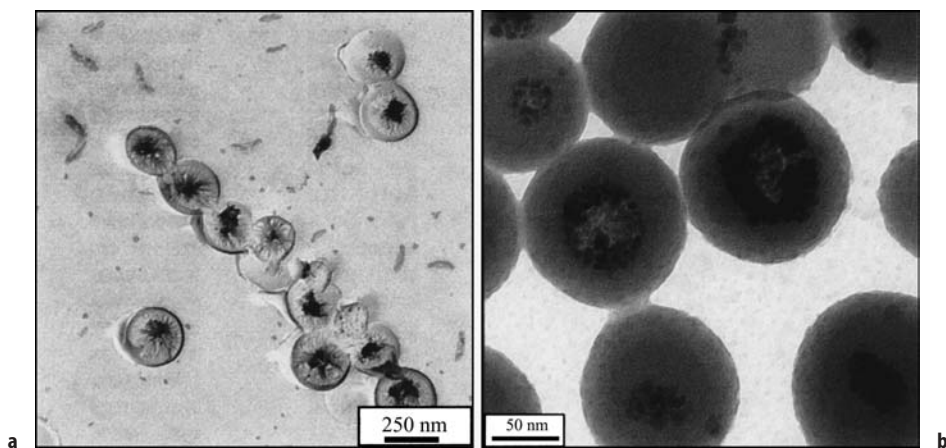


Fig. 14. Principle of encapsulation by miniemulsion polymerization

Erdem et al. described the encapsulation of  $\text{TiO}_2$  particles via miniemulsion in the two steps. First,  $\text{TiO}_2$  was dispersed in the monomer using the OLOA 370 (polybutene-succinimide) as stabilizer [105]. Then this phase was dispersed in an aqueous solution to form stable submicron droplets [106]. The presence of  $\text{TiO}_2$  particles within the droplets limited the droplet size. Complete encapsulation of all of the  $\text{TiO}_2$  in the colloidal particles was not achieved; the encapsulation of 83% of the  $\text{TiO}_2$  in 73% of the polymer was reported. Also the amount of encapsulated material was very low: a  $\text{TiO}_2$  to styrene weight ratio of 3:97 could not be exceeded [107, 108].

Nanoparticulate hydrophilic  $\text{CaCO}_3$  was effectively coated with a layer of stearic acid as surfactant system 1 prior to dispersing the pigments into the oil phase [58]. The  $-\text{COOH}$  groups act as good linker groups to the  $\text{CaCO}_3$ , and the tendency of the stearic acid to go to the second polymer/water interface was found to be low. Then 5 wt% of  $\text{CaCO}_3$  based on monomer could be completely encapsulated into polystyrene particles [58]. It was shown that the weight limit was given by the fact that, at this concentration, each polymer particle already contained one  $\text{CaCO}_3$  colloid, which was encapsulated in the middle of the latex particle (Fig. 15a).

The encapsulation of magnetite particles into polystyrene particles was efficiently achieved by a miniemulsion process using oleoyl sarcosine acid [109] or the more efficient oleic acid as first surfactant system to handle the interface magnetite/styrene, and SDS to stabilize the interface styrene/water, thus creating a polymer-coated ferrofluid (Fig. 15b). Since the magnetite particles were very small (ca. 10 nm), each polymer particle was able to incorporate many inorganic nanoparticles. A content of 20 wt% could be incorporated in this way.



**Fig. 15.** a Encapsulation of one colloid per polymer particle:  $\text{CaCO}_3$  nanoparticles in PS latex particles; b Encapsulation of many colloids per polymer particle:  $\text{Fe}_3\text{O}_4$  in PS particles

### 5.3

#### Encapsulation of Carbon Black by Co-Miniemulsion

Since carbon black is a rather hydrophobic pigment (depending on the preparation conditions), the encapsulation of carbon black in the latexes by direct dispersion of the pigment powder in the monomer phase prior to emulsification is again a suitable way [58]. Here, full encapsulation of non-agglomerated carbon particles can be provided by the appropriate choice of the hydrophobe. In this case the hydrophobe not only acts as the stabilizing agent against Ostwald ripening for the miniemulsion process, but also mediates to the monomer phase by partial adsorption. However, this direct dispersion just allows the incorporation of 8 wt% carbon black since the carbon is still highly agglomerated in the monomer. At higher amounts, the carbon cluster broke the miniemulsion, and less defined systems with encapsulation rates lower than 100%, which also contained pure polymer latexes, were obtained.

To increase the amount of encapsulated carbon to up to 80 wt%, another approach was developed [110] where both monomer and carbon black were independently dispersed in water using SDS as a surfactant and mixed afterwards in any ratio between the monomer and carbon. Then this mixture was cosonicated, and the controlled fission/fusion process characteristic for miniemulsification destroyed all aggregates and liquid droplets, and only hybrid particles being composed of carbon black and monomer remain due to their higher stability [110]. This controlled droplet fission and heteroaggregation process can be realized by high energy ultrasound or high pressure homogenization as was shown earlier.

TEM and ultracentrifuge results showed (see Fig. 16) that this process results in effective encapsulation of the carbon with practically complete yield: only rather small hybrid particles, but no free carbon or empty polymer particles, were found. It has to be stated that the hybrid particles with high carbon contents do not possess spherical shape, but adopt the typical fractal structure of carbon clusters, coated with a thin but homogeneous polymer film. The thickness of the monomer film depends on the amount of monomer, and the exchange of monomer between different surface layers is – as in miniemulsion polymerization – suppressed by the presence of an ultrahydrophobe.

Therefore the process is best described as a polymerization in an adsorbed monomer layer created and stabilized as a miniemulsion ('ad-mini-emulsion polymerization'). The process is schematically shown in Fig. 16.

### 5.4

#### Encapsulation of a Liquid – Formation of Nanocapsules

The polymerization in miniemulsion can also be performed in the presence of an oil, which is inert to the polymerization process. During polymerization, oil and polymer can demix, and many different structures such as an oil droplet encapsulated by a polymer shell, sponge like architectures, or dotted oil droplets can be formed. The formation of such structures is known from classical emul-

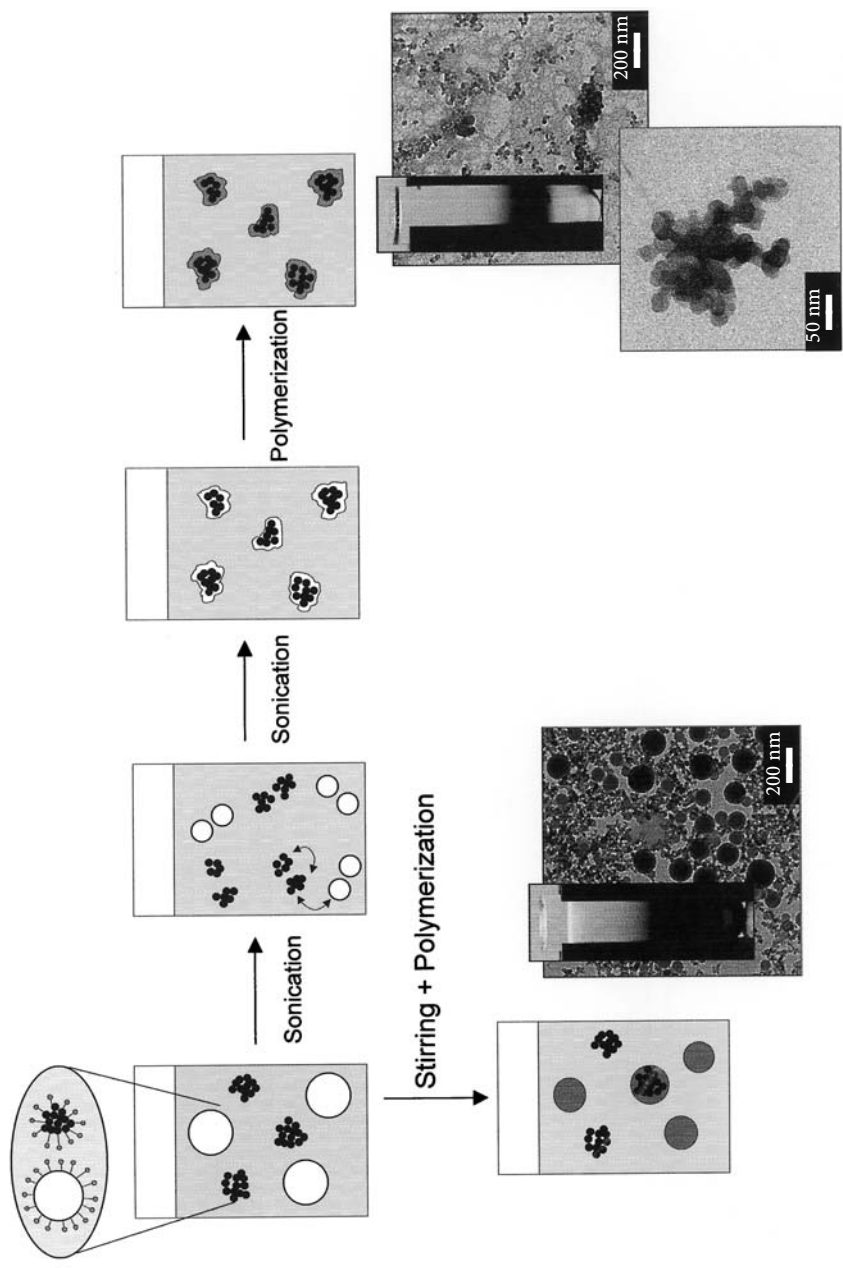


**Fig. 16.** Principle of co-mini-emulsion where both components have to be independently dispersed in water and mixed afterwards. The controlled fission/fusion process in the miniemulsification realized by high energy ultrasound or high pressure homogenization destroys all aggregates and liquid droplets, and only hybrid particles being composed of carbon black and monomer remain due to their higher stability

sion polymerization, but is usually kinetically controlled [111–113]. The synthesis of hollow polymer nanocapsules as a convenient one-step process using the miniemulsion polymerization, however, has the advantage of being thermodynamically controlled [114].

The chemical control of the expected particle morphology for an encapsulation process is a system with a complex parameter field. The particle morphology reacts sensitively on the chemical nature of the emulsifier, the polymer, and the oil, as well as on additives such as an employed additional hydrophobe, the initiator, or possible functional comonomers. It is obvious that the development of the final morphology in polymer microparticles also involves the mobility or diffusion of at least two molecular species influenced by some driving force to attain the phase-separated structure. The ease of movement may be related to the phase viscosity, but in this approach the main emphasis is laid on the driving force, which is the Gibbs free energy change of the process.

It was found that the nanocapsules are formed in a miniemulsion process by a variety of monomers in the presence of larger amounts of a hydrophobic oil. Hydrophobic oil and monomer form a common miniemulsion before polymerization, whereas the polymer is immiscible with the oil and phase-separates throughout polymerization to form particles with a morphology consisting of a hollow polymer structure surrounding the oil. The differences in the hydrophilicity of the oil and the polymer turned out to be the driving force for the formation of nanocapsules.

In the case of poly(methyl methacrylate) (PMMA) and hexadecane as a model oil to be encapsulated, the pronounced differences in hydrophilicity are suitable for direct nanocapsule formation. PMMA is regarded as rather polar (but is not water soluble), whereas hexadecane is very hydrophobic so that the spreading coefficients are of the right order to stabilize a structure in which a hexadecane droplet core is encapsulated in a PMMA shell surrounded by water [114]. In the state of miniemulsion, the monomer and the hexadecane are miscible, but phase separation occurs during the polymerization process due to the immiscibility of hexadecane and PMMA. Miniemulsions were obtained by mixing the monomer MMA and hexadecane at varying ratios together with the hydrophobic, oil-soluble initiator AIBN and miniemulsifying the mixture in an aqueous solution of SDS. After polymerization polymer capsules were obtained as shown in Fig. 17a. Nanocapsules with an increased shell stability can be obtained by using up to 10 wt% of EGDMA as crosslinking agent. It is a fortunate experimental situation that the particle size in this reaction does not change with the amount of the anionic surfactant SDS or the nonionic surfactant Lutensol AT50 (a hexadecyl modified poly(ethylene glycol)). This means that with increasing surfactant load the surface coverage also increases, and the interfacial tension at the droplet/water interface decreases. That way, the influence of the systematic variation of one of the interface tensions on the particle morphology was examined, and a continuous morphological change towards engulfed structures was found (Fig. 17b) [114].

In the case of styrene as monomer and hexadecane as model oil, the cohesion energy density of the polymer phase is closer to that of the oil and therefore the structure of the final particles depends much more on the parameters, which



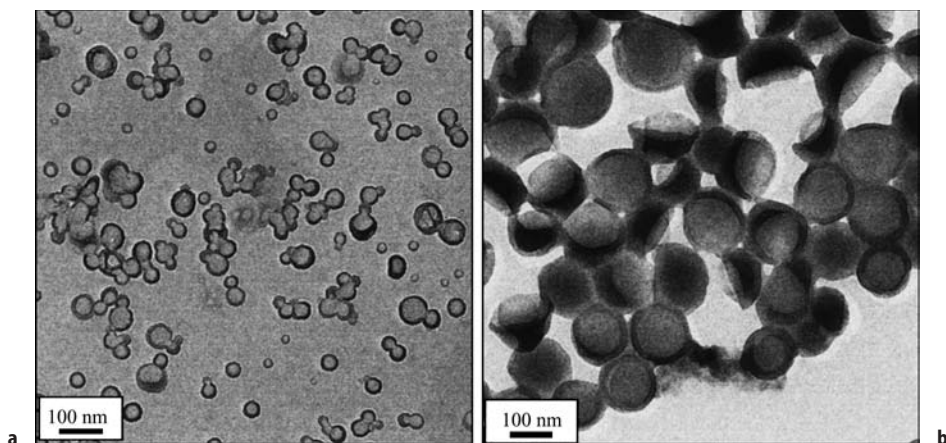


**Fig. 17.** **a** TEM micrographs of nanocapsules with an MMA to HD ratio of 1:1 using SDS as surfactant; **b** Coexistence of nanocapsules and capped particles in the case of using the surfactant Lutensol AT50

critically influence the interfacial tensions. A variety of different morphologies in the styrene/hexadecane system can be obtained by changing the spreading parameter. This was done by changing the monomer concentration, the type and amount of surfactant, as well as the initiator and the functional comonomer.

The best results were obtained by using the block copolymer surfactant SE3030 together with the nonionic initiator PEGA200 which supports interface stabilization and improves the structural perfection (Fig. 18a) of the polystyrene capsule morphology.

Another very powerful approach to improve the perfection of the capsules is the addition of a comonomer to the oil phase. Depending on the polarity of the monomer, it will enter one of the two interfaces (polymer/water or polymer/oil) and reduce the corresponding interfacial tensions and spreading coefficients. It was shown that the very hydrophobic comonomer lauryl methacrylate, which is expected to minimize the interfacial tension between styrene and the hexadecane phase, has no significant effect on the resulting morphology of the particles, meaning that this interfacial energy is of minor importance since it is already quite low. On the other hand, the slightly more hydrophilic MMA and the very hydrophilic AA affect the interfacial tension of styrene to water, and here a pronounced influence on the morphology was found. The influence depends on the partitioning coefficient: for MMA about 50 wt% of monomer was needed to create only close-to-perfect capsules, whereas 1 wt% of AA was sufficient in order to saturate the capsule surface with carboxylic groups, and hollow shell structures with constant capsule thickness were found (Fig. 18b). There is, however, a minor fraction of small homogeneous polymer latexes which we attribute to secondary nucleation due to the high content of water-soluble acrylic acid.

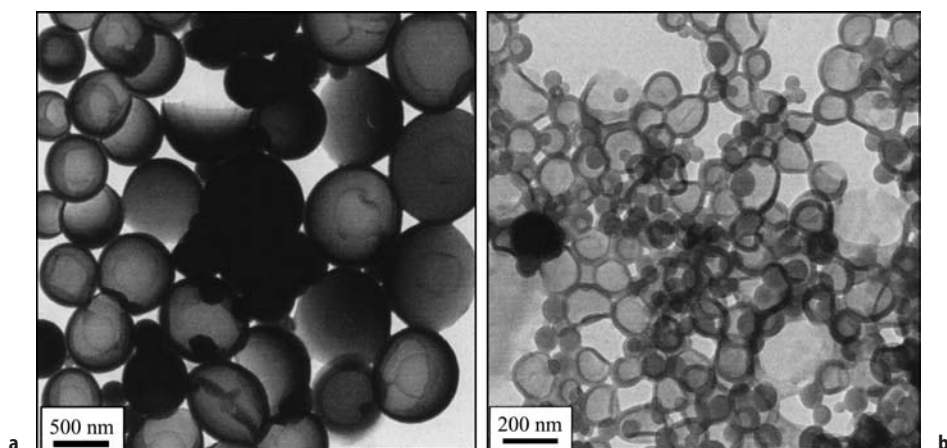


**Fig. 18a,b.** TEM micrographs of PS/hexadecane: **a** with SE3030 as surfactant and PEGA200 as initiator; **b** with AA as comonomer

## 5.5

### Surface Coating of Miniemulsions with Inorganic Nanoparticles and Crystalline Building Blocks

In many cases gas permeation or chemical sensitivity of polymer capsules is still too high to be efficient for encapsulation. Here the employment of crystalline inorganic materials, such as clay sheets of 1.5 nm thickness, can be recommended. Since those clay sheets are fixed like scales onto the soft, liquid miniemulsion droplet, the resulting objects are called ‘armored latexes’ [115]. Since clays carry a negative surface charge, miniemulsions stabilized with cationic sulfonium-surfactants represented a convenient way to generate those armored latexes or crystalline nanocapsules. Due to their high stability against changes in the chemical environment, it is possible to use miniemulsion droplets themselves, but also polymerized latex particles as templates for such a complexation process. As a result, the liquid droplets or the polymer particles are then completely covered with clay plates and therefore film formation or coalescence is prevented. A synthetic monodisperse model clay with small lateral extensions was employed. As a result, the liquid droplets or the polymer particles are then completely covered with clay plates, which is also macroscopically visible by the absence of film formation or coalescence. However, complexation with the clay plates alone was not always sufficient to prohibit the release of low  $T_g$  polymer (e.g., PBA) or liquid material. In order to glue further together the single clay sheets, silicic acid was used as a ‘mortar’. Therefore the stability of the shells can be increased by a condensation reaction with silicic acid, which reacts with itself, but also with residual surface OH-groups of the clay. In this case, film formation is indeed completely suppressed as shown by TEM for dried sample with PBA as template (Fig. 19a). The figure shows intact nanocapsules still filled with PBA with about the same size as found previously in solution. To receive an emptied, purely in-



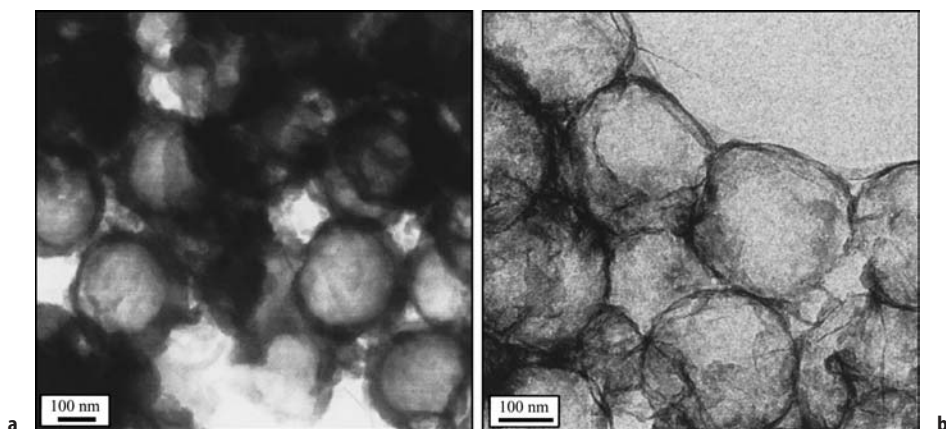


**Fig. 19a,b.** TEM of armored latexes: **a** sealed clay on PBA template particles; **b** sealed clay on PMMA template particles after removal of the PMMA in the core

organic shell, PMMA latex particles were used as templates. By intense illumination with the electron beam, PMMA depolymerizes to MMA, which uses or creates little pores in the shell to evaporate under the TEM high vacuum conditions. Figure 19b shows such emptied capsules as obtained by electron degradation. In any case the inorganic structure has not disintegrated; this means that the colloidal 'laying of bricks' was successful. These 'armored' droplets and latexes particles could be of high interest for pressure sensitive adhesives or as a new type of filler with unconventional chemical and mechanical performance.

### 5.5.1

#### *Miniemulsions with Silica Nanoparticles*

Switching from the very hydrophilic clays towards other inorganic nanoparticles, e.g., colloidal silica, leads, in the interplay with polymerization in miniemulsions, into a potential structural complexity, which covers the whole range from embedded particles (such as in the case of the calcium carbonate and carbon blacks) to surface bound inorganic layers (such as in the case of the clays). For basic research they are ideal systems to analyze complex structure formation processes in emulsions, since the original droplet shows a structure which is essentially established by molecular forces and local energy considerations, and which is ideally just solidified into a polymer structure.

It was discussed that the structure created by the ternary system oil/water/nanoparticle follows the laws of spreading thermodynamics, as they hold for ternary immiscible emulsions (oil 1/oil 2/water) [114, 116, 117]. The only difference is that the interfacial area and the curvature of the solid nanoparticle has to stay constant, i.e., an additional boundary condition is added. When the inorganic nanoparticles possess, beside charges, also a certain hydrophobic character, they become enriched at the oil-water interface, which is the physical base of the stabilizing power of special inorganic nanostructures, the so-called Picker-

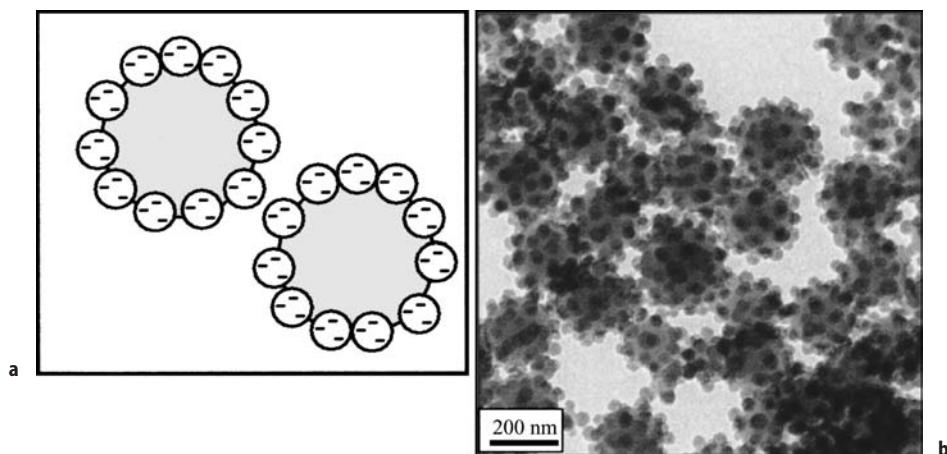


**Fig. 20.** a Scheme for using silica particles as stabilizer for monomer droplets of miniemulsions (Pickering stabilization); b Represents a latex with a monomer to silica ratio of 1:0.32

ing-stabilizers [118–120]. This means that the surface energy of the system oil/nanoparticle/water has to be lower than the sum of the binary combinations oil/water and water/nanoparticle to enable superstructure formation to occur. Since all three terms can be adjusted by the choice of the monomer and the potential addition of surfactants, this spans a composition diagram with a variety of morphologies to occur. Silica nanoparticles are quite ideal as model nanoparticles for the systematic examination of compositional phase behavior since they are easy to obtain and to control with respect to their surface structure and interacting forces. The latter is done either by variation of pH, which changes the surface charge density, or by adsorption of cationic organic components, changing the polarity of the objects.

It was shown that silica nanoparticles in the absence of any surfactant could act as a Pickering stabilizer for a miniemulsion process [121]. The high quality and small overall particle size obtained only under alkaline conditions (pH=10) and in presence of the basic comonomer 4-vinylpyridine which acts as an aminic coupler [122, 123] is shown in Fig. 20. The particle size depends on the amount of silica in the expected way: the higher the silica content, the smaller the resulting stable hybrid structures. Comparably small compound particles in the size range between 120 nm and 220 nm in diameter with rather narrow size distribution were obtained [121], speaking for the high stabilization power of the silica particles as Pickering stabilizers. This underlines the surface activity of the silica nanoparticles under the applied conditions and the kinetic-free, equilibrium type structure of a miniemulsion latex particle. Since these systems are free of low molecular weight surfactants and all chemical side products which might act as a surfactant, the measured surface tension was as high as  $71.4 \text{ mN m}^{-1}$ , which is practically the value of pure water.

The addition of a surfactant (nonionic, anionic, or cationic) to the same system resulted in a more complex zoo of structures [121]. Nonionic surfactants are

preferentially bound to the silica nanoparticles due to a preferential interaction between the silica and the ethylene oxide chains [124], which screens any interaction with the monomer mixture. Also the addition of the anionic sodium dodecyl sulfate (SDS) leads to electrostatic repulsion and a competition between surfactant and silica nanoparticles. The most pronounced morphology changes are observed with the cationic surfactant cetyltrimethylammonium chloride (CTMA-Cl). Due to charge coupling as well as induced dipole interaction, this surfactant strongly binds to silica over the whole pH-range. The surfactant is mainly adsorbed by the silica, but under standard conditions there is not enough CTMA in the recipe to counterbalance the negative charges of the system at pH=10. In the presence of 4-vinylpyridine, the strong acid-base interaction gives an additional stability. Therefore, at pH=10 a hedgehog morphology is found with a small overall diameter of 90 nm.

At higher CTMA concentrations exceeding the amount adsorbed onto the silica, a different morphology was found. Starting from a calculated surface coverage of 75%, the silica particles become incorporated into the droplets, and stable hybrid structures are obtained. The hybrids now have a raspberry morphology; however, they are rather heterogeneous with respect to loading with silica [121].

## 6

### Non-Radical Polymerizations in Miniemulsion

#### 6.1

##### Polyaddition

As already indicated in the introduction, the existence of stable, isolated nanodroplets, in which chemical reactions may, but do not have to, depend on droplet exchange (the so-called 'nanoreactors'), enables the application of the miniemulsion process in a much broader range.

In contrast to the process of creating a secondary dispersion as was used for the preparation of, e.g., polyurethanes and epoxide resins, it was shown that the miniemulsion polymerization process allows one to mix monomeric components together, and polyaddition and polycondensation reactions can be performed *after* miniemulsification in the miniemulsified state [125].

The principle of miniemulsion polymerization to polyadditions of epoxy-resins was successfully transferred to mixtures of different epoxides with varying diamines, dithiols, or diols which were heated to 60°C to form the respective polymers [125]. The requirement for the formulation of miniemulsions is that both components of the polyaddition reaction show a relatively low water solubility, at least one of them even below  $10^{-5} \text{ g l}^{-1}$ . The diepoxide bisphenol-A-diglycidylether was successfully used as epoxy component. In order to vary the obtained polymeric structure, tri- and tetra-functionalized epoxides were also used. As amino components a  $\text{NH}_2$  terminated poly(propylene oxide) with  $M_w=2032 \text{ g mol}^{-1}$ , 4,4'-diaminobenzyl, 1,12-diaminododecane, and 4,4'-diaminodicyclohexylmethane were applied. As other addition components beside amine, 1,6-hexanedithiol and Bisphenol A were used. The hydrophobic compo-

nent, which is required for the formulation of stable miniemulsions, is usually the applied epoxide itself, which has a very poor water solubility and provides sufficient retardation of the Ostwald ripening. The addition of a typical hydrophobe like hexadecane does not improve the miniemulsion stability indicating that monomer exchange is not the rate-determining step. The final polymers reveal molecular weights of about  $20,000 \text{ g mol}^{-1}$  with a dispersity of close to 2. This means that unexpectedly ideal reaction conditions are preserved during the reaction in miniemulsion, and that the proximity of the interface to water does not really disturb the reaction. Crosslinked epoxy network could be obtained by the reaction of both amine hydrogens, e.g., the molar ratio of diepoxide to diamine was chosen to be 2:1. SDS and the block copolymer SE3030 turned out to be very efficient surfactants for the polyaddition systems. With increasing amount of surfactant, the particle size decreases as expected. Using SDS as surfactant for the stabilization of the Epikote E828/Jeffamin D2000 system, the particle size ranges from 245 nm (1.7 wt% SDS relative to the monomer mixture) down to 83 nm (42 rel.% SDS). For the latexes of Epikote E828 and 1,12-diaminododecane synthesized with SDS, the particle size also shows the expected trend: with increasing amount of surfactant the particle size decreases from 816 nm (0.85 rel.% SDS) to 36 nm (25 rel.% SDS).

In general, it turned out that with increasing hydrophobicity of the reaction partner, the particle sizes also decrease, and small particles with a diameter down to 30 nm can be synthesized from a number of most hydrophobic combinations. This is about the minimal size which can be made by radical processes, i.e., we reach a limit given by the fundamental laws of colloidal stability. Figure 21a shows as a typical example the reaction product of Epikote E828 and 4,4'-diaminobenzyl: small particles with a relatively narrow size distribution are obtained.

It was also shown that polyurethane latexes can be made by direct miniemulsification of a monomer mixture of diisocyanate and diol in an aqueous surfactant solution followed by heating (see Fig. 21b) [126]. This is somewhat special since one might expect a suppression of polymerization by side reactions between the very reactive diisocyanates and the continuous phase water. Therefore, it is important that the reaction between diisocyanate and diol has to be slower than the time needed for the miniemulsification step and the side reaction of the diisocyanate with water in the dispersed state has to be slower than the reaction with the diol. The functional groups (isocyanate to alcohol groups) were employed in a 1:1 molar ratio. IR spectra of the reactants and the resulting product show the disappearance of the isocyanate group after reaction (peak at  $2300 \text{ cm}^{-1}$ ). The amide vibration at  $3300 \text{ cm}^{-1}$ , the carbonyl vibration at  $1695 \text{ cm}^{-1}$ , and the vibration at  $1552 \text{ cm}^{-1}$  are strong evidence for the formation of a polyurethane. The side reaction with water, leading to urea groups within the polyurethane, was also identified by the characteristic vibration at  $1643 \text{ cm}^{-1}$ , but turned out to be of secondary importance.

Polyaddition was also performed using chitosan stabilizer with two biocompatible costabilizers, Jeffamine D2000 and Gluadin, and a linking diepoxide in presence of an inert oil and it results, via an interface reaction, in thin but rather stable nanocapsules. Since both water and oil soluble aminic costabilizers can be

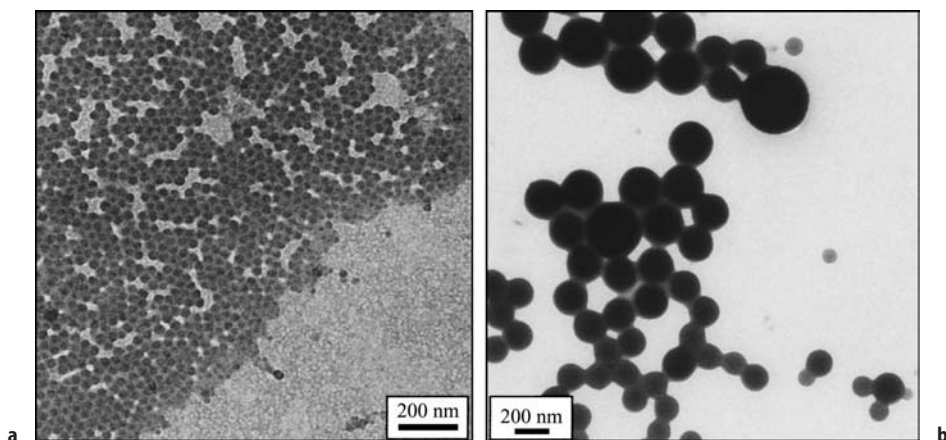


**Fig. 21.** **a** Typical latex obtained in a polyaddition process in miniemulsion (Epikote E828 (bisphenol-A-diglycidylether) and 4,4'-diaminobenzyl); **b** TEM micrograph of a polyurethane latex obtained by isophorone diisocyanate and 1,12 dodecanediol

used, these experiments show the way to a great variety of capsules with different chemical structure. These capsules are expected to be biocompatible and biodegradable and might find applications in drug delivery [127].

## 6.2

### Anionic Polymerization

For the anionic polymerization of phenyl glycidyl ether (PGE) in miniemulsion, Maitre et al. used didodecyldimethylammonium hydroxide as an 'inisurf', which acts as a surfactant and an anionic initiator by means of its hydroxy counterion at the same time [128]. As revealed by  $^1\text{H}$  NMR and FTIR, genuine  $\alpha,\omega$ -dihydroxylated polyether chains were produced. The average molecular weight could be increased by varying the initiator concentration, type and concentration of surfactants, or by adding an alcohol as costabilizer. With increasing conversion, the polymer chain length increased but remained small, with a critical polymerization degree of  $\text{DP}_{\text{max}}=8$ .

## 6.3

### Metal Catalyzed Polymerization Reactions

Ethylene can be polymerized using an aqueous miniemulsion consisting of an organo-transition metal catalyst at ethylene pressures of 10–30 bar and temperatures of 45–80°C resulting in large particles of about 600 nm [129]. A maximal productivity of 2520 kg PE per g atom active metal was achieved, which represents about 60% of the productivity of the same catalyst when used in ethylene suspension polymerization in organic phase.

## 7

**Inorganic Miniemulsions**

Miniemulsification is not restricted to organic monomers. It was shown that it can also be applied for low melting salts and metals to obtain salt or metal colloids of high homogeneity with diameters between 150 nm and 400 nm [130]. This is regarded as a very important development, since it allows the synthesis and handling of inorganic or metallic powders and their incorporation into coatings, inks, or nanocomposites by simple polymer technologies.

The extension of miniemulsions from water or polar monomers as a dispersed phase in oils or hydrocarbons as a continuous phase to salt melts or concentrated salt solutions is nevertheless demanding, since those liquids show higher cohesion energies, surface tensions, and mutual attractions than the corresponding organic matter. For that, a well-chosen steric stabilizer has to be employed, the polar part of which has to be miscible with salt melts, whereas the hydrophobic part has to be sufficiently long and tightly packed to provide sufficient steric stabilization. Again, it turned out that amphiphilic block copolymers [131] with poly(ethylene oxide) block are best suited. For the salt, one can choose from a wide variety of salts or metals, which melt below boiling or chemical decomposition of the continuous phase (which can easily be as high as 250–300°C). It is also possible to use highly concentrated salt solutions in water or to decrease the melting point by adding ternary components to the salts.

As an example, iron(III) chloride hexahydrate was melted by heating above 37°C and miniemulsified in the continuous phase (IsoparM, cyclohexane, etc.) to a stable miniemulsion using at least 5 wt% (with respect to salt) of the block copolymer stabilizer. Decreasing the temperature leads to nanoscopic salt crystals dispersed in a continuous oil phase. The average size of these particles is about 350 nm, a typical number for inverse dispersions.

Pure zirconyl chloride octahydrate melts and degrades at 150°C, but the melting temperature of the salt can easily be reduced by adding water to the salt. A 3:1  $\text{ZrOCl}_2$ /water mixture melts at about 70°C. The molten salt was added to IsoparM at 75°C. A stable miniemulsion was obtained using 10 wt% of the block copolymer poly(ethylene-*co*-butylene-*b*-ethylene oxide) (PE/B-EO), which transforms throughout cooling in a dispersion of separate  $\text{ZrOCl}_2$  nanocrystals. TEM pictures show (see Fig. 22a) that the particles are of uniform polyhedral crystalline shape.

For the preparation of nanosized metal dispersions the same procedure of high shear forces was used to prepare miniemulsions. Molten metals have very strong cohesion forces, which make them very difficult to disperse in an organic phase by conventional techniques. Gallium (mp=30°C) was melted at 45°C and emulsified in IsoparM by using 10 rel.% P(E/B-*bock*-EO). The miniemulsion was cooled to room temperature, and solid gallium particles with a size of 150 nm were obtained. Miniemulsification was also applied to disperse low melting alloys, like Wood's metal (mp=70°C) or Rose's metal (mp=110°C). Because of the very high density difference of the metal ( $\rho$  (Wood's metal)=9.67 g cm<sup>-3</sup>) and the continuous phase ( $\rho$  (IsoparM)=0.87 g cm<sup>-3</sup>), the weight-content of the metal was increased to 50 wt% (with respect to the overall dispersion) to obtain relevant volume fractions (for TEM see Fig. 22b).



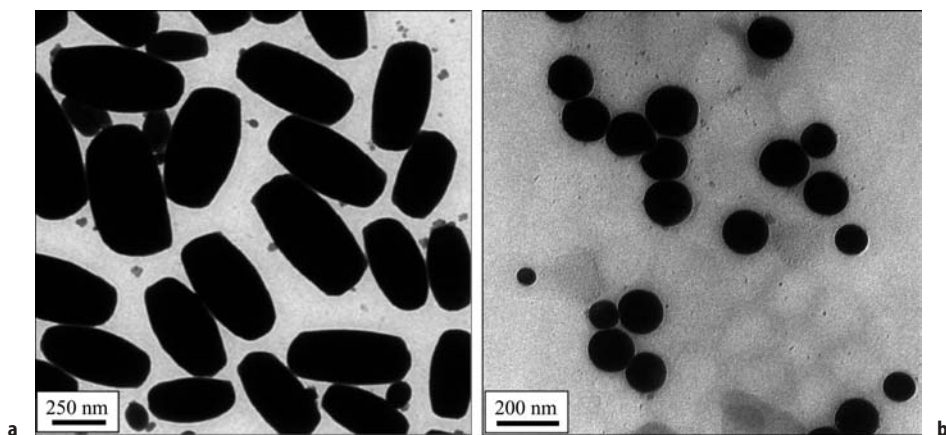


**Fig. 22a,b.** Particles obtained in an inverse miniemulsion process consisting of: **a**  $\text{ZrOCl}_2 \cdot 8\text{H}_2\text{O}$ ; **b** Wood's metal

The formation of high-melting materials can be achieved by a further reaction where the low-melting material is used as a precursor. These are subsequently transferred in a particle-by-particle fashion to the final product by reaction or precipitation, very similar to polymerization reactions of organic monomers. In the dispersed state heterophase reactions such as precipitations or oxidations can be performed, which essentially occur under preservation of the colloidal entities as single nanoreactors.

Addition of a base (pyridine or methoxyethylamine), which can mix with the continuous phase to the cyclohexane-salt miniemulsion under stirring, provides reaction to oxides and hydroxides, e.g., from iron(III) chloride hexahydrate to iron(III) oxide. Here the crystal water steps into the reaction, while pyridine from the continuous phase neutralizes the eliminated HCl. Obviously, the interface area of the miniemulsion is high enough in order to allow this reaction.

Formation of  $\text{Fe}_2\text{O}_3$  is accompanied with an increase of the particle density ( $\rho(\text{Fe}_2\text{O}_3) = 5.24 \text{ g cm}^{-3}$ ). However, light scattering values and TEM pictures show that the droplets do not shrink as a whole, but show a hollow aggregate structure with interstitial cavities between primary particles (Fig. 23a). The particle size in cyclohexane could be varied by changing the amount of surfactant between 240 nm (20 rel.% TEGO EBE45 surfactant) to 370 nm (5 rel.%) and in IsoparM between 150 nm (42.5 rel.%) and 390 nm (5 rel.%).

The confinement of two species in stoichiometric amounts within the nanodroplets also allows the synthesis of mixed species. A mixture of  $\text{Fe}^{2+}$  and  $\text{Fe}^{3+}$  salts leads to the formation of magnetite,  $\text{Fe}_3\text{O}_4$ . The final dispersion with a particle size of 200 nm is black and shows magnetic properties. As is seen in the TEM pictures (Fig. 23b), the superstructure composed of 10-nm nanoparticles as determined by WAXS is anisotropic (lemon shaped), and constituting needle shaped nanocrystals, can be identified inside the particles, arranged as bundles along the main axis of the 'lemons'.

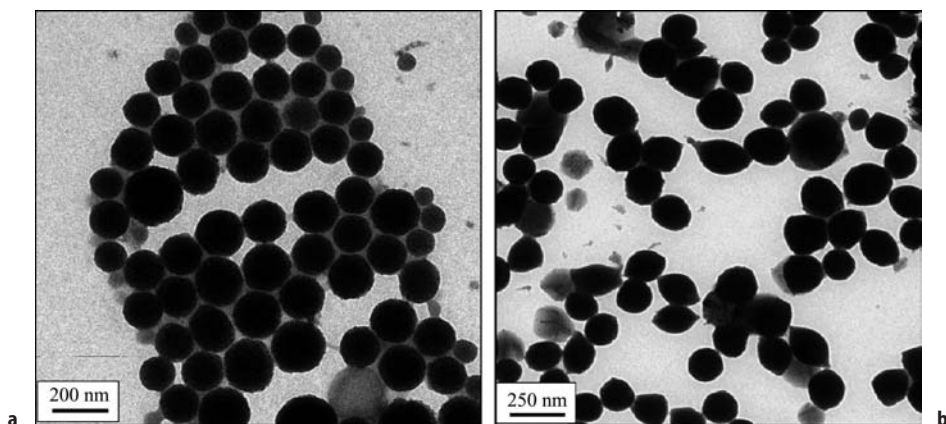


**Fig. 23a,b.** Reaction products of molten iron salt miniemulsions ('inorganic polymerizations'): **a**  $\text{Fe}_2\text{O}_3$  particles obtained from  $\text{FeCl}_3$  droplets; **b**  $\text{Fe}_3\text{O}_4$  particles obtained from  $\text{FeCl}_2/\text{FeCl}_3$  droplets

## 8 Conclusion

The main aim of this work was to summarize and combine recent progress in the field of miniemulsion. It was shown that the use of high shear, appropriate surfactants, and the addition of a hydrophobe in order to suppress the influence of Ostwald ripening are key factors for the formation of the small and stable droplets in miniemulsion. The kinetics of the reaction in the small separated nanodroplets was discussed in detail. It was shown that the strength of miniemulsion is the formation of polymeric nanoparticles consisting of polymers or polymer structures, which are hardly accessible by other types of heterophase polymerization. Non-radical polymerizations and the formation of hybrid materials by the encapsulation of inorganic materials or liquids are some examples which show the wide applicability of miniemulsions for technologically relevant problems. With the miniemulsification of molten inorganic materials in a subsequent reaction, the miniemulsions cross the border of polymers and open new possibilities in fabrication of solid particles for material science.

In my opinion, the field of miniemulsion is still on its rise in polymer and material science since there are numerous additional possibilities both for fundamental research and application. As a vision one may think of single molecules trapped and crystallized in each small droplet, which enables new types of physico-chemical experiments and handling of complex matter [132]. Since miniemulsions allow a very convenient and effective separation of objects in compartments of the size of 30–300 nm in diameter, some general new perspectives for polymer chemistry are opened. In miniemulsion droplets, it is in principle possible to isolate complex polymers or colloids strictly from each other and to react each single molecule for itself with other components, still working with significant amounts of matter and technically relevant mass fluxes. This



was called 'single (polymer) molecule chemistry' [133]. In this mode of operation, single molecule chemistry usually takes place in a highly parallel fashion, where the 3D-space is compartmentalized to small, nanometer-sized subunits or 'nanoreactors' in each of which the same reaction takes place, each on a single molecule. Although this is hardly used in classical chemistry, it is the regular case in biochemical reactions since practically all reactions take place in different compartmentalized areas of the cell [134]. The approach is not restricted to organic synthesis, but includes more complex physicochemical processes such as protein folding, which mainly takes place as a single molecular event in the nanocompartments [135]. Mimicking these processes in polymer chemistry would open a door to gain a better control of the outcome of a demanding complex process or chemical reaction.

## References

1. Blackley DC (1997) Polymer latices, 2nd edn. Chapman & Hill, London
2. Chou YJ, El-Aasser MS, Vanderhoff JW (1980) *J Dispers Sci Technol* 1:129–150
3. Ostwald WZ (1901) *Phys Chem* 37:385
4. Higuchi WI, Misra J (1962) *J Pharm Sci* 459–466
5. Webster AJ, Cates ME (1998) *Langmuir* 14:2068–2079
6. Postel M, Riess JG, Weers JG (1994) *Artif Cells Blood Substit Immob Biotechnol* 22:991–1005
7. Lowe KC (2000) *Artif Cells Blood Substit Immob Biotechnol* 28:25–38
8. Abismail B, Canselier JP, Wilhelm AM, Delmas H, Gourdon C (1999) *Ultrasonics Sonochem* 6:75–83
9. Wood RW, Loomis AL (1927) *Phil Mag* 4:417
10. Sorokin VI (1957) *Soviet Phys Acoust* 3:281–291
11. Li MK, Fogler HS (1978) *J Fluid Mech* 88:499–511
12. Li MK, Fogler HS (1978) *J Fluid Mech* 88:513–528
13. Bondy C, Söllner K (1935) *Trans Faraday Soc* 31:835–842
14. Mason TJ (1992) *Ultrasonics Sonochem* 30:192–196
15. Lauterborn W (1997) *Ultrasonics Sonochem* 4:65–75
16. Brösel S, Schubert H (1999) *Chem Eng Process* 38:533–540
17. Fontenot KJJ, Schork FJ (1992) In: Reichert KH, Moritz H (eds) *Fourth International Workshop on Polymer Reaction Engineering*. Dechema Monographs, Weinheim, Germany, vol 127, pp 429–439
18. Fontenot K, Schork FJ (1993) *Ind Eng Chem Res* 32:373–385
19. Landfester K, Bechthold N, Tiarks F, Antonietti M (1999) *Macromolecules* 32:5222–5228
20. Landfester K (2000) *Macromol Symp* 150:171–178
21. Guo JS, El-Aasser M, Vanderhoff J (1989) *J Polym Sci Polym Chem Ed* 24:861–874
22. Fontenot K, Schork FJ (1993) *J Appl Polym Sci* 49:633–655
23. Landfester K, Bechthold N, Förster S, Antonietti M (1999) *Macromol Rapid Commun* 20:81–84
24. Ugelstad J, Mork PC, Kaggerud KH, Ellingsen T, Berge A (1980) *Adv Colloid Interface Sci* 13:101–140
25. Chern CS, Chen TJ, Liou YC (1998) *Polymer* 39:3767–3777
26. Reimers J, Schork FJ (1996) *Polym React Eng* 4:135–152
27. Chern CS, Chen TJ (1998) *Colloids Surf A Physicochem Eng Aspects* 138:65–74
28. Mouran D, Reimers J, Schork J (1996) *J Polym Sci Polym Chem Ed* 34:1073–1081
29. Wang S, Poehlein GW, Schork FJ (1997) *J Polym Sci Polym Chem Ed* 35:595–603
30. Alduncin JA, Forcada J, Asua JM (1994) *Macromolecules* 27:2256–2261

31. Reimers JL, Schork FJ (1997) *Ind Eng Chem Res* 36:1085–1087
32. Ugelstad J, El-Aasser MS, Vanderhoff JW (1973) *J Polym Sci Polym Lett Ed* 11:503–513
33. Ugelstad J, Hansen FK, Lange S (1974) *Makromol Chem* 175:507–521
34. Delgado J, El-Aasser MS, Vanderhoff JW (1986) *J Polym Sci Polym Chem Ed* 24:861–874
35. Chern CS, Chen TJ (1997) *Colloid Polym Sci* 275:546–554
36. Delgado J, El-Aasser MS, Silibi CA, Vanderhoff JW (1990) *J Polym Sci Polym Chem Ed* 28:777–794
37. Reimers JL, Schork FJ (1996) *J Appl Polym Sci* 60:251–262
38. Reimers JL, Schork FJ (1996) *J Appl Polym Sci* 59:1833–1841
39. Azad ARM, Ugelstad J, Fitch RM, Hansen FK (1976) In: Piirma I, Gardon JL (eds) *Emulsion polymerization*. ACS, Washington, D.C., vol 24, pp 1–23
40. Goetz RJ, El-Aasser MS (1990) *Langmuir* 6:132–136
41. Miller CM, Venkatesan J, Silibi CA, Sudol ED, El-Aasser MS (1994) *J Colloid Interface Sci* 162:11–18
42. Wang ST, Schork FJ, Poehlein GW, Gooch JW (1996) *J Appl Polym Sci* 60:2069–2076
43. Chang H-C, Lin Y-Y, Chern C-S, Lin S-Y (1998) *Langmuir* 14:6632–6638
44. Erdem B, Sully Y, Sudol ED, Dimonie VL, El-Aasser MS (2000) *Langmuir* 16:4890–4895
45. Landfester K, Willert M, Antonietti M (2000) *Macromolecules* 33:2370–2376
46. Willert M (2001) PhD thesis, Universität Potsdam
47. Candau F (1992) In: Paleos EC (ed) *Polymerization in organized media*. Gordon and Breach Science Publisher, Philadelphia, pp 215–282
48. Candau F (1995) *Macromol Symp* 92:169–178
49. Hunkeler DJ, Hernandez-Barajas J (1996) In: Salamone JC (ed) *Polymeric materials encyclopedia*. CRC Press, New York, vol 9, pp 3322–3333
50. Chou YJ, El-Aasser MS (1980) In: Fitch RM (ed) *Polymer colloids II*. Plenum Press, New York London, pp 599–618
51. Landfester K, Bechthold N, Tiarks F, Antonietti M (1999) *Macromolecules* 32:2679–2683
52. Putlitz BZ, Hentze H-P, Landfester K, Antonietti M (2000) *Langmuir* 16:3214–3220
53. Chern CS, Liou Y-C (1999) *Polymer* 40:3763–3772
54. Capek I (1999) *Adv Polym Sci* 145:1–55
55. Lim M-S, Chen J (2000) *J Polym Sci Polym Chem Ed* 38:1818–1827
56. Wang S, Schork FJ (1994) *J Appl Polym Sci* 54:2157–2164
57. Basak G, Landfester K, Antonietti M (2000) *Macromolecules* 33:9228–9232
58. Bechthold N, Tiarks F, Willert M, Landfester K, Antonietti M (2000) *Macromol Symp* 151:549–555
59. Harkins WD (1945) *J Chem Phys* 13:381–382
60. Harkins WD (1947) *J Am Chem Soc* 69:1428–1444
61. Harkins WD (1950) *J Polym Sci* 5:217–251
62. Tauer K, Mueller H, Schellenberg C, Rosengarten L (1999) *Colloid Surf A Phys Chem Eng Aspects* 153:143–151
63. Gilbert R (1995) *Emulsion polymerization*. Academic Press, San Diego
64. Tang PL, Sudol ED, Adams ME, Silibi CA, El-Aasser MS (1992) *ACS Symp Ser* 492:72–98
65. Tang PL, Sudol ED, Silebi CA, El-Aasser MS (1991) *J Appl Polym Sci* 43:1059–1066
66. Bechthold N, Landfester K (2000) *Macromolecules* 33:4682–4689
67. Saethre B, Moerk PC, Ugelstad J (1995) *J Polym Sci Polym Chem Ed* 33:2951–2959
68. Huang H, Zhang H, Li J, Cheng S, Hu F, Tan B (1998) *J Appl Polym Sci* 68:2029–2039
69. Wang CC, Yu NS, Chen CY, Kuo JF (1996) *J Appl Polym Sci* 60:493–501
70. Wang CC, Yu NS, Chen CY, Kuo JF (1996) *Polymer* 37:2509–2516
71. Landfester K (2001) *Macromol Rapid Comm* 22:896–936
72. Landfester K, Rothe R, Antonietti M (2002) *Macromolecules* 35:1658–1662
73. Wu XQ, Schork FJ (2000) *Ind Eng Chem Res* 39:2855–2865
74. Dewald RC, Hart LH, Carroll WF Jr (1984) *J Polym Sci Polym Chem Ed* 22:2923–2930
75. Reichert K-H, Baade W (1984) *Angew Makromol Chem* 123/124:381–386
76. Baade W, Reichert K-H (1986) *Makromol Chem Rapid Commun* 7:235–241
77. Landfester K, Antonietti M (2000) *Macromol Chem Rapid Comm* 21:820–824

78. Rodriguez VS, El-Aasser MS, Asua JM, Silibi CA (1989) *J Polym Sci Polym Chem Ed* 27:3659–3671
79. Asua JM, Rodriguez VS, Silebi CA, El-Aasser MS (1990) *Makromol Chem Macromol Symp* 35/35:59–85
80. Rodriguez VS, Delgado J, Silibi CA, El-Aasser MS (1989) *Ind Eng Chem Res* 28:65–74
81. Huang H, Zhang HT, Hu F, Ai ZQ, Tan B, Cheng SY, Li LZ (1999) *J Appl Polym Sci* 73:315–322
82. Inaba Y, Daniels ES, El-Aasser MS (1994) *J Coatings Technol* 66:63–74
83. Rajatapiti P, Dimonie VL, El-Aasser MS (1995) *J Macromol Sci Pure Appl Chem* A32(8/9):1445–1460
84. Rajatapiti P, Dimonie VL, El-Aasser MS, Vratsanos MS (1997) *J Appl Polym Sci* 63:205–219
85. Landfester K, Dimonie VL, El-Aasser MS (1998) *DECHEMA Monographs*, vol 134. Wiley-VCH Weinheim, pp 469–477
86. Chern CS, Sheu JC (2001) *Polymer* 42:2349–2357
87. Chern CS, Sheu JC (2000) *J Polym Sci A Polym Chem* 38:3188–3199
88. Willert M, Landfester K (2002) *Macromol Chem Phys* 203:825–836
89. Kukulj D, Davis TP, Gilbert RG (1997) *Macromolecules* 30:7661–7666
90. Matyjaszewski K, Gaynor SG (2000) In: Craver CD, Carraher CE (eds) *Applied polymer science: 21st century*. Elsevier Science, Oxford, pp 929–978
91. Lansalot M, Farcet C, Charleux B, Vairon J-P (1999) *Macromolecules* 32:7354–7360
92. Butte A, Storti G, Morbidelli M (2000) *Macromolecules* 33:3485–3487
93. Farcet C, Lansalot M, Pirri R, Vairon JP, Charleux B (2000) *Macromol Chem Rapid Commun* 21:921–926
94. MacLeod PJ, Barber R, Odell PG, Keoshkerian B, Georges MK (2000) *Macromol Symp* 155:31–38
95. Prodpran T, Dimonie VL, Sudol ED, El-Aasser MS (2000) *Macromol Symp* 155:1–14
96. Pan G, Sudol ED, Dimonie VL, El-Aasser MS (2001) *Macromolecules* 34:481–488
97. Farcet C, Lansalot M, Charleux B, Pirri R, Vairon JP (2000) *Macromolecules* 33:8559–8570
98. de Brouwer H, Tsavalas JG, Schork FJ, Monteiro MJ (2000) *Macromolecules* 33:9239–9246
99. Matyjaszewski K, Qiu J, Tsarevsky NV, Charleux B (2000) *J Polym Sci Polym Chem Ed* 38:4724–4734
100. Qiu J, Pintauer T, Gaynor SG, Matyjaszewski K, Charleux B, Vairon JP (2000) *Macromolecules* 33:7310–7320
101. Wu XQ, Schork FJ, Gooch JW (1999) *J Polym Sci Polym Chem Ed* 37:4159–4168
102. Tsavalas JG, Gooch JW, Schork FJ (2000) *J Appl Polym Sci* 75:916–927
103. Gooch JW, Dong H, Schork FJ (2000) *J Appl Polym Sci* 76:105–114
104. van Hamersveld EMS, van Es J, Cuperus FP (1999) *Colloid Surf A Physicochem Eng Aspects* 153:285–296
105. Erdem B, Sudol ED, Dimonie VL, El-Aasser MS (2000) *J Polym Sci Polym Chem Ed* 38:4419–4430
106. Erdem B, Sudol ED, Dimonie VL, El-Aasser MS (2000) *J Polym Sci Polym Chem Ed* 38:4431–4440
107. Erdem B, Sudol ED, Dimonie VL, El-Aasser MS (2000) *Macromol Symp* 155:181–198
108. Erdem B, Sudol ED, Dimonie VL, El-Aasser MS (2000) *J Polym Sci Polym Chem Ed* 38:4441–4450
109. Hoffmann D, Landfester K, Antonietti M (2001) *Magnetohydrodynamics* 37:217–221
110. Tiarks F, Landfester K, Antonietti M (2001) *Macromol Chem Phys* 202:51–60
111. Rudin A (1995) *Macromol Symp* 92:53–70
112. Landfester K, Boeffel C, Lambla M, Spiess HW (1996) *Macromolecules* 29:5972–5980
113. Landfester K, Spiess HW (1998) *Acta Polym* 49:451–464
114. Tiarks F, Landfester K, Antonietti M (2001) *Langmuir* 17:908–917
115. Putlitz BZ, Landfester K, Fischer H, Antonietti M (2001) *Adv Mater* 13:500–503
116. Torza S, Mason SG (1970) *J Colloid Interface Sci* 33:6783
117. Berg J, Sundberg D, Kronberg B (1989) *J Microencapsulation* 6:327–337

118. Ramsden W (1903) *Proc R Soc London* 72:156–164
119. Pickering SU (1907) *J Chem Soc Commun* 91:2001
120. Briggs TR (1921) *Ind Eng Chem Prod Res Dev* 13:1008
121. Tiarks F, Landfester K, Antonietti M (2001) *Langmuir* 17:5775–5780
122. Barthet C, Hickey AJ, Cairns DB, Armes SP (1999) *Adv Mater* 11:408–410
123. Percy MJ, Barthet C, Lobb JC, Khan MA, Lascelles SE, Vamvakaki M, Armes SP (2000) *Langmuir* 16:6913–6920
124. Soler-Illia GJDA, Sanchez C (2000) *New J Chem* 24:493
125. Landfester K, Tiarks F, Hentze H-P, Antonietti M (2000) *Macromol Chem Phys* 201:1–5
126. Tiarks F, Landfester K, Antonietti M (2001) *J Polym Sci Polym Chem Ed* 39:2520–2524
127. Marie E, Landfester K, Antonietti M (2002) *Biomacromolecules* (in press)
128. Maitre C, Ganachaud F, Ferreira O, Lutz JE, Paintoux Y, Hemery P (2000) *Macromolecules* 33:7730–7736
129. Tomov A, Broyer JP, Spitz R (2000) *Macromol Symp* 150:53–58
130. Willert M, Rothe R, Landfester K, Antonietti M (2001) *Chem Mater* 13:4681–4685
131. Förster S, Antonietti M (1998) *Adv Mater* 10:195–217
132. Antonietti M, Landfester K, Mastai Y (2001) *Isr J Chem* 41:1–5
133. Antonietti M, Landfester K (2001) *Chem Phys Chem* 2:207–210
134. Stähler K, Selb J, Candau F (1999) *Langmuir* 15:7565
135. Hartl FU (1996) *Nature* 381:571

# Molecularly Imprinted Polymer Nanospheres as Fully Synthetic Affinity Receptors

Günter E. M. Tovar\*, Iris Kräuter, Carmen Gruber

Laboratory for Biomimetic Interfaces, Fraunhofer Institute for Interfacial Engineering and Biotechnology and Institute for Interfacial Engineering, University of Stuttgart, Nobelstrasse 12, 70569 Stuttgart, Germany. *E-mail: guenter.tovar@igb.fraunhofer.de*

Synthetic polymer spheres with the ability for molecular recognition represent a promising alternative to affinity binding matrices using biological molecules. This chapter describes various methods for the preparation of molecularly imprinted polymer spheres in the colloidal state. The synthesis, characterization, and performance of colloidal dispersions of molecularly imprinted polymer spheres and their application are discussed.

**Keywords.** Imprinting, Colloids, Microgels, Molecular Recognition, Templates

<b>1</b>	<b>Introduction</b>	125
1.1	General Principle of Molecular Imprinting	126
1.2	Manufacturing of Molecularly Imprinted Materials	127
<b>2</b>	<b>Controlled Synthesis of Colloidal Molecularly Imprinted Polymers</b>	128
2.1	Submicron Scale Molecularly Imprinted Particles by Precipitation Polymerization	128
2.2	Core-Shell Polymer Colloids with a Molecularly Imprinted Shell	130
2.3	One-Stage Preparation of Molecularly Imprinted Nanospheres	134
<b>3</b>	<b>Conclusions</b>	141
	<b>References</b>	143

## 1 Introduction

Recently there has been increasing interest in the use of synthetic polymers as molecularly imprinted materials for the design of artificial receptor-like binding sites in otherwise non-selective polymeric materials [1–6]. Synthetic polymers with the ability for molecular recognition represent a promising alternative to affinity binding matrices using biological molecules, such as proteins. Proteins themselves are highly functional molecules found in living organisms that have the ability to bind selectively to other molecules, carrying signals from cell to cell or catalyzing chemical reactions. Utilizing these unique properties for medical or biotechnology applications has been a logical outgrowth of proteins' unique chemical structure and functionality.

\* Corresponding author.

In medical diagnostics, enzymatic catalysis, or affinity chromatography, proteins are already in widespread use. Modern genetic methods allow for the production of even enhanced properties of various wild-type proteins. There is, however, a limiting factor for using proteins for technical purposes. In a living organism, the lifetime of a functional molecule, such as a protein, is of relatively short duration, often only several hours. Technical processes demand robust materials that are stable over long periods of time in order to be economically viable. Molecular imprinting synthetic polymers to impart the same functionality as biological proteins but with greater stability therefore became a technique of increasing interest.

To prepare molecularly imprinted polymers, a synthetic network is grown during interaction with another molecule. Under certain conditions, the network formed molds to the molecule which thus functions as a template and imprints its 'negative' shape in the growing polymer network. After polymerization, when the template molecules are removed from the polymer network, specific binding sites for the template molecules are imprinted into the synthetic polymer. Usually, such molecularly imprinted polymers are prepared by *bulk polymerization*, resulting in monoliths which must be ground and sieved before using it as functional material.

In this chapter we describe various methods for preparing molecularly imprinted polymers (MIP) in a colloidal state. The resulting materials consist of submicron scale particles dispersed in a liquid acting as fully functional synthetic affinity receptors. The synthesis, characterization, and performance of colloidal molecularly imprinted polymers are described and applications with this new class of affinity receptors is discussed.

## 1.1

### General Principle of Molecular Imprinting

The recognition sites on an MIP are formed in situ during polymerization. Polymers can thus be obtained which are either imprinted by non-covalent or by covalent interaction of an 'imprint' or template molecule with the polymer (Fig. 1). In non-covalent imprinting, a functional monomer and a crosslinker copolymerize with non-polymerizable template molecules [7]. These molecular templates are then incorporated into the growing polymer network and can easily be extracted from the polymer after polymerization is completed. If the imprinting is successful, the polymer network will be left with pores lined with sites having complementary functional groups to those of the template molecules. These functional pore sites are then used for molecular recognition reactions. The imprinted polymer specifically binds molecules by non-covalent interactions, such as hydrogen bonding, van-der-Waals forces,  $p$ - $\pi$  interactions, and, if charged compounds are used, electrostatic interactions. The physical structure of the polymer's receptor-like binding sites are molded by the shape of the template molecules and the three-dimensional arrangement of its functional units, thereby creating polymers that can be enantioselective as well [8].

For covalent imprinting, the template molecule is copolymerized into the polymer network with the monomer and crosslinker. Instead of extracting

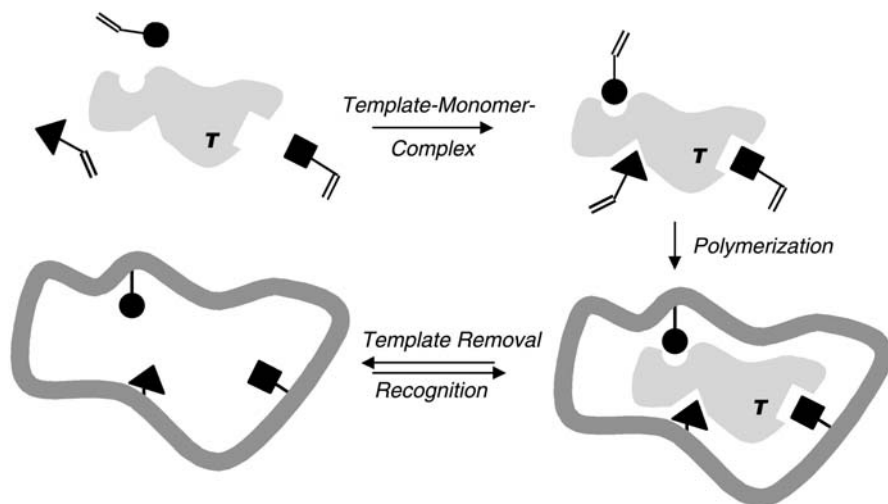


**Fig. 1.** Schematic diagram of the molecular imprinting process of specific cavities in a crosslinked polymer with the template (T) and functional monomers

the template molecule after polymerization, the template is split from the copolymer network by a chemical reaction step [9]. Requirements for the molecular template and the polymer system are much more stringent in the case of covalent imprinting compared to non-covalent imprinting. Whereas covalent imprinting requires the synthesis of special template derivatives for each polymer system, non-covalent imprinting can generally be used for all miscible molecular templates and monomer systems. Acrylic polymers and copolymers, such as poly(methacrylic acid-*co*-ethylene glycol dimethacrylate), have been successfully molecularly imprinted with a large variety of templates such as chiral amino acids, drugs, fertilizers, biocides, and peptides [10]. MIPs, so far, have been used as effective molecular selectors in liquid chromatography [11], capillary electrochromatography [12, 13], and solid-phase extraction [14–16].

## 1.2

### Manufacturing of Molecularly Imprinted Materials

The large-scale production of molecularly imprinted materials is generally limited by the synthetic polymerization method used. Usually, a molecularly imprinted polymer is prepared by *bulk polymerization* which results in a brittle monolithic polymer network. The monolith is subsequently ground in order to expose a larger surface area which is molecularly imprinted. However, the ground particles tend to have extremely broad size and shape distributions. Sieving of the particles typically yields approximately 20% of the original bulk polymer in particles of useful size [17]. The shape of individual particles however remains intrinsically irregular. The previously described preparation



method is not only inefficient but often is difficult to control. However, this procedure has enabled the synthesis of MIP polymers for use as highly selective stationary phases in HPLC separations.

Several approaches have been used to obtain molecularly imprinted particles with a controllable size and shape distribution. For example, *suspension polymerization* has been utilized to obtain monodispersed MIP particles of several microns diameter [18, 19]. Additives are put into the suspension to act as pore inducers thereby increasing the specific surface area and efficiency of the material for chromatographic applications.

Molecularly imprinted polymers with a variety of shapes have also been prepared by *polymerizing monoliths in molds*. This in situ preparation of MIPs was utilized for filling of capillaries [20], columns [21], and membranes [22, 23]. Each specific particle geometry however needs optimization of the respective polymerization conditions while maintaining the correct conditions for successful imprinting. It would be advantageous to separate these two processes, e.g., to prepare a molecularly imprinted material in one step, which then can be processed in a mold process in a separate step to result the desired shape.

Colloidal MIPs may become extremely useful in widening the applicability of MIP material as the colloidal domain offers specific advantages. A major disadvantage of the conventional bulk preparation of MIP networks is that a high amount of imprint molecules stay embedded in the polymer which cannot be extracted. This then leads to a loss of template molecules which may be an expensive substance or possibly uncontrolled leaching of the system in a later application. In any case, potential binding sites are lost for binding of target molecules in an application.

## 2

### Controlled Synthesis of Colloidal Molecularly Imprinted Polymers

Any colloidal material provides an intrinsically favorable accessibility to its surface when compared to bulk material. Therefore, the availability of receptor binding sites should be facilitated by using colloidal MIPs. Submicron scale MIPs were prepared by *precipitation polymerization*, *emulsion polymerization*, and *mini-emulsion polymerization*. Precipitation polymerization uses the insolubility of the formed polymer microgel in a certain solvent, whereas emulsion and mini-emulsion polymerization employ two solvent phases for the preparation of the colloidal polymer. The latter methods offer the opportunity for tailoring the surface of the colloids exclusively, thereby enhancing the accessibility of the binding sites. Each of the three approaches has their own characteristics and will be described in the following sections.

#### 2.1

##### Submicron Scale Molecularly Imprinted Particles by Precipitation Polymerization

Even though a particular starting monomer may be soluble in a certain solvent, the polymer formed often is not. The polymer therefore precipitates when the formed polymer reaches a certain molecular weight or size. If the polymer is



crosslinked, a microgel is thus formed. The preparation of MIPs by *precipitation polymerization* might be regarded as the easiest route to obtain nano-scale particles.

The polymerization reaction takes place in the bulk and the formation of discrete particles is a result of the good solubility of the monomer in the solvent and the low solubility of formed particles of a certain size. Because this approach is dependent on the existence of such a kind of a solubility/non-solubility regime for the monomer, crosslinker, template, and polymer network, it might be hard to find the correct combination of compounds needed to interact in the prescribed way. Additionally, there is a high risk of coagulation with this method as no surfactant is added for the stabilization of the interface between the formed polymer and the monomer containing solution.

Mosbach and co-workers developed a method to prepare molecularly imprinted polymers by *precipitation polymerization* [24]. They started from a dilute, homogenous solution of the monomer methacrylic acid (MAA) and the crosslinker trimethylolpropane trimethacrylate (TRIM) or ethylene glycol dimethacrylate (EGDMA). The polymer formed in the presence of the template molecule 17 $\beta$ -estradiol, theophylline, or caffeine contained a high proportion of discrete spheres of diameter less than a micron. Because the effect of coalescence becomes predominant with higher solid content of the reaction mixture, this approach is limited to solid contents of typically <2 wt%.

Wulff et al. prepared covalently imprinted microgels by *radical solution polymerization* at high dilutions. By choosing different solvents for the polymerization and successive binding experiments, the solubility of certain microgels under recognition conditions was achieved [25]. The microgels consisted of MAA, the model template monomer phenyl-2,3,4,6-tetra-*O*-bis(4-vinylphenylboronol)- $\alpha$ -D-mannopyranoside 1 (Fig. 2), and a crosslinker. The crosslinker was varied between EGDMA 3, TRIM 4, and 2,5-di-*O*-methacryloyl-1,4,3,6-dianhydro-D-sorbitol 5 (Fig. 2). Also varied was the crosslinker concentration during the polymerization from 50 to 90 wt%. Solvents used for the polymerization were cyclohexanone, cyclopentanone, and *N,N*-dimethylformamide (DMF), and for later recognition experiments DMF and methanol. Microgels with a molecular weight of up to  $8 \times 10^4$  g mol<sup>-1</sup> were thus prepared which showed solubility in certain solvents when the degree of crosslinking was 50% or less. There is a clear advantage to using the soluble microgels for characterization by gel permeation chromatography, viscosimetry, and membrane osmometry. Wulff and co-workers found higher experimental values for the intrinsic viscosity when compared to the theoretical value 2.5 which would be expected for spherical particles following the Einstein theory of viscosimetry. Thus it was concluded that the imprinted particles were not spherical but irregularly shaped.

The template monomer was designed for imprinting by inclusion in the microgels formed, followed by hydrolysis during suspension in methanol/water (1:1, v/v). Thus, the boronic ester was split and phenyl- $\alpha$ -D-mannopyranoside 2 (Fig. 2) was removed, leaving free binding sites in the polymer network.

Molecular recognition experiments were carried out with a racemic mixture of phenyl- $\alpha$ -mannopyranoside 2 (Fig. 2) in a heterogeneous phase as well as in a homogeneous phase depending on the solubility of the microgel in the

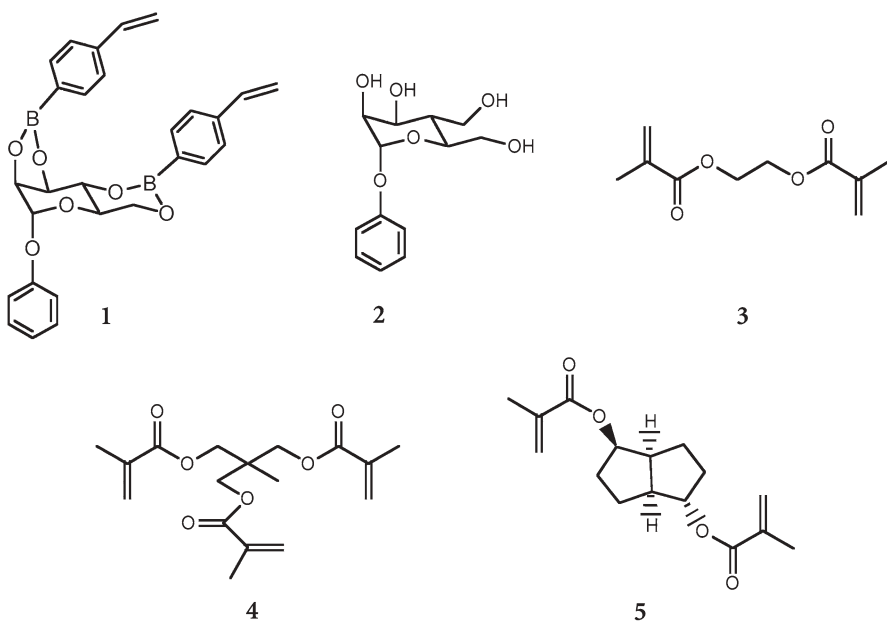


**Fig. 2.** Phenyl-2,3;4,6-tetra-*O*-bis(4-vinylphenylboronyl)- $\alpha$ -D-mannopyranoside **1**, phenyl- $\alpha$ -D-mannopyranoside **2**, EGDMA **3**, TRIM **4**, and 2,5-di-*O*-methacryloyl-1,4;3,6-dianhydro-D-sorbitol **5**

particular solvent. The separation factor  $\alpha$  is the ratio of the distribution coefficients of the D- and the L-form. A strong influence of the recognition properties was found depending on the solvent as well as the degree of crosslinking. In conclusion, the enhanced flexibility of the functional microgel groups needed to assure solubility in a certain solvent lead in consequence to a partial loss of the molecules' recognition capabilities as the "memory effect" of the binding sites was partially lost. However, the soluble microgels showed recognition properties which in some was comparable with insoluble polymer networks.

## 2.2

### Core-Shell Polymer Colloids with a Molecularly Imprinted Shell

Molecularly imprinted core-shell nanospheres were prepared by Whitcombe and co-workers using a two-stage *emulsion polymerization* [26]. The imprinting process involved a specific procedure, referred to as "sacrificed spacer method" [27]. This method is composed of a covalent imprinting step, followed by a reactive cleavage of the imprinting molecule, thus resulting in non-covalent binding sites for the specific recognition of the target molecule. This molecular target, or a close analogue which must be part of the initial imprinting molecule, was left behind by the cleavage or "sacrificed" to leave the imprinted sites.

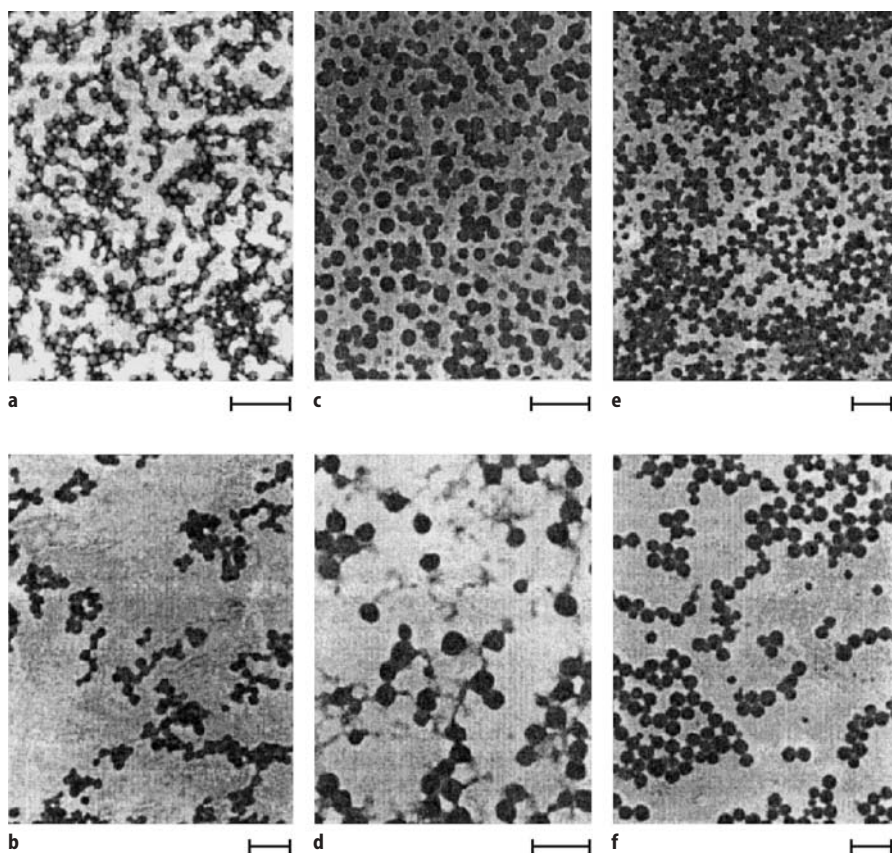


**Fig. 3a–f.** TEM photographs of polymeric nanoparticles (*scale bars represent 200 nm*) [26]

To use this method for the preparation of imprinted colloids, Whitcombe et al. applied it during the shell preparation. They synthesized a copolymer network shell consisting of poly(EGDMA-*co*-cholesteryl (4-vinyl)phenyl carbonate) using a variety of different seed particles to build the polymer core [26]. The seed particles used were 30–45 nm in diameter and the imprinted p(EGDMA-*co*-CVPC) shell resulted to a thickness of about 15 nm (Fig. 3). The specific BET surface area of the core-shell particles was typically  $80 \text{ m}^2 \text{ g}^{-1}$ .

In the next step, the cholesteryl ester entities copolymerized in the shell, were split by carbonate ester hydrolysis. The hydrolysis was carried out in sodium hydroxide in methanol. Thereby, an analogue of cholesterol, the target molecule for later recognition, was removed from the copolymer network. The particles were now ready for non-covalent binding of cholesterol. To quantify the binding behavior of colloidal MIPs, they were mixed with a cholesterol containing solution, separated from the liquid and the cholesterol concentration in the supernatant was quantified by HPLC.

Whitcombe et al. observed a strong decrease of the cholesterol concentration, and hence excellent binding for cholesterol with p(EGDMA-*co*-CVPC) shell/pMMA core particles in isohexane. When the carbonate ester was not hydrolyzed and hence no imprinted sites existed in the shell, only 2.7  $\mu\text{mol}$  cholesterol per g particles were bound corresponding to the non-specifically adsorbed templates. Slightly less cholesterol was adsorbed to particles prepared without CVPC at all thus formed with a pure pEGDMA shell ( $<2 \mu\text{mol g}^{-1}$ ).

A possible application for imprinted colloids is one where the core has a magnetic moment. To this end, Whitcombe and co-workers employed an aqueous ferrofluid containing ferromagnetic particles for inclusion in the core. Here, a p(MMA-*co*-EGDMA), prepared with a molar MMA:EGDMA ratio of 9:1 copolymer, was used to enclose the magnetic particles. Interestingly, when this EGDMA-containing core was equipped with an imprinted shell, very high recognition properties were observed once again. The ferrocolloid itself was also used as seed and allowed for direct preparation of the shell. Only slightly lower binding properties were observed. The major advantage of magnetic molecularly imprinted core-shell particles is an accelerated sedimentation when a magnetic field is applied. Sedimentation was up to 150 times faster than with gravity alone and therefore eased up the separation and purification of imprinted material significantly.

Extending this approach, Whitcombe et al. designed a template-surfactant (TS) which acted as a template and a surfactant at the same time. This approach allowed for the controlled imprinting of the core-shell particles only at the surface of the shell [28]. An example of such a template analogue is given in Fig. 4. It was proposed that the TS molecules concentrated at the water-polymer interface with the hydrophobic template region embedded in the monomer phase and the polar end group looming into the water phase during shell polymerization. The binding between template and polymer here depended principally on hydrophobic interactions instead of hydrogen bonding in contrast to the cholesterol imprinted polymers described above [26].

Whitcombe et al. concentrated on the synthesis of hydrophobic surface imprints in particles with a hydrophilic surface layer. To achieve hydrophilicity of the particles surface they chose divinylbenzene as crosslinker and an additional polymerizable surfactant (PS) (Fig. 4) with a charged end group for the shell polymerization. Thereby, imprinted particles of submicrometer scale, with good monodispersity and high surface area could be prepared. A schematic diagram of the design of hydrophobic surface imprints in particles with a hydrophilic surface layer is shown in Fig. 5.

The removal of template required only ultrafiltration and washes, thereby leaving hydrophobic cavities on the surface of charged particles. The binding properties of the imprinted particles was estimated by HPLC under aqueous conditions. Best results have been obtained using 2.5–7.5% of template-surfactant relative to polymerizable surfactant in the shell.

Following this strategy a better binding of non-polar templates in aqueous media may become possible, thus opening the MIP principle to templates with low solubility. A limitation of this approach, however, may be the fact that it requires the specific synthesis of a template analogue with surfactant properties.

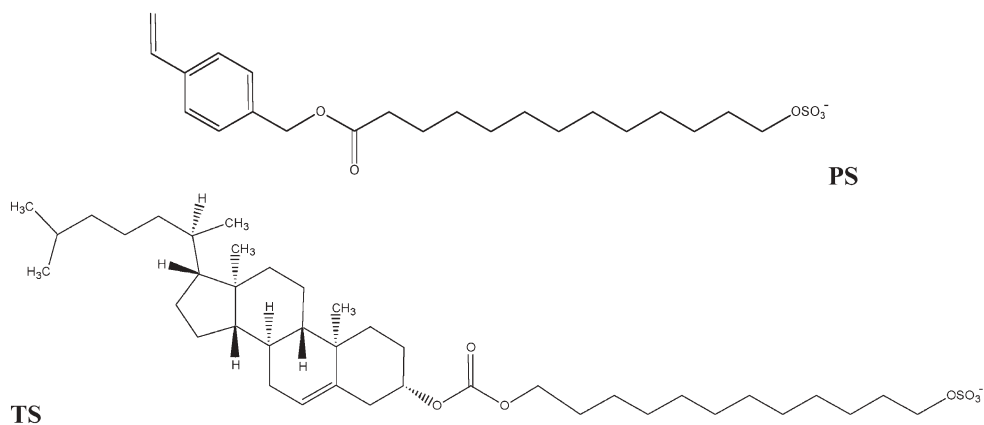


**Fig. 4.** Structures of the polymerizable surfactant (PS) and the template-surfactant (TS)

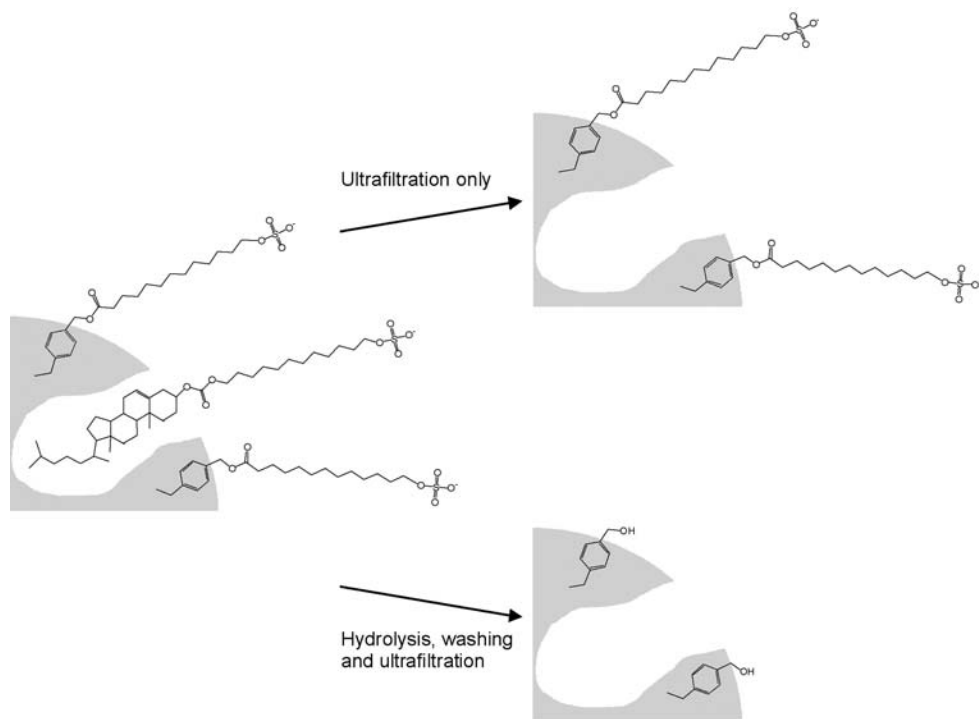


**Fig. 5.** Schematic diagram of the creation of hydrophobic surface imprints in particles with a hydrophilic surface layer (adapted from [28])

Although today there are different techniques available for the synthesis of MIPs only a few approaches use water soluble templates. Carter and Rimmer recently reported on molecularly imprinted core-shell particles for the selective recognition of caffeine in aqueous media [29]. In the first step a polymer core was formed consisting of styrene and divinylbenzene (1:1). The core particles were then coated with the imprinting monomer mixture oleyl phenyl hydrogen phosphate and EGDMA in the presence of the template molecules caffeine or theophylline. After the polymerization Rimmer and Carter removed essentially 100% of the template by extraction, thereby demonstrating one important advantage; that of more effective extraction of colloidal MIPs when compared to conventional MIPs. The binding behavior of the core-shell MIPs was characterized by Scatchard plots for the recognition of caffeine to caffeine-MIPs and theophylline to theophylline-MIPs (Fig. 6). The observed binding curves were biphasic and binding constants for caffeine and theophylline were calculated from the plots, resulting to  $200 \mu\text{mol l}^{-1}$  and  $390 \mu\text{mol l}^{-1}$ , respectively.

In contrast, the binding of caffeine to a theophylline imprinted colloid (Fig. 6c) did not lead to reasonable Scatchard plot binding data, thus indicating a clear difference in the binding behavior. Carter and Rimmer interpreted this finding by a decreased binding strength depending on the more hydrophobic nature of caffeine as compared to theophylline.

When a mixture of caffeine and theophylline was used for binding to caffeine or theophylline imprinted colloids, the caffeine imprinted particles clearly showed a higher selectivity for binding of the original template. The overall performance of the core-shell particles depended on the thickness of the imprinted shell and the best selective binding results were reported for a very thin shell of only 2 nm thickness.

### 2.3

#### One-Stage Preparation of Molecularly Imprinted Nanospheres

The principle of molecular imprinting is based on the hypothesis that monomers and templates interact in the liquid phase prior to polymerization. The molecules assume an optimum conformation driven by the gain in free energy during the interaction of complementary functional groups. This conformation is then partially conserved during the polymerization and transformed to the solid phase. A polymerization technique which allows for a simple arrangement of the MIP building blocks in the liquid phase and transforms it to solid nanoparticles would therefore be advantageous. This scenario is realized to a high degree in *mini-emulsion polymerization*. Here, nanodroplets act as small “nanoreactors”, with the monomer and the imprinting molecules already present at the beginning of the polymerization [30]. A potential thermodynamic control for the design of nanoparticles is given with this technique in contrast to the kinetically controlled precipitation and emulsion polymerization. The dictate of kinetics could cause serious problems such as lack of homogeneity or restrictions in the accessible composition of the molecularly imprinted particles. These problems are largely absent in the mini-emulsion procedure.

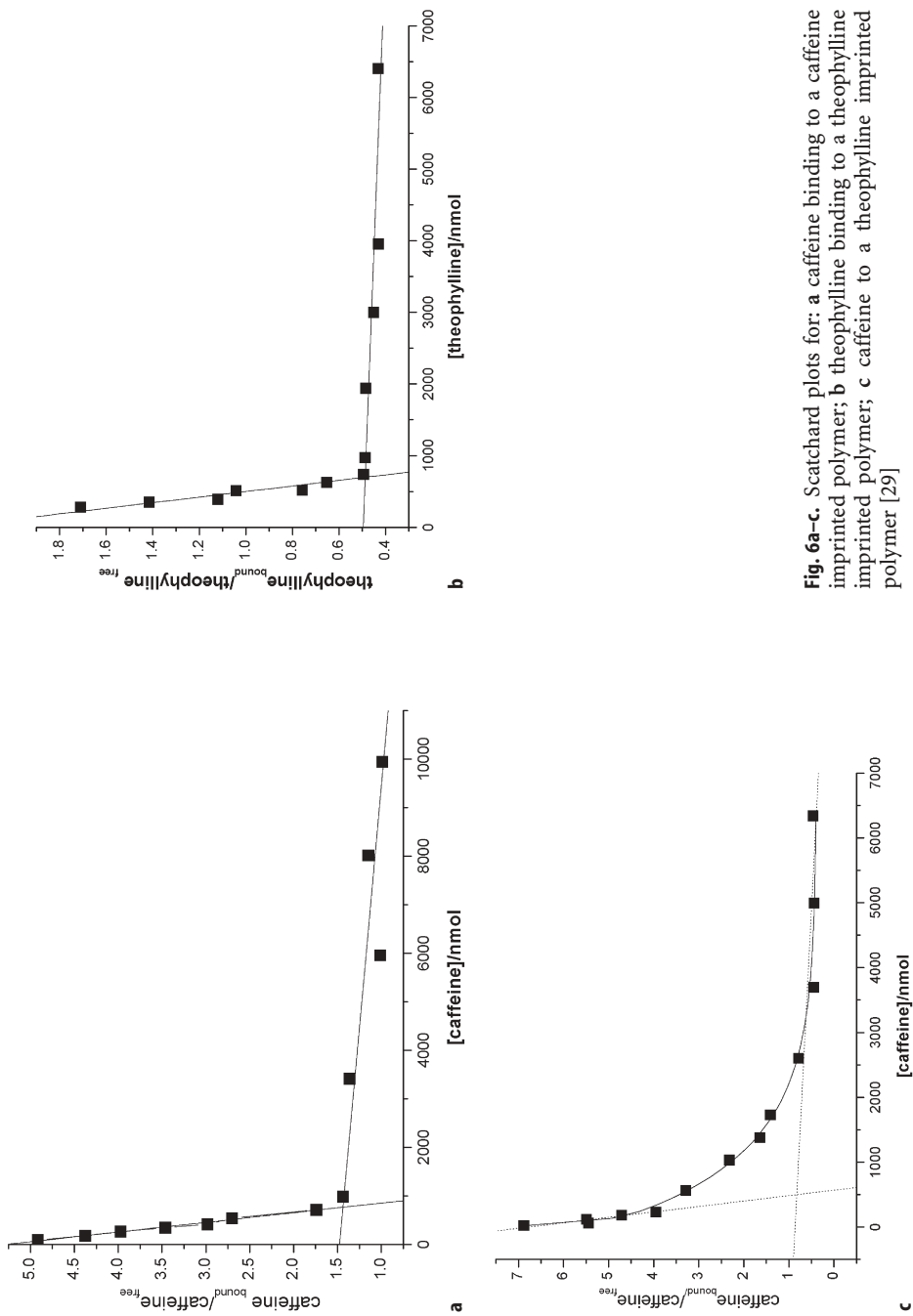


**Fig. 6a–c.** Scatchard plots for: **a** caffeine binding to a caffeine imprinted polymer; **b** theophylline binding to a theophylline imprinted polymer; **c** caffeine to a theophylline imprinted polymer [29]



*Miniemulsion polymerization* is a transformation of the suspension polymerization technique with application of high shear forces. As early as 1973, Ugelstad et al. scaled down the monomer droplet size to several hundred nanometers by shearing the suspension [31]. A co-stabilizer was added to the dispersed phase to suppress diffusion processes occurring in the continuous phase in order to create a stable emulsion with homogeneous size, so-called *mini-emulsions*. The nanodroplets are stabilized by a hydrophobic additive against Ostwald ripening during the miniemulsion polymerization. With this technique a nearly 1:1 transfer of monomer nanodroplets into polymerized nanoparticles is possible [32–34]. Miniemulsion polymerization therefore seems to be particularly suited for a one-step preparation of both covalent and non-covalent molecularly imprinted nanospheres. Figure 7 illustrates the general scheme for the preparation of molecularly imprinted nanoparticles (nanoMIPs) and their use for molecular recognition.

The preparation of nanoMIPs using the process of miniemulsion polymerization was first investigated and reported by Tovar and co-workers [30, 35]. Different types of particles, e.g., consisting of hydrophobic ethylene glycol dimethacrylate EGDMA as crosslinker and hydrophilic methacrylic acid (MAA) as functional monomer, were prepared by varying the molar ratio of monomer to crosslinker  $n_{\text{MAA}}:n_{\text{EGDMA}}$  with different templates. Water-insoluble amino acid derivatives, e.g., L- or D-boc-phenylalanine anilide (BFA) [36] were used as template molecules. With this copolymer system (Fig. 8), stable, coagulation-free dispersions were obtained with a conversion of  $98 \pm 2\%$  (Fig. 9).

Due to the high water solubility of MAA, partitioning of the MAA in the water phase was expected. After polymerization, the obtained miniemulsions (latexes) and the colloidal nanoMIPs were characterized by gravimetric analysis, dynamic light scattering (DLS), gas adsorption measurements (BET), and transmission electron microscopy (TEM) as shown in Fig. 9.

While dynamic light scattering revealed an average apparent hydrodynamic particle diameter of about  $200 \pm 20$  nm, transmission electron microscopy gave a more realistic image of the shape and the size distribution of the nanoMIPs. Figure 9 shows that spherical particles with a rather broad size distribution were formed. They had a diameter of 50 nm up to 300 nm with an average particle diameter around 110 nm and the absence or presence of the template molecule

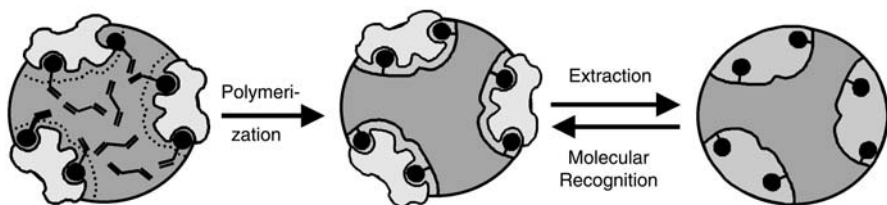


**Fig. 7.** General scheme for the preparation of molecularly imprinted nanospheres and their use for molecular recognition. Template molecules induce the formation of binding sites during the miniemulsion polymerization. The templates are extracted from the highly crosslinked particles and are molecularly recognized by the nanospheres selective binding sites



during particle preparation appeared to have no influence on the size or morphology of the resulting particles (see Fig. 9a,b, respectively). This finding for the particle morphology was proven by Brunauer-Emmett-Teller nitrogen adsorption measurements (BET) which revealed almost identical values of about  $55 \text{ m}^2 \text{ g}^{-1}$  for the specific surface of p(MAA-co-EGDMA) particles despite their preparation in the presence or absence of template molecules. An extraction of the template from the imprinted particles changed this situation drastically so that the BET-surface was substantially increased to about  $80 \text{ m}^2 \text{ g}^{-1}$ . In contrast, when a non-imprinted latex was treated with a solvent in the same way, no change in the BET-surface was observed. The increase in case of imprinting was interpreted as an indication of the formation of nanopores and a sign of successful imprinting during the polymerization.

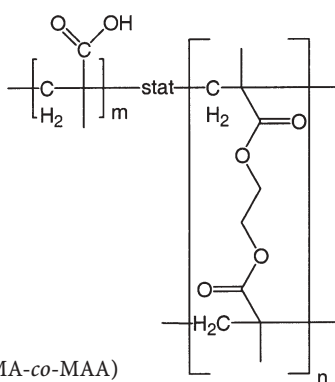


Fig. 8. Structure of p(EGDMA-co-MAA)

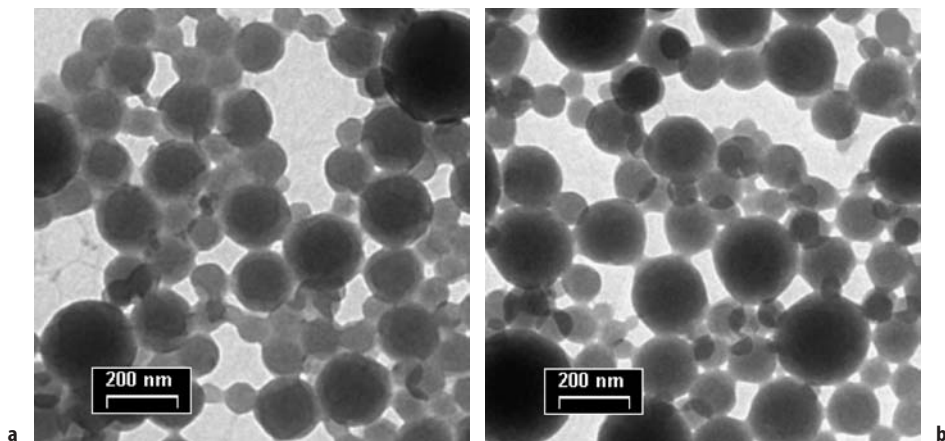


Fig. 9a,b. Transmission electron microscope photograph of MIP nanoparticles prepared by miniemulsion polymerization: **a** control polymer prepared in absence of template; **b** polymer prepared in presence of template L-BFA [30]

The inclusion of the template during the miniemulsion polymerization and its extraction from the purified imprinted nanoMIPs was also evidenced by  $^1\text{H}$ -NMR spectroscopy [30]. Figure 10 shows (a) the molecular structure of the template molecule BFA in THF and the corresponding experimental  $^1\text{H}$ -NMR spectra just as (b) the spectrum of the purified BFA imprinted nanospheres suspended in THF. All observed signals in Fig. 10b correspond to the solvent plus the template. Due to the high insolubility and immobility of the crosslinked network, no signal corresponding to the p(MAA-co-EGDMA) network was seen. Figure 10c shows the spectra of the imprinted microgel which was purified from the template BFA before measurement. The signal of BFA was significantly decreased. If the observed spectra is magnified, only traces of the template signals could be seen.

To quantify the concentration of extracted template UV spectroscopy was used. Compared to the absolute amount of template initially contained in the miniemulsion polymerization an extraction rate of up to  $95\pm 5\%$  template was observed [35]. Such efficient extraction of the template can be seen as a proof of the postulated advantage of colloidal over bulk MIP material in regard to template recovery.

Of course, the most important feature of the nanoMIPs was their ability for molecular recognition which was quantified by UV spectroscopy and HPLC. The best (enantio)selective molecular recognition properties were reported for p(MAA-co-EGDMA) nanospheres prepared with a molar ratio of the monomer to crosslinker of 0.25:1. Here, the absolute amount of particle-bound L-BFA was four times greater in case of an L-imprinted MIP than in a corresponding non-imprinted polymer and 10 times greater than the binding of the D-enantiomer in the L-imprinted microgels.

Additionally, Tovar and co-workers used microcalorimetry to monitor the heat of binding during the interaction of the nanoparticles with molecular probes. For the first time, the relatively low binding energies involved in this non-covalent interaction were quantified by a purely thermodynamic measurement. A comparison of the heat of binding using the original template or structurally closely related probe molecules showed clearly that the imprinted microgel differentiated between different molecules. Figure 11 displays the corresponding microcalorimetric titration experiment. The interaction of L-BFA **6a** (Fig. 12) with an L-BFA imprinted polymer resulted in the exothermic reaction with a binding energy of  $-21.1\pm 1.2\text{ kJ mol}^{-1}$ . The enantiomeric counterpart, D-BFA, resulted in notably less energy with  $-12.7\pm 1.2\text{ kJ mol}^{-1}$ . The heat of binding of three other amino acid derivatives interacting with the microgel showed even lower values with L-boc-phenylalanine ( $-5.1\pm 1.0\text{ kJ mol}^{-1}$ , L-boc-Phe **6b**), L-boc-tyrosine ( $-10.9\pm 0.8\text{ kJ mol}^{-1}$ , L-boc-Tyr **6c**), and L-boc-tryptophan ( $-2.8\pm 0.7\text{ kJ mol}^{-1}$ , L-boc-Trp **6d**). The investigation of the corresponding non-imprinted nanoparticles resulted in essentially zero binding energy within the experimental error.

This study clearly demonstrated the enthalpic basis of chiral molecular recognition by molecularly imprinted polymers.

Furthermore, Tovar and co-workers constituted selective layers and coatings of the nanoMIPs while taking advantage of their uniform spherical shape. For

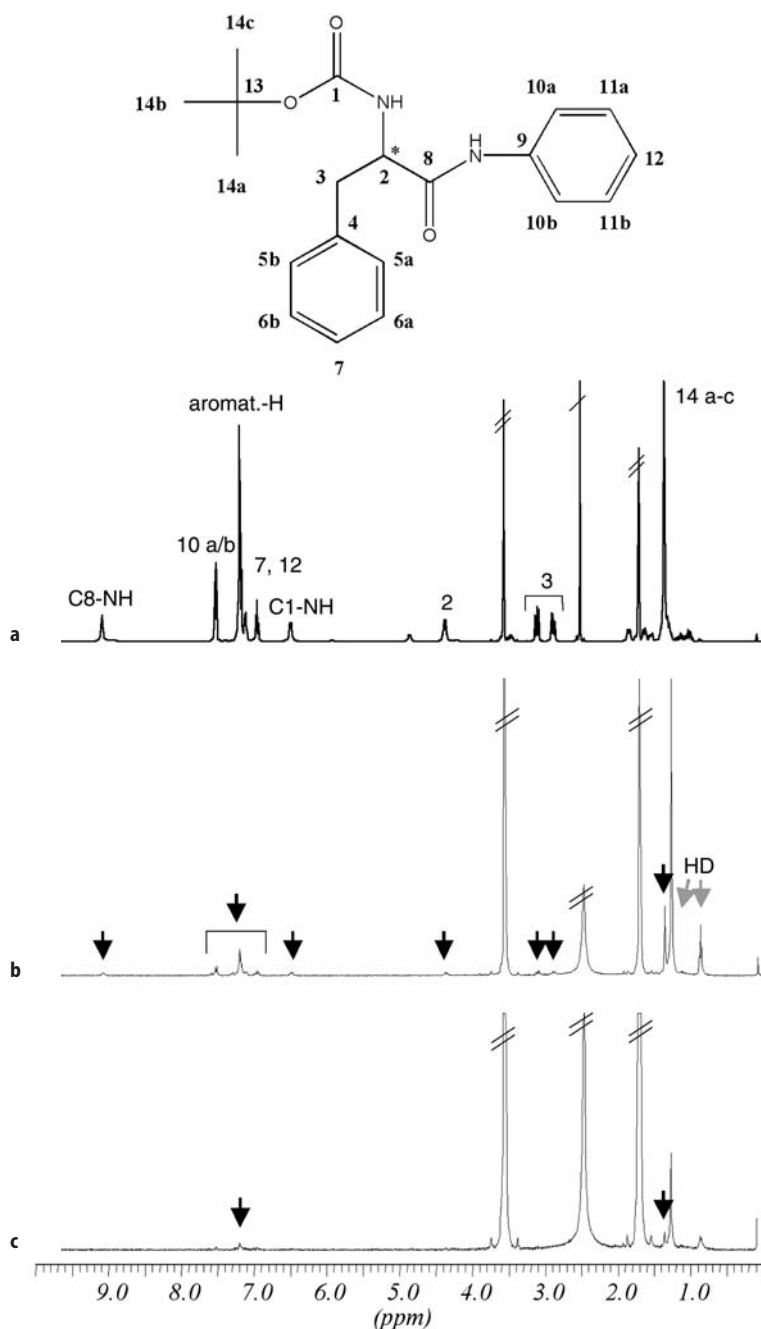


**Fig. 10a–c.** Molecular structure of BFA and  $^1\text{H}$ -NMR spectra of: a the pure template BFA; b imprinted microgel dispersed in THF- $\text{d}_8$  before extraction showing BFA-signals of high intensity; c imprinted microgel after extraction with BFA signals of very low intensity. The *barred signals* are attributed to the solvent THF- $\text{d}_8$  and water [30]

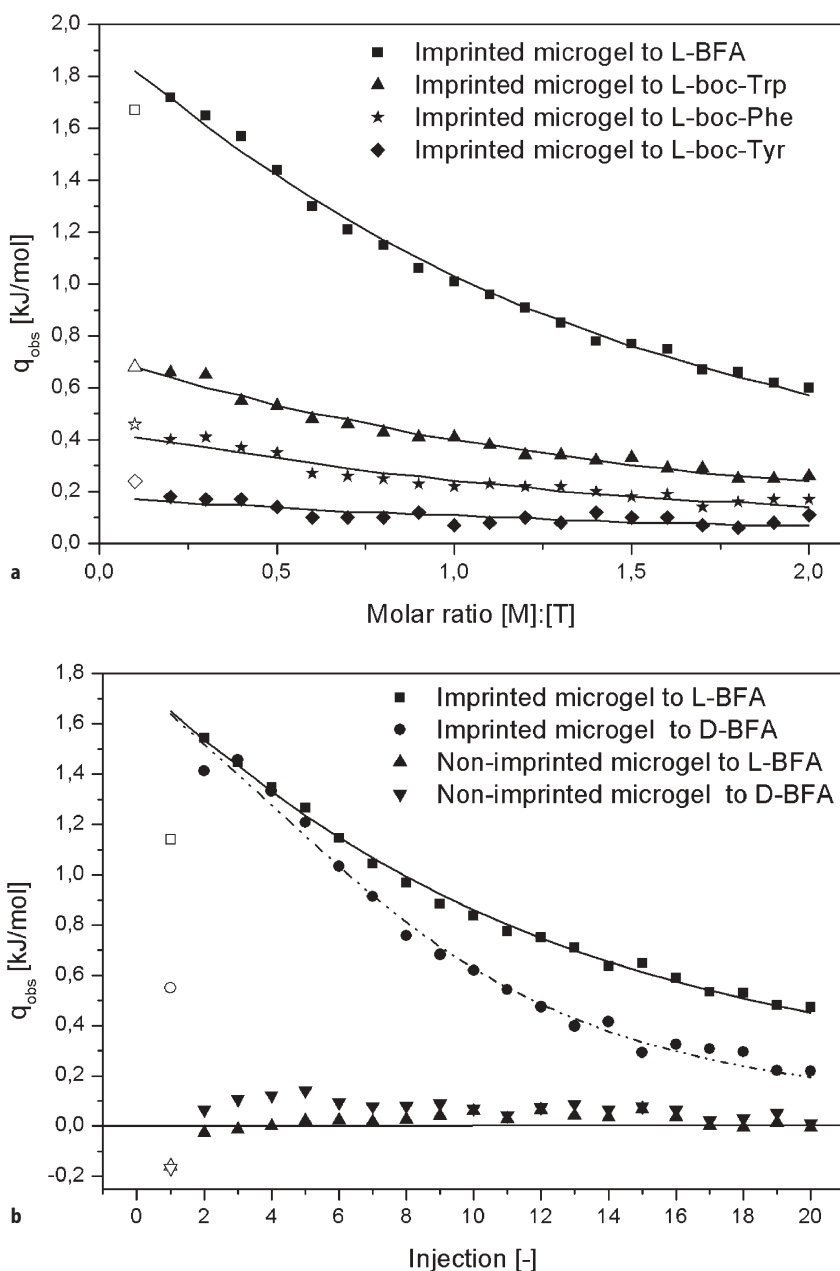


**Fig. 11.** **a** Isotherms of raw calorimetric data for the titration of L-BFA imprinted nanoMIPs with L-BFA (*squares*), L-boc-Trp (*triangles*), L-boc-Phe (*stars*) and L-boc-Tyr (*diamonds*) plotted vs the molar ratio of microgel to template [35]; **b** Isotherms of raw calorimetric data for the titration of L-BFA imprinted nanoMIPs. *Squares* show the binding isotherm of L-BFA, *circles* correspond to D-BFA. The *triangles* show the binding isotherms of the corresponding non-imprinted control polymer with L-BFA (*up-triangle*) and D-BFA (*down-triangle*) [35]

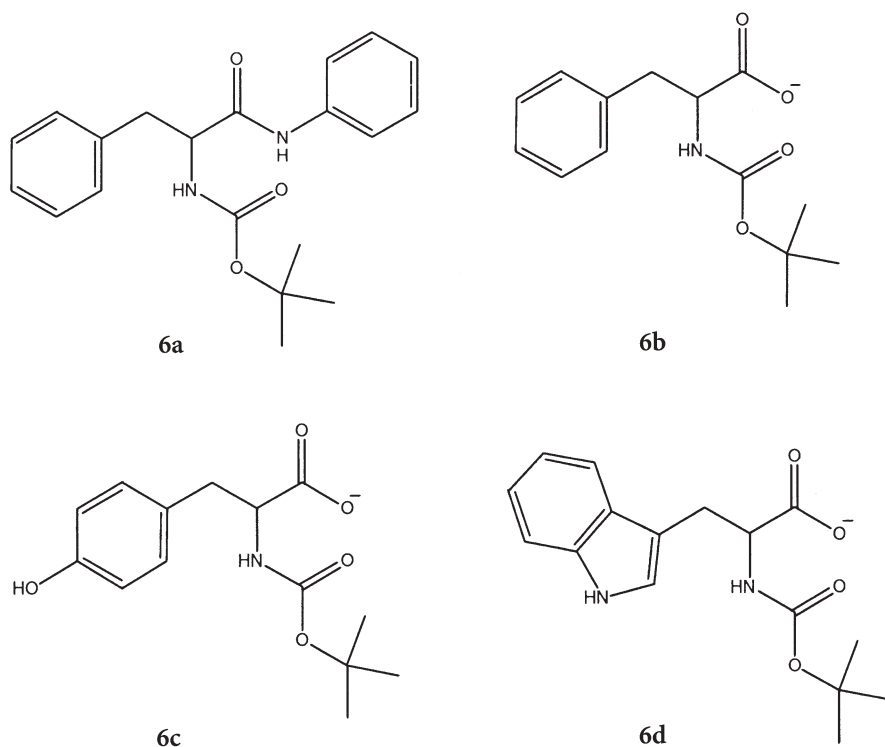


Fig. 12. Structure of the probe molecules 6a–d

example, the usefulness of colloidal MIPs as an affinity selector phase in a new composite membrane configuration was demonstrated [37]. Also, a new type of optical sensor surface was created by coating of an optical waveguide with a monoparticular layer of MIP nanospheres [38]. Due to the processability of colloidal MIPs, they further enable various useful configurations of layers and coatings and thereby constitute an attractive alternative to affinity surfaces based on rather instable biomolecules.

### 3 Conclusions

Colloidal MIPs enable for the future use of fully synthetic affinity receptors in possibly a vast range of applications. The attractive concept of generating biomimetic binding sites in chemically and structurally robust polymer materials was to date possibly but limited by the traditional preparation methods of MIPs. Bulk polymerization of the initial reaction mixture containing monomer, crosslinker, and template, followed by crushing of the formed polymer monolith networks and sieving to find the portion of useful sized polymer particles is not the way of choice for the production of technically widely applicable material.

Although this procedure was suitable for the general development of the MIP technology to date, the obtained particles were intrinsically irregularly shaped and of limited use. Forming monoliths into a desired shape is one way to achieve MIP materials for special applications. In contrast to these materials, the formation of MIPs as colloids opens up a whole new range of applications of molecular imprinting science for generating stable synthetic binding site material for use in (bio)technology.

Colloidal MIPs were recently prepared in homogeneous solutions and in emulsions. A general difference between the approaches is that the first process, *precipitation polymerization*, demands the less complex synthetic conditions to start with but often is difficult to control. If, however, for a given copolymer-template system there exists a regime for the interaction of monomers and templates before polymerization in solution and the formation of an insoluble and imprinted polymer, MIP microgels are accessible by this route. The synthesis at high dilutions and the possible occurrence of coagulation has to be accepted with this approach. The advantages might be that soluble microgels can be prepared by this route.

In contrast, *emulsion polymerization* and *mini-emulsion polymerization* use a two-phase system where the corresponding interface is stabilized by an emulsifier. Thereby, the already complex reaction mixture for the preparation of MIPs becomes even more complex. What is gained by this method however is control over the interface during the MIP synthesis, thus enabling the fine-tuning of this interface during the process. It is at this interface where the surface of the formed MIP is constructed and functionalized for its specific application. This interface and the minimization of the interfacial energy ensures a uniform spherical morphology of the microgels. Also, the widespread use of emulsion polymerization as the process of choice for the generation of polymers for production scale has the further advantages of a two-phase approach, e.g., the amount of reaction heat generated during binding of template molecules is transported easily through the emulsifying phase which is often water. Hence, the temperature during the polymerization reaction is thereby easily controlled. In the case of molecular imprinting, this may lead to more control over the polymerization reaction in general and in particular in more uniform binding sites formed during the reaction.

*Emulsion polymerization* was successfully employed for the preparation of nano-scale MIPs by synthesizing core-shell latexes with an imprinted shell. The use of a template with surfactant properties led to enhanced surface imprinting. Magnetic cores were synthesized to render MIPs which could be manipulated by magnetic fields in suspension, thereby facilitating the separation of the colloidal solid phase from the suspending solution.

By employing *mini-emulsion polymerization*, molecularly imprinted nanospheres were obtained in a one-stage process. The colloidal MIPs showed excellent recognition properties in suspension and allowed for the first time the proof of the thermodynamic origin of the MIP recognition process using Isothermal Titration Microcalorimetry. The use of colloidal MIPs for membrane and sensor applications looks very promising and takes advantage of the controlled shape of this new class of MIP material. Further exploitation of this approach can lead

to miniaturized parallel assays based on purely synthetic chip surfaces with affinities comparable to those of biomolecules but with a substantially enhanced stability.

All colloidal MIPs present a highly dispersed solid phase with specific binding sites. One unique feature of nanoMIPs in general is the efficient extraction of the template molecules after polymerization and thus a potentially large cost saving as the template is usually the most expensive compound involved in an imprinting process. Most important is that new applications can be envisaged with colloidal MIPs, e.g., they can be used for the highly specific removal of toxic compounds from complex mixtures, preconcentration of analytes for a followed analysis, pseudo-stationary phase in capillary electrochromatography that enables a substantially accelerated separation of specific analytes from a mixture [39]. If catalytically active nanospheres are prepared, they can be used in suspension to provide a very high number of easily accessible catalytic sites at their surface, thus acting as artificial enzymes.

An important advantage of colloidal MIPs might be the fact that they can be processed to surface coatings or membranes and become an attractive alternative to protein-based affinity systems. MIPs as artificial receptors are substantially more stable than typical proteins and therefore a substantial gain in the shelf-life of affinity systems can be envisaged by replacing the biological affinity molecules by nanoMIPs. The recent developments in the generation of biomimetic receptors by colloidal MIPs show just the beginning of exploitation of this new class of material. The interaction of chemical nanotechnology with the life sciences is currently creating an extremely dynamic field of new technology in which colloidal MIPs will play a prominent role.

## References

1. Wulff G (1995) *Angew Chem* 107:1958
2. Andersson LI (2000) *J Chromatogr B* 739:163
3. Asanuma H, Hishiya T, Komiyama M (2000) *Adv Mater* 12:1019
4. Sellergren B (2000) *Angew Chem* 112:1071
5. Whitcombe MJ, Vulfson EN (2001) *Adv Mater* 13:467
6. Sellergren B (2001) *Molecularly imprinted polymers*. Elsevier, Amsterdam
7. Kempe M (1996) *Anal Chem* 68:1948
8. Sellergren B, Lepistoe M, Mosbach K (1988) *J Am Chem Soc* 110:5853
9. Wulff G, Schauhoff S (1991) *J Org Chem* 56:395
10. Sellergren B, Hall AJ (2001) In: Sellergren B (ed) *Molecularly imprinted polymers*. Elsevier, Amsterdam, pp 21–57
11. Kempe M, Mosbach K (1995) *J Chromatogr A* 691:317
12. Schweitz L, Andersson LI, Nilsson S (2001) *Anal Chim Acta* 435:43
13. Vallano PT, Remcho VT (2000) *J Chromatogr A* 887:125
14. Andersson LI, Paprica A, Arvidsson T (1997) *Chromatographia* 46:57
15. Berggren C, Bayoudh S, Sherrington D, Ensing K (2000) *J Chromatogr A* 889:105
16. Chen YB, Kele M, Sajonz P, Sellergren B, Guiochon G (1999) *Anal Chem* 71:928
17. Brueggemann O, Haupt K, Ye L, Yilmaz E, Mosbach K (2000) *J Chromatogr A* 889:15
18. Hosoya K, Iwakoshi Y, Yoshizako K, Kimata K, Tanaka N (1999) *J High Resolution Chromatogr* 22:256
19. Mayes AG, Mosbach K (1996) *Anal Chem* 68:3769

20. Heegaard NHH, Nilsson S, Guzman NA (1998) *J Chromatogr B* 715:29
21. Matsui J, Miyoshi Y, Matsui R, Takeuchi T (1995) *Anal Sci* 11:1017
22. Mathew-Krotz J, Shea KJ (1996) *J Am Chem Soc* 118:8154
23. Piletsky SA, Panasyuk TL, Piletskaya EV, Nicholls IA, Ulbricht M (1999) *J Membr Sci* 157:263
24. Ye L, Weiss R, Mosbach K (2000) *Macromolecules* 33:8239
25. Biffis A, Graham NB, Siedlaczek G, Stalberg S, Wulff G (2001) *Macromol Chem Phys* 202:163
26. Pérez N, Whitcombe MJ, Vulfson EN (2000) *J Appl Polym Sci* 77:1851
27. Whitcombe MJ, Rodriguez ME, Villar P, Vulfson EN (1995) *J Am Chem Soc* 117:7105
28. Pérez N, Whitcombe MJ, Vulfson EN (2001) *Macromolecules* 34:830
29. Carter SR, Rimmer S (2002) *Adv Mater* 14:667
30. Vaihinger D, Landfester K, Kräuter I, Brunner H, Tovar GEM (2002) *Macromol Chem Phys* 203:1965
31. Ugelstad J, El Aasser MS, Vanderhoff JW (1973) *J Polym Sci Polym Lett Ed* 11:503
32. Landfester K, Willert M, Antonietti M (2000) *Macromolecules* 33:2370
33. Landfester K, Bechthold N, Förster S, Antonietti M (1999) *Macromol Rapid Commun* 20:81
34. Landfester K, Bechthold N, Tiarks F, Antonietti M (1999) *Macromolecules* 32:5222
35. Weber A, Dettling M, Brunner H, Tovar G (2002) *Macromol Rapid Commun* 23(14):824
36. O'Shannessy DJ, Ekberg B, Mosbach K (1989) *Anal Biochem* 177:144
37. Lehmann M, Brunner H, Tovar GEM (2002) *Desalination* 149:315
38. Tovar GEM, Dettling M, Sezgin S, Lehmann M, Gruber C, Weber A, Brunner H (2002) *Second International Workshop on Molecularly Imprinted Polymers*, La Grande Motte, France
39. Schweitz L, Spegel P, Nilsson S (2000) *Analyst* 125:1899



# Hollow Inorganic Capsules via Colloid-Templated Layer-by-Layer Electrostatic Assembly

Frank Caruso

Department of Chemical and Biomolecular Engineering, The University of Melbourne,  
Victoria 3010, Australia, *E-mail:* fcaruso@unimelb.edu.au

The preparation of hollow inorganic capsules of defined shape, composition and with tailored properties is of immense scientific and technological interest. This chapter highlights a recently developed layer-by-layer (LbL) assembly process for the creation of coated colloid particles (core-shell colloids), which are subsequently converted into hollow inorganic capsules. Sacrificial core template particles are coated with multiple layers of preformed inorganic nanoparticles, or inorganic molecular precursors, and oppositely charged polyelectrolyte, utilizing electrostatic attraction for construction of the layers on the particles. Calcination of the core-shell nanocomposite colloids yields hollow inorganic capsules of defined size and composition, determined by the template diameter and the nature of the charged inorganic species deposited, respectively. The capsule wall thickness can be controlled with nanoscale precision through the number of layers formed on the particles. The flexibility of the LbL strategy is demonstrated by a number of examples of nanoengineered hollow capsules. The creation of macroporous materials from the hollow capsules is also described. Additionally, the potential applications of the hollow colloid particles prepared are briefly discussed.

**Keywords.** Colloids, Nanoparticles, Multilayers, Self-assembly

<b>1</b>	<b>Introduction</b>	146
<b>2</b>	<b>Layer-by-Layer Assembly onto Colloids</b>	147
<b>3</b>	<b>Hollow Capsule Preparation and Characterization</b>	150
3.1	Preformed Nanoparticle Building Blocks	150
3.2	Inorganic Molecular Precursors	158
3.2.1	Sequential Adsorption	159
3.2.2	Sol-Gel Reactions Within Polyelectrolyte Multilayers	160
<b>4</b>	<b>Structures Composed of Hollow Capsules</b>	163
<b>5</b>	<b>Summary and Outlook</b>	164
	<b>References</b>	166

## 1

### Introduction

Hollow capsules of nanometer to micrometer dimensions represent an important class of materials in diverse technological applications, including the encapsulation and controlled release of various substances (e.g., drugs, cosmetics, dyes, and inks), catalysis, acoustic insulation, waste removal, the development of piezoelectric transducers and low dielectric constant materials, and functional materials processing [1–3]. A variety of chemical and physicochemical procedures have been employed for the manufacture of hollow polymer, glass, metal, and ceramic capsules. These include three main routes, namely nozzle reactor processes, emulsion/phase separation procedures (often combined with sol-gel processing), and sacrificial core techniques [4]. The nozzle and sacrificial core approaches generally produce coarse hollow spheres (micrometer-to-millimeter size range), while emulsion/sol-gel methods allow processing of hollow spheres of nanometer-to-micrometer dimensions. In the sacrificial core process, a coating is deposited on the core by controlled surface precipitation of inorganic molecular precursors from solution or by direct surface reactions [5–15], and the core is then removed by thermal or chemical means, leaving behind hollow spheres. Using this approach, hollow capsules with sizes from tens of nanometers to hundreds of micrometers can be prepared [5, 9–11]. Yet another approach to prepare hollow capsules has been through self-assembly. Vesicles [16, 17], dendrimers [18, 19], and block copolymer hollow capsules [20, 21] are examples of the diverse structures that can be prepared through self-assembly.

Recently, a new method that exploits both self-assembly and colloidal templating has proven to be exceptionally versatile for preparing hollow capsules of defined composition, size, and geometry [3, 22, 23]. The technique entails the nanoscale layer-by-layer (LbL) coating of colloid particles with multiple layers of various species, utilizing electrostatic interactions for the buildup of the layers, followed by removal of the core. Although numerous methods have been employed to prepare hollow capsules, a main disadvantage associated with many techniques is the lack of control over the size, geometry, wall thickness, and wall uniformity of the hollow spheres produced [1, 2]. In order to tailor the performance of hollow spheres for various technologies, control over these parameters is required [1, 2]. The LbL method overcomes many of the limitations associated with existing techniques [1, 2], providing new opportunities for constructing “nanoengineered” hollow capsules.

This chapter provides an overview of the LbL technique in preparing hollow inorganic capsules. The first part will deal with the principles of the LbL assembly technique, specifically focusing on its application to colloids. In the following part, a number of selected inorganic hollow particle systems will be illustrated to demonstrate the versatility of the LbL method. It will also be demonstrated that such capsules can be prepared by using preformed nanoparticle building blocks or inorganic molecular precursors. The control that the LbL method permits over the size, shape, composition and wall thickness of the hollow capsules formed will also be detailed. Examples demonstrating the types of structures composed of hollow capsules that are derived from the arrangement

of the LbL coated colloids will be presented. Finally, possible future research directions and areas of utilization of the LbL processed hollow capsules will be briefly discussed.

## 2


### Layer-by-Layer Assembly onto Colloids

The origins of LbL electrostatic assembly of charged species onto planar surfaces date back to the work of Iler in the mid-1960s, where it was shown that particles could be sequentially deposited onto solid substrates [24]. In the early 1990s, the pioneering work of Decher and Hong showed that polycations and polyanions (charged polymers) could also be LbL assembled onto solid supports [25, 26]. Following this, the LbL technique was widely expanded to a broad range of other charged species, including inorganic nanoparticles, biomolecules, and dyes, resulting in polyelectrolyte-composite multilayer films. Several recent reviews have been published on the preparation, characterization, and utilization of LbL assembled thin films on *planar* supports such as glass, gold and graphite [27–30].

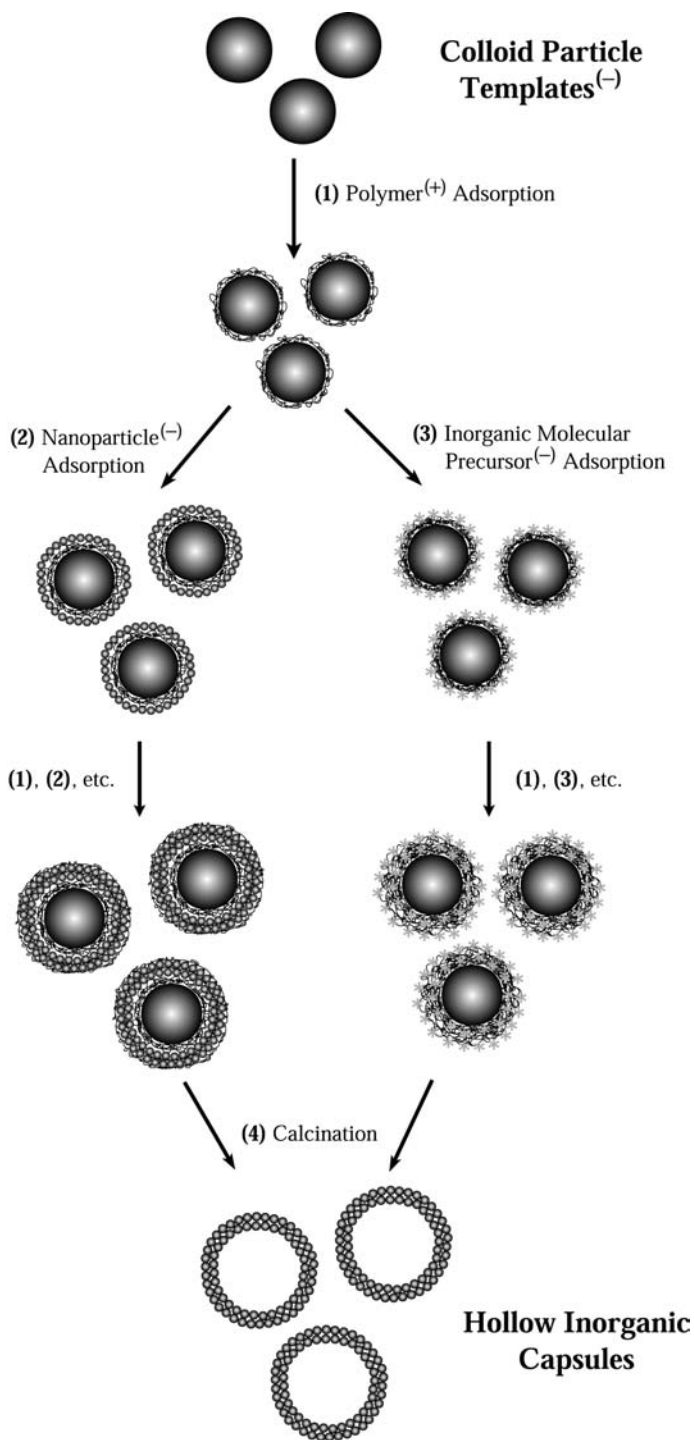
The LbL method has also been applied to *particles*, substituting planar substrates with colloids. Application of the LbL assembly method to colloids represents a promising approach to construct core-shell (or coated) particles [3, 15, 22, 23, 31, 32], the precursors to hollow capsules. Several groups have utilized the LbL approach to prepare coated colloids. For example, in 1995 Keller et al. reported the construction of alternating composite multilayers of exfoliated zirconium phosphate sheets and charged redox polymers on silane-modified silica particles [31]. Chen and Somasunduran deposited nanosized alumina particles in alternation with poly(acrylic acid), which acts as the bridging polymer, on submicrometer-sized alumina core particles [32]. Dokoutchaev et al. alternately assembled metal nanosized particles (Au, Pd, and Pt) and oppositely charged polyelectrolyte onto polystyrene (PS) microspheres [33]. In a series of detailed investigations beginning in 1998, Caruso et al. have shown that the LbL method allows the deposition of multiple layers of various polyelectrolytes on colloids in a controlled fashion [23, 34–38]. By substituting one of the charged polyelectrolyte components with preformed inorganic *nanoparticles*, it was demonstrated that a wide range of nanoparticle-based coatings could be prepared on submicrometer-sized particles via this approach. For example, these include silica [22, 39–41], zeolite [42], iron oxide [43, 44], titania [41], clay (laponite) [41], gold [45], silica-coated gold (Au@SiO<sub>2</sub>) [46], octa(3-aminopropyl)silsesquioxane (NSi8)-stabilized silver (NSi8-Ag) [47], and luminescent semiconductor (CdTe) [48, 49] nanoparticles. Additionally, the use of molecular precursors that can be LbL assembled with polyelectrolyte onto colloids to obtain multilayer coatings was reported [50–52]. Recently, Wang and coworkers [53] and Valtchev et al. [54, 55] reported the coating of PS particles with various types of zeolite nanoparticles. Dong et al. also deposited silver nanoparticles onto PS spheres by the LbL method [56]. This chapter will focus on recent work on the LbL preparation of hollow *inorganic* capsules, which are derived from multilayer-coated colloids. Details on the con-

struction of hollow polymer capsules via the LbL approach can be found elsewhere [3, 23, 35, 37].

In the LbL colloid coating (or templating) method (Fig. 1), a polyelectrolyte solution is added to a colloidal suspension (step 1). The key point is that the added polyelectrolyte has an opposite charge to that on the colloids, thereby adsorbing through electrostatic interactions. The LbL assembly of polyelectrolytes onto colloid particles can be performed in two main ways: (i) the concentration of polyelectrolyte added at each step is such that it is just enough to form a saturated layer [57], or (ii) the concentration is in excess to cause saturation adsorption [23, 34–38]. The first method requires accurate determination of the exact amount of polymer needed to saturate the particle surface, which involves separate adsorption experiments to determine the relative concentrations of polyelectrolyte and particles. In the second method, which is generally favored, the excess (non-adsorbed) polyelectrolyte is removed prior to the addition of the next oppositely charged component to prevent the formation of polyelectrolyte complexes in bulk solution. The excess polyelectrolyte can be removed by several centrifugation/wash/redispersion cycles in water [34–38], or by filtration [58]. In the coating process, particle aggregation should be suppressed at all stages of the preparation. For example, when the centrifugation/wash/dispersion approach is used, care needs to be taken not to use too high centrifugation speeds, as strongly aggregated particles in the form of a pellet are difficult to redisperse. Regardless of the method used, template particle concentrations of up to a few weight percent are used in order to avoid particle aggregation upon addition of the coating species. After adsorption of a polyelectrolyte layer, the charge on the surface of the particles is reversed, which aids in the deposition of subsequent layers of a wide range of charged components. Subsequent stepwise adsorption of oppositely charged preformed nanoparticles (step 2) or inorganic molecular precursors (step 3), and polyelectrolyte, results in the formation of nanoparticle/polyelectrolyte or precursor/polyelectrolyte multilayer coatings, respectively. Excess components are again removed either



**Fig. 1.** Schematic illustration of the LbL technique for the preparation of hollow inorganic capsules. The templates can be of different composition, size, and shape (latex particles, metal nanoparticles and nanorods, proteins, and cells). The coatings depicted are nanoparticle/polyelectrolyte and inorganic molecular precursor/polyelectrolyte multilayers. The first step (1) entails the deposition of a polyelectrolyte layer onto oppositely charged colloid particles. The charged polymer, which exhibits an opposite charge to the particle surface, is added to the colloidal suspension and allowed to adsorb via electrostatic interactions. (The case of negatively charged colloids is considered.) Step 1 can involve multiple polycation/polyanion adsorption steps to give polyelectrolyte multilayers [36]. Subsequent exposure of the polyelectrolyte coated-colloids to oppositely charged nanoparticles (step 2) or molecular precursors (step 3) results in nanoparticle and molecular precursor layers, respectively, being formed. Additional layers can be deposited by repeated deposition cycles, making use of the surface charge reversal that occurs upon adsorption of each layer. Following deposition of each layer, excess unadsorbed polyelectrolyte, nanoparticles, or molecular precursors are typically removed by repeated centrifugation/wash or filtration/wash cycles. Hollow inorganic capsules are produced by subsequent removal of the core from the coated colloids (as well as the bridging polyelectrolyte) by calcination (step 4)



by centrifugation/wash/dispersion cycles or filtration. Generally a polyelectrolyte is used to separate layers of the same materials (e.g., nanoparticles or precursors), as these polyelectrolyte interlayers act as molecular “glue” as well as provide enhanced colloidal stability to the coated particles. Hollow inorganic capsules are obtained from the coated colloids following calcination (step 4). The elevated temperature treatment removes the organic matter (i.e., sacrificial colloid core and bridging polymer) and sinters the preformed inorganic nanoparticles, hence providing structural integrity for the hollow capsules. In the case of the inorganic molecular precursors, the calcination step results in hydrolysis and condensation of the precursors to form nanoparticles, leaving behind hollow capsules comprised of sintered inorganic nanoparticles.

The following section will deal with the fabrication and characterization of a range of hollow inorganic capsules prepared by the LbL approach using preformed inorganic nanoparticles and inorganic molecular precursors as building blocks. It will be demonstrated that the LbL method allows the construction of hollow capsules of predetermined size, geometry, composition, wall thickness, and diameter-to-wall thickness ( $d:t$ ) ratio.

### 3

## Hollow Capsule Preparation and Characterization

### 3.1

#### Preformed Nanoparticle Building Blocks

Using preformed nanoparticle building blocks has the advantage that a broad range of nanoparticles of different composition and crystal phase, as well as of predefined size, can be selected to coat particles. The LbL deposition of nanoparticles and polyelectrolyte yields nanoparticle-based multilayer coatings on colloid particles [22, 39–49]. The system of  $\text{SiO}_2$  nanoparticle/polyelectrolyte multilayers on PS particles [22, 39–41] will be considered first to exemplify the LbL method of coating particles and the methods used for characterization of the coated particles. Several experimental techniques can be employed to monitor the stepwise deposition of each layer onto colloids. These include microelectrophoresis, light scattering, and electron microscopy. Microelectrophoresis provides a *qualitative* indication of layer growth. Figure 2a shows the  $\zeta$ -potential as a function of coating layer number for 640 nm diameter PS particles coated with poly(diallyldimethylammonium chloride) (PDADMAC) and  $\text{SiO}_2$  nanoparticles (25 nm diameter). The  $\zeta$ -potential of the PDADMAC/poly(styrenesulfonate) (PSS)/PDADMAC-coated PS spheres was ca. 45 mV (layer number=0), a value consistent with the outer layer being PDADMAC. (The precursor polyelectrolyte film, PDADMAC/PSS/PDADMAC, was first deposited on the PS spheres in order to provide a uniformly charged surface and to facilitate subsequent adsorption of the  $\text{SiO}_2$  nanoparticles.) The alternating  $\zeta$ -potentials indicated successful recharging of the particle surface with deposition of each layer. The positive and negative values correspond to the PDADMAC and  $\text{SiO}_2$  nanoparticle layers, respectively. The measurements were conducted at pH=5.6, which is above the isoelectric point of  $\text{SiO}_2$ ; hence the  $\text{SiO}_2$  nanoparticles have

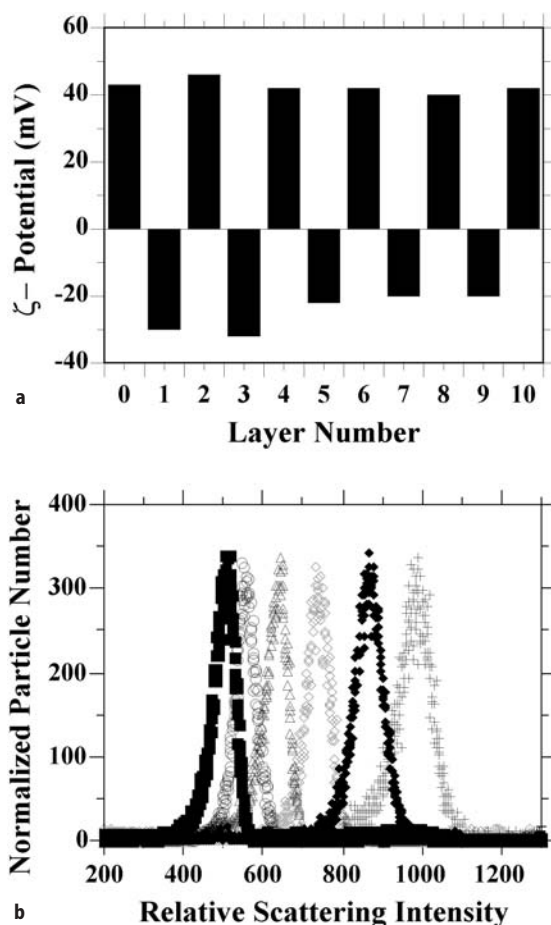


**Fig. 2.** **a**  $\zeta$ -Potential as a function of layer number for SiO<sub>2</sub> nanoparticle/PDADMAC multilayers on polyelectrolyte-modified PS particles (640 nm diameter). The  $\zeta$ -potential of the (PDADMAC/PSS/PDADMAC)-coated PS spheres is ca. 45 mV (layer number equal to zero, as shown). The odd layer numbers correspond to SiO<sub>2</sub> nanoparticle adsorption and the even layer numbers to PDADMAC deposition. The multilayer-coated PS particles were re-dispersed in air-equilibrated pure water (pH=5.6) prior to measurement of the  $\zeta$ -potential (or electrophoretic mobility). (Reproduced by permission of the American Chemical Society [40]). **b** From left to right: Normalized SPLS intensity distributions of PDADMAC/PSS/PDADMAC-coated PS spheres, and those additionally coated with one, two, three, four, and five SiO<sub>2</sub> nanoparticle/PDADMAC multilayers. The systematic shift in the SPLS intensity distributions with increasing layer number is indicative of an increase in thickness of the multilayer coating on the PS particles. The distributions shown correspond to single, coated particles. No higher order peaks, which would indicate the presence of aggregates, were observed. (Adapted from [40] by permission of the American Chemical Society)



an overall negative charge at this pH. The alternating values are characteristic of stepwise growth of multilayers on colloids, as has been demonstrated for a number of polycation/polyanion and polyelectrolyte/nanoparticle coatings [22, 23, 34–37, 39–42].

Quantitative evidence for the LbL formation of multilayers on particles was obtained by using the technique of single particle light scattering (SPLS) [59, 60]. This method is sensitive to the amount of adsorbed material on the colloid particles (analogous to ellipsometry or surface plasmon resonance for planar supports coated with thin films), and has a layer thickness resolution of about 1–2 nm. With this technique, the light scattered from a single particle at a given moment in time is recorded. Recording the light scattered from a large number of particles yields SPLS intensity distributions (Fig. 2b). SPLS is capable of distinguishing between singlets, doublets, and triplets (as well as higher order aggregates) of particles. Figure 2b shows the SPLS intensity distributions of polyelectrolyte-modified PS particles and those coated with one, two, three, four, and five SiO<sub>2</sub> nanoparticle/PDADMAC multilayers. The growth of the multilayers on the colloids was confirmed by the systematic shift in the SPLS intensity distributions with increasing layers. The data shown correspond to those of individual, coated particles. No aggregation of the coated particles was observed, as this would result in the appearance of peaks at higher intensities. The similar intensities at full-width half maximum of the SPLS distributions suggest that the coatings were of similar uniformity. The SPLS data, when fitted by using the Rayleigh-Debye-Gans theory [61], and a refractive index of 1.38 [22, 39, 40] and 1.47 [36] for the nanoparticle and polyelectrolyte layers, respectively, allow determination of the layer thicknesses. The average thickness of each SiO<sub>2</sub> nanoparticle/PDADMAC layer from SPLS was  $36 \pm 10$  nm [22, 40], suggesting that on average approximately a monolayer of SiO<sub>2</sub> nanoparticles was deposited with each nanoparticle adsorption step. The PDADMAC layer thickness was estimated to contribute ca. 2 nm of the thickness of each SiO<sub>2</sub> nanoparticle/PDADMAC layer pair. In summary, SPLS revealed regular multilayer film growth on the PS particles, and that the particles prepared were unaggregated.

Transmission electron microscopy (TEM) provided further evidence for the formation of the multilayers on the PS particles, and allowed visualization of the morphology of the coated colloids. TEM micrographs of uncoated PS particles (Fig. 3a) showed that the particles have a smooth surface, while those coated with SiO<sub>2</sub> nanoparticle/PDADMAC multilayers (Fig. 3b–d) showed increased surface roughness. Additionally, the diameter increases of the coated PS spheres (relative to uncoated PS particles (a)) were (b) 60, (c) 200, and (d) 310 nm, yielding an average diameter increment of ca. 65 nm, corresponding to a layer thickness of approximately  $32 \pm 5$  nm for each SiO<sub>2</sub>/PDADMAC layer pair. These data are in agreement with the SPLS results.

The versatility and applicability of the LbL strategy to prepare coated colloids is highlighted by the range of other nanoparticles that have been utilized to construct nanoparticle-based coatings on spheres, spanning metals (gold), metal oxides (silica, zeolite, titania, iron oxide), semiconductors (CdTe), and composite nanoparticles (Au@SiO<sub>2</sub> and NSi8-Ag). For these nanoparticles, similar to those shown for silica, regular multilayers could be formed on par-



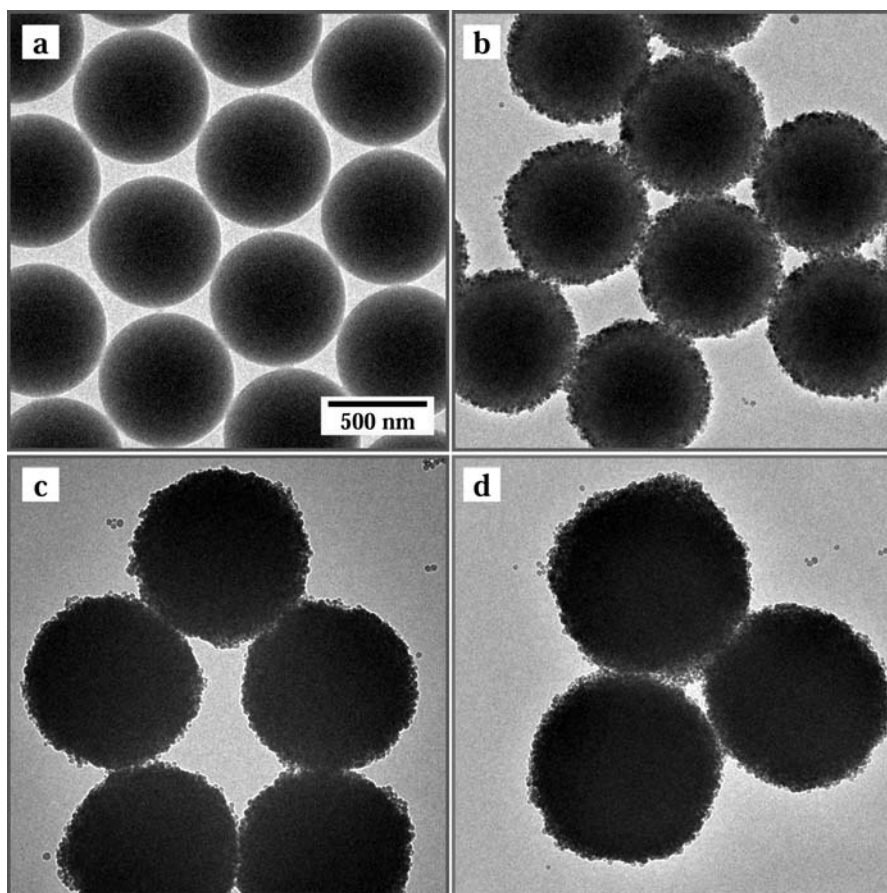


**Fig. 3a–d.** TEM images of: **a** uncoated PS particles; **b** polyelectrolyte-modified PS particles LbL coated with one; **c** three; **d** five  $\text{SiO}_2$  nanoparticle/PDADMAC multilayers. The increase in diameter of the particles with increasing layer number confirms the formation of  $\text{SiO}_2$  nanoparticle/PDADMAC multilayers on the PS particles. The *scale bar* corresponds to all four TEM images shown. The precursor polyelectrolyte film (PDADMAC/PSS/PDADMAC) on the PS particles does not cause a significant increase in diameter of the particles, or a noticeable change in the particle morphology when compared with the uncoated PS spheres. (Reproduced by permission of Wiley-VCH [3])

ticles when they were deposited in alternation with oppositely charged polyelectrolyte [41–49].

Subjecting the nanoparticle/polyelectrolyte-coated particles prepared by the LbL method to elevated temperatures (i.e., calcination) allows the production of hollow inorganic capsules, providing structural stability via sintering of the nanoparticles (Fig. 1) [3, 22]. The calcination step also removes the organic matter (core and polymer) during heating to  $450^\circ\text{C}$ , as confirmed by thermogravimetric analysis [22]. In this approach, an important prerequisite is the presence

of a dense coating of nanoparticles on the larger-sized particles. In the case of silica, this is achieved by using processing conditions that sufficiently screen the silica surface charge on the nanoparticles (e.g., salt-based solutions), thereby allowing them to pack closely on the template particle surface [22, 39, 40]. Figure 4 shows TEM micrographs of hollow silica spheres prepared by calcining PS spheres coated with (a) one, and (b–d) three  $\text{SiO}_2$  nanoparticle/PDADMAC layers. After calcination, the spheres were less electron dense, as a result of removal of the templated core (compare Fig. 4a, b with Fig. 3b,c). Close inspection of the TEM images (e.g., Fig. 4a) showed that individual silica nanoparticles

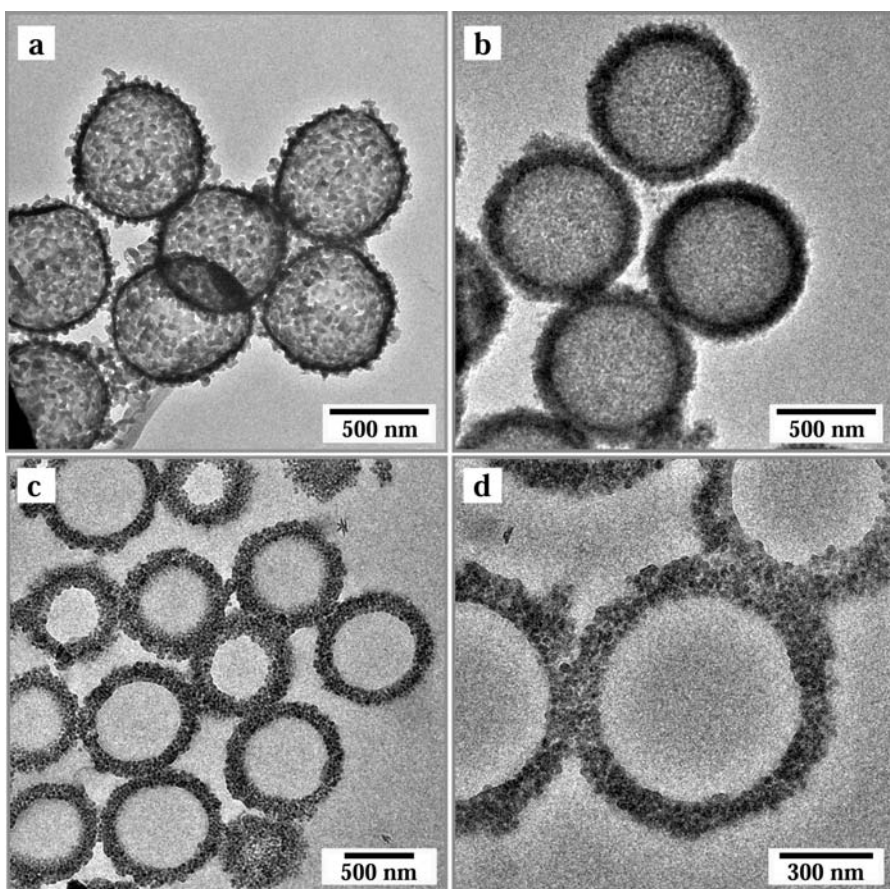


**Fig. 4a, b.** TEM micrographs of hollow silica spheres produced by calcining PS particles coated with (a) one and (b) three  $\text{SiO}_2$  nanoparticle/PDADMAC layer pairs at  $450^\circ\text{C}$ . The wall thickness of the hollow capsules is approximately three times greater for those shown in (b) compared with those shown in (a). **c, d** Cross-sections of the hollow silica spheres of the same composition as those shown in (b). The hollow silica spheres retain the spherical shape of the original PS particle templates (see Fig. 3). (Adapted from [22, 62] by permission of the American Association for the Advancement of Science and the American Chemical Society)

fused together after calcination. Sintering of nanoparticles occurred predominantly within individual capsules, rather than between capsules. The diameters of the hollow silica spheres produced were ca. 5–10% smaller than those of the initial core-shell particles. The number of  $\text{SiO}_2$  nanoparticle/PDADMAC multilayers deposited onto the PS spheres was found to influence the morphology and to determine the wall thickness of the hollow inorganic spheres [22]. Complete hollow silica spheres were obtained when the wall thickness consisted of two or more silica nanoparticle layers, with the spherical shape of the core-shell particles retained upon removal of the core. An approximate wall thickness was obtained from the dark ring on the outside of the spheres seen in the image; the difference in the thickness of the capsule wall is noticeable for the hollow spheres shown in Fig. 4a,b. TEM images of 30–50 nm thick cross-sections of the silica spheres provided an accurate measure of the wall thickness of the hollow capsules as well as confirming that they are hollow (Fig. 4c,d). The average thickness of the capsule wall for the hollow capsules prepared from PS spheres coated with three  $\text{SiO}_2$  nanoparticle/PDADMAC multilayers was approximately  $100 \pm 10$  nm. This thickness corresponds closely to that for three  $\text{SiO}_2$  nanoparticle layers deposited onto the PS spheres, as determined from SPLS and TEM. These data demonstrate that the wall thickness and the final diameter of the hollow spheres can be controlled with nanoscale precision through variation of the number of nanoparticle layers deposited on the precursor particles, thus permitting the construction of hollow inorganic capsules with predetermined  $d:t$  ratios. It was also noted that the hollow capsules were porous, as the resin used to set the hollow capsules before ultramicrotoming permeated the capsules [62].

The preceding example demonstrates that the wall thickness of the capsules can be controlled and that the size and shape of the capsules are largely predetermined by the dimensions and morphology of the sacrificial colloid template used. The following examples highlight the different types of hollow inorganic capsules with regard to composition that can be prepared by the LbL assembly method using various nanoparticles. Figure 5 shows electron microscopy images of hollow  $\text{TiO}_2$  spheres prepared by heating PS particles coated with four  $\text{TiO}_2$  nanoparticle layers, with polyelectrolyte interlayers used to electrostatically bridge the nanoparticle layers [41]. Spherical, intact, and monodisperse hollow capsules were produced after calcination. As was the case for the hollow silica spheres (Fig. 4), upon removal of the core by calcination the neighboring nanoparticles sintered, therefore conferring structural stability to the hollow spheres. Cross-sectional images (not shown) verified that the spheres were hollow. High resolution TEM indicated that the crystal phase of the titania making up the hollow spheres was anatase. Further, an overall shrinkage of ~20% in diameter occurred when the core-shell particles were calcined. The LbL technique for coating particles is adaptable, allowing small variations in the coating steps to be used to optimize the nanoparticle coatings of the different materials (in this case titania nanoparticles). Experimental parameters, such as the number of polyelectrolyte layers separating the nanoparticle layers, and the number of nanoparticle/polyelectrolyte deposition cycles, were varied to generate uniformly coated spheres with dense nanoparticle coatings. For the  $\text{TiO}_2$  nanopar-

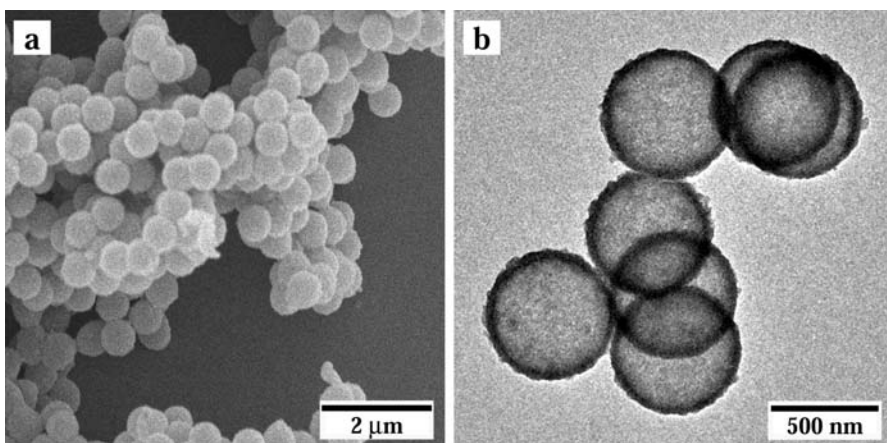


**Fig. 5.** **a** SEM image of hollow  $\text{TiO}_2$  spheres. **b** TEM image of hollow  $\text{TiO}_2$  spheres. The spheres were produced after calcining 640 nm diameter PS spheres coated with four layers of  $\text{TiO}_2$  nanoparticles (5 nm diameter). Each nanoparticle layer was separated by three polyelectrolyte layers. The hollow spheres are composed of anatase crystals. (Adapted from [41] by permission of the American Chemical Society)

ticles on the PS core templates, three polyelectrolyte interlayers were used (compared with one for the silica nanoparticles), as this yielded a close and uniform packing of the  $\text{TiO}_2$  nanoparticles on the PS core templates [41]. The hollow titania spheres may find application in the areas of photonics and microencapsulation, and may also be used as fillers and pigments.

Hollow magnetic capsules were prepared by using iron oxide ( $\text{Fe}_3\text{O}_4$ ) nanoparticles as the layer components [44]. Composite inorganic hollow spheres were also formed by depositing layers of more than one type of inorganic nanoparticle on larger particles (e.g.,  $\text{SiO}_2$  and  $\text{Fe}_3\text{O}_4$ ), interspersed with polyelectrolyte layers, and subsequently calcining the core-shell particles [44]. Hollow inorganic spheres can be produced by using nanoparticles of different size, ranging from  $\sim 5$  to 100 nm for template particles of ca. 500 nm diameter [41]. The important consideration here is the relative size of the core and that of the coating nanoparticles. The shape of the preformed nanoparticles used can also take on the form of platelets. The clay laponite, a synthetic layered silicate  $[\text{Na}_{0.7}(\text{Si}_8\text{Mg}_{5.5}\text{Li}_{0.3})\text{O}_{20}(\text{OH})_4]$ , the dimensions of which are approximately 1 nm (thickness)  $\times$  30 nm (diameter), was also used [41]. Hollow laponite spheres were prepared by calcining laponite nanoparticle/polyelectrolyte-coated PS spheres [41]. In recent work, Wang et al. [53] and Valtchev and Mintova [55] prepared hollow zeolite spheres from zeolite nanoparticle building blocks using the LbL approach.

An example of the use of *core-shell nanoparticles*, namely silica-coated gold ( $\text{Au@SiO}_2$ ) for forming composite hollow inorganic spheres is provided in Fig. 6 [46]. The use of the composite  $\text{Au@SiO}_2$  nanoparticles has several advantages: (i) the well studied surface characteristics of silica can be exploited to achieve a dense packing of  $\text{Au@SiO}_2$  nanoparticles on the template colloids – previous



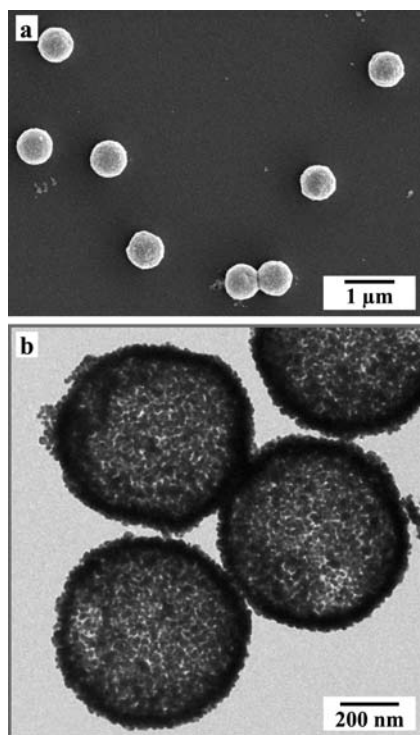


**Fig. 6.** **a** SEM micrograph of hollow Au/SiO<sub>2</sub> microspheres. **b** TEM micrograph of hollow Au/SiO<sub>2</sub> microspheres. The spheres were prepared by calcining PS particles coated with four or two Au@SiO<sub>2</sub> nanoparticle/PDADMAC layer pairs, respectively, at 450°C. (Adapted from [46], by permission of Wiley-VCH)

studies have shown that the LbL deposition of metal nanoparticles yields surface coverages less than about 30% [33, 63]; and (ii) the silica shell allows the formation of hollow Au/SiO<sub>2</sub> spheres upon calcination via sintering of the silica shell between adjacent Au@SiO<sub>2</sub> nanoparticles. The LbL prepared capsules from Au@SiO<sub>2</sub> nanoparticles were spherical (Fig. 6a) and mesoporous (Fig. 6b). Calcination caused sintering of the silica shells, as well as fusion of some of the gold nanoparticles (Fig. 6b). This fusing of the gold cores can be overcome by using Au@SiO<sub>2</sub> nanoparticles with thick (>10 nm) silica shells [64], which is important for the preparation of hollow spheres with tailored optical properties. TEM micrographs of cross-sections of the hollow Au/SiO<sub>2</sub> spheres confirmed their hollow nature [46]. Recently, it was also reported the LbL formation of hollow silica/silver spheres from particles coated with octa(3-aminopropyl)silsesquioxane (NSi8)-stabilized silver nanoparticles (NSi8-Ag) [47]. The examples presented in this chapter show that the nanoparticles used to coat the colloid templates can be of different composition, size, and shape, which opens the way to prepare hollow inorganic spheres with designed and tailored properties.

The templates employed in the LbL method can also be particles of different sizes, shapes, and composition. Typically, polystyrene and melamine formaldehyde particles in the approximate range of 0.1 to 5  $\mu\text{m}$  diameter have been utilized. Figure 7 shows an example of biological cells, glutaraldehyde-fixed echinocytes, that have been coated with  $\text{SiO}_2$  nanoparticle/polyelectrolyte multilayers, followed by removal of the core by treatment with a highly oxidizing solution to form hollow structures [3]. The coating followed the contour of the biocolloid, as the structure of the hollow inorganic-organic composite capsule formed mimicked the original shape, including the secondary structure (spikes) of the biocolloid (Fig. 7b) [3]. Calcination of these structures would yield hollow inorganic capsules. Nickel nanorods have also been used as templates for preparing hollow capsules (see Sect. 3.2.1).

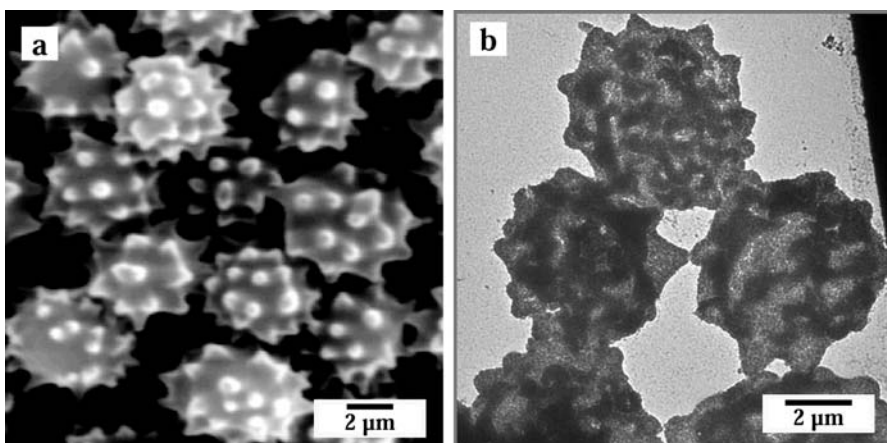


**Fig. 7.** **a** SEM image of glutaraldehyde-fixed echinocytes. **b** TEM image of hollow nanoparticle/polymer structures. The hollow composite structures were prepared by depositing three  $\text{SiO}_2$  nanoparticle/PDADMAC layer pairs on polyelectrolyte-modified echinocytes and then removing the core using an oxidizing solution. (Reproduced by permission of Wiley-VCH [3])

## 3.2

### Inorganic Molecular Precursors

The LbL deposition of inorganic molecular precursors in alternation with polyelectrolytes onto colloid particles provides an alternative means to construct core-shell colloids that may then be converted to hollow inorganic capsules. Using this approach, uniform inorganic-organic composite coatings of defined thickness can be readily formed on colloid templates by stepwise adsorption, thus eliminating the need for optimized conditions (colloid concentration, reactant quantities, pH etc.) required for the direct coating of particles with metal oxide precursors [15]. Additionally, this method avoids the separate preparation of nanoparticles prior to adsorption. This strategy is suitable for precursors that are relatively stable in aqueous solutions, and will be discussed first. For alk-

oxide precursors that are highly water sensitive, preformed polyelectrolyte multilayers can be used as nanoreactors to form coatings on particles. This second method will also be presented.

### 3.2.1

#### *Sequential Adsorption*

The LbL assembly method has been used to sequentially deposit the inorganic molecular precursor, titanium (IV) bis(ammonium lactato) dihydroxide (TALH) (chemical formula:  $[\text{CH}_3\text{CH}(\text{O}-)\text{CO}_2\text{NH}_4]_2\text{Ti}(\text{OH})_2$ ) and PDADMAC onto PS spheres at a density and distribution that is amenable to forming hollow titania spheres upon calcination [65]. The procedure used to prepare the hollow titania spheres is similar to that used for the preformed inorganic nanoparticle building blocks, as illustrated in Fig. 1. The success of this approach for forming hollow spheres hinges on the use of water-stable inorganic molecular precursors that can be assembled in alternation with polyelectrolytes. Titanium alkoxides hydrolyze rapidly in the presence of water; however TALH is relatively stable and hydrolyzes slowly at ambient temperature in neutral solution [66–68]. This prevents significant hydrolysis and condensation reactions, which would cause precipitation of titania in solution and possible aggregation of the coated particles. The precursor interacts with the polyelectrolyte coatings through electrostatic interactions [69]. Calcination of the TALH/PDADMAC-coated particles yielded hollow titania spheres as a result of hydrolysis and condensation of TALH [65].

As for the nanoparticle/polyelectrolyte-coated particles, qualitative evidence for the LbL growth of the TALH/PDADMAC multilayers on the PS particles was provided by microelectrophoresis experiments, which revealed that the sign and magnitude of the  $\zeta$ -potential of the coated particles depended on the outermost layer (PDADMAC=40 mV, TALH=-20 mV). TEM images confirmed that uniformly coated and discrete particles were formed (not shown), while energy dispersive X-ray analysis of the coated particles revealed the presence of Ti (from TALH) [65]. From TEM, an average thickness increment of ca. 5 nm was determined for each TALH/PDADMAC layer pair. Figure 8 shows electron microscopy images of the monodisperse hollow titania spheres formed after calcining the multilayer-coated particles. TALH hydrolyzes and condenses at high temperatures, forming nanoparticles [66, 67], and hence titania hollow spheres comprising nanoparticles were obtained. When heated to 450°C (Fig. 8a,b), these hollow spheres have a well-defined diameter, determined by that of the template, and uniform walls with thicknesses that are controlled by the number of layers deposited. A wall thickness of approximately 30–35 nm was estimated by TEM for the seven-layer TALH coating, that is, about 5 nm per layer. The diameters of these hollow titania spheres produced were approximately 10–15% smaller than those of the corresponding core-shell particles. A similar degree of shrinkage was observed in previous work using preformed nanoparticles to produce hollow inorganic spheres [22, 41, 42]. High resolution TEM showed that the hollow titania spheres comprised connected crystalline anatase titania nanoparticles of 6–8 nm diameter. Five TALH/PDADMAC coatings were required to form

intact hollow titania spheres when heated to 450°C [65]. Calcination at 950°C yielded hollow titania spheres (Fig. 8c) comprised of rutile-phase titania, as confirmed by electron diffraction. The titania spheres formed at 950°C had a macroporous structure, with large titania crystals observed.

The alternate assembly of TALH and PDADMAC has also been performed on nickel nanorods (average diameter ~65 nm, length ~1.5  $\mu\text{m}$ ), followed by hydrolysis of TALH upon heating under reflux (Fig. 9a). Subsequent dissolution of the nickel core yielded titania-based nanotubes (Fig. 9b) [51]. This example illustrates that the LbL method offers a promising route for the preparation of nanotubes with tailored composition and wall thickness, derived from inorganic molecular precursor and polyelectrolyte assembly. Concentric nanotubes (different composition on the inside of the nanotube from that of the surface) could also be prepared via this method.

### 3.2.2

#### *Sol-Gel Reactions Within Polyelectrolyte Multilayers*

Although metal oxide precursors are widely used to form thin inorganic coatings on surfaces, most are extremely water sensitive, hydrolyzing and condensing upon direct contact with water [70]. When applied directly to coating colloids, it is often difficult to control the precipitation of these inorganic species in solution, which can lead to non-uniform coatings and hence aggregation of the particles [15]. A further issue is that the water-sensitivity of the precursors makes their direct application in the LbL coating of colloids difficult because aqueous-based deposition solutions are commonly used. LbL preassembled polyelectrolyte multilayers on particles as nanoreactors can be used to overcome the main issue of precursor water sensitivity for coating colloids. The key points are that the particles are dispersed in organic solutions after coating and that the (sol-gel) reactions are localized within the thin polyelectrolyte coatings on the colloids [71]. Here, the water-sensitivity of the precursor is exploited to conduct the sol-gel reaction within the multilayer films, which remain hydrated to a certain extent. Once the sol-gel reaction is completed and after several washing cycles with alcohol, the particles can be readily dispersed in aqueous solution without aggregation.

Considering the example of lithium niobate ( $\text{LiNbO}_3$ ) hollow spheres, the following procedure was employed [71]. The polyelectrolyte multilayer-coated PS particles were centrifuged and redispersed in anhydrous alcohol (ethanol or isopropanol) ten times in order to replace water in the colloidal dispersion with alcohol. The precursor for  $\text{LiNbO}_3$  ( $\text{LiNb}(\text{OC}_2\text{H}_5)_6$ ) was then added to the polyelectrolyte-coated colloids in alcohol, causing it to infiltrate the multilayer shell. The presence of adsorbed water contained in the polyelectrolyte shell results in hydrolysis and condensation of the precursor (i.e., in situ sol-gel reaction), causing its gelation, and the formation of thin, inorganic-polyelectrolyte coatings of thickness defined by the number of preassembled polyelectrolyte multilayers. Hollow metal oxide spheres were subsequently obtained by calcining the coated colloids at 500°C [71]. (During calcination,  $\text{LiNbO}_3$  nanoparticles were formed and coalesced.) Figure 10 shows a TEM image of  $\text{LiNbO}_3$  hollow spheres pre-



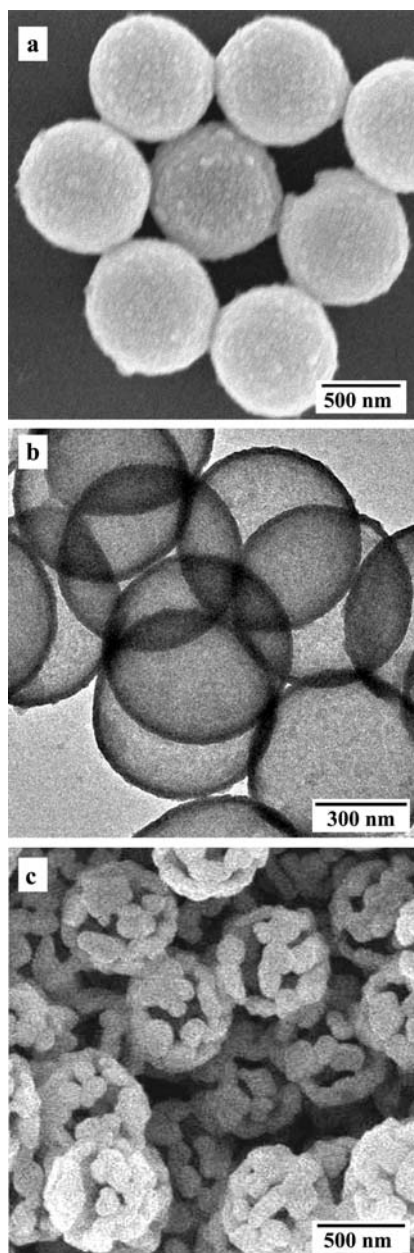


**Fig. 8a–c.** Electron microscopy images of hollow titania spheres prepared by calcination of PS spheres coated with seven layer pairs of TALH and PDADMAC at: **a, b** 450°C; **c** 950°C. **a** and **b** are hollow anatase (refractive index,  $n \sim 2.5$ ) titania spheres and **c** hollow rutile ( $n \sim 2.6$ – $2.9$ ) macroporous titania spheres. (Adapted from [65], by permission of Wiley-VCH)

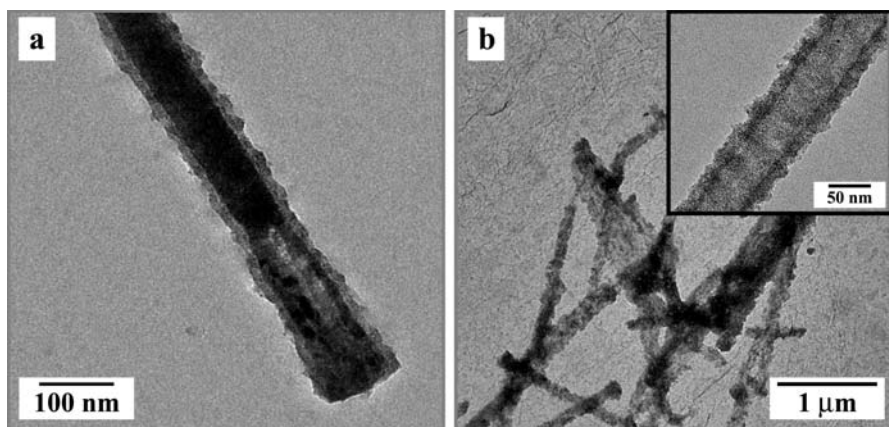


**Fig. 9a, b.** TEM images of: **a** a nickel nanorod coated with a titania/PDADMAC coating; **b** titania-based (titania/PDADMAC) nanotubes obtained following dissolution of coated nickel nanorods. The *inset* shows a higher magnification of the nanotubes shown in **b**. (Adapted from [51] by permission of the American Chemical Society)

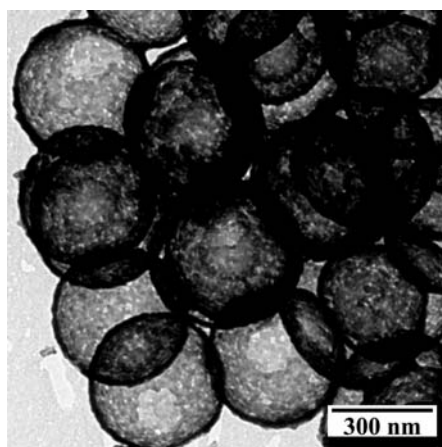


**Fig. 10.** TEM micrograph of  $\text{LiNbO}_3$  hollow spheres formed by calcining PS spheres coated with 18 polyelectrolyte layers and infiltrated with  $\text{LiNbO}_3$  precursor at  $500^\circ\text{C}$ . PS particles of diameter 640 nm were used. (Adapted from [71], by permission of the American Chemical Society)

pared by calcining PS particles coated with 18 polyelectrolyte layers ( $\text{PE}_{18}$ ) and infiltrated with  $\text{LiNbO}_3$  precursor. The spherical shape of the original template was retained. After calcination, a diameter shrinkage of about 45% was observed in comparison with the original size of the core-shell particles, which is considerably larger than that observed when using preformed nanoparticles or TALH (<20%), as described earlier. This was attributed to the lower degree of precursor loading achieved by the infiltration method. The approximate thickness of the capsule wall, estimated by TEM, was about 15–20 nm, indicating that each PE layer contributed approximately 1 nm to the final  $\text{LiNbO}_3$  capsule wall thickness. This infiltration/sol-gel procedure is rather versatile, as precursor infiltration occurs regardless of the sign of the charge of the outermost layer (e.g., polycation or polyanion), and can be applied to various inorganic molecular precursors (e.g., titanium (IV) isopropoxide) [71] to coat colloids and to form hollow inorganic spheres.

## 4

### Structures Composed of Hollow Capsules

In recent years a diverse range of three-dimensional macroporous materials have been constructed by using colloid particles as templates. A common approach has been the use of crystalline arrays of colloids, or colloidal crystals, as three-dimensional ordered scaffolds for the infiltration or synthesis of various materials using wet chemistry techniques (e.g., sol-gel processes) [72, 73]. The colloids are then removed by calcination or chemical means, resulting in a periodic and open pore structure, referred to as inverse opals. A range of inverse opals have been prepared, including metals [74, 75], metal oxides [76, 77], semiconductors [78], carbon and silicon [79, 80], polymers [81–85], and gold-silica composites [86]. To date, uncoated colloids such as silica or polystyrene spheres have predominantly been used as the template particles. The use of coated colloids, however, opens up new possibilities to construct tailored composite macroporous materials with new properties and structures. Recently, LbL coated colloids were used to prepare macroporous inorganic and inorganic-composite materials [42, 87]. These macroporous structures are composed of hollow inorganic capsules. An ordered silicalite (zeolite) macroporous monolith was formed by centrifugation of (silicalite nanoparticle (~50 nm)/polyelectrolyte)<sub>5</sub>-coated 640 nm diameter PS particles into close-packed arrays on filters, followed by calcination (Fig. 11a) [42]. The pore size (~500 nm) is about 20% less than the diameter of the template, indicating shrinkage of the structure upon calcination. TEM images showed that the walls were 200 nm thick and that the wall structure consisted of a dense array of (microporous) nanoparticles (Fig. 11b). The walls also contained disordered mesopores as a result of the interparticle voids. Electron diffraction confirmed the crystalline nature of the nanoparticles, consistent with the silicalite orthorhombic lattice (Fig. 11c). The wall thickness and pore diameters of the hierarchically ordered monolith can be controlled by the coating thickness and template diameter, respectively. Macroporous (composite) inorganic structures comprised of hollow spheres were also prepared by infiltrating sedimented, close-packed  $\text{SiO}_2$  nanoparticle/polyelec-

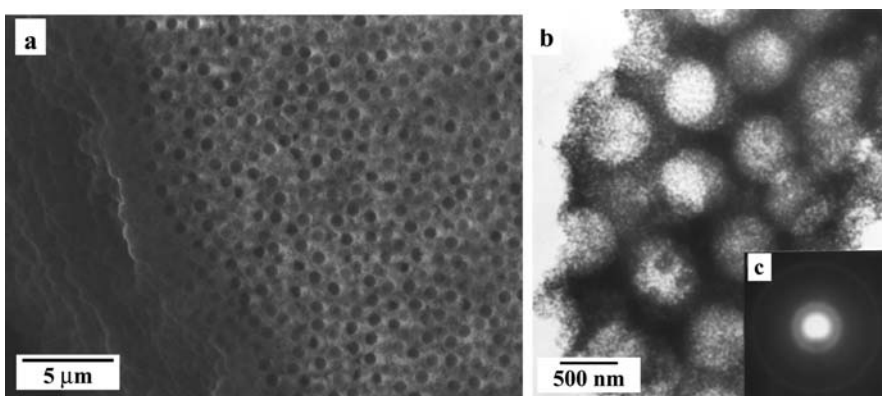


**Fig. 11.** **a** SEM image of an ordered macroporous monolith, formed by assembling PS spheres coated with five silicalite nanoparticle/polyelectrolyte layer pairs into a close-packed arrangement, and subsequently calcining. **b** TEM image of the silicalite framework in **a**. **c** Corresponding diffraction pattern. (Adapted from [42], by permission of the American Chemical Society)

trolyte-coated colloid spheres with a titanium dioxide precursor, followed by removal of the organic material by calcination (Fig. 12a) [87]. SEM and TEM images of cross-sections of the resulting  $\text{TiO}_2/\text{SiO}_2$  macroporous structure demonstrated the hollow nature of the spheres in the material (Fig. 12b,c). High resolution TEM revealed that two different types of particles with sizes of about 3 and 25 nm are present in the wall of the resulting material. The two examples described here have “closed pore” structures, as opposed to inverse opals that comprise highly ordered air spheres interconnected to each other by small channels (i.e., open pore structure) [72, 73]. The pore morphology of the macroporous structures derived from LbL coated particles was also controlled by the nature of the multilayers deposited on the colloid particles [87]. Additionally, the wall thickness of the pores was tuned by varying the number of layers deposited on the particles [87], which cannot be readily accomplished by using uncoated particles.

## 5

### Summary and Outlook

This chapter has described the application of the LbL assembly method to colloid particles for generating hollow inorganic capsules, and has illustrated the broad range of capsules that can be prepared by utilizing this highly versatile and flexible technique. Both preformed inorganic nanoparticle building blocks and inorganic molecular precursors are amenable to LbL deposition onto colloids. In the case of water-sensitive precursors, preformed polyelectrolyte multilayers on particles can be exploited as nanoreactors to localize the sol-gel reaction and thus give an inorganic coating on the particles. From the coated colloids, hollow inorganic capsules are subsequently obtained by removal of the

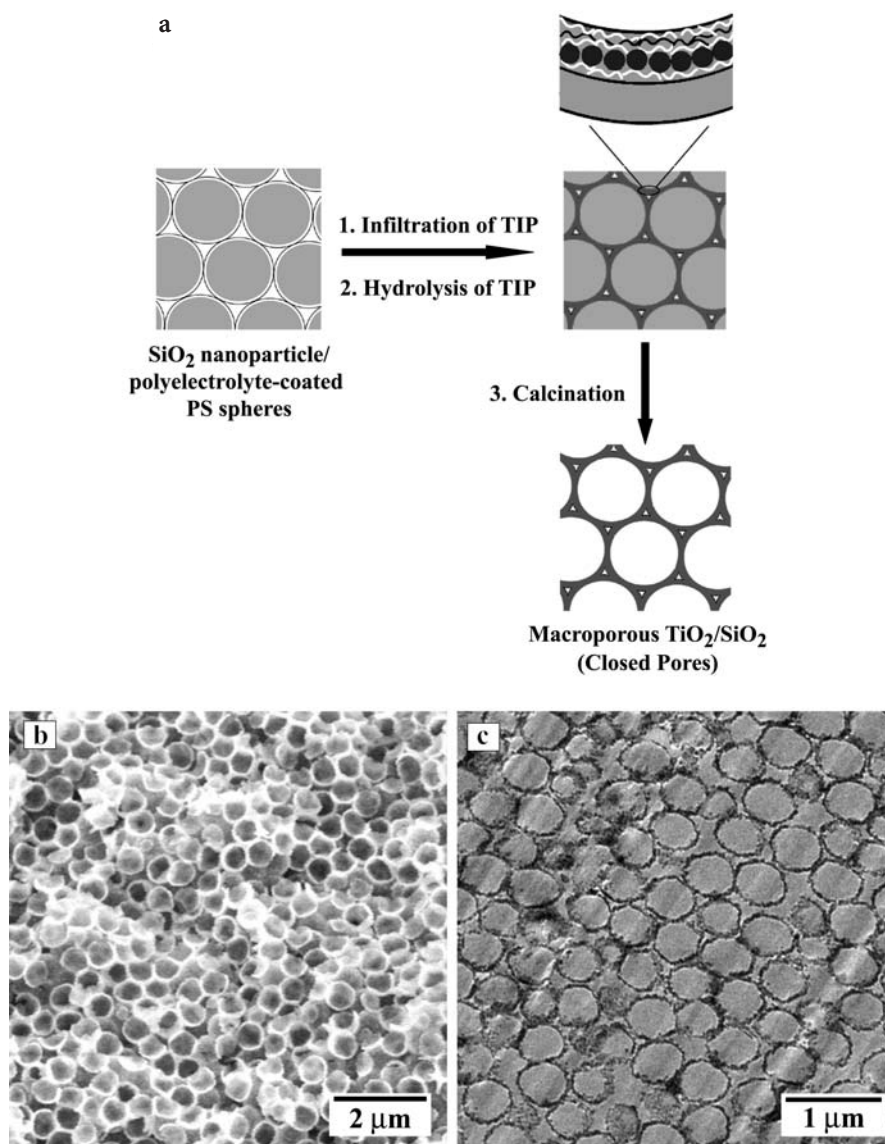


**Fig. 12.** a Illustration of the procedure used to fabricate macroporous inorganic ( $\text{TiO}_2/\text{SiO}_2$ ) structures from coated colloid spheres. A schematic representation of the wall structure and pore morphology is also shown. b SEM micrograph of cross-sections of the macroporous  $\text{TiO}_2/\text{SiO}_2$  structure. c TEM micrograph of cross-sections of the macroporous  $\text{TiO}_2/\text{SiO}_2$  structure. The structure was fabricated by templating close packed arrays of PS- $\text{SiO}_2$  nanoparticle/polyelectrolyte colloid spheres with titanium (IV) isopropoxide (TIP), followed by calcination. (Adapted from [87], by permission of the American Chemical Society)

core (and bridging polyelectrolyte). It has been demonstrated that the solution adsorption conditions to yield dense inorganic nanoparticle or highly loaded molecular precursor coatings on particles are of paramount importance for forming intact capsules upon core removal. The LbL technique can be employed to overcome problems associated with more traditional methods – it provides control over shape, size, wall thickness, and composition of the capsules. It also permits the preparation of compositionally complex hollow colloids, as the components are deposited in a stepwise sequence via self-assembly. The water-based, non-toxic process is also expected to be suited to scale-up, thus allowing the preparation of large quantities of hollow capsules.

The nanoengineered hollow capsules described make intriguing new materials available with designed and specific properties for applications in chemistry, bioscience, and materials science. For example, they are expected to find application in the areas of coatings, separations, chromatography, catalysis, and diagnostics, or to be utilized as drug delivery vehicles or reactor systems. The hollow capsules can also be used as building blocks to construct complex, hierarchical structures with predefined functions, further making them of interest in areas such as photonics and electronics. Overall, the LbL technology for producing hollow inorganic capsules is unparalleled in its versatility and simplicity, and is therefore expected to find wide application for the construction of nanoengineered hollow (as well as core-shell) colloids.

**Acknowledgement.** I extend my thanks to many outstanding colleagues for their excellent contributions to the research reported in this chapter and for fruitful collaborations: D. Wang, A. Susha, R.A. Caruso, X. Shi, M. Spasova, A.M. Dibaj, S.K. Mayya, D.I. Gittins, T. Cassagneau, and H. Möhwald (Max-Planck-Institute of Colloids and Interfaces, Potsdam); M. Giersig (Hahn Meitner Institute, Berlin); L.M. Liz-Marzan (University of Vigo, Spain); S. Mann and S.A. Davis (University of Bristol, UK). Funding from the BMBF, DFG, Volkswagen Foundation, Alexander von Humboldt Foundation, and the DAAD is gratefully acknowledged.

## References

1. Wilcox DL, Berg M, Bernat T, Kellerman D, Cochran JK (eds) (1995) Hollow and solid spheres and microspheres: science and technology associated with their fabrication and application, vol 372. Materials Research Society Proceedings, Pittsburgh
2. Cochran JK (1998) *Curr Opin Solid State Mater Sci* 3:474
3. Caruso F (2000) *Chem Eur J* 6:413
4. Wilcox DL, Berg M (1995) Microsphere fabrication and application: an overview. In: Wilcox DL, Berg M, Bernat T, Kellerman D, Cochran JK (eds) Hollow and solid spheres and microspheres: science and technology associated with their fabrication and application, vol 372. Materials Research Society Proceedings, Pittsburgh, pp 3–13
5. Kawahashi N, Matijevic E (1991) *J Colloid Interface Sci* 143:103
6. Garg A, Matijevic E (1988) *J Colloid Interface Sci* 126:243
7. Kawahashi N, Matijevic E (1990) *J Colloid Interface Sci* 138:534
8. Ohmori M, Matijevic E (1992) *J Colloid Interface Sci* 150:594
9. Giersig M, Ung T, Liz-Marzan LM, Mulvaney P (1997) *Adv Mater* 9:570
10. Giersig M, Liz-Marzan LM, Ung T, Su DS, Mulvaney P (1997) *Ber Bunsenges Phys Chem* 101:1617
11. Bamnolker H, Nitzan B, Gura S, Margel S (1997) *J Mater Sci Lett* 16:1412
12. Walsh D, Mann S (1995) *Nature* 377:320



13. Margel S, Weisel E (1984) *J Polym Sci Chem Ed* 22:145
14. Philipse AP, van Bruggen MPB, Pathmamanoharan C (1994) *Langmuir* 10:92
15. Caruso F (2001) *Adv Mater* 13:11
16. Hotz J, Meier W (1998) *Langmuir* 14:1031
17. Discher BM, Won Y-Y, Ege DS, Lee JC-M, Bates FS, Discher DE, Hammer DA (1999) *Science* 284:1143
18. Zhao M, Sun L, Crooks RM (1998) *J Am Chem Soc* 120:4877
19. Wendland MS, Zimmerman SC (1999) *J Am Chem Soc* 121:1389
20. Thurmond KB, Kowalewski T, Wooley KL (1997) *J Am Chem Soc* 119:6656
21. Thurmond KB, Huang H, Clark CG Jr, Kowalewski T, Wooley KL (1999) *Colloids Surf B Biointerfaces* 16:45
22. Caruso F, Caruso RA, Möhwald H (1998) *Science* 282:1111
23. Donath E, Sukhorukov GB, Caruso F, Davis SA, Möhwald H (1998) *Angew Chem Int Ed* 37:2201
24. Iler RK (1966) *J Colloid Interface Sci* 21:569
25. Decher G, Hong J-D (1991) *Ber Bunsen-Ges Phys Chem* 95:1430
26. Decher G, Hong J-D (1991) *Makromol Chem Macromol Symp* 46:321
27. Decher G (1997) *Science* 277:123
28. Decher G (1996). In: Sauvage J-P, Hosseini MW (eds) *Templating, self-assembly and self-organisation*, vol 9. Pergamon, Oxford, pp 507–528
29. Bertrand P, Jonas A, Laschewsky A, Legras R (2000) *Macromol Rapid Commun* 21:319
30. Hammond PT (1999) *Curr Opin Colloid Interface Sci* 4:430
31. Keller SW, Johnson SA, Brigham ES, Yonemoto EH, Mallouk TE (1995) *J Am Chem Soc* 117:12879
32. Chen T, Somasundaran P (1998) *J Am Ceram Soc* 81:140
33. Dokoutchaev A, James JT, Koene SC, Pathak S, Prakash GKS, Thompson ME (1999) *Chem Mater* 11:2389
34. Caruso F, Donath E, Möhwald H (1998) *J Phys Chem B* 102:2011
35. Sukhorukov GB, Donath E, Davis S, Lichtenfeld H, Caruso F, Popov VI, Möhwald H (1998) *Polym Adv Technol* 9:759
36. Caruso F, Lichtenfeld H, Donath E, Möhwald H (1999) *Macromolecules* 32:2317
37. Caruso F, Schüler C, Kurth DG (1999) *Chem Mater* 11:3394
38. Kurth DG, Caruso F, Schüler C (1999) *Chem Commun* 1579
39. Caruso F, Lichtenfeld H, Möhwald H, Giersig M (1998) *J Am Chem Soc* 120:8523
40. Caruso F, Möhwald H (1999) *Langmuir* 15:8276
41. Caruso RA, Susha A, Caruso F (2001) *Chem Mater* 13:400
42. Rhodes K, Davis SA, Caruso F, Zhang B, Mann S (2000) *Chem Mater* 12:2832
43. Caruso F, Susha AS, Giersig M, Möhwald H (1999) *Adv Mater* 11:950
44. Caruso F, Spasova M, Susha A, Giersig M, Caruso RA (2001) *Chem Mater* 13:109
45. Gittins DI, Susha AS, Schöler B, Caruso F (2002) *Adv Mater* 14:508
46. Caruso F, Spasova M, Salgueiriño-Maceira V, Liz-Marzán LM (2001) *Adv Mater* 13:1090
47. Cassagneau T, Caruso F (2002) *Adv Mater* 14:732
48. Susha A, Caruso F, Rogach AL, Sukhorukov GB, Kornowski A, Möhwald H, Giersig M, Eychmüller A, Weller H (2000) *Colloids Surf A Physicochem Eng Aspects* 163:39
49. Rogach A, Susha A, Caruso F, Sukhorukov G, Kornowski A, Kershaw S, Möhwald H, Eychmüller A, Weller H (2000) *Adv Mater* 12:333
50. Caruso F, Shi X, Caruso RA, Susha A (2001) *Adv Mater* 13:740
51. Mayya KS, Gittins DI, Dibaj AM, Caruso F (2001) *Nano Letters* 1:727
52. Mayya, KS, Gittins DI, Caruso F (2001) *Chem Mater* 13:3833
53. Wang XD, Yang WL, Tang Y, Wang YJ, Fu SK, Gao Z (2000) *Chem Commun* 2161
54. Valtchev V (2002) *Chem Mater* 14:956
55. Valtchev V, Mintova S (2001) *Micropor Mesopor Mater* 43:41
56. Dong AG, Wang YJ, Tang Y, Ren W, Yang WL, Gao Z (2002) *Chem Commun* 350
57. Sukhorukov GB, Donath E, Lichtenfeld H, Knippel E, Knippel M, Möhwald H (1998) *Colloids Surf A Physicochem Eng Aspects* 137:253



58. Voigt A, Lichtenfeld H, Sukhorukov GB, Zastrow H, Donath E, Bäumler H, Möhwald H (1999) *Ind Eng Chem Res* 38:4037
59. Lichtenfeld H, Knapschinsky L, Sonntag H, Shilov V (1995) *Colloids Surf A Physicochem Eng Aspects* 104:313
60. Lichtenfeld H, Knapschinsky L, Dürr C, Zastrow H (1997) *Progr Colloid Polym Sci* 104:148
61. Kerker M (1969) *The scattering of light and other electromagnetic radiation*. Academic Press, New York London
62. Caruso F, Caruso RA, Möhwald H (1999) *Chem Mater* 11:3309
63. Schmitt J, Decher G, Dressick WJ, Brandow SL, Geer RE, Shashidhar R, Calvert JM (1997) *Adv Mater* 9:61
64. Ung T, Liz-Marzán LM, Mulvaney P (2001) *J Phys Chem B* 105:3441
65. Caruso F, Shi X, Caruso RA, Susha A (2001) *Adv Mater* 13:740
66. Hanprasopwattana A, Rieker T, Sault AG, Dayte AK (1997) *Catal Lett* 45:165
67. Möckel H, Giersig M, Willig F (1999) *J Mater Chem* 9:3051
68. Baskaran S, Song L, Liu J, Chen YL, Graff GL (1998) *J Am Ceram Soc* 81:401
69. Shi X, Caruso F (2002) *Langmuir* 18:904
70. Brinker CJ, Scherer GW (eds) (1990) *Sol-gel science: the physics and chemistry of sol-gel processing*. Academic Press, San Diego
71. Wang D, Caruso F (2002) *Chem Mater* 14:1909
72. Velev OD, Kaler EW (2000) *Adv Mater* 12:531
73. Xia Y, Gates B, Yin Y, Liu Y (2000) *Adv Mater* 12:693
74. Velev OD, Tessier PM, Lenhoff AM, Kaler EW (1999) *Nature* 401:548
75. Kulinowski KM, Jiang P, Vaswani H, Colvin VL (2000) *Adv Mater* 12:833
76. Wijnhoven JEGJ, Vos WL (1998) *Science* 281:802
77. Holland BT, Blanford CF, Stein A (1998) *Science* 281:538
78. Vlasov YA, Yao N, Norris DJ (1999) *Adv Mater* 11:165
79. Zakhidov AA, Baughman RH, Iqbal Z, Cui CX, Khayrullin I, Dantas SO, Marti I, Ralchenko VG (1998) *Science* 282:897
80. Blanco A, Chomski E, Grubbschak S, Ibisate M, John S, Leonard SW, Lopez C, Meseguer F, Miguez H, Mondia JP, Ozin GA, Toader O, van Driel HM (2000) *Nature* 405:437
81. Gates B, Yin Y, Xia Y (1999) *Chem Mater* 11:2827
82. Johnson SA, Olivier PJ, Mallouk TE (1999) *Science* 283:963
83. Jiang P, Cizeron J, Bertone JF, Colvin VL (1999) *J Am Chem Soc* 121:11,630
84. Wang D, Caruso F (2001) *Adv Mater* 13:350
85. Cassagneau T, Caruso F (2002) *Adv Mater* 14:34
86. Wang D, Salgueirinho-Maceira V, Liz-Marzán LM, Caruso F (2002) *Adv Mater* 14:908
87. Wang D, Caruso RA, Caruso F (2001) *Chem Mater* 13:364

# Biorelevant Latexes and Microgels for the Interaction with Nucleic Acids

Abdelhamid Elaissari<sup>1</sup>, François Ganachaud<sup>2</sup>, Christian Pichot<sup>1</sup>

<sup>1</sup> Unité Mixte CNRS-bioMérieux, ENS – Lyon, France, 46 allée d'Italie, 69364 Lyon Cedex, France. E-mail: Hamid.Elaissari@ens-lyon.fr

<sup>2</sup> Laboratoire de Chimie Macromoléculaire, Université Pierre et Marie Curie, Paris, France

This chapter is a review of recent work devoted to polymer colloids with nucleic acids in the domain of biomedical diagnostic, in which latex particles are used as carrier. After a brief introduction concerning the applications of latex particles in the biomedical field, the first part describes the routes leading to the elaboration of reactive latexes using radical-initiated polymerization in heterogeneous media. Second, the adsorption and the chemical grafting of nucleic acids are presented as a function of pH, ionic strength, surface charge density and cationic and anionic nature of particles surface. The good knowledge of the colloidal properties of latex particles permits control of the immobilization process (adsorption and covalent binding) of functionalized single stranded DNA fragments (oligonucleotides). Finally, the last part briefly describes some fine applications based on latex-oligonucleotides in the specific capture of target DNA or RNA and also on colloidal particles for separation and concentration of nucleic acid molecules.

**Keywords.** Latex, Microgel, Nucleic acid, Adsorption, Covalent binding, Biomedical, Diagnostic

<b>1</b>	<b>Introduction</b>	171
<b>2</b>	<b>Structure and Properties of DNA and Oligonucleotides (ODN)</b>	172
<b>3</b>	<b>Latexes and Microgel Design</b>	172
<b>4</b>	<b>Nucleic Acids Immobilization</b>	175
4.1	Operating Procedure	175
4.2	Adsorption of Oligonucleotides onto Latexes and Microgel Particles	176
4.2.1	Adsorption Kinetics	176
4.2.2	Adsorption Isotherms	176
4.2.3	Effect of pH on ODN Adsorption Amount	177
4.2.4	Effect of Surface Charge Density	179
4.2.5	Effect of Ionic Strength on ODN Adsorbed Amount	179
4.3	Desorption Study	181
4.4	Chemical Grafting of Oligonucleotides Onto Reactive Latex Particles	182
4.5	Conformation of Adsorbed and Chemically Grafted ODN Onto Colloidal Particles	185

5	Some Fine Applications . . . . .	188
6	Conclusion . . . . .	190
	References . . . . .	192

## List of Abbreviations

A	Adenine
AEMH	Aminoethylmethacrylate hydrochloride
APA	<i>N</i> -(-17-Amino-3,6,9,12,15-pentaoxaheptadecyl)-3- <i>N</i> -BOC aminophenylacetamide
C	Cytosine
DNA	Deoxyribonucleic acid
dT <sub>35</sub>	Polythymidylic acid with 35 thymine
EDC	1-Ethyl-3-(3-dimethylaminopropyl)-carbodiimide
EFEP	Emulsifier-free emulsion polymerization
EGS	Ethyleneglycol bis-succinimidylsuccinate
ELOSA	Enzyme Link Oligo-Sorbent Assay
ETF	Energy Transfer Fluorescence
G	Guanine
HBV	Hepatitis B Virus
HPLC	High Permeation Liquid Chromatography
HRF	Hydroxyl Radical Footprinting
HRP	Horseradish Peroxidase
LCST	Lower Critical Solution Temperature
MBA	<i>N,N</i> -Methylene bis-acrylamide
NHS	<i>N</i> -Hydroxysuccinimide
NIPAM	<i>N</i> -Isopropylacrylamide
NIPMAM	<i>N</i> -Isopropylmethacrylamide
NMI	<i>N</i> -Methyl imidazole
ODN	Oligonucleotide
PCR	Polymerase Chain Reaction
PDC	1,4-Phenylene diisothiocyanate
PNIPAM	Poly( <i>N</i> -isopropylacrylamide)
PS	Polystyrene
RNA	Ribonucleic acid
SANS	Small Angle Neutron Scattering
SMPB	Succinimidyl 4-( <i>N</i> -maleimidophenyl)butyrate
T	Thymine
TCA	2,4,6-Trichlorotriazine
UV	Ultraviolet
V50	2,2'-Azobis(2-amidinopropane) dihydrochloride
VBAH	Vinylbenzylamine hydrochloride

## 1 Introduction

In the two last decades, the use of latex particles as a solid-phase support for biological applications received increasing attention due to their large surface area, narrow-size dispersity, and versatility in surface reactive groups [1]. Moreover, they provided polymer model colloid suitable for systematic investigations regarding the attachment (mostly through adsorption or covalent grafting) of various biomolecules such as proteins, peptides, antibodies, and nucleic acids.

Nucleic acid probes (single-stranded DNA fragments (ssDNA), oligodeoxyribonucleotides or more simply oligonucleotides) have attracted much attention because of their potential interest in the clinical both for diagnostic and therapy purposes [2–5]. In the field of clinical diagnosis, the advantages of nucleic acid probes over conventional methods lie in their specificity for the detection of infectious and genetic diseases [3, 6]. Sandwich-type assays, which require multiple discrete sequences available for hybridization of their complementary target DNA or RNA, rely on the oligonucleotide capture sequences grafted onto various types of supports [7, 8].

In that context, colloidal particles proved to be useful for the extraction of nucleic acids allowing one to enhance the detection of these species. Two main approaches have been generally considered: i) to use selected colloid particles as a collector of the prepared biological samples under appropriate conditions (as regards pH, temperature, salinity, etc.), the subsequent separation of the adsorbed nucleic acids-particles conjugates from the supernatant, their release by desorption upon changing the above medium conditions and finally their amplification using Polymerase Chain Reaction technique [9, 10]; ii) a specific extraction of the nucleic acids can be advantageously performed with latex particles bearing immobilized oligonucleotide exhibiting complementary sequences of the targeted molecules.

These applications require a good knowledge of the nature and magnitude of interactions between nucleic acids and polymer particles. To that purpose, many systematic studies were carried out by different authors and in this lab on the adsorption behavior of various nucleic acids onto various type latex microspheres, mostly cationic and anionically-charged polystyrene or hydrophilic (i.e. poly[*N*-isopropylacrylamide]) latex particles.

The design of appropriate polymer latex particles is of paramount importance and should indeed take into account that when dealing with immobilized ODNs, two major aspects should be kept in mind: i) the availability of the ODN sequences for hybridization with the target sequence and ii) the hybridability of the immobilized capture probe as compared to that of the corresponding reaction in solution. In addition, the covalent grafting of ssDNA probe is generally preferred to adsorption so as to avoid undesirable release and to favor oriented binding through the use of an terminal aminospacer arm. This is indeed an important requirement to enhance the specific extraction of targeted molecules and thus the sensitivity and reproducibility performances of the corresponding assays.

This review aims at highlighting recent studies performed in the authors' laboratory regarding the interactions of nucleic acids with two types of latex particles. The chapter will focus on the following parts:

- Structure and properties of DNA and oligonucleotides
- Latex and microgel particles synthesis design
- Nucleic acid immobilization including preliminary adsorption and desorption studies and then covalent binding
- Description of some fine applications.

## 2

### Structure and Properties of DNA and Oligonucleotides (ODN)

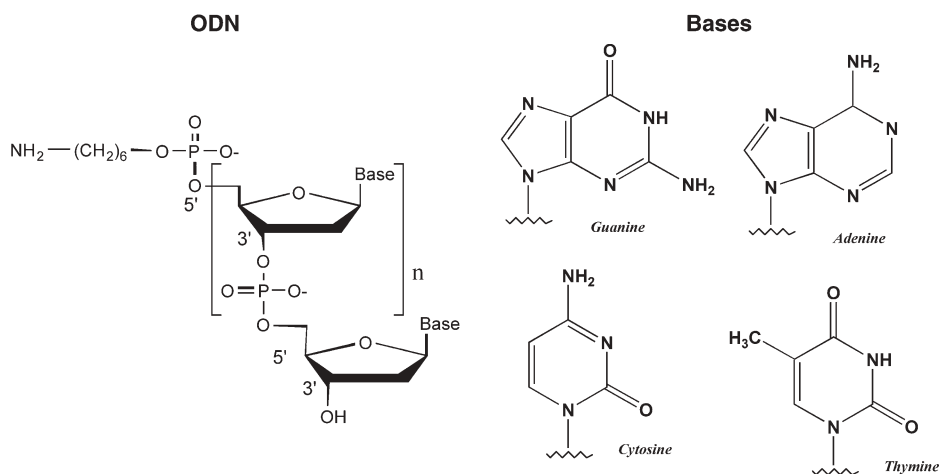
DNA is composed of two single strands composed of a chain of nucleotides. The latter are in turn composed of a phosphate group, a desoxyribose sugar, and one of the four following nucleic bases: Thymine (T), Cytosine (C), Adenine (A), and Guanine (G) (Scheme 1). The phosphate and desoxyribose groups constitute a skeleton common to all DNA. On the contrary, the order of bases along the chain is specific to each DNA and constitutes the genetic code of each person. The nucleic bases match together in pairs. Thus adenine and thymine are linked together by two hydrogen links ( $A=T$ ) (Scheme 2), as opposed to three for the couple cytosine/guanine ( $C=G$ ). The number of C/G pairs along the DNA chain partially determines the binding strength of the two strands.

ODN are fragments of small single strand DNA (generally less than 200) that can be assimilated to small polyelectrolytes. Automatic synthesis of these well structured polyelectrolytes permits their chemical modification, in particular by selective grafting of aminated functional arm at the end of the chain (amino-link arm, see Scheme 1). These ODNs can be matched with a single strand DNA fragments, hence their interest for different biological applications.

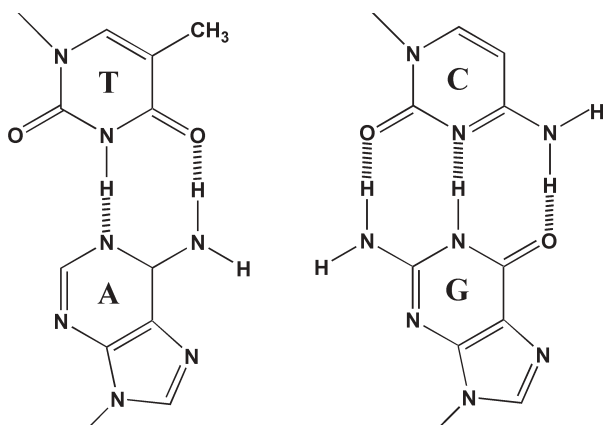
## 3

### Latexes and Microgel Design

The design of reactive polymer latex particles [11] suitable for the immobilization of DNA probes should follow most of the same criteria as required for the binding of other biomolecules (peptides, antibodies, proteins, etc.), i.e., particle size and size homogeneity (*for sake of reproducibility of the tests*), nature of the water-polymer interface (*interest of hydrophilic surfaces*), presence of ionic charges (*for enhanced colloidal stability*), and reactive groups (*for covalent coupling of biomolecules*). Particle sizes in the submicron range were usually preferred so as to favor their dispersability and to reduce sedimentation. Due the polyelectrolyte character of ODNs (anionic phosphate charges), cationically charged particles were designed in order to promote strong electrostatic interactions and to favor the approach of the DNA fragments before coupling. Amino groups in the form of cations were chosen, the reactive function being easily restored at basic pH for further covalent grafting.



**Scheme 1.** Chemical structure of single stranded DNA fragment (ODN, oligonucleotide) bearing amino-link spacer arm at it 5' position and the four bases (A: Adenine, T: Thymine, C: Cytosine, G: Guanine)



**Scheme 2.** Hybridization between complementary bases (T/A and C/G)

Two main types of latex particles were prepared based either on a polystyrene or poly[NIPAM] particle core [12]. It is well-recognized that polyalkylacrylamides exhibit an LCST, the corresponding microgel latex particles being proved suitable for controlling the hydrophilic-lipophilic balance at the interface as well as to offer a friendly environment to biomolecules. Table 1 illustrates the various latex particles investigated in the last few years together with the selected polymerization process performed for their synthesis, the particle size range, and their main properties. The control of both the surface charge and particle size

**Table 1.** Various types of reactive particles for immobilization of oligonucleotides

Type of particle	Polymerization process	Particle size range	Properties of particles	References
Cationic-amino containing polystyrene	Batch EFEP of styrene with a cationic monomer (VBAH or AEMH)	100–500 nm	Cationic surface charge controlled by VBAH or AEMH amount	[13–15]
Cationic-ended hairy PNIPAM polystyrene core	Batch EFEP of styrene and NIPAM with or without AEMH	80–500 nm	Hairy layer thickness controlled by NIPAM and AEMH amount	[16]
Cationic PNIPAM/PS core-shell particles	Two-steps protocol: 1) batch EFEP of styrene and NIPAM; 2) shot-growth <sup>a</sup> of MBA NIPAM, AEMH	300–600 nm	High surface charge density. Variable hairy layer thickness	[16, 17]
Cationically-charged microgel particles	Precipitation polymerization of NIPAM or NIPMAM with a crosslinker (MBA) and AEMH	200–1000 nm	Cationic surface charge. Swelling capacity dependent on MBA amount	[12]
Cationic PNIPAM-covered magnetic particles	Heterocoagulation of iron oxide nanoparticles onto cationic particles. Encapsulation of preformed particles by polymerization of NIPAM, BAM and AEMH	300–1000 nm	Superparamagnetic, bioreactive particles. Temperature, salinity and pH sensitive	[10, 18, 19]

Reaction temperature: 70°C, initiator=V50.

<sup>a</sup> Shot addition at about 80% conversion.

was ensured by the molar ratio of cationic monomer to main monomer (styrene or NIPAM) used in the recipe. In all cases, before any characterization, cleaning of latex particles was carried out by repetitive centrifugation in order to get free of residual monomer, electrolytes, and water-soluble polymers.

The various latexes were characterized with respect to particle size and size distribution, surface charge and functional group density, and electrophoretic mobility behavior. As observed by transmission electron microscopy all latexes were found highly monodisperse with a uniformity ratio between 1.001 and 1.010, a property due to the short duration of the nucleation period involved in the various radical-initiated heterogeneous polymerization processes. The surface charge density was determined by a colorimetric titration method reported elsewhere [13].



Cationic amino-containing particles were used for preparing submicronic magnetic particles according to a two-step protocol: i) adsorption of negatively charged iron oxide nanoparticles onto the oppositely charged latex; ii) encapsulation of the composites particles by precipitation polymerization of a mixture of NIPAM with MBA as crosslinker and a cationic amino-containing monomer (AEMH). This last procedure was also performed to encapsulate preformed magnetic particles so as to provide them with a layer of hydrophilic cationically charged PNIPAM. Another surface functionalization was recently investigated, consisting of covalent grafting a reactive polymer (which could be either a poly[maleic anhydride-*alt*-vinylmethyl ether or an *N*-acryloylmorpholine-*N*-acryloxysuccinimide random copolymer) onto preformed cationic amino-containing PNIPAM-PS core-shell particles or NIPAM-modified magnetic particles [10, 18, 19]. Such a strategy was found to be quite successful in improving strongly both the colloidal stability of the particles and the accessibility of the surface bioreactive sites groups for further covalent grafting of DNA fragments. In addition, the nature of reactive groups (anhydride or succinimide) prevents the use of an activation step for the coupling which is not the case with amino groups as will be discussed later [6, 20].

## 4

### Nucleic Acids Immobilization

Before dealing with the covalent immobilization of oligonucleotides onto reactive colloidal particles, various preliminary studies were carried out to ascertain the pertinent parameters capable of affecting the driven forces involved in the adsorption process or medium conditions able to ensure the adsorption of a large amount of ODN. In fact, the covalent immobilization is generally favored when the interactions between the biomolecules and the surface are strong, leading to adsorption. The second step consists in determining the conditions for which chemical grafting is optimal. Last, as mentioned in the introduction, the adsorption accompanying the chemical coupling of reactive ODN can lead to parasite phenomena (desorption, competition during capture, etc.) when sensitivity and specificity are required. The non-chemically grafted ODN must therefore be desorbed from the surface under specific pH and ionic strength conditions that are to be determined for each given system (colloidal particle and biomolecule).

Consequently, the purpose of the first part of this chapter is to present the results on the adsorption of oligonucleotides onto colloidal polymer particles as a function of various physical parameters such as pH, salinity, presence of surfactant, surface charge density, and nature of change of the carrier.

#### 4.1

##### Operating Procedure

The adsorption and the covalent grafting of DNA, RNA, and ODN onto colloidal particles have mostly been carried out using the classical depletion method (static method) generally used in the case of proteins and polymers. The ad-

sorbed amount,  $N_s$ , expressed in  $\text{mg m}^{-2}$ , is obtained by the difference between the concentration of nucleic acids introduced and that determined in the supernatant after adsorption. The ODN concentration can be determined using all UV technique, HPLC [20], capillary electrophoresis [6], and also fluorescence [21] and radio-labeling [22] methods.

## 4.2

### **Adsorption of Oligonucleotides onto Latexes and Microgel Particles**

The diversity of interactions between ODN and a solid surface considerably complicates the interpretation of adsorption results. Systematic investigation dealing with the conditions of the medium (pH, ionic strength, presence of surfactant, etc.) and the nature of the different partners (support and ODN) allowed some clarification of the various phenomena involved.

#### 4.2.1

##### ***Adsorption Kinetics***

The adsorption kinetics of oligonucleotides onto polymer colloids has been examined using three types of particles (sulfate charged polystyrene, cationic polystyrene particles, and cationic thermally-sensitive microgel particles). The adsorption kinetics of such small negatively charged polyelectrolytes onto negatively charged colloids has been reported to be slow as expected, a behavior mainly attributed to the repulsive electrostatic interactions. The adsorption kinetics of ODNs onto cationic particles has been found to be rapid and surface charge density dependent as shown in Fig. 1. In fact, only 10 min are needed to reach the plateau value in the amount adsorbed of ODN onto particles. The obtained results have been discussed by taking into account the magnitude of the attractive electrostatic interactions involved in the adsorption phenomena. In addition, the increase in the cationic surface charge density of the latex particles leads to increase the adsorption rate.

The adsorption kinetics of oligonucleotides onto amino-containing thermally sensitive microgel particles has also been reported to be rapid (as for cationic polystyrene latexes) and higher than amidino-containing particles. In fact, the adsorption of ODNs onto thermally-sensitive poly(*N*-isopropylacrylamide) particles bearing amidine groups is low or negligible, mainly attributed to low charge density and to the charge dilution in the highly hydrated interface layer.

#### 4.2.2

##### ***Adsorption Isotherms***

Determination of the adsorption isotherm is important, since it allows establishing of the basic relationship between the adsorbed amounts of ODN onto colloidal particles as a function of residual ODN concentration (equilibrium ODN concentration). Two major pieces of information can be deduced from the adsorption isotherm: (i) the affinity between the ODN and the particles revealed

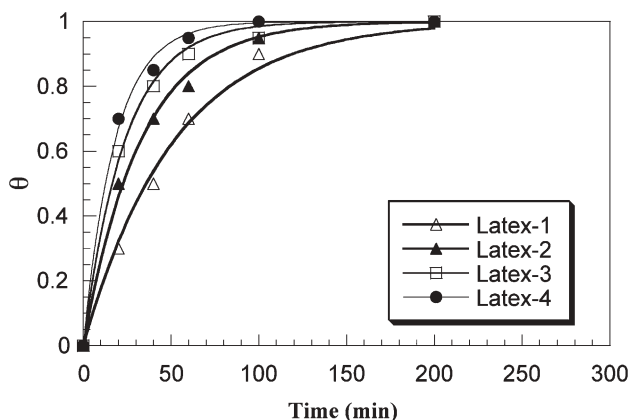


**Fig. 1.** The reduced adsorbed amount ( $\theta = N_s/N_{s,max}$ ) as a function of time with 0.1 mg/ml of polythymidylic acid on cationic polystyrene latexes at 20°C and a 10 mmol/l phosphate buffer of pH 5.2.  $\sigma_{Latex-1} < \sigma_{Latex-2} < \sigma_{Latex-3} < \sigma_{Latex-4}$ .  $\sigma$  is the surface charge density [23]

by the slope of the amount of ODN adsorbed at low ODN concentration and (ii) the plateau value deduced high ODN bulk concentration. Both the adsorption affinity and the plateau depend on surface structure and adsorption conditions.

The first reported work on the adsorption of ODNs onto charged colloids revealed marked affinity differences between sulfate- and amino-containing polystyrene latexes. In fact, low affinity has been observed for sulfated polystyrene particles, whereas high affinities are exhibited in the case of cationic (amine and amidine) polystyrene latexes (Fig. 2).

#### 4.2.3

##### *Effect of pH on ODN Adsorbed Amount*

As for adsorption of polyelectrolytes onto charged colloids, the pH of the incubation medium is one of the relevant parameters. The pH affects the charges dissociation of the solid support rather than the polyelectrolyte character of the ODN. The adsorption of oligonucleotides onto negatively charged sulfate polystyrene particles was reported to be pH independent and low in nature (less than 0.3 mg m<sup>-2</sup>) [21, 23]. The ODN adsorption onto cationic polystyrene latexes is dramatically affected by the pH of the medium as reported in Fig. 3 in which the maximal ODN adsorbed amount ( $N_{s,max}$ ) is presented as a function of pH [22, 24]. The immobilized amount of ODN decreases as the pH increases, revealing direct relationship between surface charge density and the adsorption process shown in Fig. 3. In addition, the slight surface modification by coating the particles with a nonionic surfactant (Triton x-405) affects the ODN adsorption. The behavior was attributed to an increase in the adsorption barrier principally at basic pH.

Furthermore, adsorption at basic pH, where the surface is weakly charged, was found to be low but not negligible. To explain this adsorption, Van der Waals

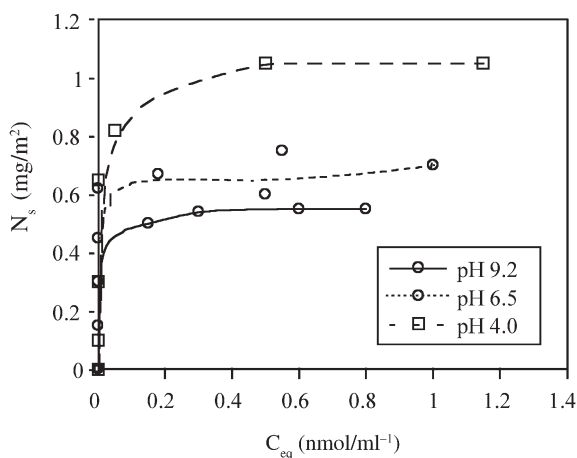


**Fig. 2.** Adsorption isotherms of oligonucleotide onto cationic polystyrene latex particles. Samples were mixed and incubated for 2 h at 20°C,  $10^{-2}$  ionic strength at a given pH [24]

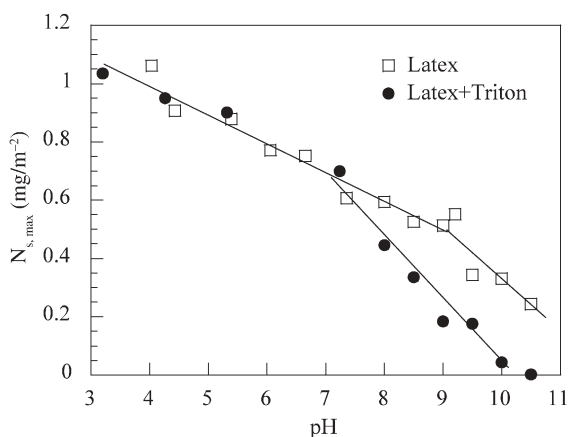


**Fig. 3.** The effect of pH on the maximal adsorbed amount of dT<sub>35</sub> onto bare and precoated latex particles (using Triton x-405) as a function of pH at 20°C and  $10^{-3}$  mol/l ionic strength [22]

forces are involved, and stacking between the aromatic compounds and the ODN bases can occur. Moreover, although charged, the amidino or amino cationic surface is relatively hydrophobic, as was revealed by contact angle measurements on various particles [25].

Last, by decreasing the hydrophilic properties of ODN by screening the charges, it is possible to increase slightly the quantities adsorbed by hydrophobic forces, though this effect has only been observed with weak ionic strengths (from  $10^{-4}$  to  $10^{-2}$  mol/l). To this end, interesting work has been reported by Walker and Grant [26] who investigated the effect of ODN hydrophobization on

sulfate charged polystyrene latexes. They pointed out that the methylation of aromatic basis of ODNs enhanced the adsorbed amount. The behavior observed has been attributed to hydrophobic adsorption process onto hydrophobic sulfate polystyrene particles.

#### 4.2.4

##### *Effect of Surface Charge Density*

The effect of surface charge density can be treated as the influence of pH on the ODN adsorption. Indeed, the increase of cationic surface charge density (or decreasing the pH to high acidic domain) leads to high ODN adsorption (Fig. 4) irrespective of pH. The extrapolated adsorbed amount at zero surface charge density was found to be close to quantities observed in the case of sulfate latexes (i.e.,  $0.3\text{--}0.4\text{ mg m}^{-2}$ ) [21, 23]. The effect of surface charge density on the adsorbed amount of ODN can be directly related to the effect of pH. In fact, the pH controls the surface ionization groups and then the attractive or the repulsive forces between the considered colloidal particles and the nucleic acid material as depicted in Fig. 3 and Fig. 4 for amino containing latex particles.

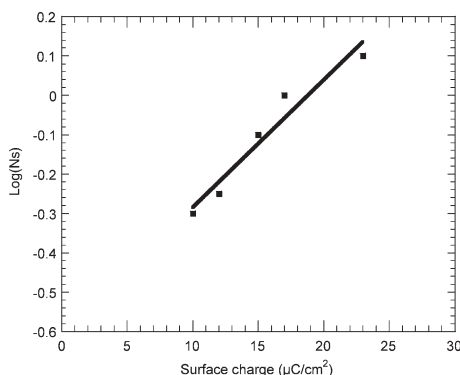


**Fig. 4.** Maximal adsorbed amount (Ns in  $\text{mg m}^{-2}$ ) of dT<sub>35</sub> on latex particles as a function of surface charge density (pH 5.0, 25°C, and ionic strength  $10^{-2}$ ) [22]

#### 4.2.5

##### *Effect of Ionic Strength on ODN Adsorbed Amount*

According to the polyelectrolyte character of ODNs, the effect of salt concentration on adsorption should be considered. Indeed, the ionic strength affects (i) the electrostatic interactions between the ODN and the adsorbent and (ii) the lateral repulsive electrostatic interactions between adsorbed ODNs.

In the case of sulfate charged latexes, the adsorption of ODN was reported to be independent of salinity. Such behavior was attributed to the hydrophobic interaction between the aromatic bases of ODN and the hydrophobic domains on the polystyrene particle surface [23].

The ODN adsorption onto cationic polystyrene latexes as a function of NaCl concentration and at acidic pH was investigated [24] and found to be slightly influenced by the salinity as given in Fig. 5. At acidic pH, the adsorbed amount of ODN decreased markedly as the salinity increases, compared to the adsorption at basic pH. For such a highly charged colloidal system, the effect of salt was attributed to the reduction in the attractive electrostatic interaction.

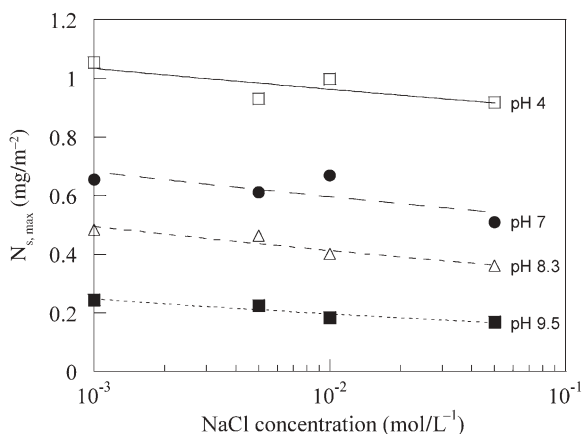


**Fig. 5.** The effect of ionic strength on the maximal adsorbed amount of dT<sub>35</sub> onto precoated amino-containing polystyrene latex particles (by adsorbing low amount of surfactant) as a function of pH [22]

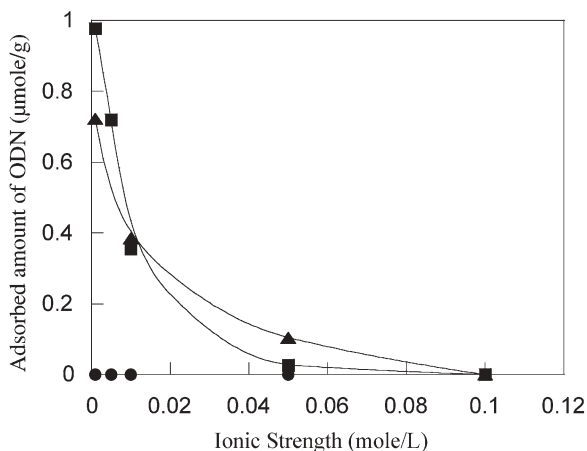


**Fig. 6.** Adsorption of oligodesoxyribonucleotides at room temperature on different amino-containing poly(*N*-isopropylacrylamide) latexes as a function of ionic strength in phosphate buffer (pH 4.5), adsorption time 2 h. Concentration of oligodesoxyribonucleotide 1 mg/ml and ionic strengths were adjusted by addition of NaCl. (amide groups 5  $\mu\text{mol g}^{-1}$ , filled circles), (amine and amide groups, 22  $\mu\text{mol g}^{-1}$ , filled squares), (amine and amide groups, 14  $\mu\text{mol g}^{-1}$ , filled triangles) [28]

The ODN adsorption onto cationic microgel poly(*N*-isopropylacrylamide) particles was reported to be dramatically affected by the salinity of the incubation medium [9] as illustrated in Fig. 6. The observed result was related to (i) the reduction in attractive electrostatic interactions between ODN molecules and the adsorbent and (ii) the drastic effect of ionic strength on the physico-chemical properties of such particles [17, 27]. In fact, the hydrodynamic size, the swelling ability, the electrokinetic properties, and the colloidal stability are dramatically affected by pH, salt concentration, and the medium temperature [27].

### 4.3

#### Desorption Study

The desorption study allows one to learn about the possibility of removing the adsorbed oligonucleotides after the covalent immobilization process. In fact, the presence of adsorbed ODNs may affect the sensitivity of the targeted biomedical tests.

The first step consists in strongly reducing the attractive electrostatic interactions by neutralizing the charges of the latex (the ODN remains negatively charged in the range of pH above 3). The enhancement of the desorption of preadsorbed oligonucleotide molecules can be ensured by changing the pH, the salinity, or upon addition of an appropriate competitor. In the case of an attractive system such as a cationic colloid, this was carried out at a highly basic pH (i.e., pH > 9), which, however, causes the particles to aggregate.

This instability can be avoided by adding a non-ionic surfactant to the surface of the latex, forming a hydrophilic layer (Triton x-405 of 30 units) on the surface of the latex [22]. In addition, this compound reduces the stacking effect by masking the hydrophobic domains (or properties) of the surface. Indeed, competition for adsorption between the ODN and the surfactant molecules can also lead to desorption. However, this effect was not observed in all reported studies, but it is in principle accessible by comparing the adsorption energies of ODN and the surfactant on the surface of the latex.

In addition, it is worth remembering that the sequence or chain length of ODN has no influence on the overall amount of adsorbed ODN (in mg m<sup>-2</sup>) on cationic colloidal polymer particles [24]. This underlines the concept that ODN are mainly adsorbed via attractive electrostatic interaction in the case of oppositely charged latexes and via hydrophobic or staking interactions when negatively hydrophobic latexes are used.

To favor the release of preadsorbed oligonucleotides, various desorption conditions have been systematically investigated. The desorption has been first examined as a function of washing steps. The results obtained revealed the decrease in the residual ODN adsorbed amount until three or four washes, after which the desorbed amounts ODN are almost nil [29] (see Fig. 7). The influence of pH on the desorption process has been reported to be the key parameter leading to high desorption of ODN. Indeed, the desorption of preadsorbed ODN at acidic pH revealed high desorption yield when high basic buffer (pH 10) was used. The behavior was attributed to the reduction in attractive electrostatic



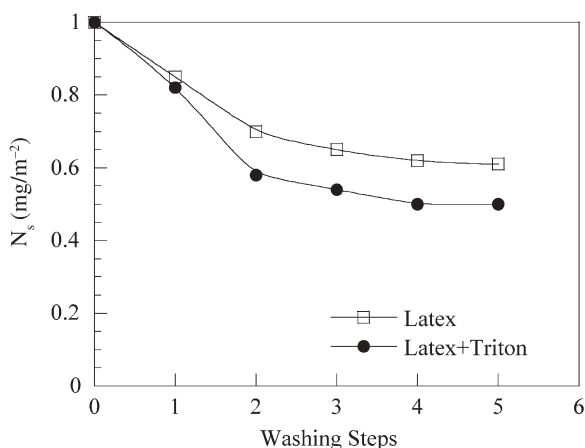


**Fig. 7.** Residual adsorbed amount of  $\text{dT}_{35}$  onto bare and precoated latex particles as a function of washing steps. Adsorption was performed onto bare latex particles at pH 5 and  $10^{-2}$  mol/l ionic strength [22]

interaction. The addition of salinity and/or small amount of surfactant (such as Triton x-405) of high affinity with the colloidal particles enhanced the desorption of adsorbed oligonucleotides as shown in Fig. 7 (for Triton) and Fig. 8 (for Triton plus NaCl).

Furthermore, a careful control of the desorption process will be suitable for monitoring the chemical grafting of functionalized oligonucleotides (mainly ODN bearing amine group at its 5' position), a point which will be delineated in the next section.

#### 4.4

##### Chemical Grafting of Oligonucleotides Onto Reactive Latex Particles

As mentioned at the beginning of this review, covalent grafting of biomolecules onto colloidal support avoids reversible immobilization. Furthermore, an extended conformation of the ODNs is a key factor for efficiently hybridizing the complementary DNA fragment (i.e., target capturing). However, implementation of immobilization is more difficult than adsorption.

An amino-functional spacer arm is introduced at the 5' position of the ODN in the last step of its automated synthesis. ODN can be grafted via various functions available on flat carriers (such as flat silicon surfaces or wafers covered in silane) or on latex particles. Table 2 shows a list of various activation agents used and the reactive group resulting from the activation depending on the compound involved; when available, the maximum grafting amount is also reported.

All reactive functions, apart from epoxide, require a preliminary amine activation step prior to chemical coupling or a reduction after grafting step (aldehyde). The quantities of chemically immobilized ODN are in the same order of magnitude than those grafted during adsorption (less than  $1 \text{ mg m}^{-2}$ ) which let one suppose that the amine functions carried by the bases also react

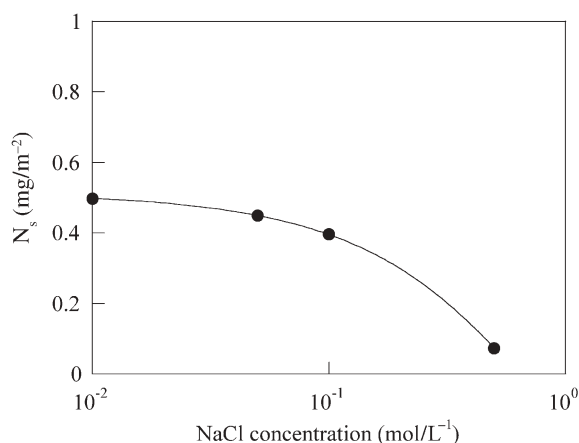


**Fig. 8.** Residual adsorbed amount of dT<sub>35</sub> onto bare latex particles as a function of ionic strength. Adsorption was performed onto bare latex particles with  $N_s=1.0 \text{ mg m}^{-2}$  at pH 5 and  $10^{-2} \text{ mol/l}$  ionic strength. The desorption was carried out after two washes using buffer (at various ionic strengths, pH 10 and 1% Triton x-405) [22]

**Table 2.** Functions involved in the covalent grafting of amino-terminated ODNs onto solid supports [30]

Functionalized support	Linker	Reactive group	Attached amount ( $\text{mg m}^{-2}$ )	Reference
$\text{NH}_2$	TCA	Chlorine	0.11	[31]
	EGS	Ester	0.30	[32, 33]
	PDC	Isothiocyanate	$\approx 5$	
Epoxy	–	–	0.37	[34]
			0.2	[35]
OH	CNBr	Imidocarbonate	0.14	[36]
SH	TCA	Chlorine		[37]
	SMPB	Maleimide	2.8	[38]
COOH	NHS	Ester		[36]
	EDC	Diazonium	1.3	[39]
	APA	Imidazole		[36]
	NMI			
	EDC			
CHO	–	–		[40]

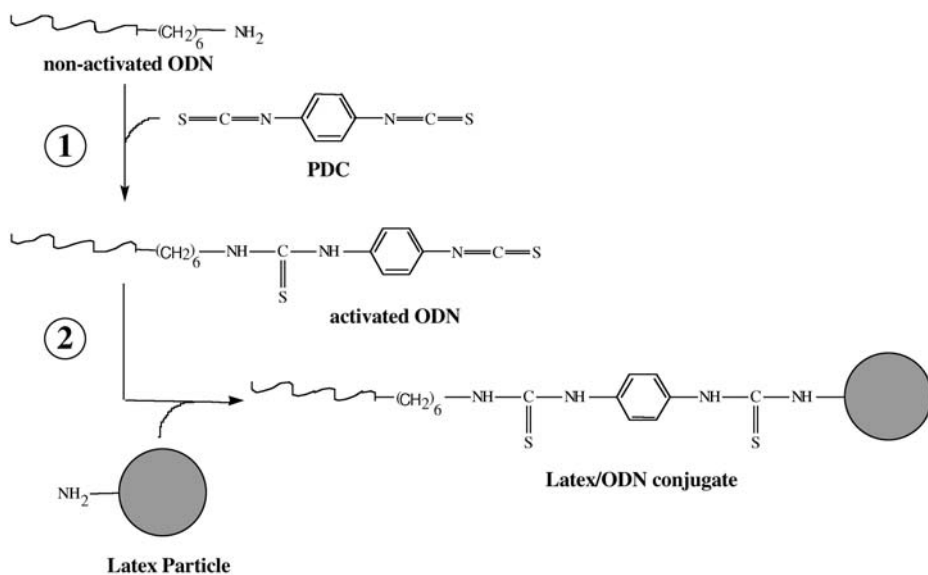
with such activated groups. Finally, hydrolysis of the reactive function implies reproducibility problems.

Selecting the appropriate reactive function leading to selective chemical grafting yield (only on the amine terminal of the ODN) and efficient chemical reaction (absence of hydrolysis of the function) is a great challenge. Here, the most often reported system is covalent grafting of ODN bearing primary amine group onto amino-containing polystyrene latex particles [30, 41]. In those works, the phenylene diisothiocyanate (PDC) was chosen for its moderate reactivity towards nucleophilic agents such as amine functions and its slow hydrolysis reaction compared to those of activated esters.

Recently, covalent grafting of ODN-bearing amino-link spacer arm onto amino-containing latex particles was reported by investigating numerous parameters from activation to covalent binding [28, 30, 41]; the principle is depicted in Scheme 3. The first step consists in activating the amine group of the ODN by PDC. A considerable surplus of this bifunctional molecule facilitates the reaction of a single isothiocyanate group. The second step consists in grafting the activated ODN on the amino-containing polystyrene latex particles.

The overall strategy consists in finding conditions where ODN adsorption occurs without avoiding grafting. Once chemical grafting is reached, desorption of non-covalently grafted ODN is performed in an appropriate conditions optimized as reported in the desorption part (basic pH, high salt amount in presence of excess non-ionic surfactant).

The maximum quantity of ODN chemically grafted on amino-containing polystyrene latexes is found to be around  $0.4 \text{ mg m}^{-2}$  irrespective of pH (from 8



**Scheme 3.** Covalent immobilization of ODNs onto aminated latex particles. Step 1: activation reaction of the ODNs by PDC. Step 2: grafting of the activated ODNs onto aminated-latex particles [30]

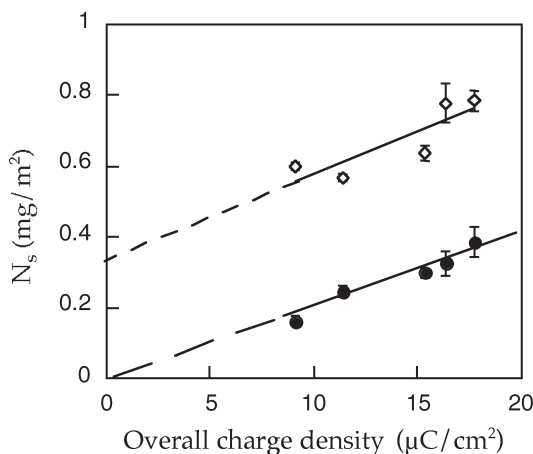


**Fig. 9.** Influence of the overall charge density of the latexes on the adsorbed and grafted poly(thymidylic) acid amounts. *Diamond*: adsorbed and grafted dT<sub>35</sub> amount. *Circle*: residual covalently grafted amount after desorption [41]

to 10) and ionic strength [41]. It is worth mentioning, that the grafting content of activated ODN onto latex particles bearing amine groups is directly related to the number of reactive functions at the particles surface as shown in Fig. 9.

The extent of the ODN activation reaction and its influence on chemical grafting was specifically studied by MALDI-TOF and the excess enzymatic digestion/HPLC experiments [30]. It turned out that activating agent (PDC) could react with the primary and secondary amine groups of the bases (of the considered ODN). For instance, poly(thymidylic) acid was shown to be very sensitive to base activation. The length and the sequence of the ODN have no influence on adsorption process [24]; however, they greatly affect the grafting yield, as illustrated in Fig. 10, in which the grafted amount is reported as a function of the number of active sites ( $n_{\text{PDC}}$ ) per ODN chain.

In addition to the chemical grafting of single strand DNA fragments, some studies [42] also described the grafting of a double-stranded ODN onto epoxy-functionalized polystyrene latexes. A protruding end of more than 15 bases was necessary for an efficient covalent grafting to occur. This behavior was attributed to non-specific reactions onto the bases. The influence of a poly (thymidylic) acid sequence added as a spacer arm onto the ODNs hybridization efficiency was also reported [43]. A spacer of at least ten bases was required for the hybridization to occur, showing that both the covalent grafting and hybridization are efficient when a thymidylic sequence is added.

#### 4.5

##### Conformation of Adsorbed and Chemically Grafted ODN Onto Colloidal Particles

The preparation of these latex/ODN conjugates is intended to capture a target single strand DNA by hybridization. Then the ODN grafted on the surface must

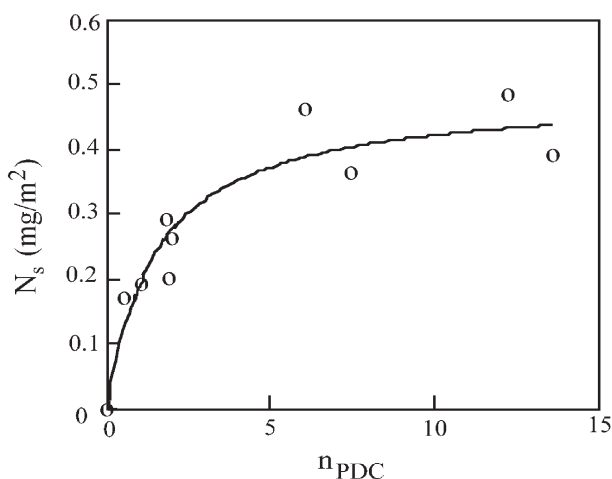


**Fig. 10.** Influence of the number of PDC per ODN chain onto the amount of ODN covalently linked to the polystyrene latex [30]

be accessible, which depends on the interactions governing the adsorption of the ODN to the interface. Consequently, knowledge of the ODN's conformation on the surface of the latex as a function of the conditions prevailing in the medium is vital. However, the nature of the system (colloidal) and the small size of the ODN restrict the number of possible analytical methods. Walker and Grant [26, 44] reported the use of different methods for studying the conformation of ODN adsorbed on anionic and cationic latex particles. A first preliminary study was carried out by this group in order to determine the thickness of the ODN layer on the surface of the latex by quasi-elastic light scattering. However, the sensitivity of this technique proved to be inadequate for accurate estimation of small thicknesses. Then, a second method often used in biology was employed, i.e., Hydroxyl Radical Footprinting (HRF). This consists in using OH radical to cleave the ODN part not in contact with the surface. The fragments obtained were analyzed by migration on gel (i.e., gel electrophoresis) and their distribution revealed the interfacial conformation of the ODN. This cleaving reaction did not occur for those ODNs whose segments are wholly adsorbed on the surface (total flat conformation). This analysis can be considered.

A recent laboratory study carried out by Charreyre et al. [45] succeeded in examining the conformation of ODN chemically grafted by its 5' end on a cationic latex by fluorescence energy transfer (FET). This method consists in using a couple of fluorescent molecules, the fluorescein (as a donor), grafted to the 3' end of the ODN and tetramethylrhodamine (as an acceptor) immobilized on the surface of the latex. The efficiency of this method varies as a function of the mean distance between the two fluorophores, (i.e., between the ODN and the surface). Fluorescence energy transfer studies of ODN grafted onto the surface of an amino-containing latex in the presence of a non-charged surfactant (Tri-

ton x-405) provided interesting information about the interfacial conformation of immobilized ODN as a function of the conditions of the medium. A “brush” type structure was observed at a basic pH (pH 10), whereas at neutral or weak acid pH (pH 6) conformation is mostly flat [45].

Recently, small angle neutron scattering (SANS), which is generally considered as accurate and appropriate method for adsorbed and grafted polymer on solid-liquid surfaces, was used by Elaissari et al. [46]. The main advantage of this technique is that it is capable of supplying both the quantity of ODN immobilized and the thickness of the layer, by eliminating the scattering specific to the latex particles dispersed in a suitable solution ( $D_2O/H_2O$  mixture). This method has been used by many authors to determine the structure of macromolecules grafted or adsorbed on carrier particles. The structure of ODN (35 base poly(thymine) as a model) adsorbed on the surface of a cationic or anionic deuterated polystyrene latex is found to be in a flat conformation [46] as demonstrated by Walker et al. by the HRF technique. This is due to the strong interactions between the ODN and the carrier resulting in a large number of contact points. ODN can be adsorbed either by its phosphodiester charged compound (via electrostatic forces), or by its nucleic bases (via stacking effect between the aromatic compounds of the bases and phenyl). The cationic latex particles carrying the adsorbed ODN analyzed at pH 5, shown in Fig. 11, reveals that the conformation is neither “brush-like” (which would be the case for  $H_T = 150 \text{ \AA}$ ), nor completely flat (for  $H_T = 10 \text{ \AA}$ ). A mean thickness from 50 to 70  $\text{\AA}$  from theory correlated with the experimental results. Similar results were obtained by varying the medium’s ionic strength and pH, for both interfaces prepared by adsorption or by coupling. The general trend of ODN conformation chemically grafted on this cationic surface is shown in Fig. 12. The ODN layer formed has an average thickness from 50 to 70  $\text{\AA}$ , as a function of the quantities immobilized.

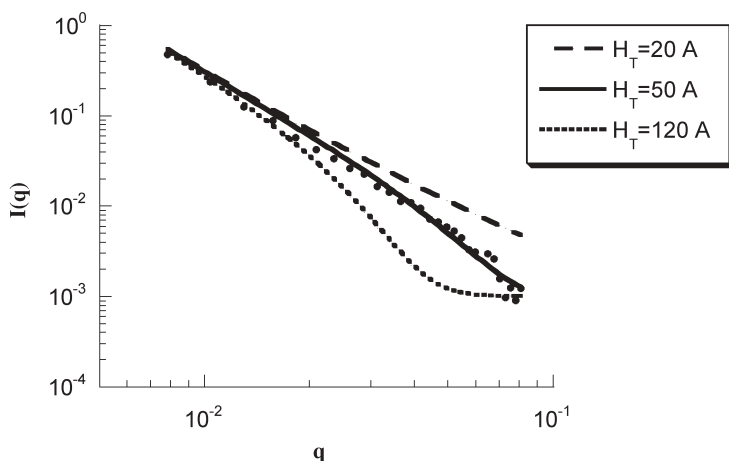


**Fig. 11.** Scattering intensity  $I(q)$  vs scattering vector ( $q$ ) in log-log scale of the coated deuterated polystyrene particles by adsorbing dT<sub>35</sub> at pH 5 and 0.01 mol/l NaCl [46]

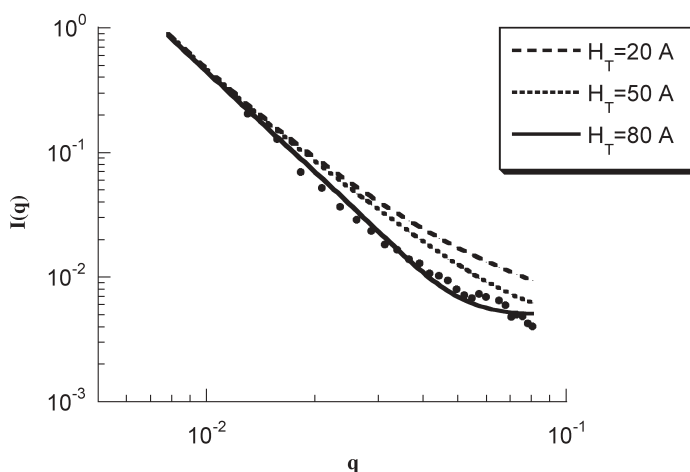


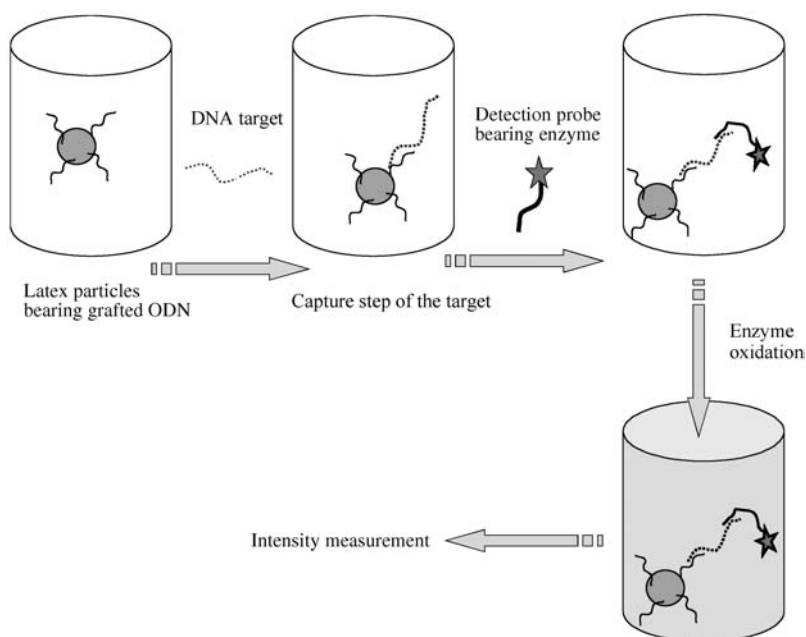
**Fig. 12.** Scattering intensity  $I(q)$  vs scattering vector ( $q$ ) in log-log scale of coated latex particles prepared by covalent grafting at pH 9.2 and  $10^{-2}$  mol/l NaCl [46]

## 5 Some Fine Applications

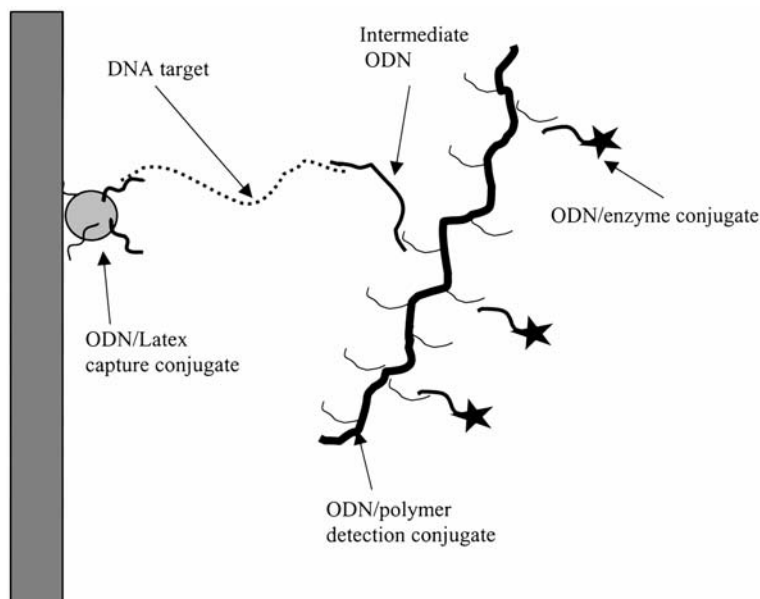
The objective of this section is to focus on some fine applications of latex particles in nucleic acids based biomedical diagnostic. In this domain, two major applications are presented: (i) specific capture and detection of targeted DNA or RNA and (ii) non-specific concentration of nucleic acids using latex particles.

The latex-oligonucleotides conjugates are principally used for capturing specifically the nucleic acid targets. In fact, when the oligonucleotides of a given sequence are chemically immobilized onto reactive colloidal particles with a good orientation, the specific capture of complementary nucleic acid (target) in biological sample is then possible as illustrated in Scheme 4. Hence, the first ODN grafted onto colloidal particles is named capture ODN bearing well defined structure in order to capture specifically target DNA or RNA from any complex biological sample. After the capture step of the target via hybridization process, the colloidal particles are then separated via physical processes using centrifugation, filtration, or magnetic separation. After the washing step to eliminate the possible contaminants and residual biological materials, the quantification of the captured targets was performed using a labeled oligonucleotide of a given sequence (bearing enzyme such as HRP) able to hybridize with a specific region of the capture target. The enzyme oxidation leads to a colored medium with intensity proportional to the target concentration. Such detection is named ELOSA (Enzyme Link Oligo-Sorbent Assay) test. The combination of latex-ODN complexes [41] with polymer-ODN conjugates [6] was found to enhance drastically the sensitivity of nucleic acids detection as recently reported [28] (Scheme 5).





**Scheme 4.** Schematic illustration of specific capture and detection of targeted DNA or RNA



**Scheme 5.** Schematic illustration of specific capture and detection of targeted DNA or RNA using colloidal particle-ODN and copolymer-ODN conjugates [28]

This type of diagnostic called genic or molecular which consists in detecting a pathogenic organism through the genetic material contained in its DNA or RNA has not been widely reported and only a few papers are dedicated to such studies. Here, the detection of HBV DNA virus is presented using the combination of latex particles and reactive copolymers. Such methodology has been applied to cationic latexes (such as polystyrene and poly(*N*-isopropylacrylamide) bearing chemically grafted oligonucleotides. The colloidal particles bearing ODN are two-dimensional assemblies adsorbed onto a solid support (inside of a pipette tip) of an automated diagnostic system [6] based on similar approach as depicted in Scheme 5.

The surface functionalization of solid phases by adsorbing latex-ODN conjugates leads to the formation of an ordered monolayer of colloidal particles. Under these conditions the performance of such system was proved, with an overall increase of sensitivity ranging from 100 to 1000 in the case of hepatitis B compared to the classical method [6, 8].

In addition to the specific capture and detection of targeted single stranded DNA fragment, the non-specific extraction and concentration of nucleic acids is of great importance. In fact, the good control of the adsorption and the desorption processes of DNA, RNA, and single stranded nucleic acid molecules onto colloidal particles was found beneficial for purification and concentration of such polyelectrolytes as recently shown using thermally sensitive poly(*N*-isopropylacrylamide) [NIPAM] based hydrophilic microgel colloidal particles [9] and cationic amino-containing hydrophilic magnetic latexes [10] (Scheme 6).

The adsorption of proteins onto such stimuli-responsive particles was found to be temperature dependent rather than pH and ionic strength (below the LCST of the corresponding homopolymer). At room temperature, the adsorption of various proteins revealed to be nil or low at room temperature in the case of poly(NIPAM) based particles [9, 10].

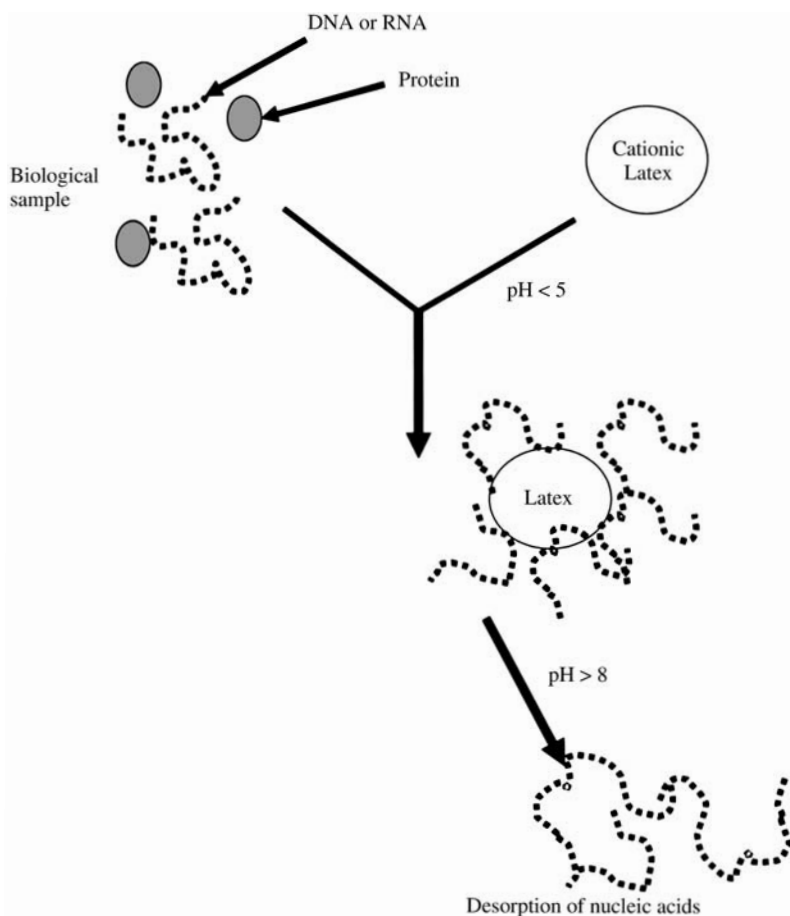
The pH-dependent properties of the hydrophilic positively charged colloidal particles favor the adsorption of negatively charged nucleic acids at acidic pH and at low salt concentration. However, the desorption is favored at basic pH and at high ionic strength. The concentration process of adsorbed nucleic acid materials was performed via centrifugation [9], filtration, or magnetic separation [10] of the used colloidal particles.

Amplification of the captured sequence can be performed directly on cationic hydrophilic particles without a release step, since they are compatible with the amplification medium, such as PCR (Polymerase Chain Reaction), or after a desorption step and the removal of colloidal particles.

## 6

### Conclusion

Colloid polymer particles bearing reactive groups are of great interest in the domain of biomedical diagnostics. Such colloids can be prepared using various polymerization processes ranging from the classical emulsion polymerization to the more complex elaboration process in dispersed media. The design of well adapted latexes for a given application needs to take into account various param-



**Scheme 6.** Principle of separation and concentration of nucleic acids using pH sensitive latex particles

eters such as particle size, size distribution, surface charge density, colloidal stability, surface morphology, and finally the surface polarity. In fact, the listed properties affect the adsorption of nucleic acid molecules and consequently their chemical grafting onto the considered colloidal particles. The presence of reactive groups (amine, aldehyde, thiol, and carboxyl) on latex particles permits the chemical grafting of biological molecules in addition to improving particle stability. Generally, these functionalized particles proved to be suitable supports for molecules with biological applications, since the adsorption of charged biomolecules onto such charged polymer particles is the driving parameter controlling the efficiency of the chemical immobilization process. The adsorption affinity of biomolecules onto charged colloidal particles is mainly related to the pH, ionic strength, and in some cases to the incubation temperature (i.e., ther-

mally sensitive particles). Prior to any real use of latex particles-biomolecules conjugates in the biomedical field, the knowledge of the adsorption phenomena of the considered biological molecules is of paramount importance. In fact, the adsorption study allows one to elaborate the effect of each parameter involved in the adsorption process and to consider the driving forces implicated in the interaction between both species.

The presence of functionalized groups on the particles surface permits the chemical grafting of various kinds of biomolecules. The covalent grafting is generally performed by considering both pH and ionic strength of the medium leading to high adsorption in order to enhance the chemical grafting step. Whatever the chemical immobilization condition, a subsequent desorption is absolutely needed for elaborating particles bearing only covalently bonded biomolecules. Stimuli responsive colloidal particles are even more promising in biomedical domains, especially for diagnostics. Thus their use to improve the sensitivity of the corresponding assays is quite significant, principally for the extraction, purification and concentration of biological entities such as nucleic acids. Obviously, the concept can be extended to more complex biomolecules and biocolloids such as viruses, bacteria, etc.

## References

1. Arshady R (1993) *Biomaterials* 14:5–15
2. Kadonaga JT, Tjian R (1986) *Proc Natl Acad Sci USA* 83:5889–5893
3. Chavany C, Le Doan T, Couvreur P, Puisieux F, Hélène C (1992) *Pharm Res* 9(4):441–449
4. Parinov S, Barsky V, Yershov G, Kirillov E, Timofeev EN, Belgovskiy A, Mirzabekov AD (1996) *Nucleic Acids Res* 24(15):2998–3004
5. Timofeev EN, Kochetkova SV, Mirzabekov AD, Florentiev VL (1996) *Nucleic Acids Res* 24:3142–3148
6. Erout MN, Troesch A, Pichot C, Cros P (1996) *Bioconjugate Chem* 7:568–575
7. Ganachaud F, Theretz A, Erout MN, Llauro MF, Pichot C (1995) *J Appl Polym Sci* 58:1811–1824
8. Charles M-H, Charreyre MT, Delair T, Elaissari A, Pichot C (2001) *STP Pharma* 11:241–263
9. Elaissari A, Holt L, Meunier F, Voisset C, Pichot C, Mandrand B, Mabilat C (1999) *J Biomater Sci Polym Edn* 10:403–420
10. Elaissari A, Roudrigue M, Meunier F, Herve C (2001) *J Magn Magn Mater* 225:127–133
11. Pichot C (1995) *Polym Adv Tech* 6:427–434
12. Meunier F, Elaissari A, Pichot C (1995) *Polym Adv Technol* 6:489–496
13. Ganachaud F, Mouterde G, Delair T, Elaissari A, Pichot C (1995) *Polym Adv Tech* 6:480–488
14. Ganachaud F, Sauzedde F, Elaissari A, Pichot C (1997) *J Appl Polym Sci* 65:2315–2330
15. Sauzedde F, Ganachaud F, Elaissari A, Pichot C (1997) *J Appl Polym Sci* 65:2331–2342
16. Duracher D, Sauzedde F, Elaissari A, Perrin A, Pichot C (1998) *Colloid Polym Sci* 276:219–231
17. Duracher D, Sauzedde F, Elaissari A, Pichot C, Nabzar L (1998) *Colloid Polym Sci* 276:920–929
18. Sauzedde F, Elaissari A, Pichot C (1999) *Colloid Polym Sci* 277:1041–1050
19. Sauzedde F, Elaissari A, Pichot C (1999) *Colloid Polym Sci* 277:846–8559
20. Ladaviere C, Veron L, Delair T, Domard A, Pichot C, Mandrand B (1997) *J Appl Polym Sci* 65:2567–2577
21. Elaissari A, Cros P, Pichot C, Laurent V, Mandrand B (1994) *Colloids Surf* 83:25–31
22. Ganachaud F, Elaissari A, Pichot C (1997) *Langmuir* 13:7021–7029

23. Elaissari A, Chauvet JP, Halle MA, Decavallas O, Pichot C, Cros P (1998) *J Colloid Interface Sci* 202:2252–2260
24. Ganachaud F, Elaissari A, Pichot C, Laayoun A, Cros P (1997) *Langmuir* 13:701–707
25. Ganachaud F, Bouali B, Veron L, Lantéri P, Elaissari A, Pichot C (1998) *Colloid Surf A Physicochem Eng Aspects* 137:141–154
26. Walker HW, Grant SB (1996) *Langmuir* 12:3151–3156
27. Nabzar L, Duracher D, Elaissari A, Chauveteau G, Pichot C (1998) *Langmuir* 14:5062–5069
28. Delair T, Meunier F, Elaissari A, Charles M-H, Pichot C (1999) *Colloids Surf A Physicochem Eng Aspects* 153:341–353
29. Elaissari A, Pichot C, Delair T, Cros P, Kurfurst R (1995) *Langmuir* 11:1261–1267
30. Ganachaud F, Laayoun A, Chaix C, Delair T, Pichot C, Elaissari A (2001) *J Disp Sci Technol* 22:473–484
31. Van Ness J, Kalbfleisch S, Petrie CR, Reed MW, Tabone JC, Vermeulen NMJ (1991) *Nucleic Acids Res* 19:3345
32. Running JA, Urdea MS (1990) *BioTechniques* 8:276–277
33. Guo Z, Guilfoyle RA, Thiel AJ, Wang R, Smith LM (1994) *Nucleic Acids Res* 22:5456–5465
34. Imai T, Sumi Y, Hatakeyama M, Fujimoto K, Kawaguchi H, Hayashida N, Shiozaki K, Terada K, Yajima H, Handa H (1996) *J Colloid Interface Sci* 177:245
35. Lamture JB, Beattie KL, Burke BE, Eggers MD, Ehrlich DJ, Fowler R, Hollis MA, Kosicki BB, Reich RK, Smith SR, Varma RS, Hogan ME (1994) *Nucleic Acids Res* 22:2121–2125
36. Ghosh S, Musso GF (1987) *Nucleic Acids Res* 13:5353–5372
37. Hakala H, Lönnberg H (1997) *Bioconjugate Chem* 8:232
38. Chrissey LA, Lee GU, O’Ferrall CE (1996) *Nucleic Acids Res* 24(15):3031–3039
39. Miller CA, Patterson WL, Johnson PK, Swartzell CT, Wogoman F, Albarella JP, Carrico RJ (1987) *J Clin Microbiol* 26:1271
40. Kremsky JN, Wooters JL, Dougherty JP, Meyers RE, Collins M, Brown EL (1987) *Nucleic Acids Res* 15(7):2891
41. Ganachaud F, Elaissari A, Pichot C (2000) *J Biomater Sci Polym Edn* 11:931–945
42. Wada T, Watanabe H, Kawaguchi H, Handa H (1995) *Methodol Enzymol* 254:595
43. Joos B, Kuster H, Cone R (1997) *Anal Biochem* 247:96
44. Walker HW, Grant SB (1996) *Colloids Surf* 119:229
45. Charreyre MT, Tcherkasskaya O, Winnik MA, Hiver A, Delair T, Pichot C, Mandrand B (1997) *Langmuir* 13:3103
46. Elaissari A, Chevalier Y, Ganachaud F, Delair T, Pichot C (2000) *Langmuir* 16:1261–1269

# Preparation of Monodisperse Particles and Emulsions by Controlled Shear

V. Schmitt<sup>1</sup>, F. Leal-Calderon<sup>1</sup>, J. Bibette<sup>2</sup>

<sup>1</sup> Centre de Recherche Paul Pascal, Avenue A Schweitzer, 33600 Pessac France

<sup>2</sup> Laboratoire de Colloïdes et Nanostructures, ESPCI, 10 rue Vauquelin, 75231 Paris cedex 05, France

Monodisperse emulsions can be obtained by applying a shear step to a crude polydisperse one [1]. In this paper, we first describe the mechanisms and conditions for the occurrence of this transformation. The fragmentation process involves two distinct regimes. At short time (shorter than one second), the droplet diameter decreases abruptly. The droplets deform into long threads that undergo a Rayleigh instability. The obtained diameter is mainly determined by the applied stress and weakly depends on the viscosity ratio between the dispersed and continuous phases. However, this last parameter is determining for monodispersity. After this first step, the resulting droplets can, once again, break up into daughter droplets. This second mechanism is much slower, with a characteristic time of several hundred seconds, and much less efficient for fragmentation. A large variety of calibrated materials (direct, inverted, multiple emulsions and suspensions) can be obtained following this monodisperse fragmentation process. PACS numbers: 82.70.Kj, 82.70.-y, 77.84.Nh

**Keywords.** Emulsions, Rayleigh instability, Controlled shear, Monodispersity

<b>1</b>	<b>Introduction</b>	196
<b>2</b>	<b>Rupture Mechanisms and Kinetics</b>	197
2.1	General Behavior	197
2.2	Analysis of the First Regime	200
2.3	Analysis of the Second Regime	201
<b>3</b>	<b>Preparation of Calibrated Materials</b>	203
3.1	Couette-Cell Description	203
3.2	Simple Emulsions	204
3.3	Suspensions	208
3.4	Multiple Emulsions	210
3.4.1	Inverted W/O Emulsion	210
3.4.2	Double Emulsion	211
3.4.3	Influence of the Internal Droplet Mass Fraction	212
3.5	Ferrofluids	213
<b>4</b>	<b>Conclusion</b>	214
	<b>References</b>	215

## 1

### Introduction

Emulsions are metastable dispersions comprised of two immiscible fluids such as oil and water. They are kinetically stabilized by the addition of surface-active species. Emulsions are widely used materials for many industrial applications such as cosmetics, foods, pharmaceuticals, paintings, coatings, etc. To reach the dispersed metastable state, energy has to be supplied and the way emulsions are prepared is of utmost importance in controlling their final properties. Indeed, the mean droplet diameter which determines most of the emulsion properties (stability, rheology, optical properties...) is strongly dependent upon the fragmentation procedure. Emulsions production is generally based on empirical considerations where an uncontrolled flow, laminar or turbulent [2], is applied to the initial mixture of oil and water. On a more fundamental level, many studies have been performed [3–17], especially in laminar flow conditions. In order to simplify the problem, isolated drops are usually considered. One can mention the pioneering work of Taylor [5, 6] who showed that, in quasi-static conditions, a drop submitted to a flow deforms and bursts if the capillary number  $Ca$ , defined as the ratio of the shear stress over half the initial Laplace pressure, exceeds some critical value  $Ca_{cr}$  that depends on the viscosity ratio  $p$  between the dispersed and continuous phases. Following Taylor's study, a more precise determination of the critical capillary number, as a function of both  $p$  and the type of flow, has been obtained [12, 18]. Other authors were more interested in the rupturing mechanisms [19, 20]. Besides the Rayleigh instability that develops at the surface of a droplet deformed onto a long cylinder [3], other scenarios such as tip streaming [21] or end pinching [16] have been identified. Up to now, the fragmentation process has been mostly explored in quasi-static conditions: the rupturing occurs either by slowly increasing the shear rate or during the cylinder relaxation once the shear is interrupted [6, 8, 9, 17, 22]. However, as showed by Hinch and Acrivos [23], if the shear is not applied slowly, some of the stationary states are not accessible anymore and as a consequence the conditions for droplet rupturing are very different. In most of the practical conditions the emulsions are fabricated under application of non-quasi-static deformations meaning that the shear is suddenly applied to the material. In such conditions Mason et al [1, 24, 25] and Mabilille et al [26–28] have shown that monodisperse fragmentation may occur.

This chapter is organized as follows. In the first part we describe the mechanisms and conditions for the occurrence of the monodisperse rupturing in non-quasi-static conditions. The fragmentation process involves two distinct regimes. At short time (shorter than one second), the droplet diameter decreases abruptly. The droplets deform into long threads that undergo a Rayleigh instability. The diameter obtained is mainly determined by the stress applied and weakly depends on the viscosity ratio between the dispersed and continuous phases. However, this last parameter is determining for monodispersity. After this first step, the resulting droplets can, once again, break up into daughter droplets. This second mechanism is much slower, with a characteristic time of several hundred seconds, and much less efficient for fragmentation. In the sec-



ond part, we present a large variety of calibrated materials (direct, inverted, multiple emulsions and dispersions) that can be obtained following this monodisperse fragmentation process.

## 2

### Rupture Mechanisms and Kinetics

The process leading to monodisperse emulsions was initially described by Mason and Bibette [1, 24, 26–28]. For that purpose, they first prepare a crude mother emulsion obtained by progressively incorporating oil into the surfactant-water phase. In a second step, they apply a simple and well-controlled shear to this crude emulsion that becomes monodisperse after no more than a few seconds. Figure 1 shows microscope images before and after application of a shear under the same conditions used by Mason and Bibette. The shear has the effect of reducing both the average diameter and the distribution width of the mother emulsion.

The aim of this first section is to describe the rupturing mechanisms and the mechanical conditions that have to be fulfilled to obtain monodisperse emulsions. A simple strategy consists of submitting monodisperse and dilute emulsions to a controlled shear step and of following the kinetic evolution of the droplet diameter. It will be demonstrated that the observed behavior can be generalized to more concentrated systems. The most relevant parameters that govern the final size will be listed. The final drop size is mainly determined by the amplitude of the applied stress and is only slightly affected by the viscosity ratio  $p$ . This last parameter influences the distribution width and appears to be relevant to control the final monodispersity.

### 2.1

#### General Behavior

To illustrate the general behavior, we consider an emulsion comprised of 2.5 wt % of 350 mPa s silicone oil dispersed in an aqueous phase. This latter contains 3 wt % of non-ionic surfactant (commercial mixture of polyethylene glycol C<sub>10</sub>E<sub>5</sub> and

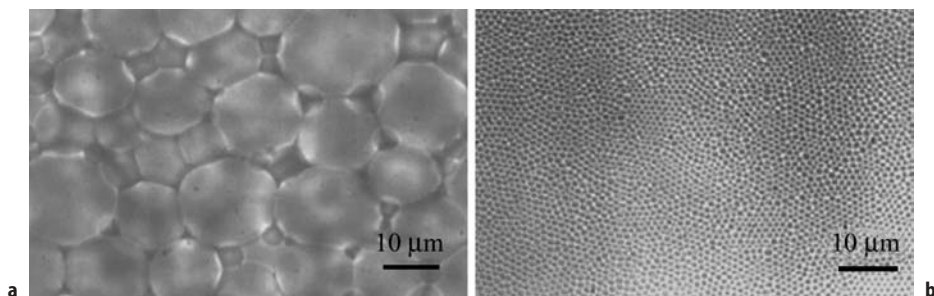


**Fig. 1.** Images of **a** a crude polydisperse emulsion with  $d=23\ \mu\text{m}$  and  $U=40\%$ , and **b**: of the same emulsion after application of a controlled shear,  $d=1\ \mu\text{m}$  and  $U=12\%$

C<sub>12</sub>E<sub>5</sub> referred to as Ifralan 205) and 2.8 wt % of a non-adsorbing polymer (alginate HF120L). The oil-aqueous phase interfacial tension  $\gamma_{\text{int}}$  is equal to 6 mNm<sup>-1</sup>. In order to obtain initially calibrated emulsions of various sizes, this emulsion is pre-sheared at different shear rates. It is then submitted to a step shear rate of 500 s<sup>-1</sup> with different step durations in order to follow the kinetics of emulsification. After the shearing process, the daughter emulsions are analyzed by static light scattering with a commercial granulometer that converts the scattered intensity into the size distribution using Mie theory. The droplet distribution is characterized in terms of the mean volume diameter  $d$  and uniformity  $U$  defined as:

$$d = \frac{\sum_i N_i d_i^4}{\sum_i N_i d_i^3}, \quad U = \frac{1}{d} \frac{\sum_i N_i d_i^3 |\bar{d} - d_i|}{\sum_i N_i d_i^3} \quad \text{where } N_i \text{ is the number of droplets of diameter } d_i, \bar{d} \text{ is the median diameter, i.e. the diameter for which the cumulative undersized volume fraction is equal to 0.5. In the following, we shall term as "monodisperse", any emulsion with uniformity smaller than 25\%. Such emulsions exhibit some crystallized domains when confined between two microscope slides.}$$

eter  $d_i$ ,  $\bar{d}$  is the median diameter, i.e. the diameter for which the cumulative undersized volume fraction is equal to 0.5. In the following, we shall term as "monodisperse", any emulsion with uniformity smaller than 25%. Such emulsions exhibit some crystallized domains when confined between two microscope slides.

The main results are reported on Fig. 2. In the case of emulsions possessing large initial diameters (11  $\mu\text{m}$ , 8  $\mu\text{m}$ ), one can clearly distinguish two regimes. For shearing times of the order of one second, the size decreases abruptly down to a value of around 6  $\mu\text{m}$ , independent of the initial size. The process of fragmentation was reproduced between two glass slides of an optical microscope (of course the shear is not controlled as it is in the rheometer) and the obtained images are reported in Fig. 3a,b. We clearly see the deformation of the initial drops into long parallel cylinders that break into identical aligned droplets with very small satellites in between them. These images reveal the existence of a Rayleigh instability that develops on the thread surface. Let us define  $d_c$  as the thread diameter just before the rupture and  $d_R$  as the droplet diameter after rupture. Considering the volume conservation and neglecting satellites contribution, we get a simple relation between  $d_c$  and  $d_R$ :  $d_c^2 \lambda = 2d_R^3/3$  where  $\lambda$  is the wavelength of the Rayleigh instability. From the data of Fig. 2, it can be deduced that  $d_R$  and therefore the product  $d_c^2 \lambda$  does not depend upon the initial drop diameter. By shearing viscous polymer blends, Rusu et al. [29] have directly observed the fragmentation of long cylinders resulting from the application of a shear. Their experiments show that all the drops undergo the Rayleigh instability at the same thread diameter. By similarity, one can hypothesize that the same scenario occurs in emulsions: all the drops deform into cylinders of various lengths and rupture at the same critical diameter under the effect of the Rayleigh instability. The uniqueness of  $d_c$  and  $\lambda$  with respect to the initial drop size explains the fact that a polydisperse emulsion, made of a mixture of different initial sizes, can be fragmented into a monodisperse one, as observed experimentally [1, 25, 26–28].

After the first fragmentation step, a second slow mechanism takes place, that further reduces the size from 6  $\mu\text{m}$  to 3.8  $\mu\text{m}$ . This regime will be described in Sect. 1.2.

To summarize, if the polydisperse emulsion is mainly composed of big drops, even after few seconds of shear, one obtains a well calibrated emulsion (with a mean diameter close to 6  $\mu\text{m}$ ); all the drops deform into threads of different

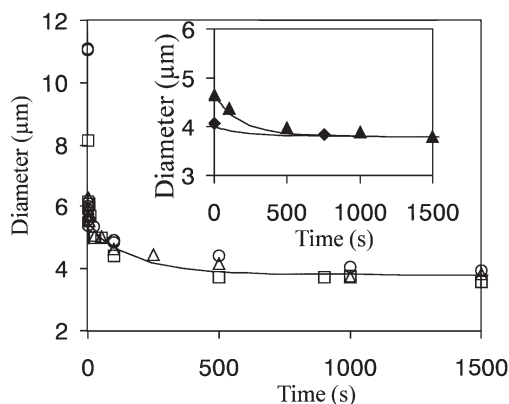


**Fig. 2.** Emulsification kinetics. All the emulsions have the same composition but different initial sizes. *Empty symbols* correspond to emulsions kinetics composed of two regimes whereas *filled symbols* (see insert) correspond to kinetics presenting only the slow regime (see text for details). Initial sizes are: ○ 11 μm; □ 8.2 μm; △ 6 μm; ▲ 4.7 μm and ◆ 4.1 μm. The lines are fits to experimental data of the second regime, using Eq. (1). Note the unique fit for all the *open symbols*

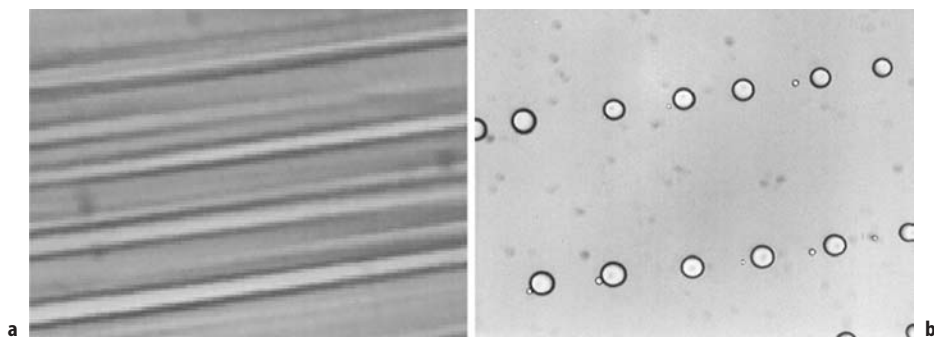


**Fig. 3.** Under shear, the drops elongate into long cylinders (a) and then break up into aligned identical droplets with a regular spacing (b)

lengths but the Rayleigh instability occurs when the same critical radius is reached by each thread. Then the second mechanism takes place and since the smaller droplets (between  $d_r$  and  $d_s$ ) also break, the size distribution becomes even narrower in the second regime. However it is clear that the most efficient process to get narrow size distributions is the initial Rayleigh instability.

The previous experiments were all performed on dilute emulsions for which the dispersed phase represents 2.5 wt % of the emulsion. As  $\phi$  increases, the relative contribution of the fast regime becomes more pronounced. As could be expected, the more concentrated the emulsion, the smaller the final size: this tendency merely reflects the fact that the emulsion viscosity and

thus the applied stress increases with droplet concentration (at constant shear rate).

We now consider a concentrated emulsion with oil mass fraction equal to 75% sheared at  $500\text{ s}^{-1}$  and  $3000\text{ s}^{-1}$  (Fig. 4). The primary emulsion is polydisperse with a mean diameter of  $57\text{ }\mu\text{m}$ . The two previously described regimes still exist. The first regime is particularly efficient in reducing the diameter since we can evaluate that one drop breaks into 160 droplets through the Rayleigh instability for an applied shear rate of  $500\text{ s}^{-1}$  ( $d_R=10.5\text{ }\mu\text{m}$ ) and into 6000 droplets for an applied shear rate of  $3000\text{ s}^{-1}$  ( $d_R=3.1\text{ }\mu\text{m}$ ). After this first step, the emulsion is already monodisperse. The second slow regime is less efficient since one drop breaks only into 3 and 6 droplets respectively.

## 2.2

### Analysis of the First Regime

The two parameters that certainly influence  $d_R$  are the applied stress  $\sigma$  and the viscosity ratio  $p$ . In order to explore the influence of  $\sigma$ , at constant shear rate  $\dot{\gamma}$ , the polymer (alginate) concentration of the continuous phase is varied from 1.6 to 2.8 wt %. The silicone oil viscosity is adjusted to keep  $p$  unchanged and it was checked that the interfacial tension  $\gamma_{\text{int}}$  remains the same. That way one can really investigate the effect of  $\sigma$  all other parameters being constant ( $\gamma_{\text{int}}=6\text{ mN}\cdot\text{m}^{-1}$ ,  $p=1$ ,  $\dot{\gamma}=500\text{ s}^{-1}$  and  $\phi=2.5\%$ ). The results are reported in Fig. 5, where the evolution of the daughter drop diameter  $d_R$  is plotted as a function of  $\sigma$ . In the insert, we see that the inverse diameter varies linearly with  $\sigma$ . From the slope of the plot, it can be deduced that the Laplace pressure of the daughter drops  $P_D=4\gamma_{\text{int}}/d_R$  is about 10 times larger than the applied shear stress.

In quasi-static conditions, it has been established both theoretically [7, 12] and experimentally [6, 12] that a drop breaks when the applied stress  $\sigma$  overcomes the product of the critical capillary number  $Ca_{\text{cr}}$  and the Laplace pressure

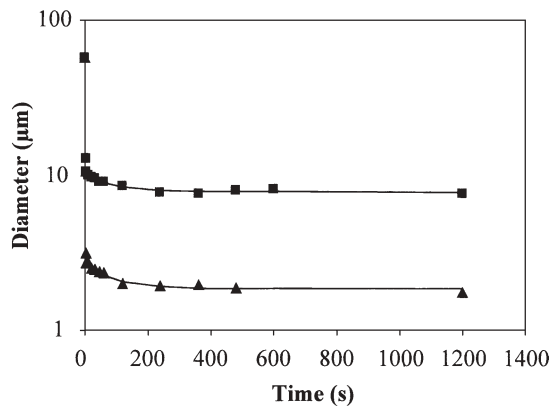


**Fig. 4.** Emulsification kinetics for emulsions containing 75 wt % of oil and sheared at: ■  $500\text{ s}^{-1}$  or ▲  $3000\text{ s}^{-1}$ . The lines are fits using Eq. (1)

of the mother drops:  $\sigma \geq Ca_{cr}^* P_M$ . In Fig. 2, one observes that the Rayleigh instability disappears by reducing the initial drop diameter. Thus, it seems that a similar criterion exists in non quasi-static conditions. From the data in Fig. 2, it can be deduced that the critical capillary number is of the order of 0.1, a value that is quite comparable to that obtained in quasi-static conditions, i.e. 0.5 for the same  $p$  value ( $p=1$ ) [5, 12, 18]. Here, we should like to stress that the previously mentioned experiments also provide an empirical law that allows predicting the droplet size resulting from the monodisperse fragmentation:  $d_R = \alpha \frac{4\gamma_{int}}{\sigma}$ ,

where  $\alpha$  is a dimensionless constant that should essentially depend on  $p$  ( $\alpha \approx 0.1$  for  $p=1$ ). This law is valid for any mother emulsion consisting of large droplets with diameters larger than  $d_R$ .

To explore the influence of  $p$ , the viscosity of the internal phase is varied over four decades, everything else being constant. As can be seen in the log-log plot of Fig. 6a,  $d_R$  (identically  $\alpha$ ) scales with the viscosity ratio as  $p^{0.2}$ : the low value of the exponent indicates that  $d_R$  (or  $\alpha$ ) is only weakly dependent on  $p$ . In quasi-static conditions, Grace [12] demonstrated that the critical capillary number diverges for  $p > 3$ , meaning that the fragmentation is no longer possible when the viscosity of the disperse phase is at least 3 times larger than that of the continuous phase. Upon sudden application of the shear, it is therefore possible to break the drops even for very high  $p$  values ( $p > 100$ ). The evolution of uniformity versus  $p$  is plotted Fig. 6b. As long as  $p$  is in the range [0.01–2], the emulsions obtained are monodisperse. For  $p$  larger than 2, the emulsion uniformity  $U$  increases reflecting the progressive loss of wavelength selectivity during the development of the Rayleigh instability.

As a conclusion, if the viscosity ratio  $p$  between the internal and external phases lies between 0.01 and 2, the shear applied on a polydisperse emulsion made of large drops leads to a monodisperse one with a mean diameter governed by the stress. This fragmentation occurs through elongation of the drops and the development of a Rayleigh instability with a characteristic time of the order of one second. The obtained monodispersity probably results from the fact that the Rayleigh instability develops under shear for a critical diameter of the deformed drops.

## 2.3

### Analysis of the Second Regime

After the first step, the resulting droplets can break again following a much slower regime. For initial droplets smaller than 6  $\mu\text{m}$ , only the second regime is observed (see insert of Fig. 2). Moreover whatever the initial size, the mean diameter converges to a unique asymptotic value of 3.8  $\mu\text{m}$ . Further shearing (one hour) of the emulsion does not reduce the diameter. This slow regime can be described considering that one droplet breaks into  $(\omega+1)$  daughter drops per unit time. Then, the variation of the number of droplets during a time interval  $dt$  is:  $dn(t) = \omega n(t) dt$ . We guess that  $\omega$  is a function of  $d$ ; the higher  $d$ , the higher the rate of droplet production. The function  $\omega(d)$  must reflect the fact that the break-up becomes less probable as  $d$  approaches the saturating diameter  $d_s$ . The

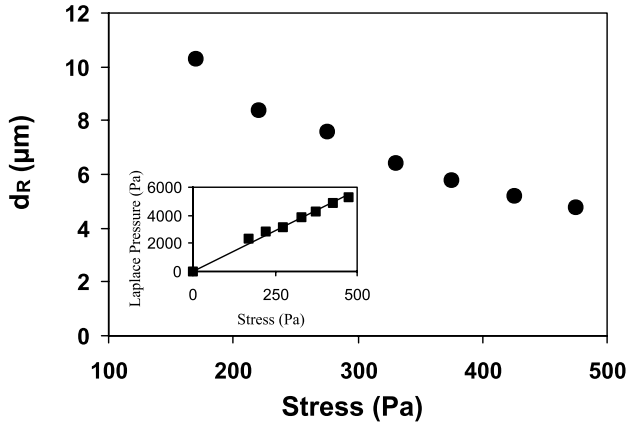


**Fig. 5.** Drops diameter resulting from the first mechanism versus shear stress. Everything except the stress is kept constant during the experiment. Insert. Laplace pressure after rupture as a function of the stress. The linear fit gives a slope of 11.5

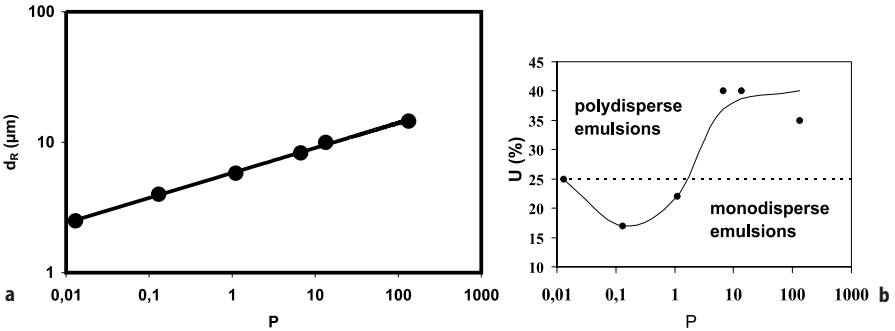


**Fig. 6.** a Mean diameter resulting from the first mechanism as a function of the internal to external phase viscosity ratio,  $p$ . The line is a power law fit giving an exponent equal to 0.2. b Corresponding uniformity versus  $p$

following simple empirical relation may be adopted:  $\omega = \omega_0(d - d_s)/d_s$  for  $d > d_s$  and  $\omega = 0$  for  $d < d_s$ . Writing the volume conservation during the break-up, the mean diameter  $d$  at time  $t$  can be written as follows:

$$d(t) = \frac{d_s}{1 - \frac{d_0 - d_s}{d_0} \exp\left(\frac{-\omega_0 t}{3}\right)} \quad (1)$$

where  $d_0$  is the initial diameter. In this model the only free parameter is  $\omega_0$ , a constant that determines how the rupturing rate depends on the current droplet size. Since all the parameters except the initial size are kept constant,  $\omega_0$  must be

the same for all the kinetics, whatever the initial size. From the best fit of the experimental curves in Fig. 2,  $\omega_0$  remains constant and equal to  $0.015 \text{ s}^{-1}$ . The inverse  $\omega_0$  corresponds to a characteristic fragmentation time of the order of 70 s. Compared to the Rayleigh instability, this second regime is extremely long and this is why the two regimes can be decoupled. For emulsions with initial diameters larger than  $6 \text{ }\mu\text{m}$ ,  $d_0$  in Eq. (1) is replaced by  $d_R$  which is the initial size for the second mechanism. For all the data, the size uniformity  $U$  remains below 25% all over the kinetic process.

### 3

#### Preparation of Calibrated Materials

From the previous section, it can be deduced that monodisperse fragmentation is obtained if two experimental conditions are fulfilled: (i) the applied shear and stress are high enough to rapidly induce the Rayleigh instability; (ii) the viscosity ratio lies in the range  $[0.01-2]$ . Hence, the most efficient way to produce monodisperse emulsions in large quantities is to use a mixer which applies a spatially homogeneous shear. That way, all the drops of the mother emulsion are directly submitted to the same shear rate and simultaneously break into daughter drops (i.e. in less than one second). However this is not a necessary condition. For example Aronson [30] described the production of emulsions having a controlled droplet size and a fairly narrow distribution using a standard mixer that does not apply a spatially homogeneous shear over the whole volume. Concentrated emulsion were fragmented for a long period of time (30–60 minutes). This ensures that the whole emulsion volume has been finally submitted to the same maximum stress. Although the application of a spatially homogeneous shear is not a *sine qua non* condition, it allows one to reduce the shear time noticeably.

Mabille et al. [26] described a device capable of producing large amounts of emulsions based on the use of a Couette-cell geometry.

#### 3.1

##### Couette Cell Description

The Couette mixer [25, 26] consisting of two concentric cylinders is schematically shown in Fig. 7. It is equipped with a syringe pump for injecting the premixed emulsion allowing batch production. The inner cylinder (rotor) of radius  $R=20 \text{ mm}$  is linked to a motor that rotates at a selected angular velocity  $\Omega$  which can reach up to  $70 \text{ rad}\cdot\text{s}^{-1}$ . The velocity  $v$  at the surface of this cylinder is  $v=R\Omega$ . The outer cylinder is fixed (stator). Three stators of different radii  $R_i$  are available, so that the shearing can be applied in three different gaps  $d_i=R_i-R$  ( $d_i=100 \text{ }\mu\text{m}$ ,  $200 \text{ }\mu\text{m}$  or  $1 \text{ mm}$ ) depending on the selected stator. For the maximum angular velocity, it is possible to reach very high shear rates  $\dot{\gamma}\sim R\Omega/(R_i-R)$  for a gap of  $d_i=100 \text{ }\mu\text{m}$ . The premixed emulsion contained initially in the syringe is pushed by a piston into the gap between the rotor and the stator. Given the covering height  $H$  between the outer cylinder and the inner one and the selected injection velocity,  $v_{\text{inj}}$ , the emulsions are sheared during about ten sec-



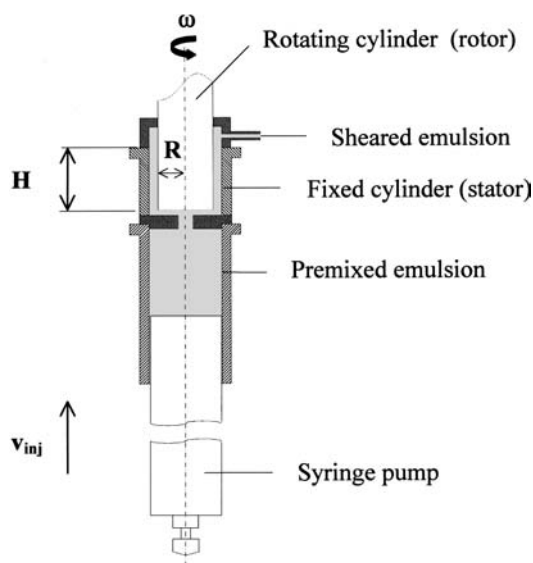


**Fig. 7.** Diagram of the Couette mixer. The premixed emulsion, initially located in the syringe, is forced by a piston into the gap between the rotor and the stator. The sheared emulsion is collected at the top of the mixer

onds. With this Couette mixer, it is possible to produce rapidly significant quantities of emulsions with narrow size distributions (up to one or two liters per hour depending on the system, at volume fractions ranging from 70% to 85%).

### 3.2 Simple Emulsions

In this section, we shall describe a large set of materials obtained following the guidance provided in Sect. 1.

Let us first consider an inverted W/O emulsion made of 10% of 0.1 M NaCl large droplets dispersed in sorbitan monooleate (Span 80), a liquid surfactant which also acts as the dispersing continuous phase. At this low droplet volume fraction, the rheological properties of the premixed emulsion is essentially determined by the continuous medium. The rheological behavior of the oil phase can be described as follows: it exhibits a Newtonian behavior with a viscosity of 1 Pa s up to 1000 s<sup>-1</sup> and a pronounced shear thinning behavior above this threshold value. Between 1000 s<sup>-1</sup> and 3000 s<sup>-1</sup>, although the stress is approximately unchanged, the viscosity ratio is increased by a factor of 4.

When sheared at 50 s<sup>-1</sup>, the crude premixed emulsion remains unchanged (Fig. 8a, b). The applied stress is insufficient to cause droplet rupture. At 1000 s<sup>-1</sup>, one can deduce from the image 8c, that fragmentation has taken place since the resulting droplets are significantly smaller than in the mother emulsion. How-

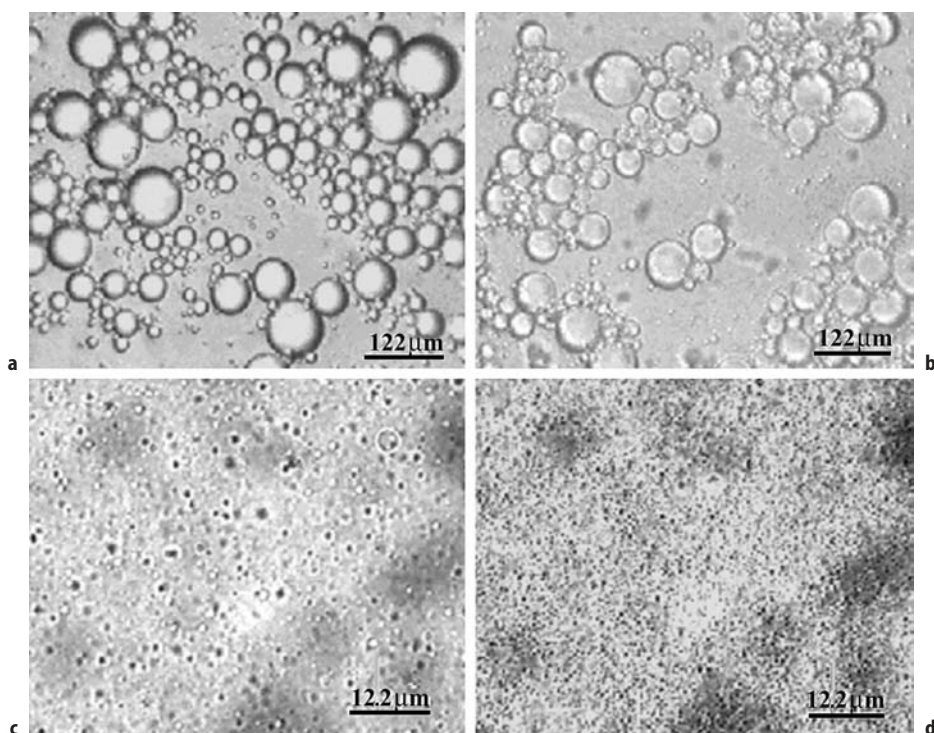


**Fig. 8.** W/O emulsions in pure Span 80 (sorbitan monooleate) **a** premixed emulsion, **b** emulsion sheared at  $50 \text{ s}^{-1}$ , **c** emulsion sheared at  $1000 \text{ s}^{-1}$ , **d** emulsion sheared at  $3000 \text{ s}^{-1}$ . Note that for images **a** and **b**, the bars represent  $122 \mu\text{m}$  whereas for images **c** and **d** they represent  $12.2 \mu\text{m}$

ever, the daughter emulsion still remains highly polydisperse. The image in Fig. 8d, corresponds to an applied shear of  $3000 \text{ s}^{-1}$ . Again fragmentation occurs but simultaneously, the size distribution becomes narrower (see Table 1). This result can be understood in the light of the previous section, where it was clearly established that the distribution uniformity is very sensitive to the viscosity ratio  $p$ ,  $U$  being smaller as  $p$  approaches unity.

We now consider a 40% silicone oil premixed emulsion dispersed in an aqueous phase. In Fig. 9 the evolution of mean diameter is plotted as a function of the applied shear rate. The dispersed phase volume fraction is kept constant at 75%, while the emulsifier concentration in the continuous medium is varied from 15 wt % to 45 wt %. The error bars show the distribution width deduced from the measured uniformity. At a given shear rate, smaller droplets with lower uniformity are produced (see Fig. 9) when surfactant concentration increases. For example at 45% of Ifralan 205 the uniformity never exceeds 15% whatever the applied shear rate, whereas it is of the order of 25% for 15% of Ifralan 205. Some microscope pictures of the emulsions obtained are given in Fig. 10. To understand the evolution, we may argue that the continuous phase viscosity increases

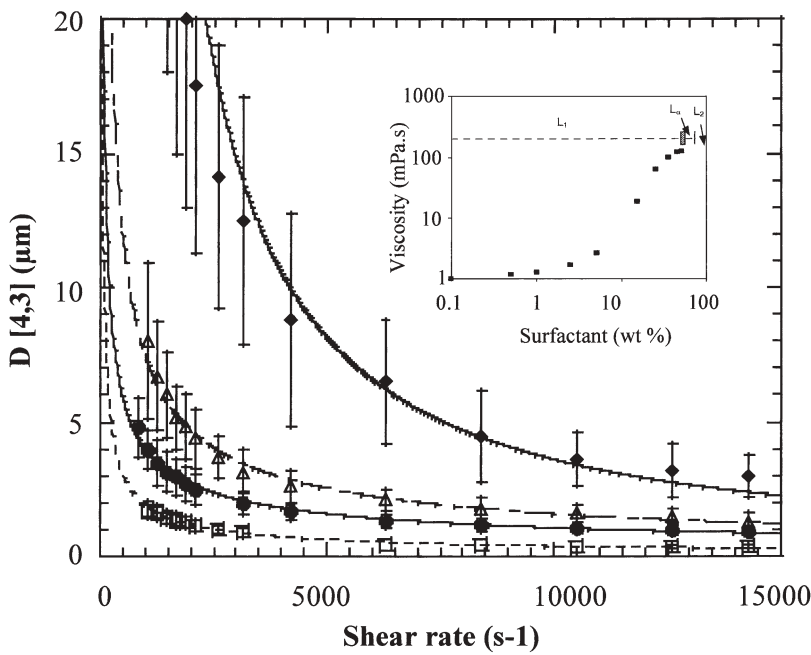


**Fig. 9.** Influence of the emulsifier concentration on the size profiles: *diamonds*  $C=15\%$ , *triangles*  $C=25\%$ , *circles*  $C=30\%$  and *squares*  $C=45\%$  of Ifralan 205. The dispersed phase is kept constant at 75% of a 350 mPa.s silicone oil. The lines are guides for the eye

**Table 1.** Droplet diameter measured by Dynamic Light Scattering experiments at  $90^\circ$  and distribution limits extracted from a multi-exponential analysis (10% brine in pure span 80)

$\dot{\gamma}$ ( $\text{s}^{-1}$ )	Mean diameter (nm)	Distribution limits (nm)
1000	300	from 90 to 735
3000	220	from 160 to 300
10,000	170	from 114 to 314

with the surfactant concentration (see insert Fig. 9). Hence for a given shear rate, the addition of surfactant has two main effects: (i) it increases the transmitted stress thus promoting fragmentation and (ii) it makes the viscosity ratio  $p$  varying (from  $p=0.06$  for 15% to  $p=0.4$  for 45% of surfactant) thus reducing the size distribution width.

Adding surfactant to the continuous phase is a possible route for improving fragmentation. However, for economic and environmental reasons, it would be beneficial to reduce it, while maintaining the viscosity of the continuous phase. This can be achieved by addition of a non-adsorbing polymer. For example, the two following aqueous phases: (i) 30 wt % of non-ionic surfactant NP7 (heptaethylene glycol nonylphenol Tergitol) in water and (ii) 3 wt % of the same sur-

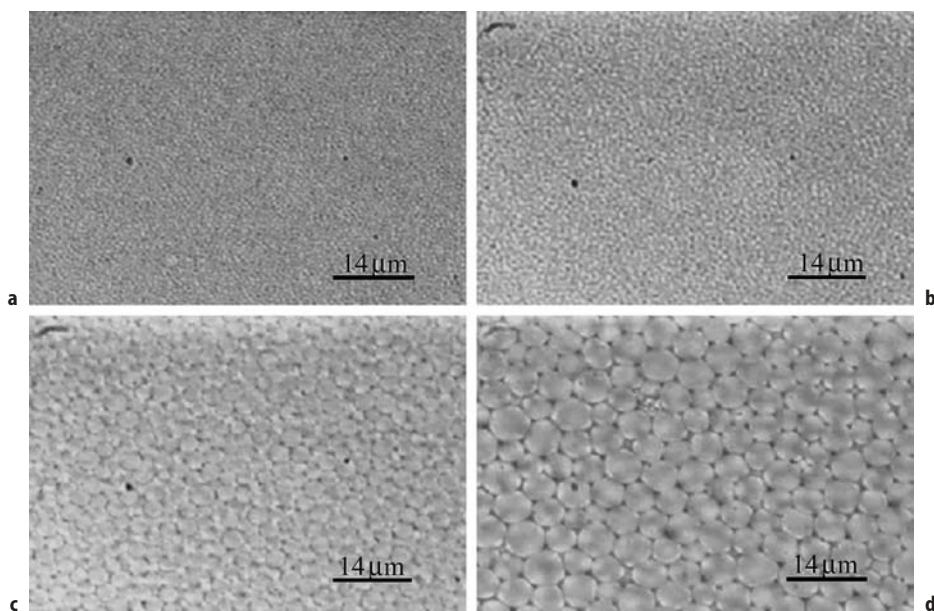


**Fig. 10.** Images of monodisperse emulsions obtained under different conditions: **a** Ifralan 55%,  $\dot{\gamma}=8400 \text{ s}^{-1}$ , **b** Ifralan 45%,  $\dot{\gamma}=2600 \text{ s}^{-1}$ , **c** Ifralan 25%,  $\dot{\gamma}=4700 \text{ s}^{-1}$ , **d** Ifralan 15%,  $\dot{\gamma}=7350 \text{ s}^{-1}$

factant with 4% of alginate in water, have the same viscosity (1 Pa s). Two mother emulsions are prepared by dispersing 30 wt % of 350 mPa s silicone oil in the two aqueous phases. When sheared at  $\dot{\gamma}=14280 \text{ s}^{-1}$ , the daughter emulsions have the same size distributions: 1  $\mu\text{m}$  and 14% of uniformity (see Fig. 11).

Surfactants are commonly used to kinetically stabilize colloidal systems. An alternative way of achieving long term metastability is to adsorb macromolecules at the interface between the dispersed and the continuous phase. Polymer chains may be densely adsorbed on surfaces where they form loops and tails with a very broad distribution of sizes and extending into the continuous phase. There is no fundamental difference regarding the fragmentation of emulsions in the presence of polymers [31, 32]. The only feature that has to be pointed out is the importance of the interfacial tension [26]. Indeed, due to their large molecular size, macromolecules reduce the interfacial tension between oil and water to a smaller extent than surfactants. In Fig. 12, the fragmentation profiles of two premixed emulsions, one stabilized by a polymer (PVAAC, copolymer of polyvinyl acetate and polyvinyl alcohol) the other by a short surfactant (Ifralan 205) have been reported for comparison [26]. The compositions have been adjusted so that the continuous phases possess the same zero-shear viscosity (100 mPa s). This is achieved with 15% PVAAC and 35% Ifralan 205 in water. The sizes obtained for the polymeric stabilized emulsions are three times larger than those obtained with the surfactant, at the same shear rate. This can be explained considering that the interfacial tension between silicone oil and the

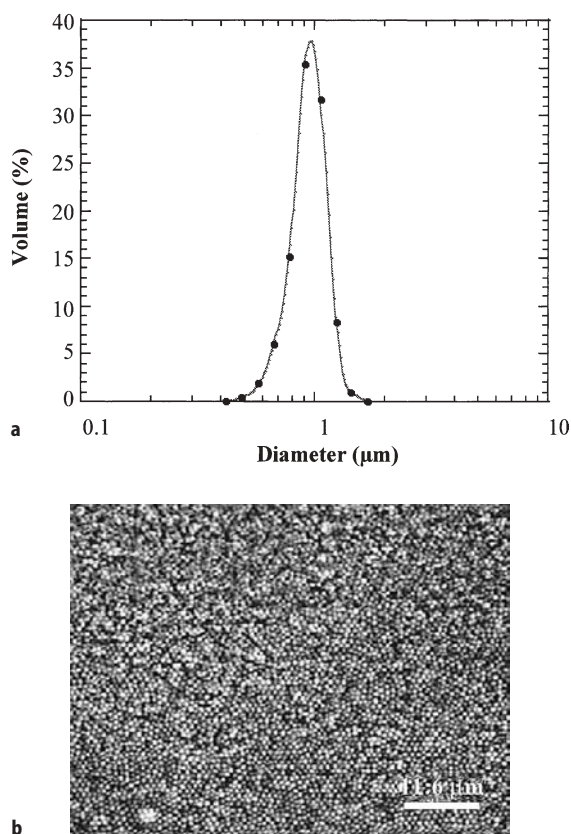


**Fig. 11.** Emulsion obtained by shearing a premixed emulsion in presence of a non adsorbing polymer. System composition. Alginate (non adsorbing polymer) 4%, non-ionic surfactant (NP7) 3%, oil volume fraction  $\phi=30\%$ . **a** size distribution, **b** microscope image

continuous medium is approximately three times larger with the polymer ( $17.2 \text{ mN} \cdot \text{m}^{-1}$ ) than with the surfactant ( $5 \text{ mN} \cdot \text{m}^{-1}$ ).

### 3.3

#### Suspensions

The monodisperse fragmentation process can be extended to produce monodisperse solid particles. The general strategy consists of performing the emulsification in conditions such that the dispersed phase is in the liquid state and to solidify the drops either by a temperature quench or through polymerization. The microscope image shown in Fig. 13 gives an illustration of this possibility. It corresponds to a solid paraffin oil dispersed in water at room temperature. The emulsification was performed in the liquid state, at a temperature above the melting point of the paraffin oil. Once fragmented, the system is cooled at am-

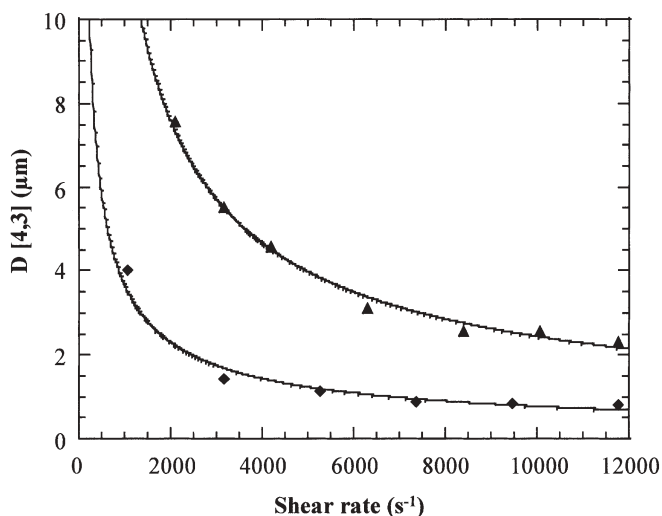


**Fig. 12.** Role of the interfacial tension on the fragmentation. *Diamonds:* Ifralan 5% - 5 mN/m, *triangles:* PVAac 15% - 17 mN/m. The lines are guides for the eye

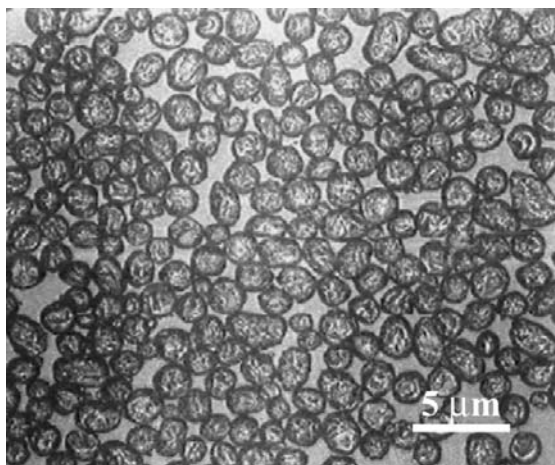


**Fig. 13.** Microscope image of a solid paraffin dispersed in water (room temperature)

bient temperature. The initially liquid spherical drops clearly adopt an anisotropic shape revealing the final solid state of the oil. Note that the monodispersity is not altered by this transformation.

All the previous examples reveal that a large variety of emulsions may be produced (in quite large quantities) by application of controlled shear and that the drop size may be tuned from 0.3  $\mu\text{m}$  to 10  $\mu\text{m}$ . In the following section, we show that the same concepts can be applied if the dispersed phase is an emulsion itself, as far as the characteristic length of the Rayleigh instability is large



compared to the average size of the primary emulsion. This allows one to fabricate the so-called double or multiple emulsions, which are materials with many potential applications.

### 3.4

#### **Multiple Emulsions**

Double emulsions may be either of the water-in-oil-in-water type (W/O/W) (with dispersed oil globules themselves containing smaller aqueous droplets) or of the oil-in-water-in-oil type (O/W/O) (with dispersed aqueous globules containing smaller oily dispersed droplets). Taking advantage of this double (or multiple) compartment structure, increasing interest has been devoted to these multiple systems. Indeed, double emulsions present many interesting possibilities for the controlled release of chemical substances initially entrapped in the internal droplets. The industrial domains showing evident interest towards the technological development of such complex systems are varied (food industry, cosmetics). The major part of applications concerns the human pharmaceutical field: water-in-oil-in-water (W/O/W) emulsions have mostly been investigated as potential vehicles for various hydrophilic drugs (vaccines, vitamins, enzymes, hormones) which would then be slowly released. Active substances may also migrate from the outer to the inner phase of multiple emulsions, in that case, providing a kind of reservoir particularly suitable for detoxification (overdose treatment) or, in a different domain, in the removal of toxic materials from waste water. In any case, the impact of double emulsions designed as drug delivery systems would be of significant importance in the controlled release field, for oral, topical or parenteral administrations, provided that the release mechanisms can be more easily monitored. Since the rates of release in double emulsions are very sensitive to the droplet and globule sizes [33, 34], the most efficient control should be achieved in the presence of emulsions that are monodisperse on the two colloidal scales [35].

The study of the effect of shear on the fragmentation of oily globules to produce W/O/W monodisperse emulsions has been developed and reported in a recent publication [36]. The authors demonstrate that the method developed for simple emulsions can be extended to produce monodisperse double emulsions within the same rheological and shearing conditions. W/O/W monodisperse emulsions are generally fabricated following a two-step procedure [34]. A monodisperse concentrated W/O emulsion stabilized by a lipophilic surfactant is first prepared. This inverted emulsion is then emulsified in an aqueous phase containing a hydrophilic surfactant. The resulting W/O/W emulsions are comprised of oily globules containing smaller water droplets, both colloids having a well-defined and controlled diameter. We report here an example taken from reference [36].

#### **3.4.1**

##### ***Inverted W/O Emulsion***

The premixed emulsion is comprised of salted water droplets dispersed in a 1:9 mixture (w/w) of dodecane and a lipophilic surfactant (Admul wol 1403) The



droplet mass fraction  $\phi_i$  is set to 80%. This crude emulsion is sheared into the Couette-type cell at constant shear rate  $\dot{\gamma}=10000 \text{ s}^{-1}$ . A monodisperse W/O emulsion with an average diameter of  $0.30 \mu\text{m}$  and uniformity  $U$  of the order of 20% is obtained. To vary the droplet volume fraction  $\phi_i$ , the emulsion is diluted with pure dodecane after the fragmentation process.

### 3.4.2

#### Double Emulsions

A given amount of the primary inverted emulsion (mass fraction  $\phi_g=70\%$ ) is dispersed in an aqueous phase containing 5%(w/w) of Synperonic PE/F 68 as the hydrophilic surfactant. In the absence of any thickening agent, the viscosity of the continuous phase is very low compared to that of the inverted emulsion. 2%(w/w) of alginate is therefore dissolved in water in order to increase the viscosity of the continuous phase. In order to predict the best conditions for obtaining quasi-monodisperse fragmentation, the evolution of the water phase viscosity  $\eta_c$  as a function of the shear rate and alginate concentration is plotted in Figure 14. For the sake of comparison, the viscosity  $\eta_d$  of the inverted emulsion at  $\phi_i=75\%$ (w/w) is reported in the same graph (up to  $1000 \text{ s}^{-1}$ ). For a 2%(w/w) alginate solution, the viscosity ratio  $\eta_d/\eta_c$  is of the order of 1 at  $1000 \text{ s}^{-1}$ , so double globules with narrow size distribution are expected in this alginate composition range. Of course, the viscosity ratio becomes smaller than 1 in presence of concentrated double globules, since the whole emulsion viscosity  $\eta_{\text{eff}}$  should to be considered instead of  $\eta_c$  ( $\eta_{\text{eff}} > \eta_c$ ). However, it was checked that the ratio remained in the adequate range, *i.e.* between 0.01 and 1, over the whole set of experiments.

The premixed double emulsion is sheared in the Couette cell at different shear rates from 0 to  $14200 \text{ s}^{-1}$ . The obtained double emulsions have diameters ranging from  $7 \mu\text{m}$  to  $2 \mu\text{m}$  and uniformity between 15% and 30%. Figure 15 is a mi-

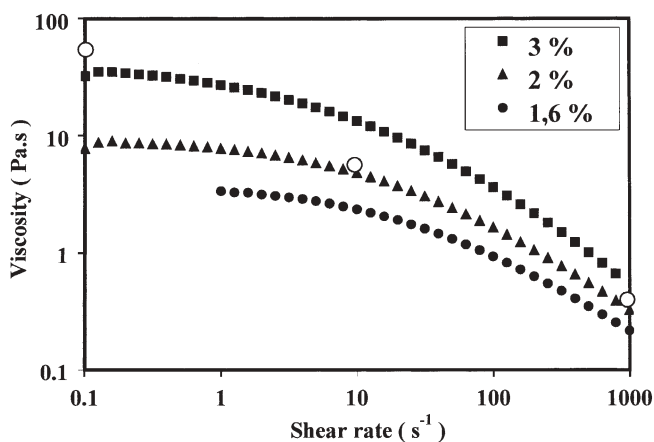


**Fig. 14.** Evolution of the water phase viscosity  $\eta_c$  as a function of the shear rate and alginate concentration (filled symbols). For the sake of comparison, the viscosity  $\eta_d$  of the inverted emulsion at  $\phi_i=75\%$  w is reported in the same graph (open symbols)

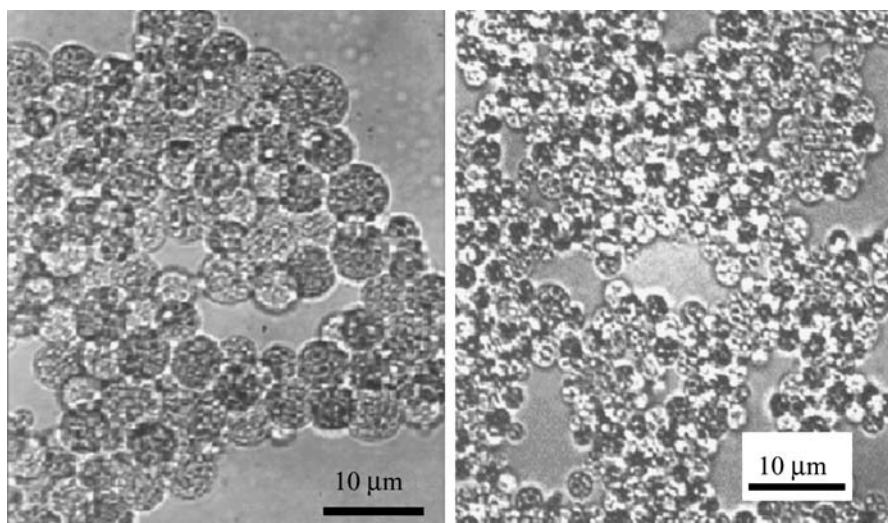


**Fig. 15.** Image of the W/O/W emulsions obtained for the system. Admul wol 1403-Synperonic PE/F 68-dodecane.  $\phi_i=65\%$ . The emulsions were diluted with water+glucose to facilitate the observation. **a**  $\dot{\gamma}=1000 \text{ s}^{-1}$  and **b**  $\dot{\gamma}=14200 \text{ s}^{-1}$

croscope image of double emulsions fabricated at different shear rates. Large oil globules very uniform in size are visible, and the smaller inverted water droplets are also distinguishable. From these results, it can be concluded that the fragmentation method that has been developed for simple emulsions can be extended to produce quasi-monodisperse double emulsions. In other words, the capillary instability occurring in simple emulsions also takes place in presence of materials such as concentrated emulsions, within the same rheological and shearing conditions. It is worth noting that in the previous experiments the final globule size is always significantly larger than the internal water droplet diameter (there is at least a factor of ten between the two diameters). In such conditions, the W/O emulsion may be considered as an effective continuous medium obeying the same fragmentation properties as a simple fluid.

### 3.4.3

#### *Influence of the Internal Droplet Mass Fraction*

The primary W/O emulsion is diluted with dodecane to vary the mass fraction  $\phi_i$  of the water droplets in the inverted emulsion. In Fig. 16 is reported the evolution of the globule diameter as a function of  $\dot{\gamma}$ , for 3 different mass fractions  $\phi_i$ . The mass fraction  $\phi_g$  of the globules in the double emulsion is always equal to 70%. It can be observed that for a given shear rate, the globule size increases with the droplet mass fraction. By varying  $\phi_i$ , the average viscosity of the inverted emulsion is also changing. The results are qualitatively identical to that obtained by Mason et al. [24] for the fragmentation of simple emulsions. By increasing

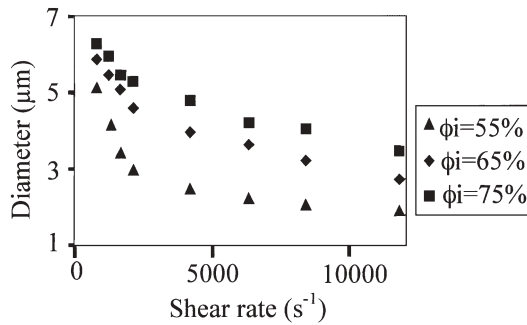


**Fig. 16.** Dependence of the globule diameter in W/O/W emulsions on the steady shear rate  $\dot{\gamma}$  for the system Admul wol 1403-SynperonicPE/F 68-dodecane, for different  $\phi_i$  values

the viscosity of the dispersed phase, they too observed that the droplet diameter increases.

### 3.5

#### Ferrofluid Emulsions

Monodisperse ferrofluid emulsions are comprised of magnetic oils dispersed in a water continuous phase. The specific magnetic and optical properties of these materials are currently exploited in research and/or technological fields. Leal-Calderon et al. [37] have developed a technique that allows one to directly determine the force distance law between tiny colloidal particles. Their technique exploits the fact that the anisotropy of the forces between dipoles causes the ferrofluid droplets to form chains. Because chains give rise to a strong Bragg diffraction of the visible light, the inter-droplet spacing is accurately measured. Moreover, because the attractive dipolar magnetic force can be varied through the intensity of the external field, the balancing repulsive force can also be measured at various spacings. This technique has been used for the measurement of colloidal forces in the presence of many different surface active species (surfactants, polymers, proteins) and has provided interesting insights in the field of colloidal forces [38].

Ferrofluid emulsions have also found a useful application in the domain of medical diagnostics. Magnetic bioseparation or biopurification of antigens, antibodies or nucleic acids with magnetic particles is both a simple and efficient alternative to column purification, centrifugation or extraction with organic solvents. For that purpose, the ferrofluid droplet surfaces are functionalized with a receptor function, i.e. a chemical function that can capture a target molecule dissolved in a biological medium (blood, food, sera, tissues,...), through a specific ligand-receptor interaction. Under the application of a magnetic field gradient, the droplets sediment and therefore isolate the target molecules which are attached to their surfaces, prior to their detection or titration. The main specifications of this technology are the following:

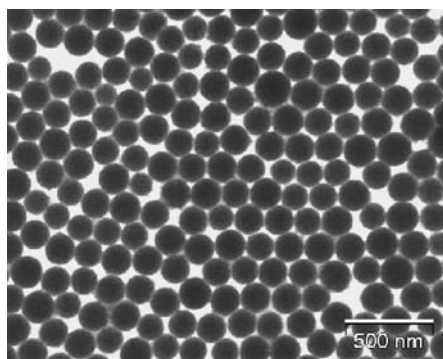


**Fig. 17.** Scanning Electron Microscope image of a ferrofluid emulsion

- large oxide content providing high magnetic susceptibility and therefore rapid separation under a magnetic field
- large specific surface area due to the small size of the magnetic particles. Moreover the particles are Brownian. The conditions are ideal for a rapid adsorption of the molecules to be attached
- high binding capacity.

The binding capacity is essentially determined by the total specific surface of the magnetic droplets. Since this parameter must be controlled with great accuracy, monodisperse emulsions become necessary.

The preparation of a ferrofluid emulsions is quite similar to that described for double emulsions. The starting material is ferrofluid oil made of small iron oxide grains ( $\text{Fe}_2\text{O}_3$ ) with a typical size of 10 nm, dispersed in oil in presence of an oil-soluble surfactant. The preparation of ferrofluid oils was initially described in a US patent [39]. Once fabricated, the ferrofluid oil is in turn emulsified in a water phase containing a hydrophilic surfactant. The viscosity ratio between the dispersed and continuous phases is adjusted in order to lie in the range where monodisperse fragmentation occurs [0.01–2]. The emulsification takes place in a Couette-type cell, leading to direct emulsions with a typical diameter around 200 nm and a very narrow size distribution as can be observed in Fig. 17.

## 4

### Conclusion

In this article we have shown how a capillary instability may generate a well-defined characteristic size. The materials that derive are essentially emulsions made of liquid or crystallizable droplets. The monodispersity make it possible to obtain materials with perfectly controlled and reproducible properties, which certainly cannot be achieved in presence of polydisperse emulsions. This is why monodisperse emulsions are not only model systems for fundamental science but also materials with commercial applications.

**Acknowledgement.** The authors would like to thank C. Mabilille, T.G. Mason, K. Pays, P. Gorria, C. Goubault, D. Olea for their contributory work and Ademtech company (Pessac, France) for providing the ferrofluid emulsions.

## References

1. Mason TG, Bibette J (1996) *Phys Rev Lett* 77: 3481
2. Walstra P, Smulders PEA (1998) In: Binks BP (ed) *Modern aspects of emulsion science*. The Royal Society of Chemistry, U.K, p 56
3. Rayleigh L (1878) *Proc London Math Soc* 10: 4
4. Rayleigh (1879) *Proc Roy Soc* 29:71
5. Taylor GI (1932) *Proc R Soc A* 138:41
6. Taylor GI (1934) *Proc R Soc A* 146:501
7. Tomotika T (1935) *Proc Roy Soc (London)* A150:322
8. Tomotika S (1936) *Proc R Soc London Ser. A* 153:302
9. Rumscheidt FD, Mason SG (1962) *J Colloid Sci* 17:260
10. Karam HJ, Bellinger JC (1968) *Ing Engng Chem Fundam* 7:576
11. Mikami T, Cox RG, Mason SG (1975) *Int J Multiphase Flow* 2:113
12. Grace HP (1982) *Chem Eng Commun* 14:225
13. Bentley BJ, Leal LG (1986) *J Fluid Mech* 167:241
14. Khakhar DV, Otino JM (1986) *J Fluid Mech* 166:265
15. Khakhar DV, Otino JM (1987) *Int. J. Multiphase Flow* 13:71
16. Stone HA, Bentley BJ, Leal LG (1986) *J Fluid Mech* 173:131
17. Palierne JF, Lequeux F (1991) *Journal of Non-Newtonian Fluid Mechanics* 40:289
18. De Bruijn RA (1989) Ph. D. Thesis Eindhoven University of Technology
19. Cohen A, Carriere CJ (1989) *Rheol. Acta* 28:223
20. Rumscheidt FD, Mason SG (1961) *J Colloid Sci* 16:238
21. De Bruijn RA (1993) *Chem Eng Sci* 48:277
22. Stone HA, Leal LG (1989) *J Fluid Mech* 198:399
23. Hinch EJ, Acrivos A (1980) *J Fluid Mech* 98:305
24. Mason TG, Bibette J (1997) *Langmuir* 13:4600
25. Bibette J, Mason TG (1999) *Emulsion manufacturing process* 5,938,581
26. Mabilille C, Schmitt V, Gorria P, Leal Calderon F, Faye V, Deminière B, Bibette J (2000) *Langmuir* 16:422
27. Mabilille C (2000) *Fragmentation in emulsions submitted to a simple shear*, University of Bordeaux I
28. Mabilille C, Leal-Calderon F, Bibette J, Schmitt V (2003) *Europhys Lett* 61:708
29. Rusu D (1997) *In-situ study of immiscible polymer blends morphology under simple shear* PhD thesis Ecole des Mines de Paris, Sophia Antipolis
30. Aronson MP (1989) *Langmuir* 5:494
31. Perrin P (1998) *Langmuir* 14:5977
32. Perrin P, Lafuma F (1998) *J Colloid Interface Sci* 197:317
33. Pays K, Kahn J, Pouligny P, Bibette J, Leal-Calderon F (2001) *Phys Rev Lett* 87
34. Pays K, Kahn J, Pouligny B, Bibette J, Leal-Calderon F (2001) *Langmuir* 17:7758
35. Bibette J, Leal Calderon F, Gorria P (1999) *Polydisperse double emulsion, corresponding monodisperse double emulsion and process to fabricate the monodisperse emulsion* WO0121297
36. Goubault C, Pays K, Olea D, Gorria P, Bibette J, Schmitt V, Leal-Calderon F (2001) *Langmuir* 17:5184
37. Leal-Calderon F, Stora T, Mondain Monval O, Poulin P, Bibette J (1994) *Phys Rev Lett* 72:2959
38. Bibette J, Leal Calderon F, Schmitt V, Poulin P (2002) *Emulsion Science: Basic Principles*. Springer, Berlin Heidelberg New York
39. Reimers G, Khalafalla S (1974) *Production of magnetic fluids by peptization techniques* US 38,435,4

---

## Author Index Volume 201–227

*Author Index Vols. 26–50 see Vol. 50*

*Author Index Vols. 51–100 see Vol. 100*

*Author Index Vols. 101–150 see Vol. 150*

*Author Index Vols. 151–200 see Vol. 200*

*The volume numbers are printed in italics*

- Achilefu S, Dorshow RB (2002) Dynamic and Continuous Monitoring of Renal and Hepatic Functions with Exogenous Markers. *222*: 31–72
- Albert M, see Dax K (2001) *215*:193–275
- Angyal SJ (2001) The Lobry de Bruyn-Alberda van Ekenstein Transformation and Related Reactions. *215*:1–14
- Astruc D, Blais J-C, Cloutet E, Djakovitch L, Rigaut S, Ruiz J, Sartor V, Valério C (2000) The First Organometallic Dendrimers: Design and Redox Functions. *210*:229–259
- Augé J, see Lubineau A (1999) *206*:1–39
- Baars MWPL, Meijer EW (2000) Host-Guest Chemistry of Dendritic Molecules. *210*:131–182
- Balczewski P, see Mikoloajczyk M (2003) *223*:161–214
- Ballauff M (2001) Structure of Dendrimers in Dilute Solution. *212*:177–194
- Baltzer L (1999) Functionalization and Properties of Designed Folded Polypeptides. *202*: 39–76
- Barré L, see Lasne M-C (2002) *222*: 201–258
- Bartlett RJ, see Sun J-Q (1999) *203*:121–145
- Bertrand G, Bourissou D (2002) Diphosphorus-Containing Unsaturated Three-Membered Rings: Comparison of Carbon, Nitrogen, and Phosphorus Chemistry. *220*:1–25
- Betzemeier B, Knochel P (1999) Perfluorinated Solvents – a Novel Reaction Medium in Organic Chemistry. *206*:61–78
- Bibette J, see Schmitt V (2003) *227*: 195–215
- Blais J-C, see Astruc D (2000) *210*:229–259
- Bogár F, see Pipek J (1999) *203*:43–61
- Bourissou D, see Bertrand G (2002) *220*:1–25
- Brand SC, see Haley MM (1999) *201*:81–129
- Bray KL (2001) High Pressure Probes of Electronic Structure and Luminescence Properties of Transition Metal and Lanthanide Systems. *213*:1–94
- Bronstein LM (2003) Nanoparticles Made in Mesoporous Solids. *226*:55–89
- Brücher E (2002) Kinetic Stabilities of Gadolinium(III) Chelates Used as MRI Contrast Agents. *221*: 103–122
- Brunel JM, Buono G (2002) New Chiral Organophosphorus catalysts in Asymmetric Synthesis. *220*:79–106
- Buchwald SL, see Muci A R (2002) *219*: 131–209
- Bunz UHF (1999) Carbon-Rich Molecular Objects from Multiply Ethynylated  $\pi$ -Complexes. *201*:131–161
- Buono G, see Brunel JM (2002) *220*:79–106
- Cadierno V, see Majoral J-P (2002) *220*:53–77
- Caminade A-M, see Majoral J-P (2003) *223*:111–159
- Carmichael D, Mathey F (2002) New Trends in Phosphametallocene Chemistry. *220*:27–51
- Caruso F (2003) Hollow Inorganic Capsules via Colloid-Templated Layer-by-Layer Electrostatic Assembly. *227*: 145–168
- Caruso RA (2003) Nanocasting and Nanocoating. *226*:91–118

- Chamberlin AR, see Gilmore MA (1999) 202:77–99
- Chow H-F, Leung C-F, Wang G-X, Zhang J (2001) Dendritic Oligoethers. 217: 1–50
- Clarkson RB (2002) Blood-Pool MRI Contrast Agents: Properties and Characterization. 221: 201–235
- Cloutet E, see Astruc D (2000) 210:229–259
- Co CC, see Hentze H-P (2003) 226:197–223
- Cooper DL, see Raimondi M (1999) 203:105–120
- Cornils B (1999) Modern Solvent Systems in Industrial Homogeneous Catalysis. 206:133–152
- Corot C, see Idee J-M (2002) 222:151–171
- Crooks RM, Lemon III BI, Yeung LK, Zhao M (2001) Dendrimer-Encapsulated Metals and Semiconductors: Synthesis, Characterization, and Applications. 212:81–135
- Croteau R, see Davis EM (2000) 209:53–95
- Crouzel C, see Lasne M-C (2002) 222:201–258
- Curran DP, see Maul JJ (1999) 206:79–105
- Currie F, see Häger M (2003) 227:53–74
- Davidson P, see Gabriel J-C P (2003) 226:119–172
- Davis EM, Croteau R (2000) Cyclization Enzymes in the Biosynthesis of Monoterpenes, Sesquiterpenes and Diterpenes. 209:53–95
- Davies JA, see Schwert DD (2002) 221:165–200
- Dax K, Albert M (2001) Rearrangements in the Course of Nucleophilic Substitution Reactions. 215:193–275
- de la Plata BC, see Ruano JLG (1999) 204:1–126
- de Meijere A, Kozhushkov SI (1999) Macrocyclic Structurally Homoconjugated Oligoacetylenes: Acetylene- and Diacetylene-Expanded Cycloalkanes and Rotanes. 201:1–42
- de Meijere A, Kozhushkov SI, Khlebnikov AF (2000) Bicyclopopylidene – A Unique Tetra-substituted Alkene and a Versatile C<sub>6</sub>-Building Block. 207:89–147
- de Meijere A, Kozhushkov SI, Hadjiraoglou LP (2000) Alkyl 2-Chloro-2-cyclopropylidene-acetates – Remarkably Versatile Building Blocks for Organic Synthesis. 207:149–227
- de Raadt A, Fechter MH (2001) Miscellaneous. 215:327–345
- Desreux JF, see Jacques V (2002) 221:123–164
- Diederich F, Gobbi L (1999) Cyclic and Linear Acetylenic Molecular Scaffolding. 201:43–79
- Diederich F, see Smith DK (2000) 210:183–227
- Djakovitch L, see Astruc D (2000) 210:229–259
- Dolle F, see Lasne M-C (2002) 222:201–258
- Donges D, see Yersin H (2001) 214:81–186
- Dormán G (2000) Photoaffinity Labeling in Biological Signal Transduction. 211:169–225
- Dorn H, see McWilliams AR (2002) 220:141–167
- Dorshow RB, see Achilefu S (2002) 222:31–72
- Drabowicz J, Mikołajczyk M (2000) Selenium at Higher Oxidation States. 208:143–176
- Ehse S, Romerosa A, Peruzzini M (2002) Metal-Mediated Degradation and Reaggregation of White Phosphorus. 220:107–140
- Eder B, see Wrodnigg TM (2001) The Amadori and Heyns Rearrangements: Landmarks in the History of Carbohydrate Chemistry or Unrecognized Synthetic Opportunities? 215:115–175
- Edwards DS, see Liu S (2002) 222:259–278
- Elaissari A, Ganachaud F, Pichot C (2003) Biorelevant Latexes and Microgels for the Interaction with Nucleic Acids. 227:169–193
- Esumi K (2003) Dendrimers for Nanoparticle Synthesis and Dispersion Stabilization. 227:31–52
- Famulok M, Jenne A (1999) Catalysis Based on Nucleic Acid Structures. 202:101–131
- Fechter MH, see de Raadt A (2001) 215:327–345
- Ferrier RJ (2001) Substitution-with-Allylic-Rearrangement Reactions of Glycal Derivatives. 215:153–175
- Ferrier RJ (2001) Direct Conversion of 5,6-Unsaturated Hexopyranosyl Compounds to Functionalized Glycohexanones. 215:277–291
- Frey H, Schlenk C (2000) Silicon-Based Dendrimers. 210:69–129



- Förster S (2003) Amphiphilic Block Copolymers for Templating Applications. 226:1–28
- Frullano L, Rohovec J, Peters JA, Geraldles CFGC (2002) Structures of MRI Contrast Agents in Solution. 221: 25–60
- Fugami K, Kosugi M (2002) Organotin Compounds. 219: 87–130
- Fuhrhop J-H, see Li G (2002) 218:133–158
- Furukawa N, Sato S (1999) New Aspects of Hypervalent Organosulfur Compounds. 205: 89–129
- Gabriel J-C P, Davidson P (2003) Mineral Liquid Crystals from Self-Assembly of Anisotropic Nanosystems. 226:119–172
- Gamelin DR, Güdel HU (2001) Upconversion Processes in Transition Metal and Rare Earth Metal Systems. 214:1–56
- Ganachaud F, see Elaissari A (2003) 227: 169–193
- García R, see Tromas C (2002) 218:115–132
- Geraldles CFGC, see Frullano L (2002) 221: 25–60
- Gilmore MA, Steward LE, Chamberlin AR (1999) Incorporation of Noncoded Amino Acids by In Vitro Protein Biosynthesis. 202:77–99
- Glasbeek M (2001) Excited State Spectroscopy and Excited State Dynamics of Rh(III) and Pd(II) Chelates as Studied by Optically Detected Magnetic Resonance Techniques. 213: 95–142
- Glass RS (1999) Sulfur Radical Cations. 205:1–87
- Gobbi L, see Diederich F (1999) 201:43–129
- Göltner-Spickermann C (2003) Nanocasting of Lyotropic Liquid Crystal Phases for Metals and Ceramics. 226:29–54
- Gouzy M-F, see Li G (2002) 218:133–158
- Gries H (2002) Extracellular MRI Contrast Agents Based on Gadolinium. 221: 1–24
- Gruber C, see Tovar GEM (2003) 227: 125–144
- Güdel HU, see Gamelin DR (2001) 214:1–56
- Guga P, Okruszek A, Stec WJ (2002) Recent Advances in Stereocontrolled Synthesis of P-Chiral Analogues of Biophosphates. 220:169–200
- Hackmann-Schlichter N, see Krause W (2000) 210:261–308
- Hadjiaraoglou LP, see de Meijere A (2000) 207:149–227
- Häger M, Currie F, Holmberg K (2003) Organic Reactions in Microemulsions. 227: 53–74
- Häusler H, Stütz AE (2001) D-Xylose (D-Glucose) Isomerase and Related Enzymes in Carbohydrate Synthesis. 215:77–114
- Haley MM, Pak JJ, Brand SC (1999) Macrocyclic Oligo(phenylacetylenes) and Oligo(phenyl-diacyetylenes). 201:81–129
- Hartmann T, Ober D (2000) Biosynthesis and Metabolism of Pyrrolizidine Alkaloids in Plants and Specialized Insect Herbivores. 209:207–243
- Haseley SR, Kamerling JP, Vliegthart JFG (2002) Unravelling Carbohydrate Interactions with Biosensors Using Surface Plasmon Resonance (SPR) Detection. 218:93–114
- Hassner A, see Namboothiri INN (2001) 216: 1–49
- Helm L, see Tóth E (2002) 221: 61–101
- Hemscheidt T (2000) Tropane and Related Alkaloids. 209:175–206
- Hentze H-P, Co CC, McKelvey CA, Kaler EW (2003) Templating Vesicles, Microemulsions and Lyotropic Mesophases by Organic Polymerization Processes. 226:197–223
- Hergenrother PJ, Martin SF (2000) Phosphatidylcholine-Preferring Phospholipase C from *B. cereus*. Function, Structure, and Mechanism. 211:131–167
- Hermann C, see Kuhlmann J (2000) 211:61–116
- Heydt H (2003) The Fascinating Chemistry of Triphosphabenzene and Valence Isomers. 223:215–249
- Hirsch A, Vostrowsky O (2001) Dendrimers with Carbon Rich-Cores. 217: 51–93
- Hiyama T, Shirakawa E (2002) Organosilicon Compounds. 219: 61–85
- Holmberg K, see Häger M (2003) 227: 53–74
- Houseman BT, Mrksich M (2002) Model Systems for Studying Polyvalent Carbohydrate Binding Interactions. 218:1–44

- Hricovíniová Z, see Petruš L (2001) 215:15–41
- Idee J-M, Tichkowsky I, Port M, Petta M, Le Lem G, Le Greneur S, Meyer D, Corot C (2002) Iodinated Contrast Media: from Non-Specific to Blood-Pool Agents. 222: 151–171
- Igau A, see Majoral J-P (2002) 220:53–77
- Iwaoka M, Tomoda S (2000) Nucleophilic Selenium. 208:55–80
- Iwasawa N, Narasaka K (2000) Transition Metal Promoted Ring Expansion of Alkynyl- and Propadienylcyclopropanes. 207:69–88
- Imperiali B, McDonnell KA, Shogren-Knaak M (1999) Design and Construction of Novel Peptides and Proteins by Tailored Incorporation of Coenzyme Functionality. 202:1–38
- Ito S, see Yoshifuji M (2003) 223:67–89
- Jacques V, Desreux JF (2002) New Classes of MRI Contrast Agents. 221: 123–164
- James TD, Shinkai S (2002) Artificial Receptors as Chemosensors for Carbohydrates. 218: 159–200
- Jenne A, see Famulok M (1999) 202:101–131
- Kaler EW, see Hentze H-P (2003) 226:197–223
- Kamerling JP, see Haseley SR (2002) 218:93–114
- Kashemirov BA, see Mc Kenna CE (2002) 220:201–238
- Kato S, see Murai T (2000) 208:177–199
- Kee TP, Nixon TD (2003) The Asymmetric Phospho-Aldol Reaction. Past, Present, and Future. 223:45–65
- Khlebnikov AF, see de Meijere A (2000) 207:89–147
- Kirtman B (1999) Local Space Approximation Methods for Correlated Electronic Structure Calculations in Large Delocalized Systems that are Locally Perturbed. 203:147–166
- Kita Y, see Tohma H (2003) 224:209–248
- Kleij AW, see Kreiter R (2001) 217: 163–199
- Klein Gebbink RJM, see Kreiter R (2001) 217: 163–199
- Klibanov AL (2002) Ultrasound Contrast Agents: Development of the Field and Current Status. 222: 73–106
- Klopper W, Kutzelnigg W, Müller H, Noga J, Vogtner S (1999) Extremal Electron Pairs – Application to Electron Correlation, Especially the R12 Method. 203:21–42
- Knochel P, see Betzemeier B (1999) 206:61–78
- Koser GF (2003) C-Heteroatom-Bond Forming Reactions. 224:137–172
- Koser GF (2003) Heteroatom-Heteroatom-Bond Forming Reactions. 224:173–183
- Kosugi M, see Fugami K (2002) 219: 87–130
- Kozhushkov SI, see de Meijere A (1999) 201:1–42
- Kozhushkov SI, see de Meijere A (2000) 207:89–147
- Kozhushkov SI, see de Meijere A (2000) 207:149–227
- Krause W (2002) Liver-Specific X-Ray Contrast Agents. 222: 173–200
- Krause W, Hackmann-Schlichter N, Maier FK, Müller R (2000) Dendrimers in Diagnostics. 210:261–308
- Krause W, Schneider PW (2002) Chemistry of X-Ray Contrast Agents. 222: 107–150
- Kräuter I, see Tovar GEM (2003) 227: 125–144
- Kreiter R, Kleij AW, Klein Gebbink RJM, van Koten G (2001) Dendritic Catalysts. 217: 163–199
- Kuhlmann J, Herrmann C (2000) Biophysical Characterization of the Ras Protein. 211: 61–116
- Kunkely H, see Vogler A (2001) 213:143–182
- Kutzelnigg W, see Klopper W (1999) 203:21–42
- Landfester K (2003) Miniemulsions for Nanoparticle Synthesis. 227: 75–123
- Lasne M-C, Perrio C, Rouden J, Barré L, Roeda D, Dolle F, Crouzel C (2002) Chemistry of  $\beta^+$ -Emitting Compounds Based on Fluorine-18. 222: 201–258
- Lawless LJ, see Zimmermann SC (2001) 217: 95–120
- Leal-Calderon F, see Schmitt V (2003) 227: 195–215
- Le Greneur S, see Idee J-M (2002) 222: 151–171
- Le Lem G, see Idee J-M (2002) 222: 151–171

- Leitner W (1999) Reactions in Supercritical Carbon Dioxide (scCO<sub>2</sub>). 206:107–132
- Lemon III BI, see Crooks RM (2001) 212:81–135
- Leung C-F, see Chow H-F (2001) 217:1–50
- Levitzi A (2000) Protein Tyrosine Kinase Inhibitors as Therapeutic Agents. 211:1–15
- Li G, Gouzy M-F, Fuhrhop J-H (2002) Recognition Processes with Amphiphilic Carbohydrates in Water. 218:133–158
- Li X, see Paldus J (1999) 203:1–20
- Licha K (2002) Contrast Agents for Optical Imaging. 222:1–29
- Linclau B, see Maul JJ (1999) 206:79–105
- Lindhorst TK (2002) Artificial Multivalent Sugar Ligands to Understand and Manipulate Carbohydrate-Protein Interactions. 218:201–235
- Lindhorst TK, see Röckendorf N (2001) 217:201–238
- Liu S, Edwards DS (2002) Fundamentals of Receptor-Based Diagnostic Metalloradiopharmaceuticals. 222:259–278
- Liz-Marzán L, see Mulvaney P (2003) 226:225–246
- Loudet JC, Poulin P (2003) Monodisperse Aligned Emulsions from Demixing in Bulk Liquid Crystals. 226:173–196
- Lubineau A, Augé J (1999) Water as Solvent in Organic Synthesis. 206:1–39
- Lundt I, Madsen R (2001) Synthetically Useful Base Induced Rearrangements of Aldonolactones. 215:177–191
- Loupy A (1999) Solvent-Free Reactions. 206:153–207
- Madsen R, see Lundt I (2001) 215:177–191
- Maier FK, see Krause W (2000) 210:261–308
- Majoral J-P, Caminade A-M (2003) What to do with Phosphorus in Dendrimer Chemistry. 223:111–159
- Majoral J-P, Igau A, Cadierno V, Zablocka M (2002) Benzyne-Zirconocene Reagents as Tools in Phosphorus Chemistry. 220:53–77
- Manners I (2002), see McWilliams AR (2002) 220:141–167
- March NH (1999) Localization via Density Functionals. 203:201–230
- Martin SF, see Hergenrother PJ (2000) 211:131–167
- Mathey F, see Carmichael D (2002) 220:27–51
- Maul JJ, Ostrowski PJ, Ublacker GA, Linclau B, Curran DP (1999) Benzotrifluoride and Derivates: Useful Solvents for Organic Synthesis and Fluorous Synthesis. 206:79–105
- McDonnell KA, see Imperiali B (1999) 202:1–38
- McKelvey CA, see Hentze H-P (2003) 226:197–223
- Mc Kenna CE, Kashemirov BA (2002) Recent Progress in Carbonylphosphonate Chemistry. 220:201–238
- McWilliams AR, Dorn H, Manners I (2002) New Inorganic Polymers Containing Phosphorus. 220:141–167
- Meijer EW, see Baars MWPL (2000) 210:131–182
- Merbach AE, see Tóth E (2002) 221:61–101
- Metzner P (1999) Thiocarbonyl Compounds as Specific Tools for Organic Synthesis. 204:127–181
- Meyer D, see Idee J-M (2002) 222:151–171
- Mezey PG (1999) Local Electron Densities and Functional Groups in Quantum Chemistry. 203:167–186
- Mikołajczyk M, Balczewski P (2003) Phosphonate Chemistry and Reagents in the Synthesis of Biologically Active and Natural Products. 223:161–214
- Mikołajczyk M, see Drabowicz J (2000) 208:143–176
- Miura M, Nomura M (2002) Direct Arylation via Cleavage of Activated and Unactivated C-H Bonds. 219:211–241
- Miyaura N (2002) Organoboron Compounds. 219:11–59
- Miyaura N, see Tamao K (2002) 219:1–9
- Möller M, see Sheiko SS (2001) 212:137–175
- Morales JC, see Rojo J (2002) 218:45–92

- Mrksich M, see Houseman BT (2002) 218:1–44
- Muci AR, Buchwald SL (2002) Practical Palladium Catalysts for C-N and C-O Bond Formation. 219:131–209
- Müllen K, see Wiesler U-M (2001) 212:1–40
- Müller G (2000) Peptidomimetic SH2 Domain Antagonists for Targeting Signal Transduction. 211:17–59
- Müller H, see Kloppe W (1999) 203:21–42
- Müller R, see Krause W (2000) 210:261–308
- Mulvaney P, Liz-Marzán L (2003) Rational Material Design Using Au Core-Shell Nanocrystals. 226:225–246
- Murai T, Kato S (2000) Selenocarbonyls. 208:177–199
- Muscat D, van Benthem RATM (2001) Hyperbranched Polyesteramides – New Dendritic Polymers. 212:41–80
- Nakayama J, Sugihara Y (1999) Chemistry of Thiophene 1,1-Dioxides. 205:131–195
- Namboothiri INN, Hassner A (2001) Stereoselective Intramolecular 1,3-Dipolar Cycloadditions. 216:1–49
- Narasaka K, see Iwasawa N (2000) 207:69–88
- Nishibayashi Y, Uemura S (2000) Selenoxide Elimination and [2,3] Sigmatropic Rearrangements. 208:201–233
- Nishibayashi Y, Uemura S (2000) Selenium Compounds as Ligands and Catalysts. 208:235–255
- Nixon TD, see Kee TP (2003) 223:45–65
- Noga J, see Kloppe W (1999) 203:21–42
- Nomura M, see Miura M (2002) 219:211–241
- Nubbemeyer U (2001) Synthesis of Medium-Sized Ring Lactams. 216:125–196
- Nummelin S, Skrifvars M, Rissanen K (2000) Polyester and Ester Functionalized Dendrimers. 210:1–67
- Ober D, see Hemscheidt T (2000) 209:175–206
- Ochiai M (2003) Reactivities, Properties and Structures. 224:5–68
- Okruszek A, see Guga P (2002) 220:169–200
- Osanai S (2001) Nickel (II) Catalyzed Rearrangements of Free Sugars. 215:43–76
- Ostrowski PJ, see Maul JJ (1999) 206:79–105
- Pak JJ, see Haley MM (1999) 201:81–129
- Paldus J, Li X (1999) Electron Correlation in Small Molecules: Grafting CI onto CC. 203:1–20
- Paleos CM, Tsiourvas D (2003) Molecular Recognition and Hydrogen-Bonded Amphiphilicities. 227:1–29
- Paulmier C, see Ponthieux S (2000) 208:113–142
- Penadés S, see Rojo J (2002) 218:45–92
- Perrio C, see Lasne M-C (2002) 222:201–258
- Peruzzini M, see Ehses M (2002) 220:107–140
- Peters JA, see Frullano L (2002) 221:25–60
- Petrus L, Petrušová M, Hricovíniová Z (2001) The Bílik Reaction. 215:15–41
- Petrusová M, see Petrus L (2001) 215:15–41
- Petta M, see Idee J-M (2002) 222:151–171
- Pichot C, see Elaissari A (2003) 227:169–193
- Pipek J, Bogár F (1999) Many-Body Perturbation Theory with Localized Orbitals – Kapuy's Approach. 203:43–61
- Ponthieux S, Paulmier C (2000) Selenium-Stabilized Carbanions. 208:113–142
- Port M, see Idee J-M (2002) 222:151–171
- Poulin P, see Loudet JC (2003) 226:173–196
- Raimondi M, Cooper DL (1999) Ab Initio Modern Valence Bond Theory. 203:105–120
- Reinhoudt DN, see van Manen H-J (2001) 217:121–162
- Renaud P (2000) Radical Reactions Using Selenium Precursors. 208:81–112
- Richardson N, see Schwert DD (2002) 221:165–200
- Rigaut S, see Astruc D (2000) 210:229–259

- Riley MJ (2001) Geometric and Electronic Information From the Spectroscopy of Six-Coordinate Copper(II) Compounds. *214*:57–80
- Rissanen K, see Nummelin S (2000) *210*:1–67
- Røeggen I (1999) Extended Geminal Models. *203*:89–103
- Röckendorf N, Lindhorst TK (2001) Glycodendrimers. *217*:201–238
- Roeda D, see Lasne M-C (2002) *222*:201–258
- Rohovec J, see Frullano L (2002) *221*:25–60
- Rojó J, Morales JC, Penadés S (2002) Carbohydrate-Carbohydrate Interactions in Biological and Model Systems. *218*:45–92
- Romerosa A, see Ehses M (2002) *220*:107–140
- Rouden J, see Lasne M-C (2002) *222*:201–258
- Ruano JLG, de la Plata BC (1999) Asymmetric [4+2] Cycloadditions Mediated by Sulfoxides. *204*:1–126
- Ruiz J, see Astruc D (2000) *210*:229–259
- Rychnovsky SD, see Sinz CJ (2001) *216*:51–92
- Salaün J (2000) Cyclopropane Derivates and their Diverse Biological Activities. *207*:1–67
- Sanz-Cervera JF, see Williams RM (2000) *209*:97–173
- Sartor V, see Astruc D (2000) *210*:229–259
- Sato S, see Furukawa N (1999) *205*:89–129
- Scherf U (1999) Oligo- and Polyarylenes, Oligo- and Polyarylenevinyls. *201*:163–222
- Schlenk C, see Frey H (2000) *210*:69–129
- Schmitt V, Leal-Calderon F, Bibette J (2003) Preparation of Monodisperse Particles and Emulsions by Controlled Shear. *227*:195–215
- Schwert DD, Davies JA, Richardson N (2002) Non-Gadolinium-Based MRI Contrast Agents. *221*:165–200
- Sheiko SS, Möller M (2001) Hyperbranched Macromolecules: Soft Particles with Adjustable Shape and Capability to Persistent Motion. *212*:137–175
- Shen B (2000) The Biosynthesis of Aromatic Polyketides. *209*:1–51
- Shinkai S, see James TD (2002) *218*:159–200
- Shirakawa E, see Hiyama T (2002) *219*:61–85
- Shogren-Knaak M, see Imperiali B (1999) *202*:1–38
- Sinou D (1999) Metal Catalysis in Water. *206*:41–59
- Sinz CJ, Rychnovsky SD (2001) 4-Acetoxy- and 4-Cyano-1,3-dioxanes in Synthesis. *216*:51–92
- Skrifvars M, see Nummelin S (2000) *210*:1–67
- Smith DK, Diederich F (2000) Supramolecular Dendrimer Chemistry – A Journey Through the Branched Architecture. *210*:183–227
- Stec WJ, see Guga P (2002) *220*:169–200
- Steward LE, see Gilmore MA (1999) *202*:77–99
- Stocking EM, see Williams RM (2000) *209*:97–173
- Streubel R (2003) Transient Nitrilium Phosphanylid Complexes: New Versatile Building Blocks in Phosphorus Chemistry. *223*:91–109
- Stütz AE, see Häusler H (2001) *215*:77–114
- Sugihara Y, see Nakayama J (1999) *205*:131–195
- Sun J-Q, Bartlett RJ (1999) Modern Correlation Theories for Extended, Periodic Systems. *203*:121–145
- Sun L, see Crooks RM (2001) *212*:81–135
- Surján PR (1999) An Introduction to the Theory of Geminals. *203*:63–88
- Tamao K, Miyauchi N (2002) Introduction to Cross-Coupling Reactions. *219*:1–9
- ten Holte P, see Zwanenburg B (2001) *216*:93–124
- Thiem J, see Werschkun B (2001) *215*:293–325
- Thutewohl M, see Waldmann H (2000) *211*:117–130
- Tichkovsky I, see Idee J-M (2002) *222*:151–171
- Tiecco M (2000) Electrophilic Selenium, Selenocyclizations. *208*:7–54
- Tohma H, Kita Y (2003) Synthetic Applications (Total Synthesis and Natural Product Synthesis). *224*:209–248

- Tomoda S, see Iwaoka M (2000) 208:55–80
- Tóth E, Helm L, Merbach AE (2002) Relaxivity of MRI Contrast Agents. 221: 61–101
- Tovar GEM, Kräuter I, Gruber C (2003) Molecularly Imprinted Polymer Nanospheres as Fully Affinity Receptors. 227: 125–144
- Tromas C, García R (2002) Interaction Forces with Carbohydrates Measured by Atomic Force Microscopy. 218: 115–132
- Tsiourvas D, see Paleos CM (2003) 227: 1–29
- Ublacker GA, see Maul JJ (1999) 206:79–105
- Uemura S, see Nishibayashi Y (2000) 208:201–233
- Uemura S, see Nishibayashi Y (2000) 208:235–255
- Valdemoro C (1999) Electron Correlation and Reduced Density Matrices. 203:187–200
- Valério C, see Astruc D (2000) 210:229–259
- van Benthem RATM, see Muscat D (2001) 212:41–80
- van Koten G, see Kreiter R (2001) 217: 163–199
- van Manen H-J, van Veggel FCJM, Reinhoudt DN (2001) Non-Covalent Synthesis of Metallo-dendrimers. 217: 121–162
- van Veggel FCJM, see van Manen H-J (2001) 217: 121–162
- Varvoglis A (2003) Preparation of Hypervalent Iodine Compounds. 224:69–98
- Verkade JG (2003) P(RNCH<sub>2</sub>CH<sub>2</sub>)<sub>3</sub>N: Very Strong Non-ionic Bases Useful in Organic Synthesis. 223:1–44
- Vliegthart JFG, see Haseley SR (2002) 218:93–114
- Vogler A, Kunkely H (2001) Luminescent Metal Complexes: Diversity of Excited States. 213: 143–182
- Vogtner S, see Kloppe W (1999) 203:21–42
- Vostrowsky O, see Hirsch A (2001) 217: 51–93
- Waldmann H, Thutewohl M (2000) Ras-Farnesyltransferase-Inhibitors as Promising Anti-Tumor Drugs. 211:117–130
- Wang G-X, see Chow H-F (2001) 217: 1–50
- Weil T, see Wiesler U-M (2001) 212:1–40
- Werschkun B, Thiem J (2001) Claisen Rearrangements in Carbohydrate Chemistry. 215: 293–325
- Wiesler U-M, Weil T, Müllen K (2001) Nanosized Polyphenylene Dendrimers. 212:1–40
- Williams RM, Stocking EM, Sanz-Cervera JF (2000) Biosynthesis of Prenylated Alkaloids Derived from Tryptophan. 209:97–173
- Wirth T (2000) Introduction and General Aspects. 208:1–5
- Wirth T (2003) Introduction and General Aspects. 224:1–4
- Wirth T (2003) Oxidations and Rearrangements. 224:185–208
- Wrodnigg TM, Eder B (2001) The Amadori and Heyns Rearrangements: Landmarks in the History of Carbohydrate Chemistry or Unrecognized Synthetic Opportunities? 215:115–175
- Yersin H, Donges D (2001) Low-Lying Electronic States and Photophysical Properties of Organometallic Pd(II) and Pt(II) Compounds. Modern Research Trends Presented in Detailed Case Studies. 214:81–186
- Yeung LK, see Crooks RM (2001) 212:81–135
- Yoshifuji M, Ito S (2003) Chemistry of Phosphanylidene Carbenoids. 223:67–89
- Zablocka M, see Majoral J-P (2002) 220:53–77
- Zhang J, see Chow H-F (2001) 217: 1–50
- Zhdankin VV (2003) C-C Bond Forming Reactions. 224:99–136
- Zhao M, see Crooks RM (2001) 212:81–135
- Zimmermann SC, Lawless LJ (2001) Supramolecular Chemistry of Dendrimers. 217: 95–120
- Zwanenburg B, ten Holte P (2001) The Synthetic Potential of Three-Membered Ring Aza-Heterocycles. 216: 93–124